Insights into auxin co-receptor formation and SCF^{TIR1}-driven AUX/IAA ubiquitylation

Kumulative Dissertation

zur Erlangung des

Doktorgrades der Naturwissenschaften (Dr. rer. nat.)

vorgelegt der

Naturwissenschaftlichen Fakultät I

Biowissenschaften

der Martin-Luther-Universität

Halle-Wittenberg,

von Michael Benedikt Niemeyer

geboren am 03.09.1990 in Goslar

Gutachter:
Prof. Dr. Steffen Abel

Prof. Dr. Andrea Sinz

Prof. Dr. Dolf Weijers

eingereicht am: 23.07.2020
verteidigt am: 11.12.2020

In the beginning, there was simplicity.

Richard Dawkins, *The Selfish Gene*

Table of Contents

List of abbreviations

2,4-D	2,4-dichlorophenoxyacetic acid
ADP	Adenosine diphosphate
AFB	AUXIN SIGNALING F-BOX
ALF4	ABERRANT LATERAL ROOT FORMATION
ARF	AUXIN RESPONSE FACTOR
ARIH1	ARIADNE
ASK	ARABIDOPSIS S-PHASE KINASE ASSOCIATED PROTEIN
At	*Arabidopsis thaliana*
ATP	Adenosine triphosphate
AUX/IAA	AUXIN/INDOLE-3-ACETIC ACID (protein)
AXR	AUXIN-RESISTANT
BDL	BODENLOS
CAND1	CULLIN-ASSOCIATED NEDD8-DISSOCIATED PROTEIN 1
CDC34	cell division cycle 34
COI1	CORONATINE INSENSITIVE 1
COP9	CONSTITUTIVE PHOTOMORPHOGENESIS 9
CP	Core particle (of the proteasome)
CRL	CULLIN RING type E3 UBIQUITIN LIGASE
CSN	COP9 SIGNALOSOME
C-terminal	carboxy-terminal
CUL	CULLIN
Da	Dalton
DEN1	DENEDDYLASE1
DNA	Deoxyribonucleic acid
dT	Degron tail, region downstream of AUX/IAA degron and upstream of its PB1 domain
DUB	Deubiquitylating enzyme
e.g.	*exempli gratia* – for example
E1	Ubiquitin activating enzyme
E2	Ubiquitin conjugating enzyme
E3	Ubiquitin ligase
EAR	ETHYLENE RESPONSE FACTOR-ASSOCIATED AMPHIPHILIC REPRESSION
FBP	F-box protein
GH3	GRETCHEN HAGEN3

GLMN	GLOMULIN
HDAC	Histone deacetylase
HECT	Homologous to E6AP C-Terminus
IAA	Indole-3-acetic acid
IAA#	A single AUX/IAA protein from *Arabidopsis thaliana* if not indicated differently
IDP	Intrinsically disordered protein
IDR	Intrinsically disordered region
IVU	*In vitro* ubiquitylation (reaction)
K_D	(equilibrium) dissociation constant
M	molar
MEF	mouse embryonic fibroblasts
MP	MONOPTEROS
N8 = NEDD8	NEURAL PRECURSOR CELL EXPRESSED, DEVELOPMENTALLY DOWNREGULATED8
NEDP1	NEDD8-SPECIFIC PROTEASE1
N-terminal	amino-terminal
Os	*Oryza sativa*
PB1	Phox and Bem1 (domain)
PTM	Post-Translational Modification
RBR	RING-betweenRING-RING
RBX	RING-box
RCE	RUB-conjugating enzyme
RING	REALLY INTERSTING NEW GENE
RP	Regulatory particle (of the proteasome)
RUB	RELATED TO UBIQUITIN
SAUR	SMALL AUXIN UPREGULATED RNA
SCF	SKP1-CULLIN1-F-box
SENP8	SENTRIN-SPECIFIC PROTEASE8
SKP	S-PHASE KINASE ASSOCIATED PROTEIN
TIR1	TRANSPORT INHIBITOR RESPONSE 1
TPL, TPD, TPR	TOPLESS, TOPLESS domain, TOPLESS-RELATED
Ub	Ubiquitin
Ub'd	Ubiquitylated
UBA	Ubiquitin activating protein/ubiquitin associated domain
UBC	Ubiquitin conjugating (domain/protein)
UbL	Ubiquitin-like

UPS	Ubiquitin Proteasome System
XL-MS	Cross-linking mass spectrometry
a.k.a.	Also known as

Throughout this thesis protein-protein interactions (PPIs) include the following symbol "~". Covalent modifications such as ubiquitylation are depicted as *e.g.* Ub~IAA7, while non-covalent protein-protein, and protein-ligand interactions in complexes include the following symbol "·" *e.g.* TIR1·auxin·AUX/IAA. For amino acids the three-letter or one-letter code is used according to IUPAC-IUB (recommendations 1983). In various stances, specific protein domains are annotated as $Protein^{Domain}$. The word proteasome refers to the population of capped proteasomes including 26S and 30S proteasomes and others proteasome subtypes are specifically mentioned.

1. Introduction

1.1 The ubiquitin proteasome system arranges protein pools

In eukaryotic cells, spatiotemporal regulation of protein levels is driven by the covalent attachment of ubiquitin (Ub) to target proteins, a.k.a. ubiquitylation substrates (Kim et al., 2013; Aguilar-Hernández et al., 2017). Almost every single cellular process depending on the rapid adjustment of protein pools, including translation, protein trafficking, cell cycle control, or responses to external and internal cues, *e.g.* immunity and hormone signaling, is impacted by protein ubiquitylation (Komander and Rape, 2012; Mendes et al., 2020). Ubiquitylation, at its core, depends on an enzymatic cascade requiring the activity of three protein classes: E1 ubiquitin activating enzymes, E2 ubiquitin conjugating enzymes, and E3 ubiquitin ligases (**Figure 1**) (Komander and Rape, 2012; Callis, 2014). E1, E2 and E3 enzymes are highly conserved among eukaryotes, and most of the ubiquitylation knowledge gathered over the past centuries in mammals and yeast, is considered to be valid in plants (Haas and Rose, 1982; Ling et al., 2000; Bachmair et al., 2001; Callis, 2014). During

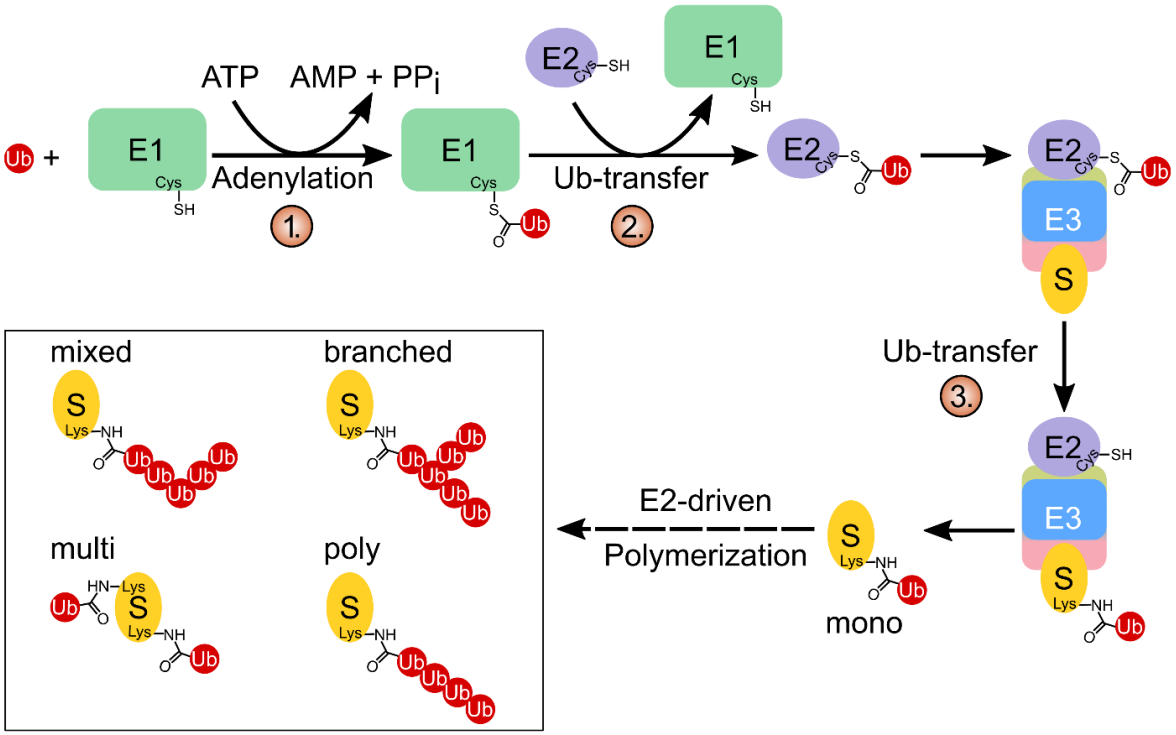

Figure 1: An enzymatic cascade ubiquitylates substrate proteins. Ubiquitin (Ub, red circles) is bound and activated by the ubiquitin activating enzyme E1 (light green) coupled to ATP hydrolysis. Cysteine-bound Ub is transferred from the E1 to a Ub conjugating enzyme E2 (lilac) *via* transesterification. The E2 docks on an E3 Ub ligase, which directly and specifically recruits the substrate (yellow oval (S)). Ub is either transferred directly from the E2, or *via* an Ub~E3 intermediate onto the substrate. Substrate ubiquitylation can occur in multiple facets ranging from mono-ubiquitylation, to multi-ubiquitylation, in one or multiple sites. Poly-ubiquitylation as homotypic, branched or mixed Ub chains results from consecutive ubiquitylation cycles, where substrate-attached Ub acts itself as a substrate.

the first step of ubiquitylation, a ubiquitin activating enzyme (E1; UBAs) activates ubiquitin *via* adenylation, followed by thioester formation on the active site cysteine (Hann et al., 2019). A Ub-loaded E1 interacts further with a ubiquitin conjugating enzyme (E2; UBCs), enabling Ub transfer to the catalytic cysteine of the E2 *via* trans-thioesterification. Next, a ubiquitin ligase (E3) confers substrate specificity exerting its function at least in two different ways. During Ub-transfer to the substrate, Ub is either directly transferred from the E2 enzyme to the E3-bound substrate; or an Ub~E3 intermediate is formed followed by ubiquitin transfer to the substrate usually on exposed lysine residues *via* an isopeptide bond (Komander and Rape, 2012). Prior substrate ubiquitylation, an E3 ligase must recruit the substrate in a controlled manner, which is ensured by specific sequence signals, such as short linear motifs (SLiMs). Degrons (degradation signal) represent the most prominent SLiM in substrate proteins that undergo ubiquitin-mediated proteasomal degradation (Skaar et al., 2013; Guharoy et al., 2016). In this case, substrate recruitment to an E3 ligase and its subsequent specific ubiquitylation, results in its recognition and degradation by the proteasome (Finley, 2009). This cascade of events constitutes the backbone of the ubiquitin proteasome system (UPS). Initiation of substrate binding by the E3 often involves, molecular triggers, which activate or expose the degron in substrates. Degrons might undergo conformational changes or specific post-translation modifications (PTMs) *e.g.* phosphorylation prior proteolysis of cell cycle-regulating proteins (cyclins, p27) (Ye et al., 2004; Holt, 2012; Skaar et al., 2013); processing and modification of specific N-terminal amino acids (N-degron pathway) during hypoxia responses in plants (Dissmeyer, 2019); oxygen-dependent prolyl hydroxylation in HIF1α at normal oxygen levels in mammals (Ravid and Hochstrasser, 2008); or non-covalent induction *via* small molecules such as phytohormones, which enhance substrate binding to E3s (Tan et al., 2007; Skaar et al., 2013).

1.1.1 Ubiquitylation determines substrate's fate

The fate of the ubiquitylated substrate defines such a recognition motif as a degron, and the substrate's fate is determined by the type of ubiquitylation (**Figure 1 & 2**). Monoubiquitylation of proteins occurs when a single Ub moiety is attached to the substrate, which escapes further ubiquitylation cycles (Komander and Rape, 2012). In other cases, ubiquitylation continues in (possibly) multiple cycles. These can either enable targeting of lysines in the substrate (multiubiquitylation), or the already-attached Ub undergoes itself ubiquitylation (poly-

ubiquitylation). In this case, any of the seven lysines in Ub (K6, K11, K27, K29, K33, K48, K63), or its N-terminal methionine, might act as Ub acceptor sites (Komander and Rape, 2012). Cycles of ubiquitylation on ubiquitin result the formation of chains on substrates. Ub chains can be homotypic, if the same lysine residue in each Ub undergoes ubiquitylation, heterotypic, if different lysines are used as acceptor sites within one chain (**Figure 1, box**) (Akutsu et al., 2016; Stolz and Dikic, 2018). A ubiquitin chain on substrate proteins becomes a distinct signal, that facilitates recognition by other proteins containing Ub receptor domains (Husnjak and Dikic, 2012).

The proteasome is a multi-subunit ATP-driven protease, which contains multiple Ub receptors on its surface for recognition, engagement and proteolysis of ubiquitylated substrates (Yu and Matouschek, 2017). These receptors, namely Rpn1, Rpn10 and Rpn13, reside in the 19S regulatory particle (RP) of the proteasome (Martinez-Fonts et al., 2020). The RP is attached either one site (26S proteasome) or on both sites (30S proteasome) of the barrel-shaped 20S core particle (CP). The RP controls the entry to the CP *via* substrate binding and unfolding, while the CP itself, confers the

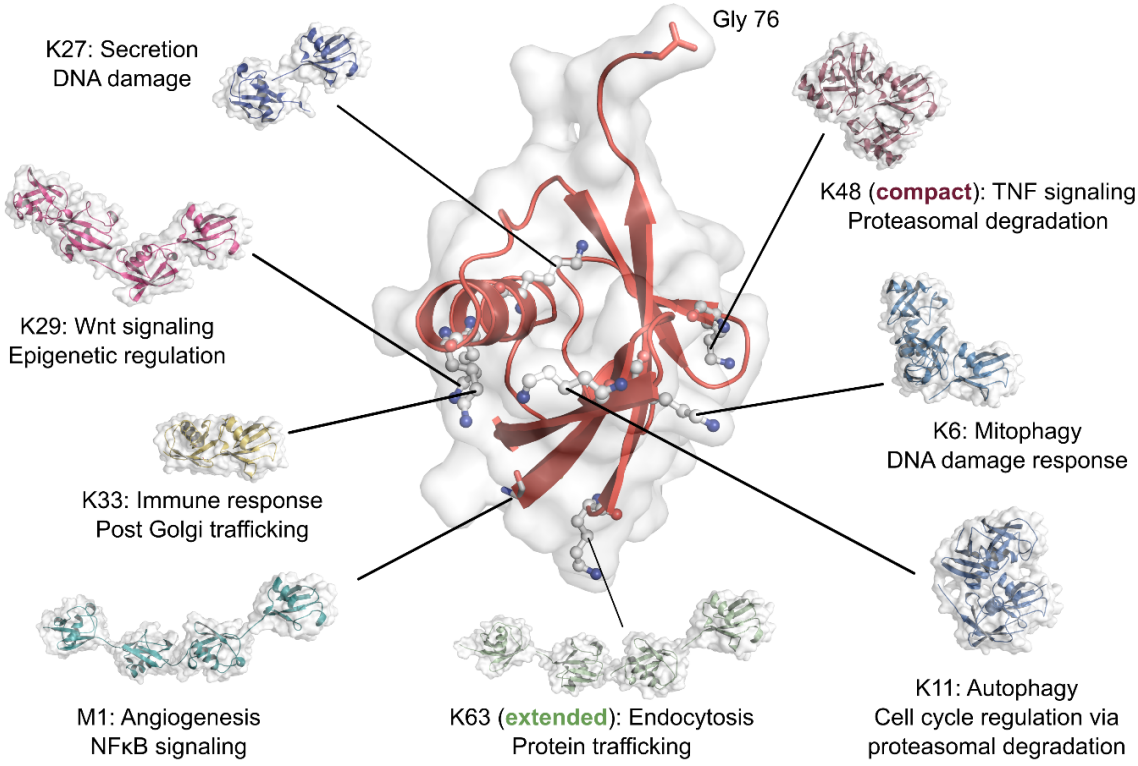

Figure 2: Lysine-specified ubiquitin chain topology determines protein fate. Ub (red cartoon & white transparent surface) undergoes ubiquitylation through one of eight residues (seven lysines and the N-terminal methionine; stick & spheres representation). The resulting Ub chains show different topologies: from globular (*e.g.* K48- or K11-linked) to elongated (K63- or K29-linked). Different Ub chain types on substrates can be recognized by Ub binding proteins (UBPs), Ub receptors and Ub-associated proteins through their overall shape, and multiple (specifically exposed) interaction interfaces. The recognition of Ub chains results in different processing of target proteins, enabling numerous cellular functions as indicated for each linkage-type.

proteolytic activity to the proteasome (Tanaka, 2009). In this manner, the overall architecture of the proteasome, shields its protease sites from the cellular environment, preventing unspecific degradation of proteins (Finley et al., 2016; Yu and Matouschek, 2017). Specific Ub receptors at the RP discriminate substrates by the attached ubiquitin chains, and allow tight substrate engagement, leading to the translocation into the proteolytic core (Finley, 2009; Finley et al., 2016; Yu and Matouschek, 2017; Bard et al., 2019). If one considers homotypic chain types only, K48-linked and K11-linked Ub chains constitute preferred signals on substrates for recruitment by the proteasome (Yu and Matouschek, 2017). Degradation signals are versatile though and heterotypic or branched/mixed Ub chains on substrates serve also as tags for proteolysis (Xu et al., 2009; Meyer and Rape, 2014; Ohtake et al., 2018; Bard et al., 2019). Added complexity and specificity during ubiquitin-mediated protein degradation is given by the activity of ubiquitin-like (UbL) proteins, and ubiquitin binding proteins (UBPs), which can act as shuttles to bring ubiquitylated proteins to the proteasome (reviewed in: Husnjak and Dikic, 2012; Yu et al., 2016; Tsuchiya et al., 2017). Prerequisites for engagement and efficient degradation of substrates by the proteasome include: a disordered (unstructured) initiation site and correctly placed ubiquitin chains of the above specified types along their protein sequence (Prakash et al., 2004; Guharoy et al., 2016; Yu et al., 2016; Bard et al., 2019).

Ub receptors or Ub binding domain (UBD)-containing proteins recognize Ub chains by their topology and length (**Figure 2**) (Husnjak and Dikic, 2012). The differences in homotypic chain topology are visualized in **Figure 2** and vary from highly compact forms (K48-, or K11-linked) to extended chains (K63-linked and linear) (Eddins et al., 2007; Bremm et al., 2010). Besides the overall topology, the linkage type defines the accessibility of interaction surfaces on Ub. Recently, heterotypic (branched and mixed) ubiquitin chains were found to prompt proteasomal degradation of proteins in cells (Ohtake et al., 2016; Ohtake et al., 2018; Swatek et al., 2019). Mixed chains, where none of the ubiquitins is modified by two ubiquitins at the same time, seem to keep the signals encoded by each of the connected chains (Nakasone et al., 2013). At the same time, chains branched *via e.g.* K11/K48 linkages on one ubiquitin can increase the functionality, and exhibit different affinities to Ub receptors than their homotypic counterparts alone (Boughton et al., 2020).

While degradation at the proteasome is one of the most studied, and the most prominent fate of ubiquitylated substrates, various additional outcomes result from protein ubiquitylation *e.g.* DNA

damage response, endocytosis, and trafficking (as reviewed in Mendes et al., 2020). For example, H2B monoubiquitylation, for instance, modulates nucleosomes and chromatin structure and thereby transcription (reviewed in: Meas and Mao, 2015). K63-linked polyubiquitin chains on proteins play a predominant role during endocytosis of numerous membrane-bound receptors and transporters, such as the auxin efflux carrier PIN2 or the iron transporter IRT1 (Leitner et al., 2012; Dubeaux et al., 2018; Romero-Barrios and Vert, 2018; Martinez-Fonts et al., 2020; Romero-Barrios et al., 2020). In addition, protein localization, activity and assembly into complexes is regulated on multiple levels *via* ubiquitylation (Komander and Rape, 2012).

While ubiquitylation of Ub is essential during chain formation, Ub can be subjected to other posttranslational modifications (PTMs) such as phosphorylation, deamidation, and acetylation, which has the potential of altering interactions with E2/E3 pairs or shielding lysines from further ubiquitin attachment, thereby restricting Ub chain elongation (Swatek and Komander, 2016). It was recently shown, Ub also undergoes inactivation *via* ADP-ribosylation by bacterial effector proteins (Yan et al., 2020). Protein ubiquitylation is probably one of the main drivers of signal integration, allowing cells to constantly and rapidly react to their close and far environment (Miricescu et al., 2018; Kliza and Husnjak, 2020). Multiple signals are translated into all kinds of PTMs, such as ubiquitin chains, which govern the fate of substrate proteins. The diverse ways, in which ubiquitylation occurs, and is modulated embody a molecular code, where the E1(s), E2s and E3s serve as the writers of the ubiquitin code. Specifically, E2 and E3 enzymes ensure Ub chain type, and substrate specificity across tissues and developmental stages (Komander and Rape, 2012; Swatek and Komander, 2016).

1.1.2 Diversity of E2s and E3s drive Ub chain formation

The variety and combinatorial potential of ~40 E2 Ub conjugating (UBCs) enzymes and more than 600 or 1400 E3s, in mammals or in plants, respectively, drive the precise coding capabilities of the ubiquitin system (Callis, 2014; Morreale and Walden, 2016). The mechanisms of ubiquitin chain formation on target proteins, specifically, how distinct E2s, and E2/E3 or even E3/E3 pairs dictate Ub chain types, and Ub chain elongation, will be revised in the next section.

E2s or UBCs are conserved protein families among yeast, mammals, and the model plant *Arabidopsis thaliana* (Kraft et al., 2005; Stewart et al., 2016). In *Arabidopsis*, 37 proteins are considered active ubiquitin-conjugating enzymes, and all but two were shown to be active *in vitro* (Kraft et al., 2005; Callis, 2014; Kowarschik et al., 2018). E2 activity is embedded in the highly conserved core catalytic UBC domain, that harbors the active site, a cysteine needed for transthioesterification during the ubiquitylation cascade. The UBC domain harbors conserved and partially overlapping E1 and E3 binding sites, which make E1 and E3 binding mutually exclusive (Stewart et al., 2016). In addition, E2s carry unique specificity determinant regions for either chain formation or E3 selectivity (Stewart et al., 2016; Gundogdu and Walden, 2019). Monomeric E2s, for example, ensure chain specificity by facilitating acceptor ubiquitin recognition using extensive noncovalent interactions with the donor or acceptor Ub (Wickliffe et al., 2011; Middleton and Day, 2015). In general, two major classes of E2s can be defined, based on their intrinsic reactivity: E2s with lysine reactivity, which carry out direct substrate ubiquitylation; and cysteine-reactive E2s, which participate in ubiquitylation reactions where an Ub~E3 intermediate is formed (Stewart et al., 2016).

The most diversity in the UPS is provided by the numerous E3 ligases, which not only contribute to linkage specificity, but more importantly select specifically the ubiquitylation substrates (Callis, 2014). E3s can be divided in three main classes: HECT (Homologous to E6AP C-Terminus)-type E3 ligases, which form an E3~Ub intermediate *via* an additional transthioesterification step at their active site cysteine; RING (REALLY INTERESTING NEW GENE)-type E3 ligases, which bind an E2 loaded with Ub (Ub~E2), and facilitate direct Ub transfer to the E3-bound substrate without the formation of a covalent intermediate (Metzger et al., 2014). RING-betweenRING-RING (RBR) E3 ligases, on the other hand, combine the mechanism of action of the other two types of E3s, namely RING-dependent E2 recruitment, and the formation of an Ub~E3 intermediate (Morreale and Walden, 2016). While the RBR and HECT E3 ligases represent only ~10% of the E3s identified in plants, RING-type E3 ligases constitute the majority of E3 ligases in plants (Callis, 2014).

In numbers, 350 or 490 RING domain-containing proteins are described in humans and *Arabidopsis*, respectively (Callis, 2014; Medvar et al., 2016). Those numbers account only for the RING domain-containing proteins themselves and disregard multimeric complexes with interchangeable subunits, which increase the number of RING E3s dramatically. Probably one of

the structurally most complex RING-type E3 ligases is the ANAPHASE-PROMOTING COMPLEX/CYCLOSOME (APC/C) with at least 11-13 core subunits in eukaryotes (Heyman and Veylder, 2012). APC/C functions during cell cycle control, and is essential for proper growth and development in many organisms (Watson et al., 2019). One of the core subunits, APC2, shows similarity with a group of proteins named cullins, which act as scaffolds for many multimeric RING-type E3 ligases.

Multimeric cullin-RING ligases (CRLs) consist of a RING-containing RING Box 1/2 (RBX1/2) protein, one of multiple cullins, or cullin-like proteins (APC2, CUL1, CUL2, CUL3(A/B), CUL4, CUL5, CUL7), and a substrate receptor (SR) module, which is usually comprised of a cullin adaptor protein, and a versatile protein-protein interaction (PPI) domain (Sun et al., 2020). Cullins bridge the E2-binding subunit, RING domain-containing RBXs, on one site, and substrate specific SR modules, on the other (Thomann et al., 2005; Zimmerman et al., 2010). The SR modules built by S-PHASE KINASE-ASSOCIATED PROTEIN 1 (SKP1), and F-box containing proteins (FBPs) associate with CUL1 forming SCF-type ubiquitin E3 ligases. Similarly, CUL2 and CUL5-containing CRLs use Elongins as adaptors, and interact with substrates *via* different BC-Box proteins. BROAD COMPLEX/TRAMTRACK/BRIC-ABRAC (BTB)-containing SRs associate with CUL3, and CUL3-associated BTB proteins directly bind substrates without an adaptor protein (Hua and Vierstra, 2011; Rusnac and Zheng, 2020). CUL4-type E3 ligases contain a DCAFs/DWD SR module, adopting a structurally distinct fold based on WD40-like β-propeller domains (Zimmerman et al., 2010). Interesting is the fact, that the variability of receptor modules likely broadens substrate specificity of each CRL tremendously. The *Arabidopsis* genome encodes for close to 700 FBPs, ~80 BTBs, and 85 DDB1/DWD SRs (Hua and Vierstra, 2011). This evidences a pivotal role for E3s presumably controlling ubiquitylation and fate of 100s, if not 1000s of proteins, thereby impacting all sort of signaling pathways for plant growth and development (Saracco et al., 2009; Kim et al., 2013; Svozil et al., 2015; Romero-Barrios et al., 2020).

1.1.3 E2-E3 pairing defines Ub chain types

Coordination of efficient protein ubiquitylation and ubiquitin chain formation relies on the adequate combination of E2-E3 pairs. To ensure correct chain formation on a substrate, E2-E3 pairing involves multiple specificity-determining factors (Mattiroli and Sixma, 2014). The basic

pairing principle relies on E2 reactivity for either lysines, or cysteines, combined with selective binding to either RING or HECT domains in E3s (Stewart et al., 2016). These two E2 parameter constraints enable selection for classic RING E3s, RBRs or HECT-type E3s ligases. Cysteine-reactive E2s act unlikely during specific Ub chain elongation, and only transfer Ub to an HECT or RBR-type E3. Thereby, chain specificity is rather determined by the interacting E3 or by another secondary E2 (Deol et al., 2019). During ubiquitylation, the transfer of the first ubiquitin to the substrate protein, or to an Ub~intermediate forming E3, differs from subsequent chain elongation events, and distinct E2s or even E3s carry out this so-called priming event (Wu et al., 2010; Scott et al., 2016; Deol et al., 2019). Similarly, multiple E2s can be involved in the formation of defined mixed Ub chains, where one E2, first "seeds" some short Ub chains *via* a certain linkage type, *e.g.* K63, while a different E2 elongates the chain with a different linkage type, such as K48. This is the case with APC/C-interacting E2s (Wickliffe et al., 2011; Brown et al., 2016; Ohtake et al., 2018).

E2 enzymes ensure specific Ub chain-type formation based on multiple contacts with the acceptor Ub, the donor Ub, and E3s, creating a beneficial micro-environment for ubiquitin conjugation towards one defined Lys in Ub (Mattiroli and Sixma, 2014). Since E2s cannot stay bound to the E3 during Ub recharging by the E1, a rapid cycling of Ub~E2 assemblies, and Ub discharge facilitates Ub chain formation, while the substrate remains bound to the E3 (Kleiger et al., 2009b). Some E2s, and E2/E3 combinations produce more than one linkage type, which is counteracted by the action of deubiquitylating enzymes (DUBs). DUBs constitute a family of proteases specialized to cleave ubiquitins of Ub chains and substrates (Nielsen and MacGurn, 2020). Upon DUB action, a further modification of a Ub chain is possible, and might shift the fate of a substrate, or counteract unwanted side reactivities (Lee et al., 2016; Niu et al., 2019).

Various activity assays have revealed specificity in the E2 family for certain RING/U-BOX E3 ligases (Kraft et al., 2005; Ramadan et al., 2015; Turek et al., 2018). For example, UBC34 showed only activity in combination with two E3s of the RING-H2 subtype (Kraft et al., 2005). Specificity can be introduced by domains or proteins in complex with the E2-binding RING/U-BOX domain (Turek et al., 2018) such as the WHB domain in the CUL1 subunit of an SCF complex (Kleiger et al., 2009a; Spratt and Shaw, 2011). Other E2s, such as those belonging to the UBC8 subgroup (VI) have shown activity with many E3s of different subtypes (Kraft et al., 2005). Some E2s are not only promiscuous while interacting with RING/U-Box E3 ligases, but additionally form active complexes with E3s of

the other two types, RBR and HECT E3 ligases (Stewart et al., 2016). This behavior is not surprising given the hierarchical interaction potential of ~40 E2s with the many hundreds E3s present in both humans and plants (Callis, 2014; Metzger et al., 2014; Morreale and Walden, 2016). Multimeric RING-type E3 ligases seem to facilitate the specific interaction with a subgroup of E2s *via* an acidic tail in the E2 (Kleiger et al., 2009a). In addition, their RING domain activates E2s by the stabilization of their closed, catalytically active state during ubiquitin transfer (Plechanovová et al., 2012; Pruneda et al., 2012; Branigan et al., 2020). Besides the conserved UBC domain, which contains already multiple described interaction surfaces, some E2s have expanded sequences, likely acting as additional specificity determinants (Stewart et al., 2016).

1.1.4 CRL1 or SCF-type E3 ligases integrate plant signaling cascades

Compared to humans, plants exhibit a 10-fold increase in FBPs, enabling the potentially ~700 FBP-containing SCF-type E3 ligases to function as versatile protein targeting tools for ubiquitylation and degradation (Stefanowicz et al., 2015; Abd-Hamid et al., 2020). FBPs interchangeably assemble with SCFs *via* their F-box domain that is recruited by ASK adaptor proteins (Tal et al., 2020). The FBP substrate-recruiting subunit consists of one of various known protein-protein interaction domains, such as Kelch, WD-40 or leucine-rich repeat (LRR) domains (Skaar et al., 2013). These versatile domains facilitate the specific recognition of target proteins through degrons (Skaar et al., 2013). During the last decades, various SCFs have been shown to be pivotal for integration of cellular responses, particularly for hormone-mediated signal transduction (Lechner et al., 2006; Tal et al., 2020). Phytohormones often act as triggers enabling SCF-substrate interactions for target ubiquitylation and degradation (Santner and Estelle, 2010). During hormone signaling, FBPs can either directly participate in hormone perception, *e.g.* for auxin and jasmonate (JA; jasmonic acid) signaling, or indirectly, during gibberellic acid (GA) and strigolactone (SL)-mediated processes (Stefanowicz et al., 2015; Tal et al., 2020). The small molecules auxin and JA trigger the recruitment of AUXIN/INDOLE-3-ACETIC ACID (AUX/IAA), and JASMONATE-ZIM DOMAIN (JAZ) repressor proteins, respectively, by enhancing the interaction between TRANSPORT INHIBITOR RESPONSE 1 (TIR1) and AUX/IAAs, or CORONATINE INSENSITIVE 1 (COI1) and JAZs (Tan et al., 2007; Yan et al., 2009). Other than that, GA and SL induce a conformational change in their receptors (GID1 and D14, respectively), which enables the recruitment of the receptors, and

associated proteins to cognate FBPs SLEEPY1 (SLY1)/SNEEZY (SNZ) for GA, or *Os*D3/*At*MAX2 in case of SL signaling (Tal et al., 2020). In all four cases, the small molecule-triggered interaction with the cognate SCF complexes lead to the ubiquitylation of transcriptional regulators, followed by their proteasomal degradation (Blázquez et al., 2020). The coupling of hormone-triggered substrate degradation, which happens within seconds to minutes, and transcriptional reprogramming allows the rapid UPS-dependent adjustment of protein pools (Xing and Xue, 2012; Stefanowicz et al., 2015; Černý et al., 2016; Guo et al., 2017; Pu et al., 2019). How SCF complex assembly and activity is regulated to ensure the timed availability of specific SCFs (*e.g.* for hormone signaling) on demand, will be laid out in detail in the next section.

1.1.5 SCFs undergo complex regulation allowing broad functionalization

Protein degradation is an energetically very costly process, as cells not only loose most of the energy invested during protein synthesis, but they need to invest additional energy for the destruction itself. Besides protein synthesis, ubiquitylation, and unfolding-coupled translocation at the proteasome are ATP-dependent energy-costly processes, which require tight regulation (Berg et al., 2012). The multimeric nature of SCF-type E3 ligases with interchangeable subunits provides a cost-efficient, adjustable protein targeting platform and allows additional control over substrate degradation *via* the remodeling and activity control of SCF ligase complexes (**Figure 3**). Especially the additional modification of the CUL1 backbone and the exchange of SRs constitute regulatory potential.

The post-translational modification of the CUL1 backbone by the UbL protein NEDD8 (neural precursor cell expressed, developmentally downregulated8; N8) functions as an activation switch, where NEDD8 or RUB (RELATED TO UBIQUITIN; N8 in plants) conjugation allows highly processive target ubiquitylation by CRLs (Pan et al., 2004; Duda et al., 2008; Baek et al., 2020). Similar to Ub, NEDD8 is conjugated to specific substrates *via* an enzymatic cascade that includes an E1, E2 and, sometimes, E3 enzymes (Huang et al., 2004; Enchev et al., 2015). NEDD8 conjugation (neddylation) to cullins leads to a conformational shift in the C-terminus of cullins, as NEDD8 acts as a nucleating factor. The conformational shift reduces the distance between the catalytic Ub~E2·RBX1 site and the SR-bound substrate, increasing thereby the catalytic efficiency of the SCF-type E3 ligase by more than 2000-fold (Duda et al., 2008; Baek et al., 2020).

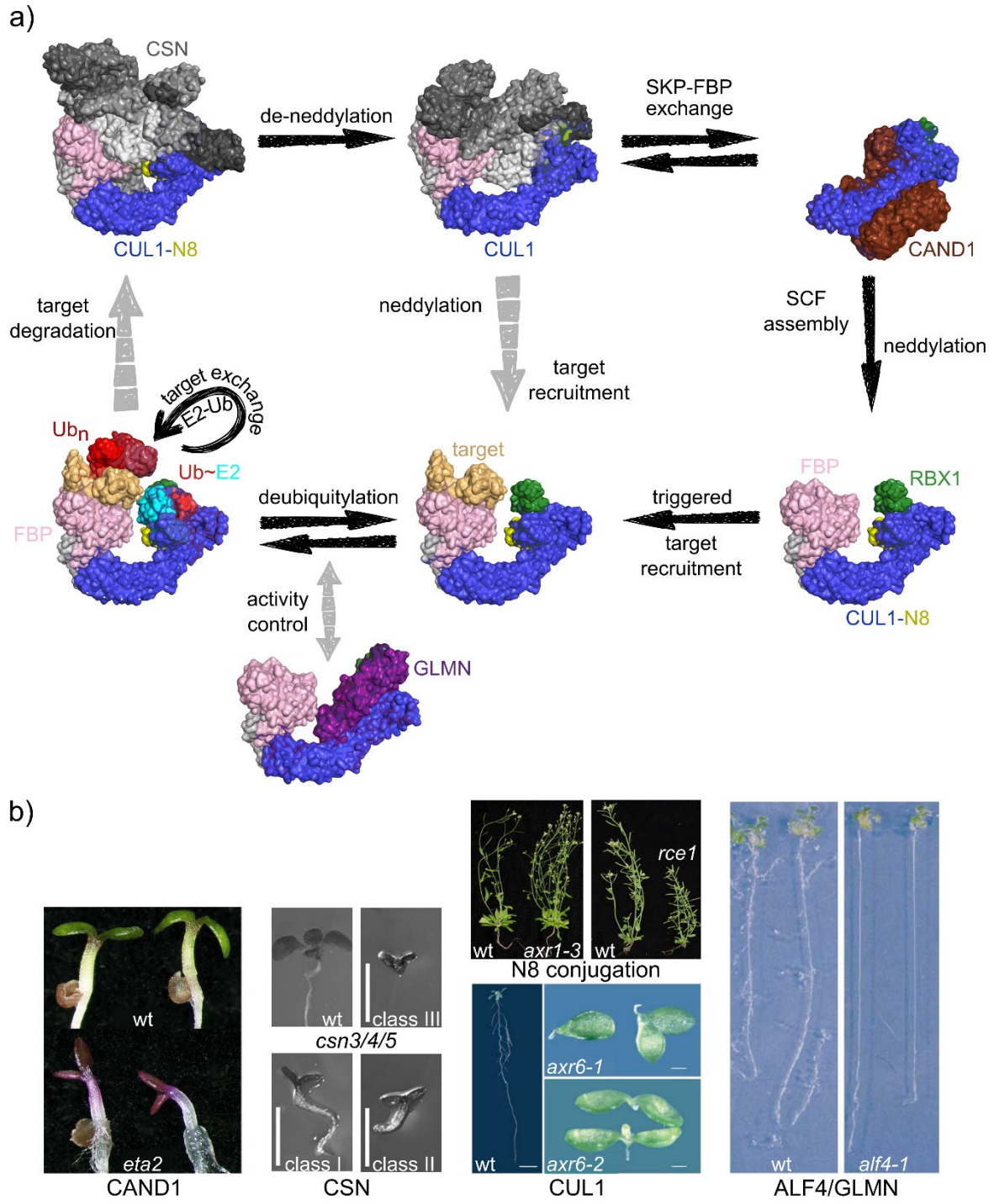

Figure 3: SCF-type E3 ligase activity is highly regulated through multiple interconnected mechanisms. **a**) All SCF complexes share the CUL1 backbone (dark blue) and their assembly into specific active complexes is facilitated *via* the action of multiple activating and inactivating proteins. Assembled substrate receptor(gray/lightpink)-containing SCFs get activated *via* neddylation (N8, yellow) leading to the efficient transfer of ubiquitin (red) onto the target (lightorange). GLMN (purple) and potentially ALF4 regulate this process competing with E2s (aquamarine) for RBX1 (green) binding. Ubiquitylated substrates dislodge from the E3 Ub ligase complex and are targeted for proteasomal degradation. The SCF complex is subsequently inactivated by the CSN complex (shades of gray) removing N8 from the CUL1 subunit. Non-neddylated CUL1 can be bound by CAND1 (brown), which enhances substrate receptor exchange. b) Perturbations in the function of SCF components, or the regulatory proteins lead to diverse and severe phenotypes (Hobbie et al., 2000; Chuang et al., 2004; DiDonato et al., 2004; Parry et al., 2006; Dohmann et al., 2008).

This effect is strongly connected to the rate-limiting transfer of the first ubiquitin, which is known as the priming or initiation event (Baek et al., 2020). Besides directly enhancing the catalytic efficiency for Ub transfer, CUL1 neddylation (N8~CUL1) allows the recruitment of the RBR-type E3 ligase ARIADNE (ARIH1), which also facilitates substrate priming, but does not appear to be involved in Ub chain elongation (Scott et al., 2016).

Neddylation is a reversible process, and NEDD8 deconjugation is carried out by two types of proteases: ubiquitin c-terminal hydrolases (UCH) and DEN1/NEDP1/SENP8 (DENEDDYLASE1 (NEDD8-SPECIFIC PROTEASE1/SENTRIN-SPECIFIC PROTEASE8) proteins deconjugate NEDD8 from non-cullin substrates and NEDD8 precursors in order to maintain an intracellular available NEDD8 pool (Mergner and Schwechheimer, 2014; Mergner et al., 2015; Mergner et al., 2017). CONSTITUTIVE PHOTOMORPHOGENESIS 9 (COP9) SIGNALOSOME (CSN), on the other hand, deconjugates NEDD8 from neddylated cullins *via* its CSN5 subunit (Cope et al., 2002). Binding of CSN to SCF-type E3 Ub ligases mutually exclude substrate binding to the SCF complexes, and inhibits substrate ubiquitylation (Enchev et al., 2012). De-neddylation counteracts NEDD8 conjugation, and the CSN renders SCF-type E3 ligases inactive (Emberley et al., 2012; Enchev et al., 2012).

De-neddylation of cullins by CSN, allows also the binding of another SCF regulator, CULLIN-ASSOCIATED NEDD8-DISSOCIATED PROTEIN 1 (CAND1) (Liu et al., 2002; Enchev et al., 2012). CAND1 binding can only occur on non-neddylated cullins, as CAND1 wraps around cullin and occupies its NEDD8 conjugation site (Liu et al., 2002; Zheng et al., 2002; Goldenberg et al., 2004). CAND1-binding to cullins also appears to expel SR modules from SCFs hindering their ubiquitylation activity *in vitro* (Zheng et al., 2002), while promoting target ubiquitylation *in vivo* (Liu et al., 2018). This apparent paradox is explained by the fact that CAND1 functions as an SR exchange factor (Lo and Hannink, 2006; Zhang et al., 2008; Pierce et al., 2013; Straube et al., 2017). After SR release, CAND1 facilitates NEDD8 re-conjugation and the association with (other) SRs. In this manner, CAND1 expedites the switch from one active SCF complex to another, depending on substrate and SR availability (Liu et al., 2018). The interplay between SCFs, CSN, CAND1 and N8~CUL1 allows the rapid cycling through active SCFs in physiologically relevant timescales (**Figure 3a**) (Pierce et al., 2013; Liu et al., 2018). This dynamic E3 regulatory mechanism is essential in plant systems, as it allows the adaptive SR exchange required for timely and accurate adaptation

of functional protein pools in response to developmental and environmental cues (Chuang et al., 2004; Feng et al., 2004).

As genetic evidence, plants carrying mutations in SCF components, or SCF regulators, show severe and often pleiotropic phenotypes (**Figure 3b**). Homozygous *axr6/cul1* mutants, for instance, show severe defects during embryogenesis leading to growth arrest after germination (Hobbie et al., 2000). Impaired cullin neddylation in *axr1* (N8-activating enzyme E1) and *rce1* (N8-conjugating enzyme E2) mutants results in reduced growth, loss of apical dominance, and reduced responsiveness to the phytohormone auxin (Lincoln et al., 1990; Leyser et al., 1993; Dharmasiri et al., 2003). Loss of *CAND1* function (in *cand1-1* or *eta2-1*), results in delayed flowering and impaired fertility, while *csn* mutants exhibit growth arrest in seedling stage (Chuang et al., 2004; Dohmann et al., 2008).

1.1.6 Newly characterized CRL regulators GLMN/ALF4 likely control E2 binding to CRLs

GLOMULIN (GLMN) was first identified in humans, and homologues genes were found in other higher eukaryotes (mouse, rat, *Drosophila melanogaster, Danio rerio, Xenopus laevis, Tetraodon nigroviridis*) (Brouillard et al., 2002). Mutations in human GLMN were found to be the cause of the disease glomuvenous malformation, which affects patients carrying a second somatic mutation, and is evidenced as venous, purplish blue lesions in affected skin areas (Brouillard et al., 2002; Brouillard et al., 2013). At the molecular level and similar to CAND1, GLMN interacts with multiple cullins (CUL1, CUL3, CUL4A, CUL2), which assemble in CRLs containing RBX1, but not its closest homolog RBX2 (Tron et al., 2012). GLMN binding to cullins neither discriminate between their neddylation status, nor substrate receptor binding to the CRL (Duda et al., 2012; Tron et al., 2012). *In vitro* experiments have shown GLMN binding to CRLs inhibits substrate ubiquitylation on the one hand, and cullin neddylation on the other (Tron et al., 2012). Both is thought to happen through the same mechanism, as GLMN binds to RBX1, and masks the E2 binding site, consequently impeding E2s, *e.g.* UBC12 (N8 conjugating E2), from docking onto the CRL (Duda et al., 2012). Contrary to the *in vitro* experiments, a knock-out or knock-down of *GLMN* or reduction of GLMN protein levels results in stabilization of UPS substrates *in vivo* (Tron et al., 2012). Apparently, the absence of functional GLMN leads to the destabilization of SRs and cullins. Since the CRL

destabilization partially relies on proteasome activity, the loss GLMN in *glmn* mutants probably allows an uninhibited binding of active E2s to CRLs, and reduced de-neddylation. This evidently leads to autoubiquitylation and subsequent degradation of CRL components (Enchev et al., 2012; Tron et al., 2012).

GLMN is encoded as a single gene not only in animals, but across kingdoms including *Arabidopsis thaliana* (Brouillard et al., 2002). Based on sequence homology the ABERRANT LATERAL ROOT FORMATION4 (*ALF4*) gene encodes for the GLMN ortholog in *Arabidopsis thaliana*. *alf4* mutant plants have been isolated from a screen for defective auxin-induced lateral root (LR) formation, and *alf4-1* mutant plants grow bushy, without lateral roots (LRs), and exhibit male sterility (Celenza et al., 1995). Similar to *csn*, *cand1* and *axr1/ecr1* mutants, *alf4* mutant plants show partial auxin resistance, as auxin signaling relies on the correct and timely assembly of the $SCF^{TIR1/AFB1-5}$ complex (Celenza et al., 1995; DiDonato et al., 2004). This is an indication of a presumptive role of ALF4 during $SCF^{TIR1/AFBs}$-mediated auxin signaling. How auxin perception is integrated in $SCF^{TIR1/AFB1-5}$-dependent ubiquitylation and complex assembly is described in the following section.

1.2 A short nuclear cascade senses changes in auxin concentration

The natural phytohormone auxin (*e.g.* indole-3-acetic acid, IAA) shapes the entire plant body, as auxin coordinates cell division, differentiation and elongation, and participates in extensive crosstalk with other phytohormones (Mockaitis and Estelle, 2008; Lavy and Estelle, 2016; Leyser, 2018; Altmann et al., 2020). Natural auxins, such as IAA, or synthetic ones *e.g.* 2,4-dichlorophenoxyacetic acid (2,4-D) or α-naphthaleneacetic acid (α-NAA), trigger the interaction between the FBPs TIR1/AFB1-5 and the transcriptional repressor proteins AUX/IAAs (Zenser et al., 2001; Dharmasiri et al., 2005b).

TIR1/AFB-bound AUX/IAAs undergo polyubiquitylation, which triggers their rapid proteasomal degradation (Gray et al., 2001; Dreher et al., 2006; Maraschin et al., 2009). The auxin-driven and $SCF^{TIR1/AFB1-5}$-dependent degradation of AUX/IAAs relieves the transcription factors AUXIN REPONSE FACTORs (ARFs) from repression, enabling the transcription and expression of auxin-responsive genes (**Figure 4**) (Worley et al., 2000; Tiwari et al., 2001; Zenser et al., 2001; Tiwari et al., 2004).

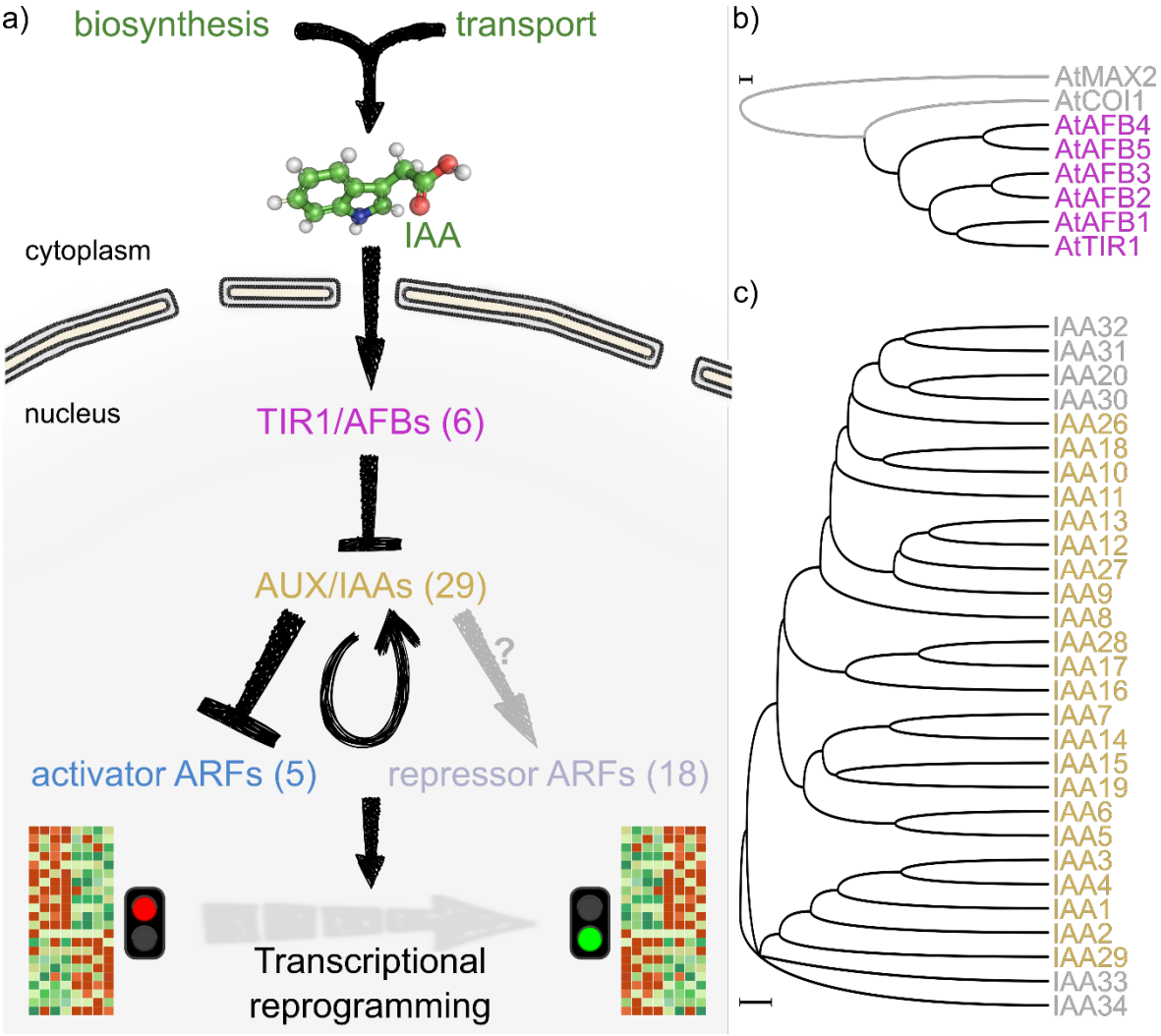

Figure 4: Auxin signal transduction relies on the UPS, and auxin is sensed and transduced *via* a short nuclear cascade consisting of multigene families. a) Upon transport to or synthesis at specific cells, IAA diffuses into the nucleus, where it is sense *via* a co-receptor system consisting of TIR1/AFBs (magenta) and AUX/IAAs (orange). Subsequently, ARF-repressing AUX/IAAs undergo ubiquitylation and degradation *via* the UPS and auxin-responsive genes are turned on by ARF activator-dependent transcription. **b)** The TIR1/AFB protein clade (magenta) consists of 3 closely-related gene pairs and show similarities to other plant FBPs that control diverse plant hormone signaling pathways (grey). **c)** 29 *At*AUX/IAA proteins occur as sister pairs. 23 AUX/IAAs carry a canonical degron (orange), 5 AUX/IAAs lack a degron (grey), and IAA31 contains a degenerated degron.

Therefore, in plants and specifically *Arabidopsis* transmission of the auxin signal, which is based on changing auxin concentration gradients across tissues, relies essentially on 3 protein families (**Figure 4 & 5**): The FBP TIR1 and its five homologs AUXIN SIGNALING F-BOX PROTEIN 1-5 (AFB1-5), 29 transcriptional repressors AUXIN/INDOLE-3-ACETIC ACID (AUX/IAA) proteins and 23 transcription factors named AUXIN RESPONSE FACTORs (ARFs), including five ARF activators and 18 ARF repressors (Leyser, 2018).

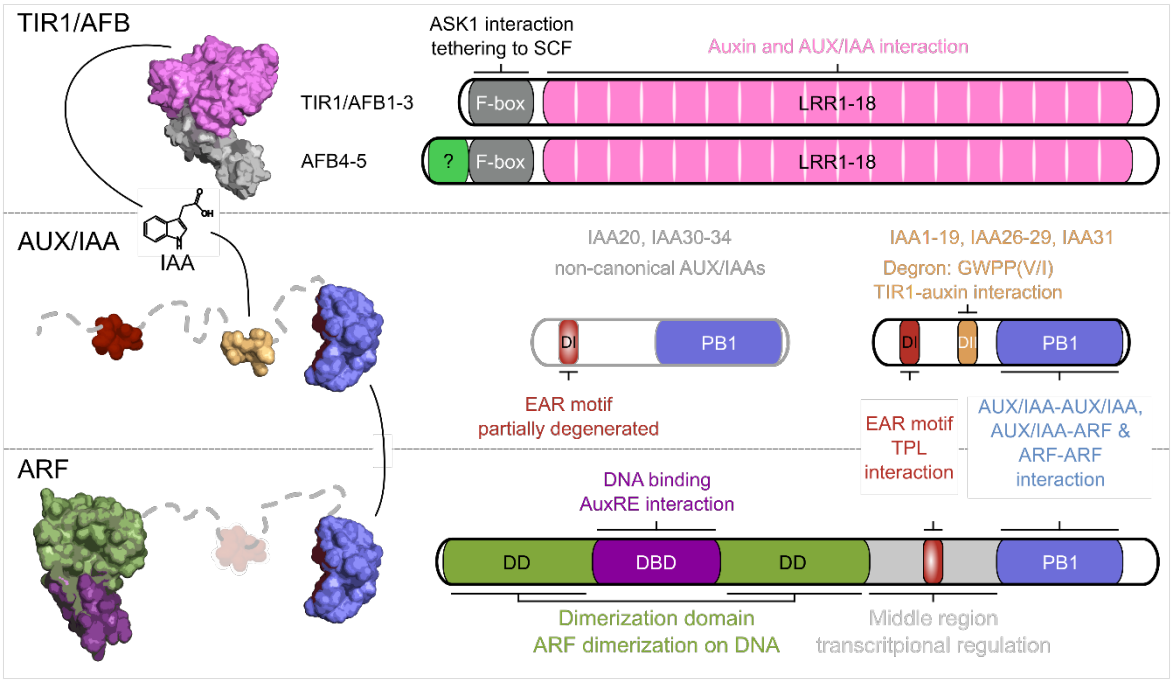

Figure 5: Domain structures of the three key protein families during auxin signal transduction. TIR1/AFBs (light pink) exhibit a solenoid fold and consists of an F-box domain for ASK1 (gray) interaction and a leucine-rich repeat (LRR) domain for target recognition. AFB4-5 carry an N-terminal extension (green) of unknown function. The TIR1/AFBs LRR domain interacts with the AUX/IAA core degron (DII, light orange) in an auxin-dependent manner. AUX/IAAs have flexible regions connecting the degron with the N-terminal DI (red) responsible for TPLinteraction and the C-terminal PB1 domain (blue). The PB1 domain is shared with the ARF transcription factors. ARFs comprise a combined DNA binding and dimerization domain (green and purple), and a connecting middle region (gray), that determines their function as either activators or repressors. Black lines between domains indicate their interaction.

Under low local auxin concentrations, AUX/IAAs are bound to (activator) ARFs through their shared Phox and Bem 1 (PB1) domain, which is located at the C-terminus of AUX/IAAs, and repress ARF activity (Liscum and Reed, 2002; Han et al., 2014; Piya et al., 2014; Tao and Estelle, 2018). This repression is facilitated by the recruitment of TOPLESS (TPL) co-repressors *via* the AUX/IAA's ETHYLENE RESPONSE FACTOR-ASSOCIATED AMPHIPHILIC REPRESSION (EAR) motif (Kagale and Rozwadowski, 2011; Ke et al., 2015; Martin-Arevalillo et al., 2017). In this manner, AUX/IAA·ARF interaction results in a downregulation of ARF-targeted auxin-responsive genes (Ulmasov et al., 1997; Maraschin et al., 2009).

Increasing nuclear auxin concentration leads to recognition of short-lived AUX/IAAs by the $SCF^{TIR1/AFBs}$ E3 ubiquitin ligase (Dharmasiri et al., 2005a; Kepinski and Leyser, 2005; Tan et al., 2007; Maraschin et al., 2009) (**Figure 4 & 5**). Recruitment of AUX/IAAs by TIR1/AFBs depends on a 13 amino acid short degron motif present in 23 of the 29 *At*AUX/IAAs (Details in chapter 1.4) (Gray et al., 2001). The degron is embedded in the variable N-terminal half the AUX/IAA proteins, which additionally harbors the KR motif, important for degradation, and the aforementioned TPL-

recruiting EAR motif (**Figure 5**) (Dreher et al., 2006). Stabilizing mutations due to a single amino acid exchange in the AUX/IAA degron, hinder AUX/IAA recruitment by the TIR1/AFB1-5 proteins, rendering plants insensitive to auxin (Worley et al., 2000; Ramos et al., 2001b). The resulting phenotypes vary depending on the affected AUX/IAAs, and include *e.g.* the lack of LRs in *solitary root* (*slr*) (IAA14) mutants, agravitropism and reduced shoot growth in *axr2-1* (IAA7) or the absence of a primary root in case of *bodenlos* (IAA12) or (Hamann et al., 1999; Nagpal et al., 2000; Fukaki et al., 2002). The range of mutant phenotypes shows diverse and partially specialized functions of the proteins in the AUX/IAA family. Non-canonical AUX/IAAs, which do not contain a degron are rather stable proteins (Dreher et al., 2006) (**Figure 4 & 5, gray**).

1.3 Auxin perception dissected – mechanistic insights into auxin-dependent TIR1·AUX/IAA interactions

While in 2005, TIR1 was identified as an auxin receptor (Dharmasiri et al., 2005a; Kepinski and Leyser, 2005), a few years later it was shown that TIR1 and related AFBs interact with AUX/IAAs in an auxin- and degron-dependent manner, and as a result control auxin signaling by forming an auxin co-receptor system (Dharmasiri et al., 2005b; Calderón Villalobos et al., 2012). Instead of acting as an allosteric ligand, auxin(s) occupies a deep pocket in TIR1 without changing its overall structure, as it was revealed from the ASK1·TIR1·auxin·IAA7 degron crystal structure (Tan et al., 2007) (**Figure 6)**. The TIR1 auxin binding pocket is built by 18 LRRs, and is decorated with residues directing selectivity for auxin(s) (Uzunova et al., 2016). The first and last LRRs of TIR1 contact each other resulting in a solenoid fold with the inositol hexakisphosphate (IP_6) co-factor at its base (Tan et al., 2007). IP_6 is fixed in place by multiple basic residues (K74, R113, R114, R484, K485, R509), likely acting as a LRR nucleation factor (Tan et al., 2007; Calderón Villalobos et al., 2012). When IAA is bound to TIR1, it is surrounded by mostly hydrophobic residues (F79, F82, F380), additionally forming a salt bridge and hydrogen bonds with its carboxyl group (**Figure 6**, dotted lines), which orients it in the TIR1 pocket (Tan et al., 2007). By occupying the pocket in TIR1, auxin creates a continuous hydrophobic interface *via* its indole ring, which allows high affinity binding of the AUX/IAA core degron (VGWPPV). Auxin contacts the degron *via* its tryptophan (W86) and

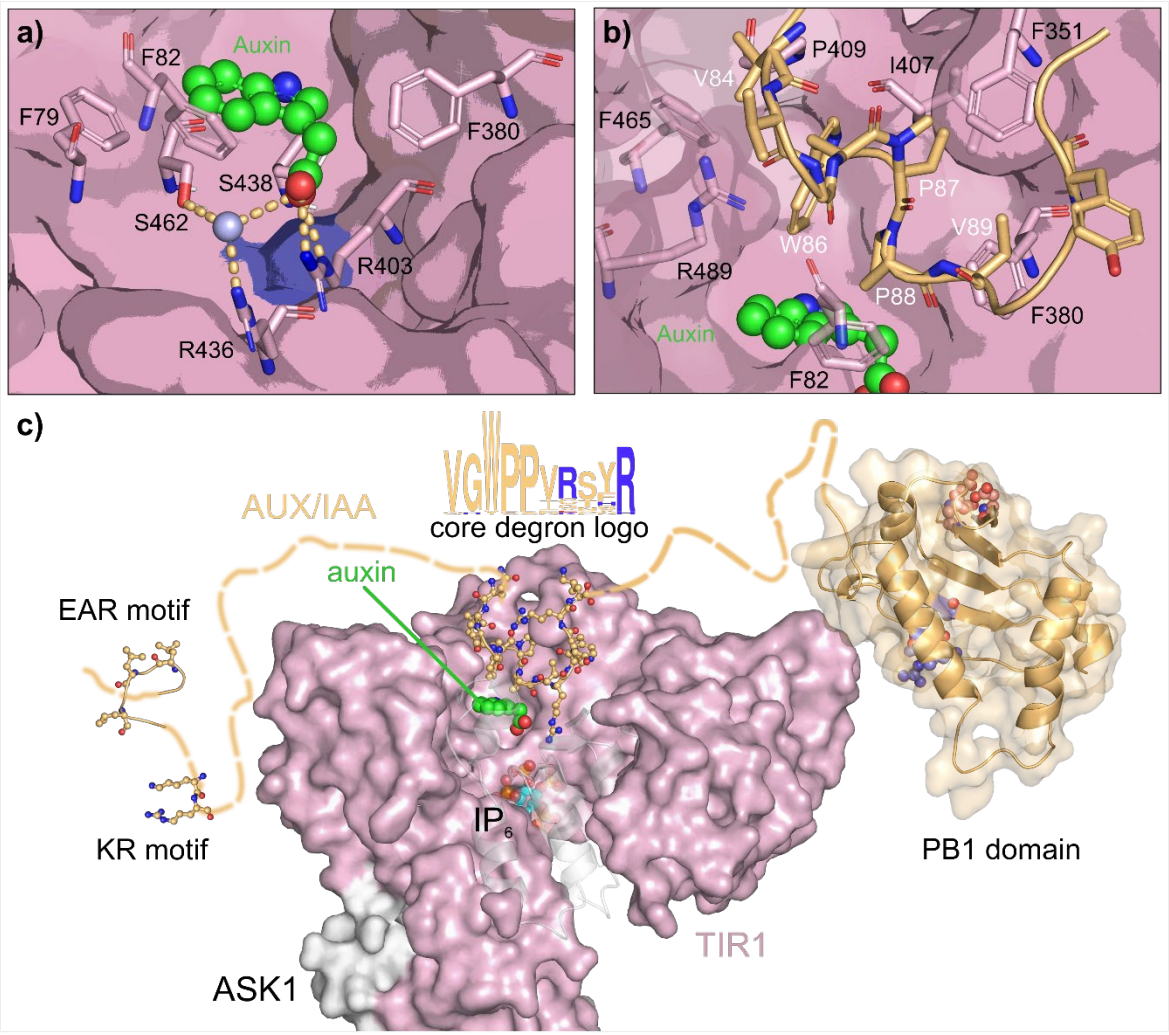

Figure 6: Auxin acts as a molecular glue enhancing TIR1 and AUX/IAA degron interactions. a) Auxin (IAA, green spheres) is located in a deep pocket in TIR1 (light pink) and surrounded by hydrophobic residues (F79, F82, F380). Its carboxylic group is orientated *via* H-bonding and salt bridges (dashed lines) pointing towards the IP_6 binding site by the action of two guanidino groups (R403 and R436). **b)** Auxin facilitates interactions with the AUX/IAA core degron residues (V84, W86, P87, P88) by expanding the hydrophobic interaction interface (F82, F351, F380, I407, P409, F465). **c)** IAA stabilizes the interaction between the ASK1·TIR1 dimer and AUX/IAAs (light orange, lower panel). Key auxin binding and AUX/IAA-interacting residues in TIR1 are shown as sticks (based on Tan et al. (2007), PDB: 2P1Q). The sequence logo of the core degron residues is shown on top of the structure (basic residues in blue). Degron residues are labeled in white, and TIR1 residues in black.

the second proline (P88), and the adjacent degron residues (V84 & P87) contact hydrophobic residues of TIR1 (Tan et al., 2007).

The auxin binding mode in which TIR1 and the AUX/IAA degron sandwich auxin explains elegantly the dramatic impact of single amino acid exchanges in the degron of AUX/IAAs. A number of non-auxin-responsive gain of function AUX/IAA mutants, including *iaa1/axr5-1, iaa3/shy2, iaa6/shy1, iaa7/axr2, iaa12/bdl, iaa14/slr, iaa16/iaa16-1, iaa17/axr3, iaa18/crane, iaa19/msg2, iaa28/iaa28-1* (Liscum and Reed, 2002; Yang et al., 2004; Rinaldi et al., 2012).

The concerted action of TIR1 and the AUX/IAA degron tightly bind auxin, and high auxin binding affinities are likely driven by the sequential association/dissociation of auxin and the AUX/IAA degron and *vice versa* (Hellmuth, 2017). Taking into account six different TIR1/AFBs with the potential of recruiting 23 degron-containing AUX/IAAs, a diverse auxin co-receptor system landscape is probable in *Arabidopsis thaliana* (**Figure 4**). The high conservation of the core AUX/IAA degron allowed originally to hypothesize that auxin binding capabilities of different receptors were similar among TIR1-AUX/IAAs receptor pairs (**Figure 6**). Instead, it turned out that the resulting auxin binding affinities of distinct auxin receptors are variable, and highly dependent on the specific AUX/IAA protein incorporated in the receptor complex (Calderón Villalobos et al., 2012). While TIR1 is the archetype and most studied FBP to date, the other AFBs, but AFB2, tend to contribute less prominently to auxin perception than TIR1 (Dharmasiri et al., 2005b; Calderon-Villalobos et al., 2010; Calderón Villalobos et al., 2012).

Although only a partial biochemical characterization of auxin coreceptors have been carried out as yet, TIR1/AFB1-5 interact directly to a major or lesser degree with degron-containing AUX/IAAs (Calderón Villalobos et al., 2012; Hellmuth, 2017). Intriguingly, some interaction specificities have been observed *in vitro*. For instance, IAA3 interacts with TIR1, AFB1 and AFB2, but not to AFB5, while IAA7 interacts with all 6 TIR1/AFBs (Dharmasiri et al., 2005b; Calderón Villalobos et al., 2012; Prigge et al., 2016). The FBP-derived specificity expands towards the small molecule binding, as, for example, the more distantly related AFB4 and AFB5 in complex with IAA7 exhibit stronger binding affinities for the synthetic auxin picloram than the auxin co-receptor complex TIR1·IAA7 (Calderón Villalobos et al., 2012; Prigge et al., 2016).

The range of binding affinities for different natural and synthetic auxinic compounds by TIR1/AFBs·AUX/IAA auxin co-receptor complexes ranges from physiologically relevant nanomolar to higher less-relevant micromolar concentrations. The specific affinities of co-receptors consisting of TIR1 and variable AUX/IAAs for the most abundant natural auxin, IAA, are rather in the physiological nanomolar range (Calderón Villalobos et al., 2012; Lee et al., 2014; Hellmuth, 2017). Biochemical studies on various TIR1·AUX/IAAs complexes prompted the conclusion that the core AUX/IAA degron, although essential, is only partially defining the variable auxin binding affinities of the auxin co-receptors. TIR1·IAA7 and TIR1·IAA12 show high (~17 nM) and low (~270 nM) auxin binding affinities (K_d), respectively. Changing the IAA12 core degron

(GWPPIG) to the degron in IAA7 (GWPPVR), increases the affinity only to ~72 nM, which is still ~4-fold lower than the affinity of a TIR1·IAA7 co-receptor (Calderón Villalobos et al., 2012). Thus, altering IAA14 residues adjacent to its core degron, tune auxin binding and subsequent IAA14 degradation (Guseman et al., 2015). Additionally, a KR motif located in the N-terminal region upstream of the degron in AUX/IAAs contributes to differential auxin binding and AUX/IAA degradation (Dreher et al., 2006; Calderón Villalobos et al., 2012; Moss et al., 2015). These observations indicate that residues outside the core degron, not directly contacting auxin in the pocket, modulate the differential binding capabilities of TIR1/AFBs·AUX/IAAs auxin co-receptors, potentially affecting AUX/IAA ubiquitylation (Calderón Villalobos et al., 2012; Moss et al., 2015; Hellmuth, 2017). Degron flanking regions that harbor the KR motif and are adjacent to a folded PB1 domain, represent around 50% of the AUX/IAA sequences. Whether the well-folded PB1 domain in AUX/IAAs contributes also to auxin receptor formation is not known. Opposing effects on auxin binding, and AUX/IAA degradation seen for PB1 truncations in IAA1 and IAA28, hint towards complex multifarious TIR1·AUX/IAA interaction mechanisms (Calderón Villalobos et al., 2012; Moss et al., 2015). Interestingly, regions flanking the degron exhibit the highest variability, regarding length and sequence composition, among AUX/IAA family members (see chapter 7.2, Suppl. Fig. 1). These regions have eluded structural as yet, due to apparent inherent conformational flexibility.

1.4 Auxin-triggered & $SCF^{TIR1/AFBs}$-dependent AUX/IAA ubiquitylation results in AUX/IAA turnover

As a result of auxin receptor assembly, $SCF^{TIR1/AFB1-5}$-bound AUX/IAAs are processed by the UPS in two consecutive steps initiated by $SCF^{TIR1/AFB1-5}$ E3 ligase activity. Ubiquitylated AUX/IAAs are captured by the 26S proteasome leading to their rapid degradation (Maraschin et al., 2009). Auxin-triggered AUX/IAA degradation set to be a singular feature of the AUX/IAA protein family early on (Ramos et al., 2001b; Tian et al., 2003). High instability due to their degrons and half-lives between 5-60 minutes, as well as steady state levels mostly below LC-MS detection limits *in planta*, made AUX/IAAs difficult to study (Worley et al., 2000; Ramos et al., 2001a; Dreher et al., 2006; Mergner et al., 2020). Therefore, multiple synthetic approaches utilizing heterologous systems have

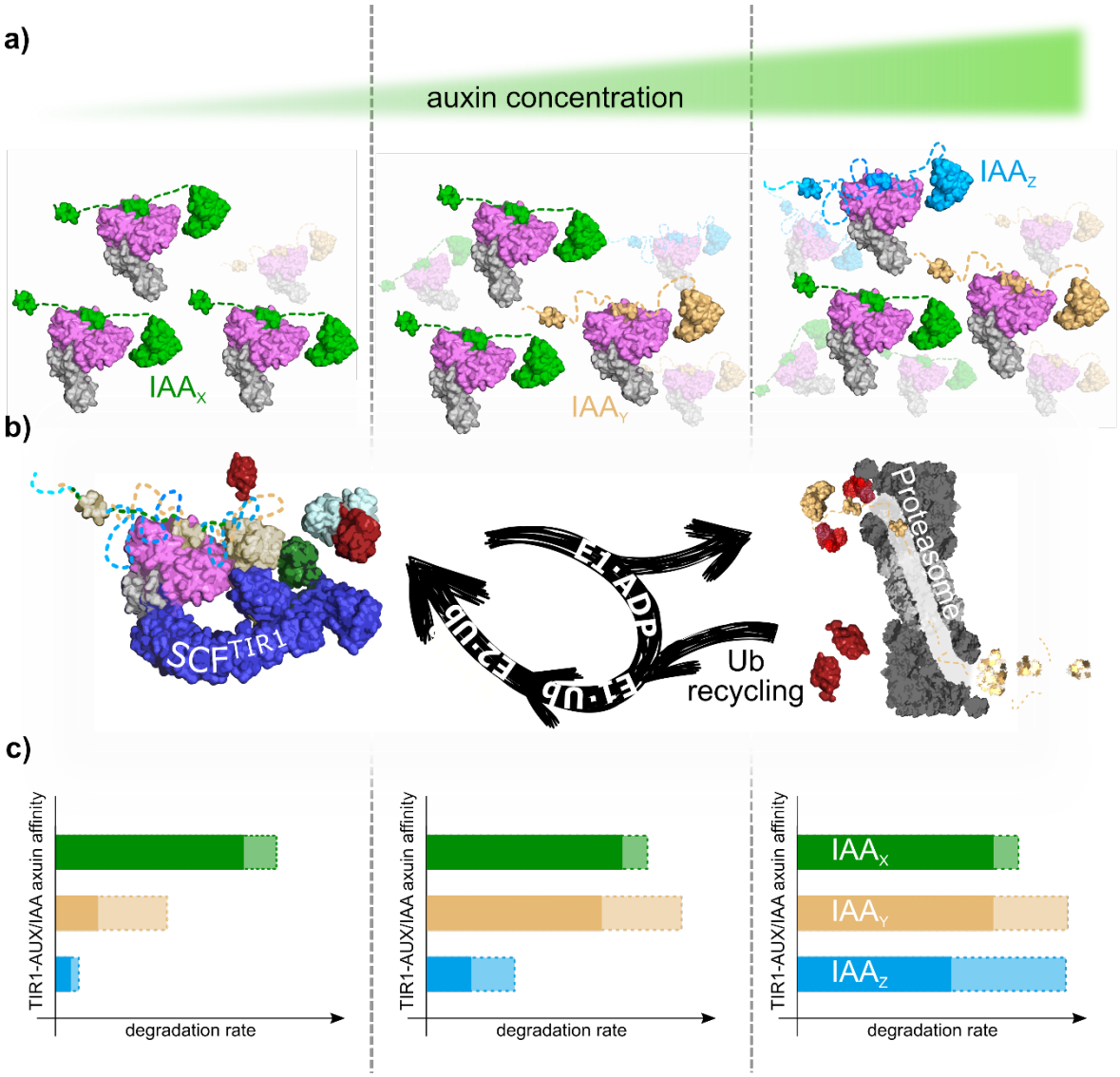

Figure 7: Efficient degradation of UPS targets, such as AUX/IAAs, rely on triggered interaction with E3s and intrinsic features in their sequences. a) AUX/IAAs greatly contribute to the auxin binding affinities of TIR1/AFB·AUX/IAA auxin co-receptor systems. **b)** The UPS ensures AUX/IAA destruction thanks to the presence of degrons and other sequence features *e.g.* flexibility of degradation initiation sites, and the type of Ub chains on the substrate. **c)** At low auxin concentrations, mainly AUX/IAAs incorporated in high-affinity receptors (green) are efficiently degraded, while at medium and high auxin concentrations, additional structural and ubiquitylation-related features, might become increasingly important for AUX/IAA turnover. This possibly results in the preferred or similar degradation of medium (orange) and low (blue) affinity receptor forming AUX/IAAs, and uncouples auxin binding from AUX/IAA turnover.

been developed over the years to trace auxin signaling output and AUX/IAA degradation (Havens et al., 2012; Wend et al., 2013; Shimizu-Mitao and Kakimoto, 2014; Moss et al., 2015). The derived degradation rates and half-lives substantiate the influence of AUX/IAAs on their auxin-triggered ubiquitylation and degradation. Those experiments further indicated the combinatorial potential of six TIR1/AFBs and 29 AUX/IAAs leading to a range of responsiveness in the system based in the AUX/IAA degradation dynamics (Calderón Villalobos et al., 2012; Havens et al., 2012; Shimizu-Mitao and Kakimoto, 2014). Additionally, some TIR1/AFB·AUX/IAA combinations show

specificity for certain auxins such as 4-Cl-IAA and PAA (Shimizu-Mitao and Kakimoto, 2014). Differences between AUX/IAA degradation rates at a fixed (high) IAA concentration and the auxin-responsiveness of AUX/IAA degradation hint towards a less studied mechanism, that causes the discrepancy between auxin co-receptor binding capabilities, auxin responsiveness and AUX/IAA degradation rates (Dreher et al., 2006; Calderón Villalobos et al., 2012; Havens et al., 2012; Lee et al., 2014; Shimizu-Mitao and Kakimoto, 2014; Guseman et al., 2015; Moss et al., 2015) (**Figure** 7). The UPS connects initial auxin binding and proteasome-dependent AUX/IAA degradation through AUX/IAA ubiquitylation. Each event is highly regulated (see previous chapters), and could explain how similar binding or responsiveness lead to differential degradation (Chapman and Estelle, 2009; Santner and Estelle, 2010; Kelley and Estelle, 2012; Lavy and Estelle, 2016; Leyser, 2018) (**Figure** 7).

Despite the relevance of the ubiquitylation event, we lack information about the specificity and mechanistic of ubiquitylation *in planta*, *e.g.* the SCF regulatory cycle, and Ub chain types on a given substrate under specific conditions. Thus, the dynamics of AUX/IAA ubiquitylation, and its dependency on auxin levels, leading to AUX/IAA degradation, remains to be study (Gray et al., 2001; Ramos et al., 2001b; Tian et al., 2003; Maraschin et al., 2009; Gilkerson et al., 2015; Jing et al., 2015).

Application of MG132, a proteasome inhibiting peptide, on plants or protoplasts stabilizes tagged versions of IAA1, IAA2, IAA3, IAA7, IAA12, MdIAA12, IAA17 and OsIAA26, which is considered a general feature for degron-containing AUX/IAAs (Gray et al., 2001; Ramos et al., 2001a; Tian et al., 2003; Maraschin et al., 2009; Hellmuth, 2017; Chen et al., 2018; Wang et al., 2018). Similarly, it is considered that AUX/IAA degradation is ubiquitylation-dependent even though direct evidence for AUX/IAA ubiquitylation is reported only for IAA1, IAA3, IAA12 and OsIAA26 (Maraschin et al., 2009; Gilkerson et al., 2015; Chen et al., 2018). In protoplasts, IAA3 and IAA12 ubiquitylation is auxin-dependent, and limited by the levels of functional TIR1 (Maraschin et al., 2009).

In plants, low AUX/IAA abundance, and a high AUX/IAA turnover rate seem to be absolutely crucial as even the mutation of all 16 lysines in IAA1, acting as Ub acceptor sites, does not fully abrogate ubiquitylation and subsequent degradation (Gilkerson et al., 2015). Instead, the non-canonical serine, threonine and tyrosine residues act as ubiquitylation sites, forming oxyester linkages between Ub and IAA1 (Gilkerson et al., 2015). The reduction (11/16 Lys) or complete unavailability of lysines impaired IAA1 degradation only moderately. This reduced degradation

could be a direct result of the lower ubiquitylation level or the instability of the oxyester linkage resulting in continuous disassembly. The different distribution of the non-canonical acceptor sites along the sequence could further impair degradation.

SCF-type E3 ligases are quite flexible, and can handle slightly shifted target residues during ubiquitin transfer while the substrate is still bound. Optimal proteasomal degradation on the other hand, requires Ub chains to be positioned precisely (Duda et al., 2008; Inobe et al., 2011; Baek et al., 2020). Which exact AUX/IAA residues are ubiquitylated is still unknown. The degradation efficiency of proteasome substrates is determined at large, by the spacing between ubiquitylation sites, and an unstructured initiation region, which further affects degradation depending on the sequence composition (**Figure 7**) (Fishbain et al., 2015; Guharoy et al., 2016). The unresolved N-terminal half of the AUX/IAAs potentially serves as this initiation site depending on its structural character. In addition to the correct spacing between initiation site and Ub site, the ubiquitin chain type attached, specifies whether AUX/IAAs are degraded efficiently, and both remains to be studied so far. The type of ubiquitylation defines binding to the Ub receptors in the 19S cap of the proteasome and its unfolding ability (Reichard et al., 2016; Martinez-Fonts et al., 2020).

The main predicted outcome of auxin-triggered AUX/IAA ubiquitylation is degradation, but more subtle effects, such as altered recruitment by *e.g.* SCF^{TIR1}, or changes in AUX/IAA interaction profiles, might also be relevant outcomes of AUX/IAA ubiquitylation. Which complexes are remodelled upon AUX/IAA ubiquitylation, and how different interactions might be involved is described in the next section.

1.5 AUX/IAA ubiquitylation enables ARF-dependent gene activation

Besides TIR1/AFBs·AUX/IAA associations, the AUX/IAAs participate in repressor complexes by directly engaging in heteromeric interactions with ARF transcription factors (Han et al., 2014; Piya et al., 2014). ARFs bind to auxin response elements (AuxREs) in the promoter region of auxin-responsive genes *via* their B3-type DNA-binding domain (DBD) (Guilfoyle et al., 1998) (**Figure 5 & 8**). ARFs act either as transcriptional activators (class A) or repressors (class B and C) depending on their middle region (MR), and activator and repressor ARFs can compete for the same promoters (Lavy et al., 2016; Weijers and Wagner, 2016; Kato et al., 2020). Under low auxin concentrations,

auxin-independent PB1 domain-driven interactions dominate AUX/IAA PPIs. AUX/IAAs and ARFs share the PB1 domain, and establish the core of a transcriptional repressor complex *via* PB1·PB1 heteromers. Structural studies have shown that PB1·PB1 multimerization depends on two distinct charged patches on opposite faces of each PB1 domain (Korasick et al., 2014; Nanao et al., 2014; Dinesh et al., 2015; Kim et al., 2020) (**Figure 6 & 8**). These mostly ionic interactions between PB1·PB1 dimers span medium nanomolar and low micromolar affinities (in K_D values) (Han et al., 2014). Assembly of heteromeric AUX/IAA·ARF complexes seem to be more favorable than AUX/IAA·AUX/IAA and ARF·ARF homomeric complexes, as reflected by higher dimerization affinities of heteromeric complexes formed by *e.g.* PB1 domains of IAA7 and ARF5 (Han et al., 2014; Kim et al., 2020).

ARF-bound AUX/IAAs likely form high order multimers with enhanced transcriptional repression activity due to the recruitment of TPL, and probably several AUX/IAA subunits contacting additional ARFs (Korasick et al., 2014; Dinesh et al., 2016). TPL and its homologs TOPLESS-RELATED (TPR1-4) homo-tetramerize *via* their N-terminal TPL domain (TPD) (Ke et al., 2015; Martin-Arevalillo et al., 2017) (**Figure 8**). TPL/TPR multimers allow high avidity-driven complexes to form with multiple AUX/IAAs, and ensure tight transcriptional repression, which can be further enhanced by direct ARF·TPL interactions and histone deacetylases (HDAs) (Korasick et al., 2014; Liu et al., 2014; Ma et al., 2017; Kato et al., 2020). The resulting DNA-bound complex consists of (multiple) ARFs, TPL tetramers and at its core AUX/IAA oligomers nucleating the formation of the repressor complex (Ke et al., 2015; Dinesh et al., 2016; Martin-Arevalillo et al., 2017).

Rising nuclear auxin concentrations result in the disassembly of such a repressor complex, through AUX/IAA ubiquitylation and degradation, which favor auxin-dependent gene expression (Maraschin et al., 2009; Weijers and Wagner, 2016). Subsequently derepressed ARFs can recruit BRAHMA/SPLAYED (BRM/SYD) chromatin remodeling complexes (Wu et al., 2015). The loosened chromatin is now accessible for additional TFs, and transcription inducing factors (*e.g.* histone acetyl transferases) enabling activation of auxin responsive genes (**Figure 6**). Specific AUX/IAA·ARF complex compositions, ARF and AUX/IAA expression domains and protein levels, and auxin binding affinities of respective TIR1/AFB·AUX/IAA complexes allow fine-tuned specified responses (Hamann et al., 2002; Vernoux et al., 2011; Calderón Villalobos et al., 2012; Piya et al., 2014; Farcot et al., 2015; Weijers and Wagner, 2016; Kato et al., 2020).

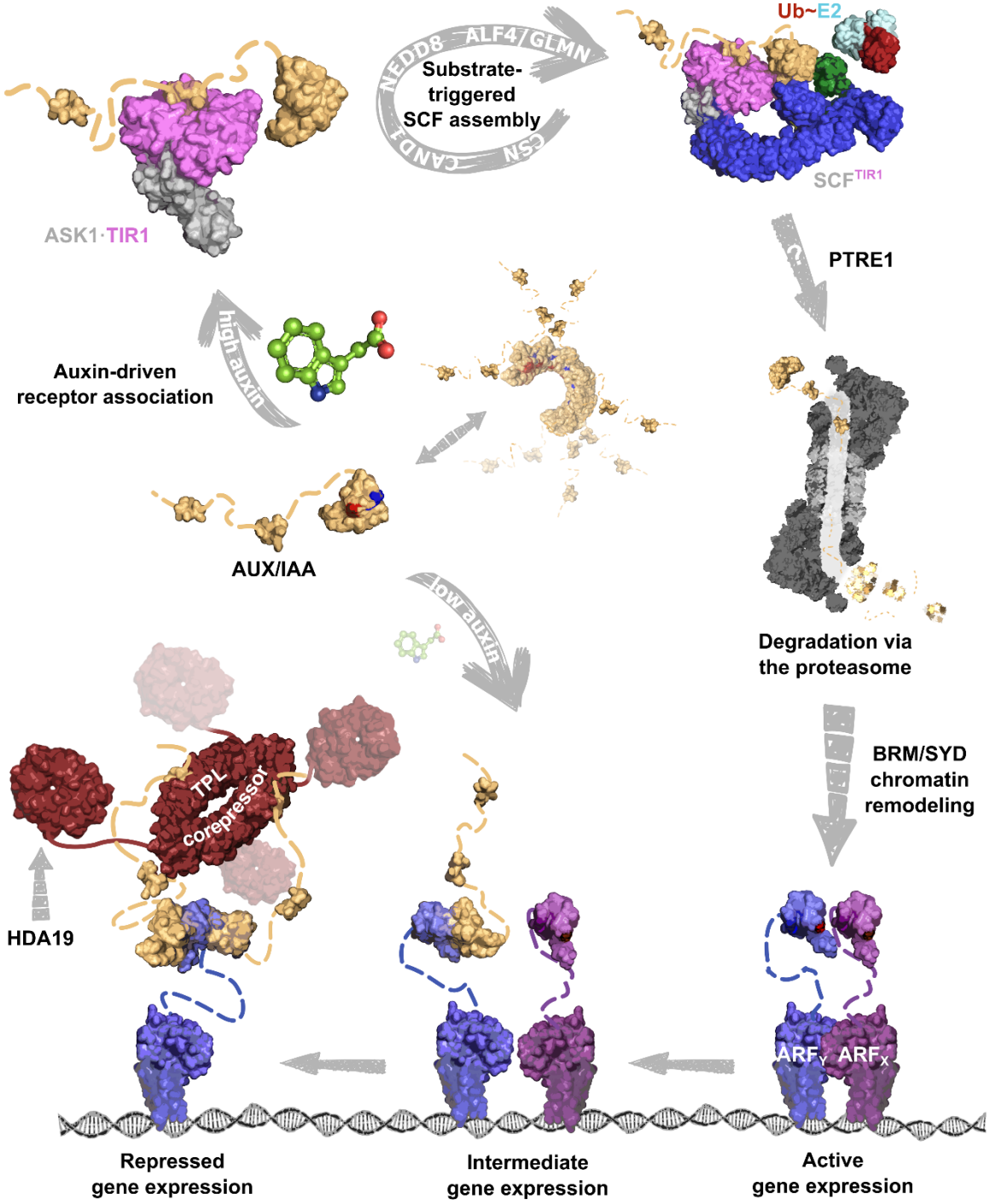

Figure 8: Auxin shifts the composition of AUX/IAA-containing complexes. Various multimeric complexes, involving AUX/IAAs, which assemble and collapse depending on cellular auxin (green) levels. AUX/IAAs (light orange) either nucleate repressor complexes for ARF inhibition when auxin is low, or AUX/IAAs are recruited by $SCF^{TIR1/AFBs}$ E3 ubiquitin ligases (gray, lightpink, blue, green) in response to auxin. This leads to AUX/IAA ubiquitylation (red), and degradation by the proteasome (gray). Proteolysis of AUX/IAAs is being further regulated by PROTEASOME REGULATOR 1 (PTRE1) in an auxin-dependent manner (Yang et al., 2016). AUX/IAAs can also form oligomeric structures of high molecular weight, which possibly include ARFs (purple, lilac). Transcriptional activation is further enhanced by BRM/SYD complexes, while repression is facilitated by TPL corepressors (dark red), and histone deacetylases *e.g.* HDA19.

Transcriptional activation of auxin-responsive genes requires AUX/IAAs to be dislodged from the repressor complex. Whether and how the auxin-driven recruitment of AUX/IAAs by TIR1/AFBs, $SCF^{TIR1/AFBs}$-driven AUX/IAA ubiquitylation, binding by Ub receptors, or their ultimate degradation at the proteasome initiate destabilization of repressor complexes, is currently unknown. While the PB1 domain is probably deeply embedded in such a complex, the core degron is connected *via* a flexible linker (degron tail) and is likely available to initiate repressor complex disassembly (**Figure 8**). Thereby, it is presumed, but not shown so far, that the recruitment of the core AUX/IAA degron to TIR1/AFBs in response to auxin drives a transcriptional switch from a repressive to an activated state.

It will be intriguing to investigate how TIR1·AUX/IAA complex formation and AUX/IAA ubiquitylation is modulated structurally. Thus, details on the mechanistic of AUX/IAA ubiquitylation remain unknown at large. Understanding the molecular mechanisms involved in AUX/IAA ubiquitylation, and the structural prerequisites for precise ubiquitin chain assembly will present a tremendous advancement for the auxin and the UPS fields (**Figure 9**).

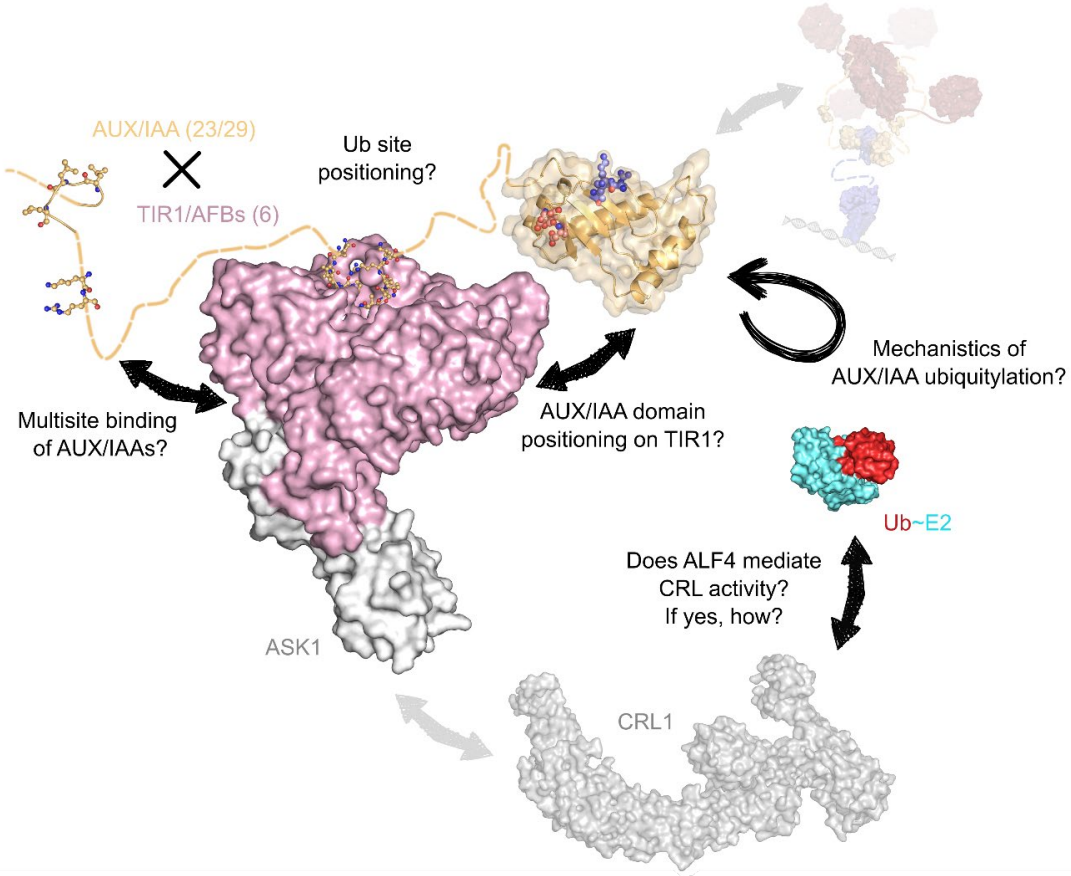

Figure 9: Many open questions remain regarding the structural and mechanistic basis of AUX/IAA ubiquitylation. The combinatorial aspects of auxin-mediated TIR1·AUX/IAA interactions draw attention to structural determinants in AUX/IAAs that can alter or modulate their recognition, and ubiqutiylation.

1.6 Questions addressed in this thesis

Ubiquitylation of AUX/IAAs occurs based on their auxin-dependent recruitment to the $SCF^{TIR1/AFB1-5}$ E3 Ub ligases (Gray et al., 2001; Zenser et al., 2001). The complex formed by $SCF^{TIR1/AFBs}$ and an AUX/IAA target, at same time, constitutes an auxin co-receptor system (Dharmasiri et al., 2005b; Dharmasiri et al., 2005a; Kepinski and Leyser, 2005; Calderón Villalobos et al., 2012). Thus, auxin co-receptor formation, its auxin sensing capabilities, and auxin-prompted AUX/IAA ubiquitylation are directly intertwined. While auxin-triggered recruitment of AUX/IAAs to TIR1 depends on their short degron, highly variable regions outside of the degron modulate the auxin binding capabilities of the corresponding co-receptor (Tan et al., 2007; Calderón Villalobos et al., 2012). How regions outside the AUX/IAA degron (upstream: DI and linker; downstream: degron tail and PB1 domain), exert a modulatory function for auxin perception remain to be established. Thus, we lack information of how AUX/IAA configuration(s) and architecture might affect TIR1/AFB1-5 interactions, and subsequent ubiquitin transfer. Initial approximations to understand AUX/IAA ubiquitylation, have left open questions regarding the pacing at which AUX/IAAs become modified by ubiquitin, as well as the specific drivers for lysine recognition and ubiquitin chain elongation (Maraschin et al., 2009; Gilkerson et al., 2015) (**Figure 9**). Therefore, mechanistic and structural studies pursuing TIR1/AFB·AUX/IAA auxin co-receptor formation, where full length AUX/IAAs (and not only their degron) are resolved, will shed light on AUX/IAA processing. Importantly, we have little knowledge of the structural requirements for correct positioning of substrates on SCF-type E3 ligases for efficient ubiquitin transfer. to understand how auxin-mediated remodeling of protein pools occurs. Exploring the contribution of flexible degron flanking regions in AUX/IAAs to auxin sensing has the potential to illuminate non-covalent small molecule-driven substrate recruitment by the UPS, in general.

In addition, SCF-dependent ubiquitylation of proteins is a highly regulated process involving multiple proteins and protein complexes that guide assembly of SCF subunits and SCF activation (Enchev et al., 2012; Liu et al., 2018). SCF regulators are shared among plants and animals, and impairing their function results in auxin-related growth phenotypes in plants. The role of ALF4, the plant ortholog of *Hs*GLMN, during SCF regulation has yet to be established. ALF4 might modulate the ubiquitylation of substrates, such as the AUX/IAAs, DELLAs, JAZs and other transcriptional repressors in hormone signaling pathways, as well as, other cullin-RING ligase (CRL) targets.

Molecular and biochemical studies towards understanding ALF4 action, can further shed light on phytohormone-driven ubiquitylation of proteins.

My doctoral studies sought to address the following specific questions from a biochemical perspective based on structure-function relationships:

- How do the unresolved AUX/IAA regions outside of the degron influence auxin receptor formation, and AUX/IAA ubiquitylation?
- How is AUX/IAA ubiquitylation paced and mechanistically regulated?
- Could comparative structure-function relationships of AUX/IAAs have the potential to explain the expansion of the AUX/IAA protein family in land plants, and their specific contributions to auxin sensing?
- What is the mechanistic basis of ALF4 action?
- Does ALF4 regulate CRLs activity by an E2 selection mechanism?

For transparency, I implemented extensive biochemical and structural approaches including crosslinking-coupled mass spectrometry, yeast-two-hybrid, immunoprecipitation, pull-down and radioligand binding assays in order to address auxin co-receptor formation, as well as in silico protein analysis, circular dichroism spectroscopy, and size exclusion chromatography for studying AUX/IAA folds. I also, extensively optimized a cell-free system for studying protein ubiquitylation dynamics and detection of ubiquitylation sites.

The findings of my doctoral studies have been peer-reviewed and published, and the three resulting manuscripts are the backbone of this cumulative thesis.

2 Publications and Results

The following section comprises my published work including three manuscripts in peer-reviewed scientific journals: **Two (2) in Nature Communications (2017 and 2020), and one (1) in EMBO Journal (2018)**.

My investigations on the ubiquitylation of two AUX/IAAs (IAA6 and IAA19) have been instrumental in the evolution of **Winkler *et al.*, Nat Commun 2017**. The identified ubiquitylation sites agglomerate in fast-diverging, potentially flexible regions adjacent to the core degron in AUX/IAAs, which has been shown to be crucial for differences in auxin binding capabilities of auxin co-receptors. How the nature of those flanking regions in AUX/IAAs impact, not only on auxin binding properties of co-receptors, but especially AUX/IAA ubiquitylation have been the focus of my doctoral studies and resulted in the core findings of **Niemeyer *et al.*, Nat Commun 2020**. Further biochemical investigations on ALF4, a postulated regulator of SCF^{TIR1}-dependent AUX/IAA ubiquitylation resulted in the collaborative work **Bagchi *et al.*, EMBO J 2018**.

2.1 Winkler M. *et al.* Variation in auxin sensing guides AUX/IAA transcriptional repressor ubiquitylation and destruction

Winkler M, **Niemeyer M**, Hellmuth A, Janitza P, Christ G, Samodelov S, Wilde V, Majovsky P, Trujillo M, Zurbriggen M, Hoehenwarter W, Quint M, Calderón Villalobos LIA (2017). Variation in auxin sensing guides AUX/IAA transcriptional repressor ubiquitylation and destruction ***Nat Commun*** Jun 7;8:15706; doi: 10.1038/ncomms15706.

2.1.1 Aims and summary of the results

In this publication we sought to understand why closely related *Arabidopsis thaliana* AUX/IAA ohnologs, IAA6 and IAA19, were retained during evolution after gene duplication events. The auxin co-receptor system is formed by one of 23 auxin-sensitive AUX/IAAs, and any of 6 F-box proteins TIR1/AFB1-5. Different auxin binding capabilities depend primarily on the AUX/IAA incorporated in the receptor complex. In AUX/IAAs, regions outside the auxin-contacting degron seem to play an important role in modulating auxin sensitivity. We investigated, how these regions in IAA6 and IAA19 directly contribute to auxin binding, as well as the dynamics of IAA6 and IAA19 ubiquitylation and degradation. We found that despite of the high sequence similarity between IAA6 and IAA19, they interact differently with TIR1, AFB1 and AFB2. We showed that IAA6 is more selective towards AFB1, while IAA19 interacts stronger with all TIR1/AFBs tested, which is also reflected by a higher affinity for auxin in complex with ASK1·TIR1. In order to reveal the connections between auxin binding and AUX/IAA ubiquitylation, we reconstituted IAA6 and IAA19 ubiquitylation *in vitro*. We showed that auxin binding by TIR1·IAA6 and TIR1·IAA19 auxin co-receptors, and SCF^{TIR1}-dependent IAA6 and IAA19 ubiquitylation are directly coupled. We further identified ubiquitylation sites in regions of high sequence divergence in IAA6 and IAA19. While we traced distinct lysines in IAA6 and IAA19 targeted for ubiquitylation *in vitro*, the ubiquitin chain types we identified are comparable, validating the role of E2s mediating ubiquitin chain extension. Ubiquitylation site analysis on IAA6 and IAA19 revealed that most of the ubiquitylation occurs in structurally unresolved regions, which are highly variable segments between known AUX/IAA motifs and domains. Further, AUX/IAA interaction strength with TIR1/AFB1-2, auxin binding and ubiquitylation correlate with IAA6 and IAA19 stability of *in vivo*.

2.1.2 Contributions

Own contributions:

In Winkler *et al.*, I was involved in the characterization of IAA6 and IAA19 ubiquitylation. I developed a biochemical cell-free assay (*in vitro* ubiquitylation, IVU) to trace the dynamics of auxin- and SCF^{TIR1}-dependent ubiquitylation of IAA6 and IAA19. I further adapted the IVU assay to identify ubiquitylation sites on AUX/IAAs, and ubiquitin chain types *via* LC-MS/MS. Our IVU approach is pioneering as, to our knowledge, this was the first time that all single subunits of a plant-derived multimeric SCF-type E3 ligase were recombinantly expressed with high purity, and full reconstitutionof an E1-E2-E3 cascade *in vitro* enabled highly specific recapitulation of substrate ubiquitylation.

Estimated percentage-based author (M. Niemeyer) contribution to experimental work:

Protein expression and purification of IVU-related proteins (50%), *in vitro* ubiquitylation assays (IVU) (70%), LC/MS/MS sample preparation for ubiquitylation site detection (70%). Data analysis: IVU data (80%), ubiquitylation site LC/MS/MS (70%), ubiquitin chain analysis (100%)

Estimated percentage-based author (M. Niemeyer) contribution to written manuscript:

Writing (10%), design, preparation of 3 main figures, 4 supplementary figures, and 1 table (40%).

Other contributions:

30% supervision of a master student (Gideon Christ), involved fulltime in this study

See "Author Contributions" section at the end of the manuscript for detailed description of input and experimental support from our scientific collaborators in this study.

2.1.3 Original publication

See next page. Supplementary Material in Chapter 7.1.

nature COMMUNICATIONS

ARTICLE

Received 9 Oct 2015 | Accepted 21 Apr 2017 | Published 7 Jun 2017

DOI: 10.1038/ncomms15706 OPEN

Variation in auxin sensing guides AUX/IAA transcriptional repressor ubiquitylation and destruction

Martin Winkler[1,†], Michael Niemeyer[1], Antje Hellmuth[1], Philipp Janitza[2], Gideon Christ[1], Sophia L. Samodelov[3,6], Verona Wilde[1], Petra Majovsky[4], Marco Trujillo[5], Matias D. Zurbriggen[3,7], Wolfgang Hoehenwarter[4], Marcel Quint[2] & Luz Irina A. Calderón Villalobos[1]

Auxin is a small molecule morphogen that bridges $SCF^{TIR1/AFB}$-AUX/IAA co-receptor interactions leading to ubiquitylation and proteasome-dependent degradation of AUX/IAA transcriptional repressors. Here, we systematically dissect auxin sensing by SCF^{TIR1}-IAA6 and SCF^{TIR1}-IAA19 co-receptor complexes, and assess IAA6/IAA19 ubiquitylation *in vitro* and IAA6/IAA19 degradation *in vivo*. We show that TIR1-IAA19 and TIR1-IAA6 have distinct auxin affinities that correlate with ubiquitylation and turnover dynamics of the AUX/IAA. We establish a system to track AUX/IAA ubiquitylation in IAA6 and IAA19 *in vitro* and show that it occurs in flexible hotspots in degron-flanking regions adorned with specific Lys residues. We propose that this signature is exploited during auxin-mediated SCF^{TIR1}-AUX/IAA interactions. We present evidence for an evolving AUX/IAA repertoire, typified by the IAA6/IAA19 ohnologues, that discriminates the range of auxin concentrations found in plants. We postulate that the intrinsic flexibility of AUX/IAAs might bias their ubiquitylation and destruction kinetics enabling specific auxin responses.

[1] Department of Molecular Signal Processing, Leibniz Institute of Plant Biochemistry (IPB), Halle (Saale) D-06120, Germany. [2] Institute of Agricultural and Nutritional Sciences, Martin Luther University Halle-Wittenberg, Halle (Saale) D-06120, Germany. [3] Institute of Synthetic Biology, University of Düsseldorf, Düsseldorf D-40225, Germany. [4] Proteome Analytics Research Group, Leibniz Institute of Plant Biochemistry (IPB), Halle (Saale) D-06120, Germany. [5] Independent Junior Research Group Ubiquitination in Immunity, Leibniz Institute of Plant Biochemistry (IPB), Halle (Saale) D-06120, Germany. [6] Spemann Graduate School of Biology and Medicine (SGBM), University of Freiburg, Freiburg D-79104, Germany. [7] Cluster of Excellence on Plant Science (CEPLAS), University of Düsseldorf, Düsseldorf D-40225, Germany. † Present address: Institute of Biochemistry, ETH Zurich, Zurich 8093, Switzerland. Correspondence and requests for materials should be addressed to L.I.A.C.V. (email: LuzIrina.Calderon@ipb-halle.de).

Ubiquitin-dependent dynamic turnover of transcriptional regulators via E3 ligases in response to phytohormones is pivotal for growth and development[1–5]. Auxin or indole-3-acetic acid (IAA) is one of the major plant regulators, and triggers extensive transcriptional reprogramming through a very short nuclear cascade[6]. Auxin drives nuclear events by modulating the recruitment of mostly short-lived AUXIN/INDOLE-3-ACETIC ACID (AUX/IAA) transcriptional repressors by multimeric SKP1/CUL1/F-Box (SCF)-type E3 ubiquitin ligases. $SCF^{TIR1/AFBs}$ E3s control auxin-triggered molecular networks by acting at the site of auxin sensing. In a tight and regulated manner and bypassing an autocatalytic mechanism, TRANSPORT INHIBITOR RESPONSE 1 (TIR1)/AUXIN SIGNALLING F-BOX (AFB1-5) proteins assemble in an $SCF^{TIR1/AFBs}$ complex and recruit the core degron of multifunctional AUX/IAA proteins in response to fluctuations in intracellular auxin levels[7–10]. By increasing the hydrophobic interactions between TIR1/AFBs and their AUX/IAA targets, auxin behaves as a molecular glue which is hereby sensed by this co-receptor system. Given the expansion of *TIR1/AFBs* and *AUX/IAA* genes in *Arabidopsis*, with six and 29 members, respectively, a broad range of auxin concentrations is likely differentially sensed via combinatorial assembly of $SCF^{TIR1/AFB}$-AUX/IAA co-receptor complexes[11]. Through heterodimerization of their C-terminal PB1 domains[12–15], AUX/IAAs interact with DNA-binding proteins of the auxin response factor (ARF) family, which specifically occupy auxin-responsive elements (AuxREs) in numerous auxin-regulated genes[16]. The primary structures of most AUX/IAAs share four regions of sequence conservation[17] including an N-terminal domain (DI) for recruitment of transcriptional co-repressors, a core degron flanked by rate motifs[18], and the C-terminal ubiquitin-like PB1 domain that mediates homotypic as well as heterotypic interactions (reviewed in ref. 19). AUX/IAA's inherent structural flexibility seems to allow them to accommodate different binding partners exploiting different binding modes. As AUX/IAAs are often products of early auxin-responsive genes, their repressor activity establishes robust negative feedback loops[6,20]. AUX/IAAs probably also undergo cyclophilin-catalysed isomerization[21] stimulated by auxin, which facilitates recognition by $SCF^{TIR1/AFBs}$. An increase of the nuclear auxin concentration is registered by the formation of a ternary TIR1/AFB:auxin:AUX/IAA co-receptor complex (reviewed in ref. 19). Once recruited, AUX/IAAs are predicted to be tagged with polymeric ubiquitin (Ub) chains leading them to destruction by the 26S proteasome[22]. Interestingly, an auxin-inducible degron technology has been widely utilized for conditional auxin-based depletion of proteins in various eukaryotic systems such as yeast, *Drosophila melanogaster*, *Caenorhabditis elegans* and recently mammalian cells using a combination of auxin-inducible degron tagging and CRISPR/Cas[23,24]. Although the core of the AUX/IAA degron located in conserved domain II (DII) is necessary for TIR1-AUX/IAA associations, it is not sufficient for full auxin-binding properties of a co-receptor *in vitro* or AUX/IAA turnover *in vivo*[11,18]. In fact, a bona fide AUX/IAA degron for ubiquitin-proteasome system (UPS)-mediated degradation likely consists of three elements (tripartite): the primary degron motif recognizable by cognate $SCF^{TIR1/AFB}$-E3 ligases; a secondary degron with one (or multiple neighbouring) lysine(s) present on a ubiquitylation zone[25]; and a tertiary degron in a disordered locally flexible site located proximal to (or overlapping with) the secondary degron for engaging the proteasome[25–27]. Hence, rate motifs that flank the primary degron and are located in AUX/IAA-disordered regions could also modulate $SCF^{TIR1/AFB}$-AUX/IAA interactions and AUX/IAA degradation dynamics[11,18]. It has been proposed that $SCF^{TIR1/AFB}$-mediated AUX/IAA proteolysis, and the combinatorial diversity of auxin-triggered TIR1/AFB-AUX/IAA interactions build an intricate network controlling complex genetic programs[6,28]. The understanding of the global dynamics of auxin co-receptor assembly and its immediate impact on AUX/IAA ubiquitylation and degradation is not fully understood. Furthermore, while most studies have focused on the downstream events of auxin sensing, we lack a detailed explanation for the co-existence of the plethora of co-receptor complexes. Studies on how the $SCF^{TIR1/AFBs}$-auxin system senses various auxin concentrations differentially targeting AUX/IAA proteins leading to their ubiquitylation and degradation are still in their infancy. Therefore, we seek to understand the evolutionary retention of AUX/IAA genes and identify paramount features that lead to SCF^{TIR1} discrimination and processing. Additionally, aiming to dissect biochemically ubiquitin conjugation of AUX/IAAs, we set to establish a tunable system to assess SCF^{TIR1}-AUX/IAA assembly and specific auxin-triggered AUX/IAA ubiquitylation.

Here, we analyse inter- and intra-specific sequence variation in a selected sister pair of canonical *Arabidopsis* AUX/IAAs, *IAA6* and *IAA19*, and characterize biochemically the SCF^{TIR1}-IAA6 and SCF^{TIR1}-IAA19 auxin co-receptors. We also define their affinity for auxin, the kinetics of SCF^{TIR1}-target assembly for these two co-receptors, and report distinct ubiquitylation patterns of IAA6 and IAA19 repressors. Ultimately, we present a model for how related proteins, that are functionally specialized to sense specific small molecule concentrations, might interpret those signals into differential stability of transcriptional regulators, regulating gene expression and developmental responses.

Results

IAA6 and IAA19 differ in expression and selection patterns. AUX/IAA transcriptional repressors exist as sister pairs, or ohnologues, with high sequence similarity, which have been retained in an unusually high proportion of cases after whole-genome duplication events, and have therefore been diverging for the same length of time[29,30] (Supplementary Fig. 1). Functional shifts by neo- or sub-functionalization or selection for dosage balance in protein complexes contribute to the retention of such gene duplicates[31]. Among 29 AUX/IAA proteins in *Arabidopsis*, IAA6 and IAA19 ohnologues carry a degron motif and share high sequence identity (61.4%) (Supplementary Data 1). Nevertheless, dominant degron mutations, *iaa6/shy1* and *iaa19/msg2,* and swapping IAA6 and IAA19 N-terminal repressor domains (DI) indicate that IAA6 and IAA19 have distinct as well as shared functions in auxin signalling[17,32–36]. As *IAA6* and *IAA19* gene expression might reflect specific functions at the molecular level, we compared available data on mRNA expression profiles in different tissues, developmental stages, and *Arabidopsis thaliana* accessions (Fig. 1a and Supplementary Fig. 2a–c, Supplementary Note 1). Consistently, *IAA19* exhibited significantly higher expression than *IAA6*, indicating that albeit their relative conserved promoter regions[29], the two genes are differentially regulated. Selective constraints on gene-coding sequences have been shown to increase with expression level[31]. As *IAA6* and *IAA19* orthologs are not present in *Carica papaya*, the duplication event seems to have occurred after *Brassicaceae* and *Caricaceae* separated. In the most simple scenario, one of the two sister genes keeps the function of the original single-copy gene in the last common ancestor, while the other gene either pseudogenizes or is free to sub- or neo-functionalize. Pseudogenization in this case has obviously not occurred. As *IAA19* expression is significantly higher than *IAA6*, *IAA19* is likely the gene that retained the original function. It is often

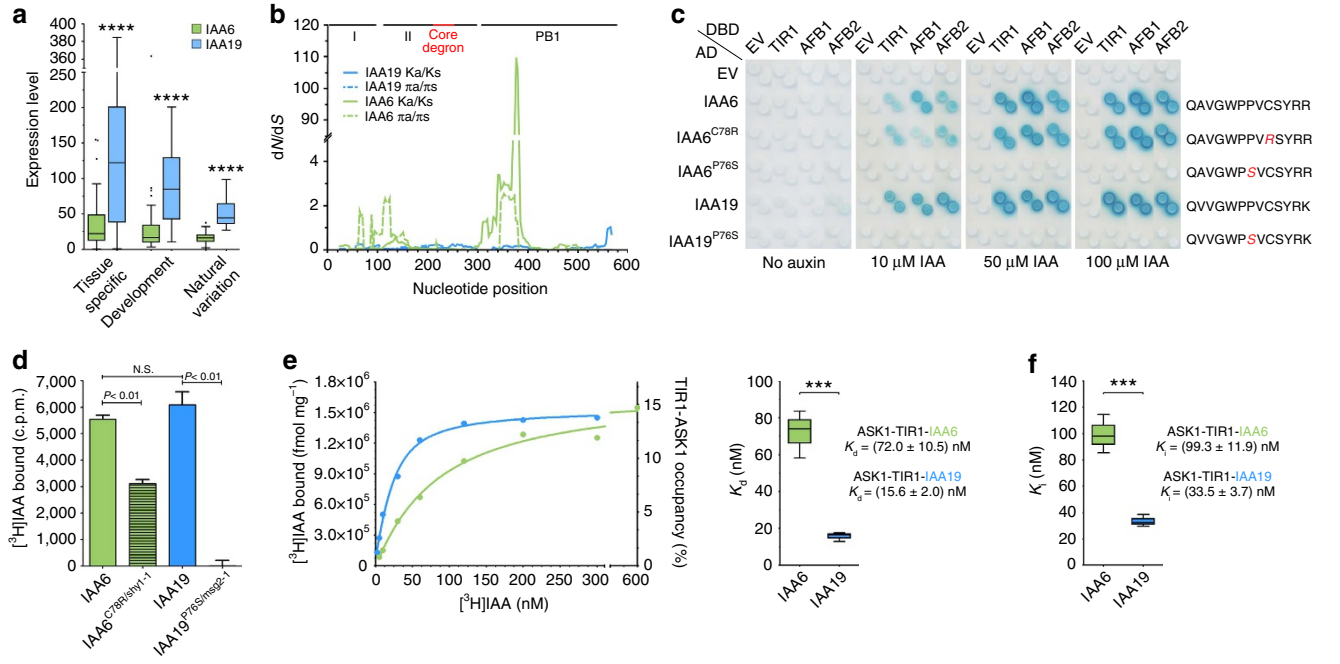

Figure 1 | *IAA6* and *IAA19* ohnologues exhibit different selection pressure signatures and their TIR1-containing receptor complexes show dissimilar auxin binding properties. (**a**) Comparison of available *A. thaliana IAA6* (green) and *IAA19* (blue) expression data. Box plots depict IQR and the median of three different datasets obtained from the *Arabidopsis* eFP browser[78]. Outliers were defined as 1.5 × IQR. Graphs for different conditions in each data set are shown in Supplementary Fig. 2. IQR, interquartile range. (**b**) Sliding window plots of nucleotide sequence divergence between *IAA6* and *IAA19* in *A. thaliana*, *A. lyrata*, *A. halleri* and *C. rubella*. d*N*/d*S* ratios are plotted against the midpoint position of each 50 bp window. Black bars (top) display positions of the different protein domains. See Supplementary Data 1 for detailed AUX/IAA domain structure. (**c**) Y2H interaction matrix for TIR1, AFB1, AFB2 with IAA6, IAA19, and their putative dominant mutant versions[32,33,35]: IAA6$^{C78R/suppressor\ of\ hy2\ (shy1-1)}$, IAA6^{P76S}, IAA19$^{P76S/massugu\ (msg2-1)}$, carrying mutations in the degron (right). Yeast diploids containing LexA DBD-TIR1/AFBs and AD-AUX/IAAs were spotted on selective medium with increasing IAA concentrations, and β-galactosidase reporter expression indicates IAA-induced TIR1/AFB1/2-AUX/IAA interactions. EV, empty vector. (**d**) One-point saturation binding assays using 200 nM [^{3}H]IAA to recombinant ASK1-TIR1-AUX/IAA ternary complexes. IAA6$^{C78R/shy1-1}$ and IAA19$^{P76S/msg2-1}$ mutants that mimic stabilized version of the proteins affect significantly specific auxin binding. (**e**,**f**) IAA6 and IAA19 provide ASK1-TIR1-containing complexes different auxin-sensing capabilities. (**e**) Representative saturation binding curves for IAA6 and IAA19 (left). ASK1-TIR1-IAA19 complexes bind auxin with high affinity (K_d = 15.6 ± 2.00 nM), whereas IAA6-containing co-receptor complexes provide fivefold lower affinity for auxin (K_d = 72.0 ± 10.5 nM) (right). (**f**) Homologous competition experiments were performed using 50 or 25 nM [^{3}H]IAA for ASK1-TIR1-IAA6 or -IAA19, respectively. IC_{50}s were obtained from curve fitting, and K_i values were calculated using the Cheng–Prusoff equation given the observed dissociations constants from saturation binding experiments. Error bars, s.d. (**d**) or minimum and maximum values (**e**,**f**) of three independent biological replicates. Asterisks denote significant statistical differences (P < 0.001 (***), and P < 0.0001 (****)) calculated using either two-tailed Student's *t*-test (**e**,**f**), or one-way ANOVA (**a**,**d**) followed by Tukey's honest significant difference test. ANOVA, analysis of variance.

possible to detect this trend by testing for positive selection between the two sister genes. However, the evolutionary signal present in these sequences among four *Brassicaceae* orthologues for each of the genes was not strong enough (or not present) to identify significant signatures of positive selection (based on the branch-site model in CodeML from the PAML package (version 4.9c))[37]. We therefore asked whether sequence divergence between the two genes differs by comparing the *IAA6* and *IAA19* orthologous *Brassicacae* sequences for each gene separately (Fig. 1b). While both full length sequences seemed rather conserved between the four *Brassicaceaes* tested (overall d*N*/d*S* *IAA6* = 0.132; d*N*/d*S* *IAA19* = 0.087), sliding window analyses revealed regions of increased sequence divergence in *IAA6*. These encompass the upstream region of the core degron and a conspicuous peak (d*N*/d*S* > 100) in the PB1 domain (Fig. 1b). Since *IAA6* and *IAA19* orthologous sequences lacked indels in the vast majority of comparisons, these peaks must be driven by amino acid substitutions. A similar trend can be observed when intraspecific sequence divergence based on 80 resequenced *A. thaliana* accessions is assessed. Here, *IAA19* is once more highly conserved (d*N*/d*S* = 0.169), while *IAA6* seems to be under relaxed selective constraints (d*N*/d*S* = 0.660). Hence, although comparison of *IAA6* with *IAA19* did not reveal direct evidence for positive selection, *IAA6* but not the highly expressed *IAA19* includes regions with extensive sequence variation between *Brassicaceaes* when gene sequences were analysed separately (Fig. 1b and Supplementary Data 2). In addition, relaxed selective constraints indicate that within the *A. thaliana* germplasm *IAA6* may be in the process of sub-functionalizing.

TIR1-IAA6 and TIR1-IAA19 receptors discriminate auxin levels. To address functional differences on the protein level, we then asked whether IAA6 and IAA19 vary in their potential to interact with TIR1, and AFBs in response to auxin in conventional yeast two-hybrid assays (Y2H). IAA6 and IAA19 interacted in an auxin-dependent manner with TIR1, AFB1 and AFB2 (Fig. 1c, Supplementary Figs 3 and 4). Particularly, low micromolar concentrations of naturally occurring auxins IAA, 4-chloro-IAA and, to a lesser extent, the synthetic auxin 1-naphthalene acetic acid (1-NAA) triggered TIR1/AFB1/AFB2-IAA6/19 associations (Fig. 1c and Supplementary Fig. 3). Overall, IAA19 interacted more strongly with TIR1/AFBs than IAA6, demonstrating that IAA6 and IAA19

differ in strength of auxin-dependent TIR1/AFB-AUX/IAA interactions. We hypothesize that these differences might arise from the unique amino acids in their degron-flanking regions (Supplementary Data 1), which may affect AUX/IAA ability to assemble into auxin co-receptor complexes.

Since it is possible that TIR1-IAA6 and TIR1-IAA19 co-receptors exhibit biochemical differences that enable specialized functions, we next assessed their auxin-binding properties via saturation binding assays using increasing concentrations of radiolabelled IAA (Fig. 1d,e). TIR1-IAA19 binds IAA with a K_d of ~15.6 nM compared to a K_d ~72.0 nM by TIR1-IAA6, indicating that TIR1-IAA19 co-receptor has a comparatively higher affinity for IAA than TIR1-IAA6 (Fig. 1e, Supplementary Figs 5 and 6). TIR1-auxin-AUX/IAA ternary complex formation was significantly compromised when the receptors consisted of TIR1-iaa19/msg2-1, or -iaa6/shy1-1 dominant mutants (Fig. 1c,d). We then directly compared the auxin affinity of TIR1-IAA6 and TIR1-IAA19 co-receptors via competitive binding assays, and determined IC_{50} and K_i values for each of the complexes using increasing concentrations of unlabeled IAA as competitor (Fig. 1f). At equilibrium, unlabeled IAA chased [^{3}H]IAA consistently three times more efficiently from TIR1-IAA19 than TIR1-IAA6 ($K_i = 33.5 \pm 3.7$ nM and $K_i = 99.3 \pm 11.9$ nM, respectively), mirroring the affinity of the co-receptors for IAA determined in saturation binding experiments (Fig. 1f and Supplementary Fig. 7). Hence, IAA6 confers essentially lower auxin binding affinity than IAA19 to TIR1-AUX/IAA co-receptor complexes.

Tracking specific SCF^{TIR1}-mediated AUX/IAA ubiquitylation. E3-target affinity determines a time interval in which Ub transfer to targets takes place[25]. Hereafter, we speculated that the strength of the SCF^{TIR1}-IAA6 and SCF^{TIR1}-IAA19 associations might impact AUX/IAA ubiquitylation and specifically, that the stability of SCF^{TIR1}-AUX/IAA complexes affects the site of ubiquitylation, Ub-chain extension, or the dynamics of Ub-conjugation. To analyse Ub-conjugation dynamics, we developed a TIR1-dependent, cell-free *in vitro* ubiquitylation assay (IVU). A typical IVU consists of recombinantly expressed and highly purified E1 (*At*UBA1), E2 (mostly *At*UBC8), mammalian *Hs*Cul1-*Mm*RBX1 (ref. 38), Ub, *At*TIR1-ASK1 (ref. 9), and GST-tagged IAA6 or IAA19 targets (Fig. 2 and Supplementary Fig. 8). Thus, correct assembly of an *Hs*Cul1-*Mm*RBX1-ASK1-F-box^{TIR1} complex in our IVUs allows the recruitment and activation of a Ub-charged E2 (E2~Ub) for Ub-conjugation of AUX/IAA *in vitro* (Supplementary Fig. 9).

To confirm the requirements for *in vitro* Ub-conjugation of IAA6 and IAA19, we pre-assembled SCF^{TIR1} complexes and performed IVUs when either one of the components was removed from the reaction. As expected, UBA1 (E1), UBC8 (E2), and SCF^{TIR1} (E3) were unambiguously required for IAA6 and IAA19 ubiquitylation (Fig. 2a). Moreover, SCF^{TIR1} showed strong E3 ligase activity *in vitro*. SCF^{TIR1} is a cullin-based RING ligase and since RING-E3s do not form a thioester intermediate with Ub, the linkage specificity of Ub-chain formation is likely conferred by the E2 (refs 39,40). Therefore, the topology of Ub-chains assembled on a target by the RING-E3 can change with the nature of the E2 (refs 40–42). Also, while E1 function is universal and both *Arabidopsis* E1s (UBA1 and UBA2) show almost equal specificity in transferring activated Ub to a variety of *Arabidopsis* E2s (ref. 43), various E2-E3 combinations may affect E3 ligase activities. We then assessed how three E2s from different subclades out of the 37-member Ub E2 family in *Arabidopsis*[44], namely UBC1, UBC4 and UBC8 catalyse Ub-conjugation to IAA6 and IAA19 (Fig. 2b and Supplementary Fig. 10). UBC1, 4 and 8 form a thioester linkage between the E2 and Ub, indicating these E2s can be charged with ubiquitin *in vitro* (Supplementary Fig. 9)[44,45]. Whereas, UBC1 and UBC8 triggered comparable IAA6 and IAA19 poly-ubiquitylation, only low molecular ubiquitin conjugates could be detected when using UBC4 as E2 in IVUs (Fig. 2b and Supplementary Fig. 10). This shows E2-SCF^{TIR1} selectivity and discrimination for auxin-mediated ubiquitylation of targets. These observations also suggest that the AUX/IAA ubiquitylation tracked in the IVU system is the consequence of the attachment of Ub polymers with different topologies. We therefore incorporated in our assays Ub variants bearing individually substituted lysine residues (K to R mutants), that have been widely used to characterize E2-E3 linkage specificity[46]. Hence, availability of a Ub mutant containing only a single lysine residue, either Lys29, Lys48 or Lys63 forces, if permitted by the E2-SCF^{TIR1} interaction, the formation of polyubiquitin chains on AUX/IAA targets via the single available lysine (Fig. 2b). We found that restricting ubiquitin concatenation leads to an alternate conjugation pattern, and there is an apparent loss of ubiquitin chain formation as compared with reactions containing wild-type ubiquitin (Fig. 2b). This implies ubiquitin conjugates on IAA6 and IAA19, in dependency of UBC8, are the product of different linkage types leading to alternative topologies, most likely several poly-mono-ubiquitylation and/or multi-, poly-ubiquitylation events. E2-E3 combinations determine specific chain formation by positioning the acceptor Ub in a defined orientation to favour linkage of the donor Ub on the selected lysine[25]. Therefore, it remains to be established, which E2-SCF^{TIR1} combinations occur, and whether Lys29, Lys48, Lys63 Ub-chains or a combination of them render IAA6 and IAA19 unstable *in vivo*.

AUX/IAA ubiquitylation mirrors auxin receptor affinity. Next, we determined how IAA6 and IAA19 ubiquitylation is influenced by auxin. First, we monitored auxin-dependent ubiquitylation of AUX/IAAs over time using fluorescein-labelled ubiquitin, and fluorescent secondary antibodies for accurate and non-enzymatic detection of ubiquitin conjugates in a single image. We detected steady and rapid (<10 min) Ub-conjugation to IAA6 and IAA19 in the presence of auxin (750 nM IAA) (Fig. 2c and Supplementary Fig. 8b–d). Albeit much less efficient, as depicted by the relative Ub signal (+IAA/−IAA) (depicted in lower panel Fig. 2c), we observed AUX/IAA ubiquitylation in the absence of IAA, which is probably the result of basal interactions between SCF^{TIR1} and AUX/IAAs[7–9,11,47–49]. IVU reactions in the presence of ~10× and ~50× [IAA] higher than the observed auxin affinity of TIR1-IAA6 and TIR1-IAA19 co-receptor complexes, respectively (Fig. 1e), did not provide evidence for significant differences in the ubiquitylation status of IAA19 over IAA6 (depicted in lower panel Fig. 2c and Supplementary Fig. 8b–d). Intriguingly, when we further evaluated ubiquitylation of AUX/IAAs with increasing nanomolar concentrations of IAA, we detected a surge in high molecular weight species in IAA19 compared to IAA6 (Fig. 2d). While a steady increase in Ub-conjugation of IAA6 took place at 0.1–2 μM [IAA] after 10 min, Ub-conjugation of IAA19 spiked already at the lowest IAA concentration (Fig. 2d and Supplementary Fig. 8e,f). This suggests a greater efficiency of the ubiquitylation machinery acting upon IAA19 at low auxin concentrations. Taken together, these experiments are the first to demonstrate reconstitution of SCF^{TIR1} assembly and AUX/IAA ubiquitylation.

AUX/IAA Ub-site selection depends on local flexibility. Having developed a tool for investigating IAA6 and IAA19 recognition by

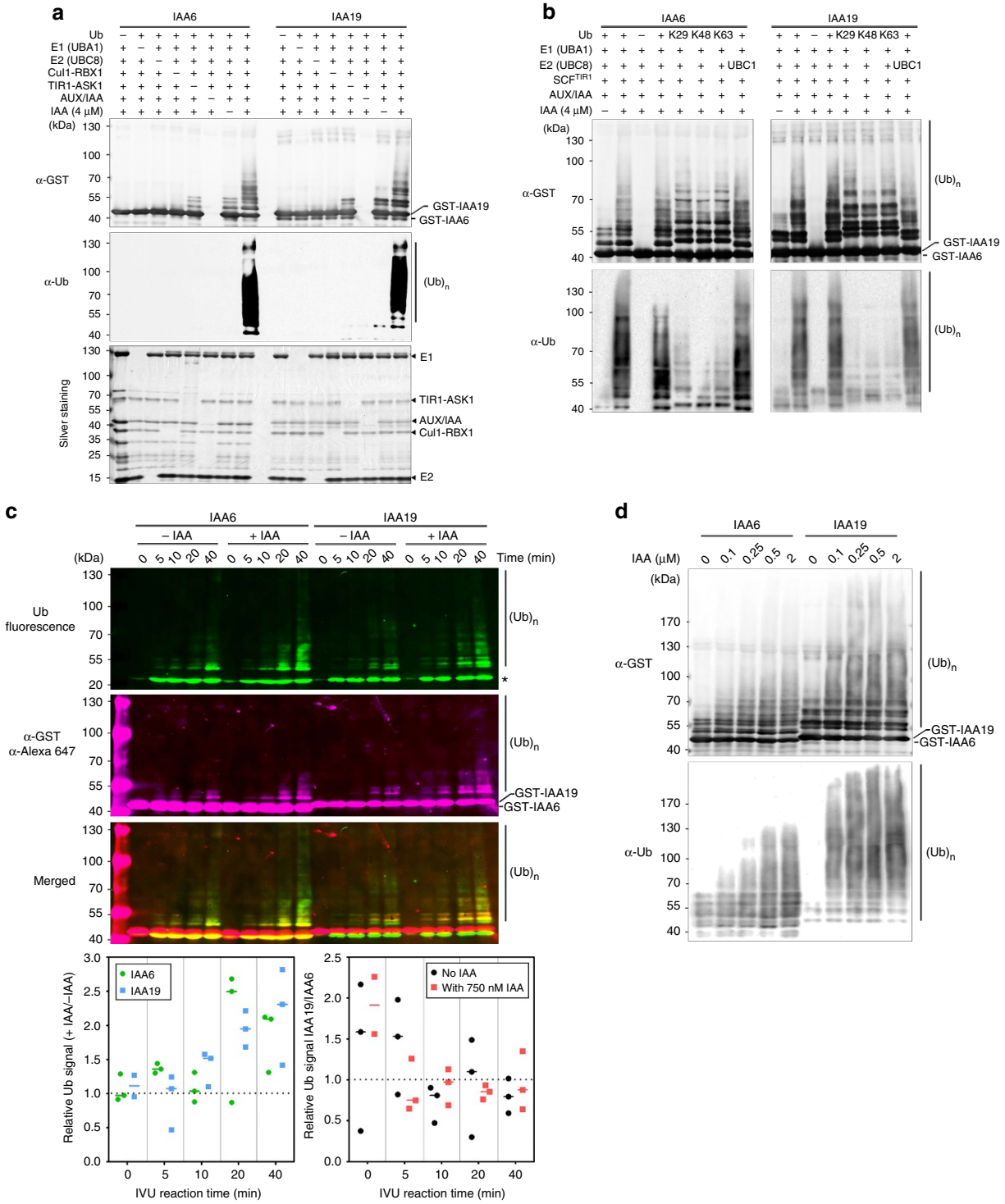

Figure 2 | SCF^{TIR1}-dependent and specific IAA6 and IAA19 ubiquitylation is enhanced by auxin. (**a**) IVU assays with recombinant GST-IAA6 or GST-IAA19, E1 (*At*UBA1), E2 (*At*UBC8), reconstituted SCF^{TIR1} (*At*SKP1-TIR1, *Hs*Cul1 and *Mm*RBX1), *At*Ub and IAA (auxin). AUX/IAA ubiquitylation is dependent on each component. Anti-GST, as well as anti-Ub antibodies recognize IAA6 and IAA19 ubiquitylated species. IVU reaction time 10 min (**b**) UBC8 and UBC1 Ub-conjugating enzymes (E2s) elicit poly-Ub-conjugation of IAA6 and IAA19 after 10 min *in vitro*. UBC8 promotes various Ub-linkages as seen by the reduction of IAA6 and IAA19 ubiquitylated species using either one of the chain-specific Ub-donors, Lys-29, Lys-48 or Lys-63 (Supplementary Fig. 9). (**c**) Rapid IVU of IAA6 and IAA19 is auxin- and time-dependent. Time course IVU reactions were performed using fluorescein isothiocyanate-labelled ubiquitin with or without 750 nM IAA. Ubiquitylation was monitored using the ubiquitin fluorescent signal (green, top) and Alexa Fluor 647-conjugated secondary antibodies for detection of GST:AUX/IAAs (magenta, middle). (*) Asterisk depicts ubiquitylated Cullin1 as previously reported[79]. ImageQuant TL software was used for quantification and generation of merged image (bottom). Ratios for auxin- and target-dependent ubiquitylation were calculated from three independent IVUs ($n=3$; see Supplementary Fig. 8b–d for replicates) and the single measurements are depicted in the corresponding scatter dot plots with line at median. A two-way ANOVA ($P>0.05$) showed no significant differences for the relative Ub signal between IAA6 and IAA19 in a specific time point (left), or for the IAA19/IAA6 ratio with or without 750 nM IAA. (**d**) Increased nanomolar concentrations of IAA promote IAA6 or IAA19 ubiquitylation after 10 min IVU reactions and higher molecular ubiquitylated species occurred on IAA19.

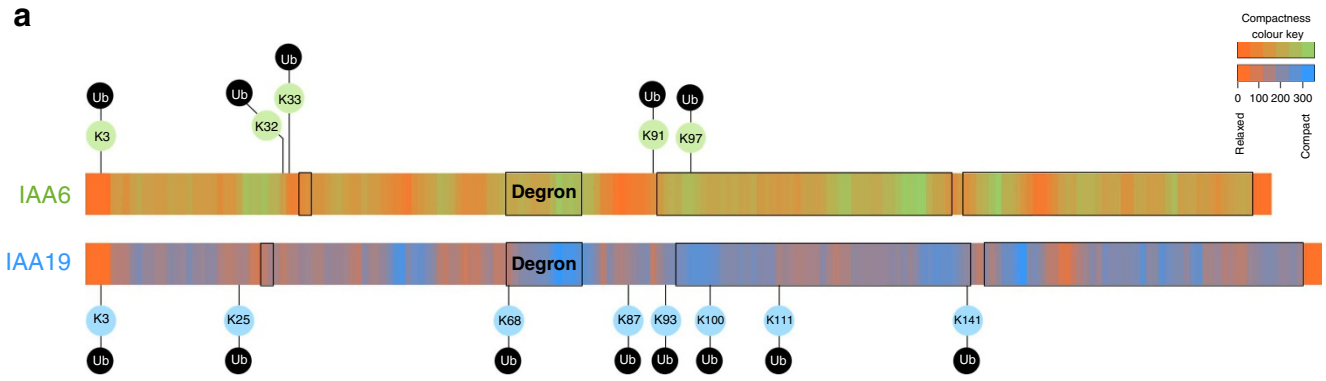

b

Ub site	Tryptic peptide sequence	Ion score[1]
K3	AGFMA*K*EGLALEITELR	90
K3	KAGFMA*K*EGLALEITELR	85
K32, K33	LGLPGDNYSEISVCGSS*KK*	83(K32)§, 85(K33)
K32, K33	LGLPGDNYSEISVCGSS*KK*K	42(K32)§, 39(K33)
K91	KNNEEAS*K*AIGYVK	37
K91	NNEEAS*K*AIGYVK	93§
K97	AIGYV*K*VSMDGVPYMR	62

Ub site	Tryptic peptide sequence	Ion score[1]
K3	AGFME*K*EGLGLEITELR	84§
K25	DVAE*K*MMK	32
K68	VNDSPAA*K*SQVVGWPPVCSYR	66§
K87, K93	NSC*K*EASTT*K*VGLGYVK	46
K93	EASTT*K*VGLGYVK	58§
K100	VGLGYV*K*VSMDGVPYLR	88
K111[2]	*K*MDLGSSQGYDDLAFALDK	156§
K141	GIGVAL*K*DGDNCEYVTIYEDK	104

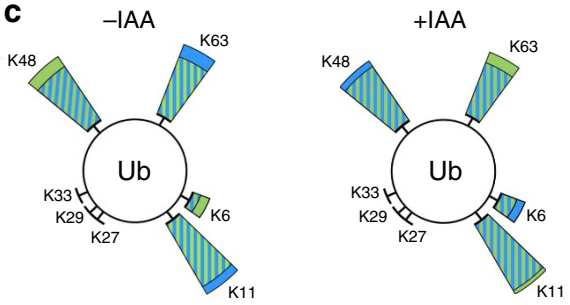

Figure 3 | IAA6 and IAA19 exhibit high intrinsic disorder offering a broad ubiquitylation zone with likely limited lysine availability. (**a**) Putative lysine ubiquitylation in IAA6 and IAA19 concentrate in hotspots with low compactness. Meta-structure of IAA6 and IAA19 was quantified by sequence-derived parameters, compactness and local secondary structure. Residue-specific compactness is displayed in green-orange (IAA6), and blue-orange (IAA19) 2-colour sequential variation (see colour key), where folding corresponds to values above 300 from DisProt database (see Supplementary Fig. 14 for details). IAA6 and IAA19 IVU samples were analysed via LC-MS and putative ubiquitylation sites were mapped relative to their domain structure (black boxes). (**b**) List of Ub-modified IAA6 (green) and IAA19 (blue) peptides and their ion scores (Mascot[1]) identified by mass spectrometry. Specific ubiquitylated Lys-residues of cleaved peptides are shown in red, and (§) symbol depicts the site is also covered by the Lys-Arg-Gly-Gly (LRGG) remnant, which is further confirmation that the site is genuine. Ub-conjugation on Lys111 in IAA19 (ref. 2) is also supported by the LRGG remnant, reducing the uncertainty caused by the N-terminal location on the peptide. See Supplementary Figs. 11 and 12 for information about reproducibility and FDR. (**c**) Distribution of identified ubiquitin linkage types. IVU reactions for IAA6 (green) and IAA19 (blue) with or without IAA were analysed via LC-MS, and ubiquitin peptides corresponding to different ubiquitin linkage types were identified (for details see Supplementary Fig. 13).

the SCF^{TIR1}-E3 ligase and subsequent ubiquitylation *in vitro*, we next sought to determine the residue(s) within IAA6 and IAA19 that function as attachment sites for Ub (Fig. 3a,b). We processed IVU samples containing IAA6- and IAA19-ubiquitin conjugates for liquid chromatography coupled with tandem mass spectrometry (LC-MS) and inspected MS/MS spectra for peaks with a mass difference representing LRGG (trypsin miscleavage product of Ub C-terminus) and di-Gly modified residues (Fig. 3b, Supplementary Figs 11–13 and Supplementary Table 1, Supplementary Table 2). We found Lys-ubiquitylation on IAA6 and IAA19 in regions with low or intermediate compactness (Fig. 3a and Supplementary Fig. 14a,b) and more Ub-modified peptides for IAA19 than for IAA6 independently of auxin present in the IVU reactions. Reproducible ubiquitylated sites in independent replicates comprise Lys3, Lys32, Lys33, Lys91 and Lys97 in IAA6 (27% total Lys); and Lys3, Lys25, Lys68, Lys87, Lys93, Lys100, Lys111 and Lys141 in IAA19 (47% total Lys) (Fig. 3a,b). Ubiquitylated Lys3 is a conserved residue among a subgroup of AUX/IAAs including IAA6, 19, 8, 9, 34, 32. Neighbouring Lys32 and Lys33 in IAA6 appear to be equivalent to Lys25 in IAA19. These residues are located in the vicinity of the completely conserved but not ubiquitylated KR motif in a region decorated with additional multiple unmodified lysines (Supplementary Data 1). Similarly, ubiquitylated Lys91 in IAA6 coincides with K87 and K93 in IAA19, also located in a region downstream of the canonical degron including a rate motif and DIII in the PB1 domain. Specifically, ubiquitin modified Lys97 in IAA6 akin Lys100 in IAA19 are completely conserved among *Arabidopsis* AUX/IAAs, which encourages the idea that this is a common ubiquitylation site in the AUX/IAA family (Supplementary Data 1). Interestingly, ubiquitylation of Lys97 of IAA6, and Lys100 and Lys111 of IAA19 could serve as a mechanism to dislodge AUX/IAA interaction partners by interfering with their oligomerization interface (Supplementary

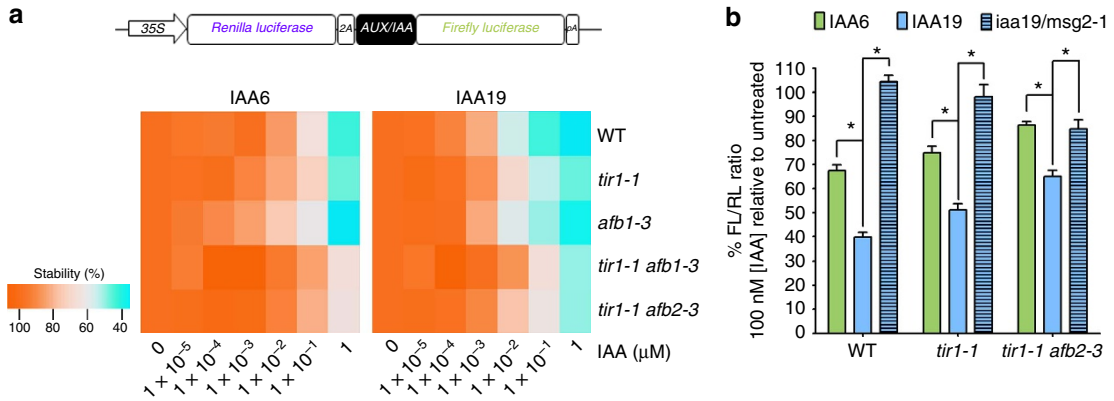

Figure 4 | IAA6 and IAA19 stability is differentially impacted by their ability to form auxin coreceptor complexes with variations in affinity. (**a**) Ratiometric luminescence auxin biosensor constructs comprising IAA6 or IAA19 coding sequences flanked by Renilla luciferase (RL), and a C-terminal fusion with Firefly luciferase (FL) under the 35S constitutive promoter. 2A oligopeptide (2A) and poly(A) tail (pA) elements allow stoichiometric co-expression of RL and IAA6 or IAA19 FL fusions, and maturation of messenger RNA for their translation, respectively. *A. thaliana* protoplasts of *Col-0* (wild type, WT), *tir1-1, afb1-3* single and *tir1-1 afb2-3* and *tir1-1 afb3-4* double mutant plants transformed with IAA6 or IAA19 auxin biosensors were incubated for 30 min in IAA-supplemented medium (10 pM–1 μM IAA) prior luciferase activity determination. Auxin dose response on AUX/IAA stability is calculated as percentage of a decrease in FL/RL of untreated samples at a given IAA concentration. Heat map displays means ($n=6$) of FL/RL ratios of IAA6 and IAA19 sensors. Detailed graphs for each sensor in each genotype are shown in Supplementary Fig. 15. (**b**) Sensitivity of IAA6, IAA19 or IAA19$^{P76S/msg2\text{-}1}$ sensors in protoplasts of *Col-0* (WT), *tir1-1*, and *tir1-1 afb2-3* plants. Ratiometric luciferase activities are shown as percentage (%) of FL/RL ratio at 100 nM [IAA] relative to untreated samples. Statistical differences (*) were calculated by two-way ANOVA of the absolute data. Error bars, s.e.m. Data were considered statistically significant if the P value was <0.05.

Fig. 14c,d). In addition, although these are highly or completely conserved residues, we did not identify Lys68, or Lys111 ubiquitylated peptides in IAA6. We therefore cannot rule out that our MS-based analysis might be affected by the fidelity of the ubiquitylation *in vitro*, permitting only a subset of possible ubiquitylation sites to be detected. Non-canonical ubiquitylation of AUX/IAAs was previously proposed, as substitution of 16 lysines in IAA1 is not sufficient to abrogate its localization, turnover and function[50]. In our assays non-canonical IAA6 and IAA19 ubiquitylation might not be favoured, due to its low probability, the relative instability of the thioester bond to Cys in MS analysis, and the less frequent and also less kinetically stable hydroxyester linkages to Ser, and Thr[51]. Nevertheless, IAA6 and IAA19 ubiquitylation might rather depend on the structural adaptability around the ubiquitylation surface, namely local flexibility, enabling a choice of multiple lysines to be modified[27,52]. Concertedly, the *in vitro* tracking of Lys-ubiquitylation on IAA6 and IAA19 is placed on putatively exposed flexible regions flanking structured domains, so that AUX/IAA Ub-site selection depends on a specific local environment (Fig. 3a and Supplementary Fig. 14). Thus, our data nicely support recent findings showing that Ub-sites on targets exhibit striking propensity to occur within intrinsically disordered regions in a specific determinant sequence neighborhood[27].

Various linkages of polyubiquitin chains which are determined either by the E2 or less frequently, by the E3 ligase[53], confer distinct fates to target proteins[54]. Therefore, we surveyed the relative abundance of ubiquitin linkage types in our IVUs by making a direct estimate from the number and frequency of peptide spectrum matches (PSMs) from ubiquitylated lysine residues in ubiquitin. Independently of auxin, primarily K48-, K11-, K63-, and to a much lesser extent K6-linked chains were identified in the samples (Fig. 3c and Supplementary Fig. 13). It has been shown that ubiquitin chains on targets adopt either compact or open conformations affecting the proteasome ability to unfold and degrade the target[55]. So, K48- or mixed linkage-chains, adopting compact conformations, lead to a greater turnover than K63-linked chains[54]. Combinations of homologous, heterologous and branched ubiquitin chains on IAA6 and IAA19 possibly endow their degradation by the proteasome.

Auxin co-receptor affinity tunes AUX/IAA turnover. *In vivo,* many factors may influence auxin co-receptor formation and IAA6 and IAA19 processing. Therefore, we quantitatively assessed IAA6 and IAA19 degradation in various TIR1/AFB mutant backgrounds, and monitored their response to auxin. We generated IAA6 and IAA19 ratiometric luminescent sensor constructs[56] for transient expression in *Arabidopsis* leaf protoplasts, and measured auxin-dependent degradation as a decrease in firefly relative to renilla luminescence (FL/RL ratio) (Fig. 4 and Supplementary Figs 15 and 16). IAA6 and IAA19 sensors showed auxin concentration-dependent degradation in the wild-type genetic background, rapidly responding towards low levels of exogenously applied IAA. While IAA concentrations between 100 pM to 1 nM triggered IAA19 degradation, 10 nM IAA was required for comparable turnover of IAA6 (Supplementary Fig. 15). In *tir1-1* and *tir1-1 afb2-3* or *tir1-1 afb3-4* double mutant backgrounds, IAA6 and IAA19 degradation was reduced, requiring ~10 times more IAA to reach wild-type degradation rates (Fig. 4a and Supplementary Fig. 15). Interestingly, the differences we observed between IAA6 and IAA19 coincide with estimates for relative speed of auxin-induced turnover for IAA6 and IAA19 in a synthetic approach[57]. Additionally, incorporating MG132 proteasome inhibitor stabilized IAA6 and IAA19 (Supplementary Fig. 16b). Thus, degradation of IAA6 and IAA19 sensors in our protoplast system is proteasome-dependent consistent with previous observations[58], and sensors carrying dominant mutations in the degron displayed increased stability (Supplementary Fig. 16a). Also, specific structural features of IAA6 and IAA19 might contribute to fine-tuning their turnover. A structural approach in the future will surely corroborate whether rate motifs[18] on IAA6 and IAA19 degron-flanking regions amplify or mitigate turnover dynamics. For instance, slightly longer rate motifs enriched with Gly residues in IAA19 (Supplementary Fig. 1b) could eventually confer much

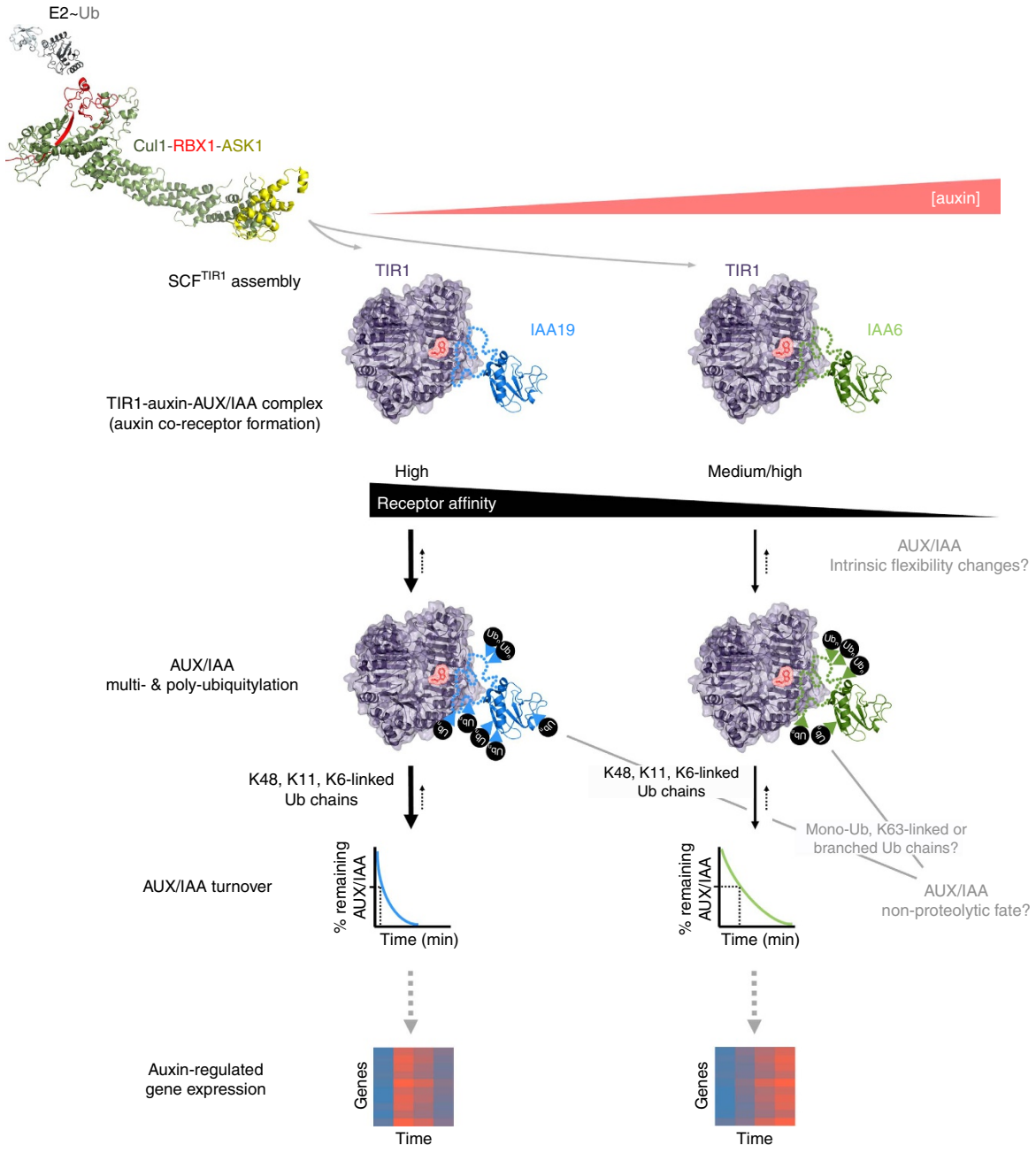

Figure 5 | Simplified model of auxin sensing by SCF^{TIR1}-IAA6 and SCF^{TIR1}-IAA19 co-receptor complexes. A Cullin-RING E3 ligase[80] from the SCF-type is formed when TIR1 or its paralogs AFB1-5 interchangeably assemble with the adaptor protein ASK1. SCF^{TIR1} interacts with both E2~Ub and IAA6 or IAA19 degradation targets in response to intracellular auxin levels. TIR1 recruits IAA19 at low nanomolar concentrations of IAA and forms a high affinity co-receptor complex, while TIR1-IAA6 displays only a medium IAA affinity. Co-receptor complex dissociation is possible but unfavored in the presence of auxin (reverse dotted arrows). A degron and intrinsically disordered regions (unstructured dotted line) most likely fit on top of auxin in the TIR1-auxin-binding groove. It is currently unknown whether the two-pronged PB1-like IAA6 and IAA19 homo- and heterodimerization domains III-IV (folded structure) directly contribute to auxin binding. IAA binding affinities of TIR1-IAA6 and TIR1-IAA19 complexes yield differential Ub-conjugation at different sites. Lysines (K) along the IAA19 structure probably become ubiquitylated with Lys48-, Lys6-, Lys11-chain linkage types offering multiple ubiquitylation signatures for efficient and rapid degradation by the 26S proteasome. Putatively IAA6 ubiquitylation on lysine residues might be less efficient, leading to a comparably slower IAA6 turnover. Other residues in flexible and/or intrinsically disordered regions of IAA6 and IAA19 eventually become ubiquitylated *in vivo*. Since the outcome of AUX/IAA ubiquitylation depends on the distinct types of ubiquitin topologies, K63-linked ubiquitin chains, monoubiquitylation or mixed chains on IAA6 and IAA19 could affect their function and have a non-proteolytic role. Conceivably, AUX/IAA ubiquitylation can be counteracted by the activity of deubiquitylases (reverse dotted arrows). AUX/IAA ubiquitylation, particularly initial rounds, might trigger temporal- and auxin- dependent SCF^{TIR1}-AUX/IAA binding specificity variations through intrinsic flexibility changes. IAA19 has a very short half-life, its ohnologue IAA6, although also unstable, exhibits longer half-life, which is a reflection of their differential affinity for auxin when in TIR1-containing co-receptor complexes. Consequently, IAA6- and IAA19-dependent specific transcriptional outputs, in different tissues and in response to different auxin concentrations, are likely impacted by AUX/IAA processing.

more flexibility, so that amino acid composition affects the conformational ensemble and facilitates processivity on IAA19.

Discussion

Here, we propose a model (Fig. 5) in which IAA6 and IAA19 ohnologues have evolved functionally specialized auxin sensitivity through differential auxin co-receptor formation, auxin sensing, and ubiquitylation. Despite high amino acid sequence similarity, IAA19 associates more strongly with TIR1/AFBs than IAA6 does, forms a higher affinity TIR1-auxin-IAA19 ternary complex, and is ubiquitylated with higher processivity at lower auxin concentrations. As ubiquitylation is highly dynamic, SCF^{TIR1} complex formation and stability as well as AUX/IAA isomerization and deubiquitylation may also affect IAA6 and IAA19 Ub-conjugation status, pacing their processing and degradation dynamics in a cellular context.

Our studies on the dynamics of TIR1-IAA6 and TIR1-IAA19 co-receptor formation and outcome suggest that a subtle AUX/IAA sequence divergence drives functional specialization, thereby dictating AUX/IAA Ub-conjugation, and most likely degradation. Thus, these events ultimately impinge on ARF interactions and auxin-dependent gene activation. It is quite remarkable that differences between sister genes like *IAA6* and *IAA19* might already leave traces on both expression level, and sequence divergence of each single gene. Regions of increased sequence divergence in *IAA6* coincide with ubiquitylation hotspots in *IAA19*. Whether these regions in *IAA6* with relaxed selection have a functional relevance and provide, for instance, a different landscape for ubiquitin conjugation affecting AUX/IAA stability, or are merely an effect of genetic drift remains, so far unknown.

The higher ubiquitylation processivity we observed for IAA19 compared to IAA6 in response to auxin may be a function of higher auxin affinity of TIR1-IAA9 versus TIR1-IAA6. Higher auxin affinity likely confers greater stability to the SCF^{TIR1}-IAA19 interaction, which may prolong the time interval in which IAA19 is available to the E3 ligase for Ub-conjugation. Structural constraints may preclude targeting residues limiting the E3's area of action[25], so alternative and differential IAA6 and IAA19 ubiquitylation could depend on how such residues are available in IAA6 and IAA19 ubiquitylation zones[59,60]. Interestingly, some E3s generate ubiquitin-rich foci on proteins that act as stable recruitment platforms for DNA and/or cognate protein partners[55]. For instance, multi-monoubiquitylation or Lys63-linked chains act as transient mediators of protein interactions[61]. The relevance of such Ub-modifications on IAA6 and IAA19 remains to be determined in future studies. Our results allow us to postulate that the UBC8-SCF^{TIR1} combination yields Ub-chains on IAA6 and IAA19 that most presumably confer recognition by the proteasome and a degradation outcome.

We propose that although a single polyubiquitin chain on one Ub-site might be sufficient for targeting IAA6 and IAA19 for degradation, the relative location of additional ubiquitylation sites such as Lys particularly in flexible regions serve as backup sites for differential ubiquitylation in response to auxin. We demonstrate that SCF^{TIR1}-mediated ubiquitylation of IAA6 and IAA19 can occur via lysine residues on flexible disordered regions, each of which could be sufficient to induce the rapid degradation of IAA6 and IAA19 *in vivo*. Given the vast scope for variation in Ub-linkage types and their associated topologies, it is also plausible that only specifically linked Ub-chains on IAA6 and IAA19 via isopeptide bonds at certain lysines result in proteasomal degradation. Conversely, mono-, multi-monoubiquitylation or poly-ubiquitylation with distinct Ub-chain topology might alter AUX/IAA localization, and/or its intrinsic properties thereby conditioning IAA6 and IAA19 turnover in a cellular environment. Alternatively, the same events leading to differential AUX/IAA ubiquitylation might regulate auxin signalling non-proteolytically by controlling AUX/IAA activity or offering a signal for recruiting or modulating interaction with partners such as ARFs.

Together, we combined quantitative *in vitro* and *in vivo* tools to reveal underlying mechanisms and consequences of discriminatory auxin perception and response. In the future, combining genetic studies of early-diverging land plants with biochemical tools, such as those we have developed and implemented here, will surely give a unique insight into the evolution, dynamics and the wiring of the auxin response system. Our results illustrate how evolution of primary protein structure may be amplified through interaction with small molecules and protein complexes downstream. In our system, the consequence of these differential interactions is distinct degradation kinetics of transcriptional repressors central to auxin response. It is likely that similar mechanisms specify responses among not only the other AUX/IAA proteins, but also among the many other protein families that participate in small molecule sensing. Thus, we offer a model strategy for interpretation of small molecule concentrations into fine-tuned control of gene expression.

Methods

Population genetic and gene expression analyses. AtGenExpress (http://jsp.weigelworld.org/AtGenExpress/resources/) and *Arabidopsis* expression data deposited at the eFP browser (http://www.bar.utoronto.ca/) were used to retrieve and compare *A. thaliana* expression profiles for *IAA6* and *IAA19* in different tissues (full citation list in Supplementary Note 1), developmental stages[62] and natural accessions[63].

Sequence divergence between *Brassicaceaes*. *IAA6* and *IAA19 A. thaliana* sequences and the BLASTp (BLAST version 2.2.21) reciprocal best hit in *A. lyrata, A. halleri and C. rubella* were used to generate sequence alignments using the L-INS-i option in MAFFT[64]. The resulting protein alignment and the corresponding nucleotide sequences were used to compute codon alignments with Pal2Nal (ref. 65). Based on the codon alignments, nucleotide divergence was computed with a sliding window analysis (window size: 50, step: 3) with DnaSPv5.1 (ref. 66).

Phylogeny of AUX/IAA proteins in *A. thaliana*. *A. thaliana* AUX/IAA amino acid sequences were aligned using the L-INS-i option in MAFFT[64]. JTT + F + G was selected as best fitting amino acid substitution model according to the Bayesian Information Criterion in the MEGA-CC Model Selection analysis[67]. To reconstruct the phylogeny, the maximum likelihood (ML) algorithm with a bootstrap test (1000 replications) implemented in MEGA-CC was applied (additional settings: No of Discrete Gamma Categories = 5, Site Coverage Cutoff (%) = 95, ML Heuristic Method = Nearest-Neighbor-Interchange (NNI), Initial Tree for ML = Make initial tree automatically, Branch Swap Filter = None, Gaps/Missing Data Treatment = Partial deletion). The unrooted phylogenetic tree was obtained with MEGA Tree Explorer[68].

Protein expression and purification. Preparations of recombinantly expressed GST-tagged ASK1-TIR1 protein complex from SF9 insect cells were essentially performed as previously published[9,11]. GST-tagged *Arabidopsis* AUX/IAAs were expressed in *Escherichia coli* BL21 (DE3) cells carrying N-terminal GST-tagged IAA6 (AT1G52830) and IAA19 (AT3G15540) plasmids. Cells were harvested by centrifugation (5000g, 15 min) and resuspended in lysis buffer (50 mM Tris pH 8.0, 200 mM NaCl, 2.5 mM DTT, and cOmplete EDTA-free protease inhibitor (Roche)). After lysis by sonication, lysates were cleared by centrifugation, and the supernatant was used for purification either via gravity flow using GSH agarose (SERVA), or via an ÄKTA pure FPLC system using a GSTrap 4B column 1 ml (GE Healthcare). The supernatants were loaded on the column, washed with at least 5 column volumes (CV) of lysis buffer. GST-tagged proteins were eluted using 10 mM glutathione in lysis buffer, and corresponding fractions were pooled, concentrated, buffer exchanged to lysis buffer containing 15% glycerol and stored at 4 °C until use or directly used.

GST-tagged ASK1-TIR1 was expressed in Sf9 or Hi5 insect cells and purified in a similar fashion. After affinity purification using a FPLC system, the GST-tag was cleaved of by TEV protease treatment and further purified using anion exchange (MonoQ, GE Healthcare) and gel filtration chromatography (Superdex 200, GE Healthcare). Appropriate fractions were pooled, buffer exchanged to glycerol-containing buffer, concentrated, frozen in liquid nitrogen and stored at − 80 °C until use.

6xHis-UBA1 and 6xHis-UBC8 were expressed and purified from *E. coli* BL21-AI after 5 h of induction (0.01% L-Arabinose) at 28 and 22 °C, respectively. Cells were lysed in 25 mM Tris-HCl, pH 8.0, 500 mM NaCl, 20 mM imidazole, 2 mM DTT, 1 mM EDTA, 1 mM PMSF, protease inhibitor cocktail (Roche, cOmplete mini, EDTA-free). Cleared lysates were supplemented with 5 mM $MgCl_2$ and loaded onto a pre-equilibrated (wash buffer: 25 mM Tris-HCl, pH 8.0, 350 mM NaCl, 20 mM imidazole, 2 mM DTT) HisTrap FF 5 ml column (GE Healthcare) at 2 ml min^{-1}. The column was washed with 5 CV of wash buffer including 65 and 100 mM imidazole for 6xHis-UBA1 and 6xHis-UBC8, respectively. 6xHis-UBC8 was eluted with 25 mM Tris-HCl, pH 8.0, 350 mM NaCl, 400 mM imidazole, 2 mM DTT, whereas 6xHis-UBA1 was eluted with 250 mM imidazole in the same buffer. 6xHis-UBC8 was concentrated by centrifugation (10 kDa MWCO Centricon, Millipore), dialyzed and finally stored in 50 mM Tris-HCl, pH 8.0, 200 mM NaCl, 2 mM DTT and 25% (v/v) GlyOH. Elution fractions of 6xHis-UBA1 were combined, diluted with 15 volumes of anIEX equilibration buffer (50 mM Tris-HCl, pH 8.0, 5 mM NaCl, 2 mM DTT) and applied to a HiTrap Q XL 1 ml column (GE Healthcare). Elution was initiated without any wash step by a linear gradient from 5 mM NaCl to 1 M NaCl (0–100% anIEX elution buffer in 50 CV; 50 mM Tris-HCl, pH 8.0, 1 M NaCl, 2 mM DTT). 6xHis-UBA1 eluted at a salt concentration of ~330 mM NaCl. Appropriate fractions were pooled, concentrated and loaded onto a HiLoad S200 16/60 pg (GE Healthcare). 6xHis-UBA1 eluted at a retention volume of ~65 ml. 6xHis-UBA1-containing fractions were pooled, concentrated and stored as described for 6xHis-UBC8.

*Hs*Cul1-*Mm*RBX1 purification was performed using the split'n coexpress system[69]. Briefly, *E. coli* BL21 (DE3) cells expressing GST-tagged *Hs*Cul1-*Mm*RBX1 were harvested, resuspended (for buffer composition, see GST-AUX/IAA purification) and lysed by sonication. Cleared lysate was subjected to affinity chromatography using a GSTrap 4B 5 ml (ÄKTA system, GE Healthcare). Appropriate fractions were pooled, concentrated and incubated with thrombin (SERVA, see manufacturer's protocol for cleavage conditions). After dilution to approx. 40 mM NaCl, the solution was subjected to anion exchange and gel filtration chromatography. *Hs*Cul1-*Mm*RBX1-containing fractions were pooled, buffer exchanged to 15% glycerol-containing lysis buffer, frozen in liquid nitrogen and stored at −80 °C.

[^{3}H]-labelled auxin binding assay. Radioligand binding assays were performed using 20 nM purified ASK1-TIR1 protein complexes, as well as 2–15 μM GST-tagged AUX/IAAs (except Supplementary Fig. 88e,f, where GST has been cleaved off IAA6) or their GST-aux/iaa dominant mutant versions, and [^{3}H]IAA with a specific activity of 25 Ci/mmol from American Radiolabeled Chemicals, Inc. All reactions were carried out in a volume of 100 μl (for additional details see[11,70]). Nonspecific binding was determined using at least 500 × excess of cold IAA with respect to [^{3}H]IAA. Specific binding was calculated as the average of at least two measurements of nonspecific binding subtracted from total binding. For saturation-binding assays, samples were prepared as above and incubated with at least six IAA concentrations on either side of the K_d of a given co-receptor pair. The saturation-binding curves were fitted to the Morrison equation for tight binding[71]. Since nonspecific binding exceeded 10% of total binding in all independent experiments, total binding data were additionally analysed according to Swillens, *Mol Pharm*, 1995 (ref. 72). For homologous competition binding assays, ASK1-TIR1 as well as GST-tagged AUX/IAA proteins were incubated with a fix concentration of either 50 or 25 nM [^{3}H]IAA for experiments with IAA6 and IAA19, respectively. Data of three independent experiments ($n = 3$) were plotted against the concentration of cold IAA and fitted with built-in analysis (one-site fit logIC50) of Prism5, GraphPad Software, Inc. Importantly, formation of ASK1-TIR1-IAA-AUX/IAA complexes cannot be strictly described using the above models *per se*. Auxin co-receptor complex formation is expected to be consisting of reversible binding events with yet unknown hierarchy. An intuitive model would assume that TIR1 and auxin form first a TIR1:auxin complex. This partial reaction is described by the dissociation constant K_D^{auxin}. Next, the TIR1:auxin complex binds the AUX/IAA with a high-affinity $K_D^{AUX/IAA}$. Using an excess of AUX/IAA over TIR1, thus allows to assume a bimolecular association between ASK1-TIR1-AUX/IAA co-receptors and [^{3}H]IAA. In radioligand binding assays, neither dissociation constant of the partial reactions is assessable. Therefore, it can be assumed that in the auxin binding assays, one actually determines the apparent dissociation constant K_D' for ternary complex formation from the reactants, *i.e.* the net binding reaction.

E2-charging assays. Reactions for E2~Ub thioester formation were performed using 50 μM *At*Ubiquitin (*At*Ub) or *Hs*Ubiquitin mutants containing one Lys residue available (Boston Biochem, UM-HK480-01M, UM-HK630-01M, UM-HK290-01M), 2 μM of 6 × His-UBA1 and 20 μM 6xHis-E2 protein (UBC1, UBC4 or UBC8) mixed in thioester buffer (10 mM HEPES, pH 7.5, 100 mM NaCl, 4 mM ATP and 20 mM $MgCl_2$). Reactions were incubated at room temperature for 10 min, and subsequently mixed with reducing (containing 40 mM DTT) or non-reducing (without DTT) SDS-sample buffer. Samples were boiled for another 10 min and afterwards resolved by 15% SDS-PAGE followed by Coomassie staining or immunoblot detection using 1:500 or 1:1,000 dilution of monoclonal anti-Ub (P4D1) (Santa Cruz, SC-8017), and 1:10,000 anti-mouse HRP (Thermo Scientific, Cat. # 31430).

***In vitro* reconstitution of Ub-conjugation.** Proteins were prepared as described above and amounts are expressed relative to AUX/IAA concentrations ([AUX/IAA]). Two mixtures (mix A and mix B) were prepared in parallel. Mix A contained 7.5 to 10 fold molar excess of Ub (either 6xHis-*Hs*Ub or *At*Ub), 6xHis-*At*UBC8 (1x [AUX/IAA]) and 6xHis-Uba1 (0.1–0.2x [AUX/IAA]) in reaction buffer (30 mM Tris-HCl, pH 8.0, 100 mM NaCl, 2 mM DTT, 5 mM $MgCl_2$, 1 μM $ZnCl_2$, 2 mM ATP. Mix B was prepared by mixing 0.1x [AUX/IAA] of Cul1-RBX1, 0.1x [AUX/IAA] of ASK1-TIR1 with AUX/IAA in reaction buffer. Mix B was aliquoted and supplemented with indicated amounts of IAA. Mixtures A and B were separately incubated for 5 min at 25 °C with shaking at 500 rpm. Equal volumes of mix A and B were combined to initiate the ubiquitylation reaction (0 min). Aliquots were taken at specified time points and reactions were stopped by denaturation in 2X Laemmli buffer. Protein samples were electrophoretically separated in either 8% or 5–15% mini- or maxi- polyacrylamide gradient gels, and transferred onto nitrocellulose membranes. Immobilized Ub-conjugated proteins were detected with monoclonal anti-Ub (P4D1) as described above, or with 1:10,000 dilution of polyclonal anti-GST in rabbit (Sigma, G7781), and 1:10,000 anti-rabbit HRP in goat (Santa Cruz, SC-2004) as secondary antibody.

For quantification of ubiquitin conjugates, IVU reactions were performed as described above with the following modifications. 50 μM fluorescein-labelled ubiquitin (UBPBio, S20C) instead of *At*Ub was included in the reactions. IVU reactants were adjusted accordingly: Mix A contained 10 fold molar excess of fluorescein-labelled Ub, 6 × His-AtUBC8 (0.4x [AUX/IAA]) and 6xHis-Uba1 (0.04x [AUX/IAA]); and Mix B contained 0.2 × [AUX/IAA] of Cul1-RBX1, 0.2 × [AUX/IAA] of ASK1-TIR1 with AUX/IAA and 750 nM IAA. Mix A and Mix B were prepared in reaction buffer and IVU reactions were incubated at 25 °C between 0 and 40 min. IVU reactions were separated by SDS − polyacrylamideage followed by immunoblotting using primary anti-GST antibody (1:10,000; Sigma, G7781) and secondary anti-rabbit Alexa Fluor Plus 647 antibody (1:20,000) (Thermo Fischer Scientific, A32733). Nitrocellulose membranes were scanned using a Typhoon FLA9500 system (473 nm excitation wavelength and LPB filter for ubiquitin signal detection and 635 nm excitation wavelength and LPR filter for GST signal). Fluorescent signals located between GST-tagged AUX/IAAs, and ubiquitylated Cullin (~50 kDa), which correspond to IAA6- and IAA19-ubiquitin conjugates (see Fig. 2c) were quantified for each lane using ImageQuant TL software automatic lane detection. Background subtracted signals were used to generate ratios between auxin-dependent and independent ubiquitylation of GST-IAA6 and GST-IAA19. In the same way, the relative ubiquitin signal corresponding to the ratios between ubiquitin conjugates on GST-IAA19 over GST-IAA6 were generated. Two fluorescence signals were excluded (T0) due to their low intensity, which otherwise would have resulted in artificial high ratios. To evaluate for significance, a two-way ANOVA with Bonferroni multiple comparisons post-tests was performed using GraphPad Prism software.

LC-MS analyses. IVU reactions were performed as described above. Three sets of IVUs, corresponding to three independent (biological) replicates, were carried out on consecutive weeks using AUX/IAA proteins from different batch preparations. After 30 min, 20 μl IVUs were stopped by denaturing with 1 volume 16M urea. Proteins were further reduced by adding 0.5 μl of 200 mM dithiothreitol (DTT), and alkylated by adding 2 μl of 200 mM iodoacetamide. The reactions were quenched with 2 μl of 200 mM DTT, and subsequently 320 μl of 50 mM ammonium bicarbonate pH 8.5 were added. Alternatively, samples were also processed without reduction and alkylation. Proteins in the IVU reactions were digested with trypsin (enzyme to substrate 1:50 (w/w)) at 37 °C with gentle agitation overnight. Reactions were quenched by adding formic acid (FA) to a final concentration of 0.1%, and the peptides were desalted as previously described[73]. Dried peptides were dissolved in 5% acetonitrile, 0.1% trifluoric acid, and 0.5 μg were injected into the LC-MS system. Peptides were separated using liquid chromatography C18 reverse phase chemistry employing a 120 min gradient increasing from 5 to 40% acetonitrile in 0.1% FA, and a flow rate of 250 nl min^{-1}. Eluted peptides were electrosprayed online into a QExactive Plus mass spectrometer (Thermo Fisher Scientific). The spray voltage was 1.9 kV, the capillary temperature 275 °C and the Z-Lens voltage 240 V. A full MS survey scan was carried out with chromatographic peak width set to 15 s, resolution 70,000, automatic gain control (AGC) 3E + 06 and a max injection time (IT) of 200 ms. MS/MS peptide sequencing was performed using a Top10 DDA scan strategy with HCD fragmentation. MS/MS scans were acquired with resolution 17,500, AGC 5E + 04, IT 150 ms, isolation width 1.6 *m/z*, normalized collision energy 28, under fill ratio 3%, dynamic exclusion duration 40 s, and an intensity threshold of 1E + 04. Peptides were identified and ubiquitylated residues on identified peptides were mapped using both the Mascot software v2.5.0 (Matrix Science) linked to Proteome Discoverer v1.4 (Thermo Fisher Scientific), and the MaxQuant software v1.5.0.0. A precursor ion mass error of 5 and ,7 p.p..m respectively and a fragment ion mass error of 0.02 Da and 20 m.m.u. ,respectively were tolerated in searches of a custom made database containing the IVU proteins. GG and LRGG on lysine (K) and on serine, threonine and cysteine (S,T,C), as well as oxidation of methionine (M) were tolerated as variable modifications. Cysteine carbamidomethylation was set as a fixed modification in searches of reduced and alkylated samples. A PSM, and peptide level false discovery rate (FDR) threshold of 0.01 was applied for peptide identification employing the target-decoy database model. All ubiquitylated

peptides that were also identified in IVUs lacking Ub (negative control) were discarded. Only in three cases, ubiquitylated peptides were identified in which K ubiquitylation produced the same scores as S,T,C ubiquitylation, in all other cases K ubiquitylation scored higher. Therefore in those cases when the ubiquitylation site(s) was alternatively mapped to a K or a S,T or C residue on the same peptide, S,T,C ubiquitylation was deprecated. An FDR specifically for the identification of ubiquitylated peptides was calculated. Ubiquitylated peptides in the IVUs lacking Ub (negative control) were used to model the H_0 of random peptide spectral matching and estimate the number of false positives (FP). Ubiquitylated peptides identified in the IVUs containing Ub (supplemented with AUX/IAA or not) were used to estimate the number of true and false positives (TP + FP), because while all Ub identifications in the negative control are FP by design, only some in the IVUs containing Ub will also be FP. The number of acquired MS/MS spectra and PSMs was essentially the same for the negative control and targets (190272, 178910, 182152 MS/MS spectra and 38994, 38984, 40288 PSMs respectively) underscoring the validity of the H_0 model. The simple FDR was calculated as FP/TP + FP. The percentage incorrect in target (FP in denominator; PIT) was estimated by determining the ratio of non-significant to total peptide identifications by the Mascot software. The simple FDR was adjusted accordingly (for further explanations see[74]). All mass spectrometry proteomics data have been deposited to the ProteomeXchange Consortium via the PRIDE[75] partner repository (http://www.ebi.ac.uk/pride/archive/) with the data set identifier PXD004027 and 10.6019/PXD004027.

Meta-structure analyses. Meta-structure analyses for compactness were carried out using the primary structure of IAA6 and IAA19. Plots of compactness and secondary structure are predictions based on collected pdb structures and aa contacts[76].

Ratiometric analysis in *Arabidopsis* protoplasts. Sensor constructs for expression in plant protoplasts were generated as described in (ref. 56). In brief, the cDNAs of IAA6, IAA19 or their dominant mutated versions iaa6/shy1-1 or iaa19/msg2-1 were amplified and Gibson cloned into the existing pMIR expression vector, where the sensor module (L2min17-Luc) was replaced. Sensors encode for renilla-2A-SM-firefly fusions under the control of a CaMV 35S promoter.

For protoplast isolation, two to three-week old plants *of A. thaliana* (*Col-0*) or *tir1-1, afb1-3, afb1-2 afb2-3, tir1-1 afb2-3, tir1-1 afb3-4* grown at a 16 h light regime at 23 °C were used. Tissue pre-plasmolysis, digestion, protoplast isolation and transformation were performed according to (ref. 77). For each ratiometric construct tested, five separate transformations with 500,000 protoplasts in a final volume of 1.6 ml were made in a six-well plate, sealed with parafilm, and incubated in the dark for 24 h. Before induction with different IAA concentrations, the replicate transformations were pooled and 1 ml of protoplast solution was transferred into a 2 ml deep-well storage plate for every auxin concentration to be tested. Serial dilutions of IAA solutions in PCA-M medium (PCA salts, 600 mOsm mannitol, pH 5.8) were prepared at 11-fold concentration, and 100 µl were added to the protoplasts to obtain the appropriate final auxin concentration. For luminescence determinations, 80 µl of protoplast suspensions of each *A. thaliana* genetic background transformed with the sensor constructs were transferred to 96-well flat-bottom white plates. After addition of 20 µl of either firefly luciferase substrate (20 mM Tricine, 2.67 mM $MgSO_4$, 0.1 mM EDTA, 33.3 mM DTT, 0.52 mM ATP, 0.27 mM acetyl-CoA, 5 mM NaOH, 0.264 mM $MgCO_3$, 0.47 mM luciferin), or renilla luciferase substrate (472 µM coelenterazine stock solution in methanol; diluted 1:15 in PBS directly before use). Samples were incubated in the dark for 30 min upon which firefly and renilla luminescence were monitored using either a Synergy 4 multimode microplate reader (BioTek Instruments Inc., Winooski, VT) or an Infinite M200 Pro (Tecan Group Ltd., Männedorf, Switzerland). Firefly and Renilla values for the different sensors in the different backgrounds were normalized and one- or two-way ANOVA statistical analyses were performed using RLPlot version 1.5, together with Bonferroni post-tests in GraphPad Software, Inc. Heat maps were generated in R (http://www.R-project.org/) using the gplots package with default parameters.

Statistical analysis. Statistical analyses were performed using GraphPad Prism version 6.0, GraphPad Software, La Jolla,1 California, USA. Data were analysed by either Student's *t*-tests (two-tailed), one-way ANOVA with Tukey's honest significant difference as *post hoc* test, or two-way ANOVA with Bonferroni tests to correct for multiple testing unless otherwise stated. All experiments were repeated at least three times consisting of three-independent biological replicates. Heatmaps were generated in R (www.r-project.org) using the gplots package.

Data availability. The authors declare that all data supporting the finding of this study are available within the article and its Supplementary Information or are available from the corresponding author upon request. Multiple sequence alignments have deposited in Figshare: https://figshare.com/s/6e202a97eb8034bbb1d9 and the mass spectrometry proteomics data have been deposited to the ProteomeXchange Consortium via the PRIDE partner repository with the data set identifier PXD004027 and Project DOI:10.6019/PXD004027.

References

1. Kelley, D. R. & Estelle, M. Ubiquitin-mediated control of plant hormone signaling. *Plant Physiol.* **160,** 47–55 (2012).
2. Stone, S. L. & Callis, J. Ubiquitin ligases mediate growth and development by promoting protein death. *Curr. Opin. Plant Biol.* **10,** 624–632 (2007).
3. Hua, Z. & Vierstra, R. D. The cullin-RING ubiquitin-protein ligases. *Annu. Rev. Plant Biol.* **62,** 299–334 (2011).
4. Genschik, P., Marrocco, K., Bach, L., Noir, S. & Criqui, M. C. Selective protein degradation: a rheostat to modulate cell-cycle phase transitions. *J. Exp. Bot.* **65,** 2603–2615 (2014).
5. Thomann, A., Dieterle, M. & Genschik, P. Plant CULLIN-based E3s: phytohormones come first. *FEBS Lett.* **579,** 3239–3245 (2005).
6. Chapman, E. J. & Estelle, M. Mechanism of auxin-regulated gene expression in plants. *Annu. Rev. Genet.* **43,** 265–285 (2009).
7. Dharmasiri, N., Dharmasiri, S. & Estelle, M. The F-box protein TIR1 is an auxin receptor. *Nature* **435,** 441–445 (2005).
8. Kepinski, S. & Leyser, O. The *Arabidopsis* F-box protein TIR1 is an auxin receptor. *Nature* **435,** 446–451 (2005).
9. Tan, X. *et al.* Mechanism of auxin perception by the TIR1 ubiquitin ligase. *Nature* **446,** 640–645 (2007).
10. Yu, H. *et al.* Untethering the TIR1 auxin receptor from the SCF complex increases its stability and inhibits auxin response. *Nat. Plants* **1,** 14030 (2015).
11. Calderón Villalobos, L. I. *et al.* A combinatorial TIR1/AFB-Aux/IAA co-receptor system for differential sensing of auxin. *Nat. Chem. Biol.* **8,** 477–485 (2012).
12. Boer, D. R. *et al.* Structural basis for DNA binding specificity by the auxin-dependent ARF transcription factors. *Cell* **156,** 577–589 (2014).
13. Han, M. *et al.* Structural basis for the auxin-induced transcriptional regulation by Aux/IAA17. *Proc. Natl Acad. Sci. USA* **111,** 18613–18618 (2014).
14. Korasick, D. A. *et al.* Molecular basis for auxin response facTOR protein interaction and the control of auxin response repression. *Proc. Natl Acad. Sci. USA* **111,** 5427–5432 (2014).
15. Nanao, M. H. *et al.* Structural basis for oligomerization of auxin transcriptional regulators. *Nat. Commun.* **5,** 3617 (2014).
16. Guilfoyle, T. J. & Hagen, G. Auxin response factors. *Curr. Opin. Plant Biol.* **10,** 453–460 (2007).
17. Overvoorde, P. J. *et al.* Functional genomic analysis of the auxin/indole-3-acetic acid gene family members in *Arabidopsis thaliana*. *Plant Cell* **17,** 3282–3300 (2005).
18. Moss, B. L. *et al.* Rate motifs tune Aux/IAA degradation dynamics. *Plant Physiol.* (2015).
19. Dinesh, D. C., Calderón Villalobos, L. I. & Abel, S. Structural biology of nuclear auxin action. *Trends Plant Sci.* **21,** 302–316 (2016).
20. Krogan, N. T., Yin, X., Ckurshumova, W. & Berleth, T. Distinct subclades of Aux/IAA genes are direct targets of ARF5/MP transcriptional regulation. *New Phytol.* **204,** 474–483 (2014).
21. Jing, H. *et al.* Peptidyl-prolyl isomerization targets rice Aux/IAAs for proteasomal degradation during auxin signalling. *Nat. Commun.* **6,** 7395 (2015).
22. Gray, W. M., Kepinski, S., Rouse, D., Leyser, O. & Estelle, M. Auxin regulates SCF(TIR1)-dependent degradation of AUX/IAA proteins. *Nature* **414,** 271–276 (2001).
23. Nishimura, K., Fukagawa, T., Takisawa, H., Kakimoto, T. & Kanemaki, M. An auxin-based degron system for the rapid depletion of proteins in nonplant cells. *Nat. Methods* **6,** 917–922 (2009).
24. Natsume, T., Kiyomitsu, T., Saga, Y. & Kanemaki, M. T. Rapid protein depletion in human cells by auxin-inducible degron tagging with short homology donors. *Cell Rep.* **15,** 210–218 (2016).
25. Mattiroli, F. & Sixma, T. K. Lysine-targeting specificity in ubiquitin and ubiquitin-like modification pathways. *Nat. Struct. Mol. Biol.* **21,** 308–316 (2014).
26. Fishbain, S. *et al.* Sequence composition of disordered regions fine-tunes protein half-life. *Nat. Struct. Mol. Biol.* **22,** 214–221 (2015).
27. Guharoy, M., Bhowmick, P., Sallam, M. & Tompa, P. Tripartite degrons confer diversity and specificity on regulated protein degradation in the ubiquitin-proteasome system. *Nat. Commun.* **7,** 10239 (2016).
28. Weijers, D. & Wagner, D. Transcriptional responses to the auxin hormone. *Annu. Rev. Plant Biol.* **67,** 539–574 (2016).
29. Remington, D. L., Vision, T. J., Guilfoyle, T. J. & Reed, J. W. Contrasting modes of diversification in the Aux/IAA and ARF gene families. *Plant Physiol.* **135,** 1738–1752 (2004).
30. Kalluri, U. C., Difazio, S. P., Brunner, A. M. & Tuskan, G. A. Genome-wide analysis of Aux/IAA and ARF gene families in *Populus trichocarpa*. *BMC Plant Biol.* **7,** 59 (2007).

31. Gout, J. F., Kahn, D. & Duret, L. The relationship among gene expression, the evolution of gene dosage, and the rate of protein evolution. *PLoS Genet.* **6,** e1000944 (2010).
32. Kim, B. C., Soh, M. S., Kang, B. J., Furuya, M. & Nam, H. G. Two dominant photomorphogenic mutations of *Arabidopsis thaliana* identified as suppressor of *hy2*. *Plant J.* **9,** 441–456 (1996).
33. Reed, J. Roles and activities of Aux/IAA proteins in *Arabidopsis*. *Trends Plant Sci.* **6,** 420–425 (2001).
34. Muto, H., Watahiki, M. K., Nakamoto, D., Kinjo, M. & Yamamoto, K. T. Specificity and similarity of functions of the Aux/IAA genes in auxin signaling of Arabidopsis revealed by promoter-exchange experiments among MSG2/IAA19, AXR2/IAA7, and SLR/IAA14. *Plant Physiol.* **144,** 187–196 (2007).
35. Tatematsu, K. *et al.* MASSUGU2 encodes Aux/IAA19, an auxin-regulated protein that functions together with the transcriptional activator NPH4/ARF7 to regulate differential growth responses of hypocotyl and formation of lateral roots in *Arabidopsis thaliana*. *Plant Cell* **16,** 379–393 (2004).
36. Li, H., Tiwari, S. B., Hagen, G. & Guilfoyle, T. J. Identical amino acid substitutions in the repression domain of auxin/indole-3-acetic acid proteins have contrasting effects on auxin signaling. *Plant Physiol.* **155,** 1252–1263 (2011).
37. Yang, Z. PAML 4: phylogenetic analysis by maximum likelihood. *Mol. Biol. Evol.* **24,** 1586–1591 (2007).
38. Li, T., Pavletich, N. P., Schulman, B. A. & Zheng, N. High-level expression and purification of recombinant SCF ubiquitin ligases. *Methods Enzymol.* **398,** 125–142 (2005).
39. Ye, Y. & Rape, M. Building ubiquitin chains: E2 enzymes at work. *Nat. Rev. Mol. Cell Biol.* **10,** 755–764 (2009).
40. Kelly, A., Wickliffe, K. E., Song, L., Fedrigo, I. & Rape, M. Ubiquitin chain elongation requires E3-dependent tracking of the emerging conjugate. *Mol. Cell* **56,** 232–245 (2014).
41. Christensen, D. E., Brzovic, P. S. & Klevit, R. E. E2-BRCA1 RING interactions dictate synthesis of mono- or specific polyubiquitin chain linkages. *Nat. Struct. Mol. Biol.* **14,** 941–948 (2007).
42. Meyer, H. J. & Rape, M. Enhanced protein degradation by branched ubiquitin chains. *Cell* **157,** 910–921 (2014).
43. Hatfield, P. M., Gosink, M. M., Carpenter, T. B. & Vierstra, R. D. The ubiquitin-activating enzyme (E1) gene family in *Arabidopsis thaliana*. *Plant J.* **11,** 213–226 (1997).
44. Kraft, E. *et al.* Genome analysis and functional characterization of the E2 and RING-type E3 ligase ubiquitination enzymes of *Arabidopsis*. *Plant Physiol.* **139,** 1597–1611 (2005).
45. Zhao, Q. *et al.* A plant-specific *in vitro* ubiquitination analysis system. *Plant J* **74,** 524–533 (2013).
46. Hong, J. H., Ng, D., Srikumar, T. & Raught, B. The use of ubiquitin lysine mutants to characterize E2-E3 linkage specificity: mass spectrometry offers a cautionary 'tail'. *Proteomics* **15,** 2910–2915 (2015).
47. Dharmasiri, N. *et al.* Plant development is regulated by a family of auxin receptor F box proteins. *Dev. Cell* **9,** 109–119 (2005).
48. Gray, W. M. *et al.* Identification of an SCF ubiquitin-ligase complex required for auxin response in *Arabidopsis thaliana*. *Genes Dev.* **13,** 1678–1691 (1999).
49. Kepinski, S. & Leyser, O. Auxin-induced SCFTIR1-Aux/IAA interaction involves stable modification of the SCFTIR1 complex. *Proc. Natl Acad. Sci. USA* **101,** 12381–12386 (2004).
50. Gilkerson, J., Kelley, D. R., Tam, R., Estelle, M. & Callis, J. Lysine residues are not required for proteasome-mediated proteolysis of the auxin/indole acidic acid protein IAA1. *Plant Physiol.* **168,** 708–720 (2015).
51. McDowell, G. S. & Philpott, A. Non-canonical ubiquitylation: mechanisms and consequences. *Int. J. Biochem. Cell Biol.* **45,** 1833–1842 (2013).
52. Hochstrasser, M. Lingering mysteries of ubiquitin-chain assembly. *Cell* **124,** 27–34 (2006).
53. David, Y. *et al.* E3 ligases determine ubiquitination site and conjugate type by enforcing specificity on E2 enzymes. *J. Biol. Chem.* **286,** 44104–44115 (2011).
54. Komander, D. The emerging complexity of protein ubiquitination. *Biochem. Soc. Trans.* **37,** 937–953 (2009).
55. Komander, D. & Rape, M. The ubiquitin code. *Annu. Rev. Biochem.* **81,** 203–229 (2012).
56. Wend, S. *et al.* A quantitative ratiometric sensor for time-resolved analysis of auxin dynamics. *Sci. Rep.* **3,** 2052 (2013).
57. Havens, K. A. *et al.* A synthetic approach reveals extensive tunability of auxin signaling. *Plant Physiol.* **160,** 135–142 (2012).
58. Maraschin Fdos, S., Memelink, J. & Offringa, R. Auxin-induced, SCF(TIR1)-mediated poly-ubiquitination marks AUX/IAA proteins for degradation. *Plant J.* **59,** 100–109 (2009).
59. Fischer, E. S. *et al.* The molecular basis of CRL4DDB2/CSA ubiquitin ligase architecture, targeting, and activation. *Cell* **147,** 1024–1039 (2011).
60. Tang, X. *et al.* Suprafacial orientation of the SCFCdc4 dimer accommodates multiple geometries for substrate ubiquitination. *Cell* **129,** 1165–1176 (2007).
61. Xia, Z. P. *et al.* Direct activation of protein kinases by unanchored polyubiquitin chains. *Nature* **461,** 114–119 (2009).
62. Schmid, M. *et al.* A gene expression map of *Arabidopsis thaliana* development. *Nat. Genet.* **37,** 501–506 (2005).
63. Lempe, J. *et al.* Diversity of flowering responses in wild *Arabidopsis thaliana* strains. *PLoS Genet.* **1,** 109–118 (2005).
64. Katoh, K., Kuma, K., Toh, H. & Miyata, T. MAFFT version 5: improvement in accuracy of multiple sequence alignment. *Nucleic Acids Res.* **33,** 511–518 (2005).
65. Suyama, M., Torrents, D. & Bork, P. PAL2NAL: robust conversion of protein sequence alignments into the corresponding codon alignments. *Nucleic Acids Res.* **34,** W609–W612 (2006).
66. Librado, P. & Rozas, J. DnaSP v5: a software for comprehensive analysis of DNA polymorphism data. *Bioinformatics* **25,** 1451–1452 (2009).
67. Kumar, S., Stecher, G., Peterson, D. & Tamura, K. MEGA-CC: computing core of molecular evolutionary genetics analysis program for automated and iterative data analysis. *Bioinformatics* **28,** 2685–2686 (2012).
68. Tamura, K. *et al.* MEGA5: molecular evolutionary genetics analysis using maximum likelihood, evolutionary distance, and maximum parsimony methods. *Mol. Biol. Evol.* **28,** 2731–2739 (2011).
69. Petroski, M. D. & Deshaies, R. J. *In vitro* reconstitution of SCF substrate ubiquitination with purified proteins. *Methods Enzymol.* **398,** 143–158 (2005).
70. Hellmuth, A. & Calderón Villalobos, L. I. Radioligand binding assays for determining dissociation constants of phytohormone receptors. *Methods Mol. Biol.* **1450,** 23–34 (2016).
71. Morrison, J. F. Kinetics of the reversible inhibition of enzyme-catalysed reactions by tight-binding inhibitors. *Biochim. Biophys. Acta* **185,** 269–286 (1969).
72. Swillens, S. Interpretation of binding curves obtained with high receptor concentrations: practical aid for computer analysis. *Mol. Pharmacol.* **47,** 1197–1203 (1995).
73. Majovsky, P. *et al.* Targeted proteomics analysis of protein degradation in plant signaling on an LTQ-Orbitrap mass spectrometer. *J. Proteome Res.* **13,** 4246–4258 (2014).
74. Kaell, L., Storey, J. D., MacCoss, M. J. & Noble, W. S. Assigning significance to peptides identified by tandem mass spectrometry using decoy databases. *J. Proteome Res.* **7,** 29–34 (2008).
75. Vizcaino, J. A. *et al.* update of the PRIDE database and its related tools. *Nucleic Acids Res.* **44,** D447–D456 (2016).
76. Konrat, R. The protein meta-structure: a novel concept for chemical and molecular biology. *Cell Mol. Life Sci.* **66,** 3625–3639 (2009).
77. Ochoa-Fernandez, R. *et al.* in *Optogenetics—Methods and Protocols*. (ed. K. A.) (Springer, New York, 2015).
78. Winter, D. *et al.* An 'electronic fluorescent pictograph' browser for exploring and analyzing large-scale biological data sets. *PLoS ONE* **2,** e718 (2007).
79. Duda, D. M. *et al.* Structural insights into NEDD8 activation of cullin-RING ligases: conformational control of conjugation. *Cell* **134,** 995–1006 (2008).
80. Zheng, N. *et al.* Structure of the Cul1-Rbx1-Skp1-F boxSkp2 SCF ubiquitin ligase complex. *Nature* **416,** 703–709 (2002).

Acknowledgements

We thank Elisabeth J. Chapman for helpful discussions and comments to the manuscript. We also acknowledge Kristian Ullrich for the initial assessments on molecular population genetics; Roman Lassig for support with E2 expression; Robert Konrat and Dariush Hinderberger for advice on IDPs and compactness and data handling; and Carolin Delker for help with heat maps and statistical analyses. We gratefully acknowledge financial support from the Deutsche Forschungsgemeinschaft (DFG CA716/2-1), and IPB core funding from the Leibniz Association. We dedicate this work to the memory of Andreas Winkler.

Author contributions

M.W. and L.I.A.C.V. prepared the manuscript and designed the experiments. M.W. and M.N. performed the experiments and analysed the data. A.H. and L.I.A.C.V purified TIR1-ASK1 complex, and A.H., M.W. and V.W. generated constructs and performed Y2H assays. P.J. and M.Q. carried out population genetic and gene expression analyses. M.T. provided E1 and E2 expression clones. G.C. carried out E2-charging assays, and M.N. and M.W. executed and validated IVU and MassSpec data. P.M. and W.H. performed and hosted LC-MS analyses, respectively, and W.H. processed the data. S.S. and M.Z. designed, carried out ratiometric experiments, and analysed the data. M.Z., M.Q., M.T., W.H. provided input to the manuscript. L.I.A.C.V oversaw the project and all authors approved the intellectual content.

Additional information

Supplementary Information accompanies this paper at http://www.nature.com/naturecommunications

Competing interests: The authors declare no competing financial interests.

Reprints and permission information is available online at http://npg.nature.com/reprintsandpermissions/

How to cite this article: Winkler, M. *et al.* Variation in auxin sensing guides AUX/IAA transcriptional repressor ubiquitylation and destruction. *Nat. Commun.* **8**, 15706 doi: 10.1038/ncomms15706 (2017).

Publisher's note: Springer Nature remains neutral with regard to jurisdictional claims in published maps and institutional affiliations.

2.2 Niemeyer M. *et al.* Flexibility of intrinsically disordered degrons in AUX/IAA proteins reinforces auxin co-receptor assemblies

Niemeyer M, Moreno Castillo E, Ihling CH, Iacobucci C, Wilde V, Hellmuth A, Hoehenwarter W, Samodelov SL, Zurbriggen MD, Kastritis PL, Sinz A, Calderón Villalobos LIA. (2020) Flexibility of intrinsically disordered degrons in AUX/IAA proteins reinforces auxin co-receptor assemblies. ***Nat Commun*** May 8;11(1):2277. doi: 10.1038/s41467-020-16147-2.

2.2.1 Aims and summary of the results

In Niemeyer et al., we aimed at unveiling the structural properties of fast-diverging, unresolved regions in AUX/IAAs, that were shown to be ubiquitylated in Winkler *et al.*. These regions are the most variable feature within the AUX/IAA protein family, and potentially drive the differential auxin sensing capabilities of distinct TIR1·AUX/IAA auxin co-receptor systems. I sought to go beyond mechanistic studies and addressed how conformational flexibility and intrinsic disorder in AUX/IAAs impact auxin sensing, and further processing by the degradation machinery. We structurally characterized the distantly-related AUX/IAAs, IAA7 and IAA12, and experimentally categorized their degron flanking regions as intrinsically disordered. Intrinsic disorder regions (IDRs) adjacent to the core AUX/IAA degron were predicted to be a general feature of most AUX/IAA members. Through a structural proteomics and biochemistry approach, I uncovered how structural disorder in AUX/IAAs shapes their conformational ensembles by exposing and bridging TIR1·AUX/IAA interaction sites. The accumulation of ubiquitylation sites in AUX/IAA IDRs suggests they are either favorably placed or exposed upon SCF^{TIR1}·AUX/IAA complex formation. In order to investigate how IDRs are positioned when TIR1 and AUX/IAAs interact, we analyzed the overall TIR1·AUX/IAA complex topology in presence of IAA using XL-MS. Crosslinks of the TIR1·auxin·AUX/IAA complex revealed that AUX/IAAs lay extended on TIR1, spanning the entire width of TIR1 LRRs mainly contacting two distinct patches opposite sides of TIR1. One patch secures the flexible N-terminus around the KR, and EAR motifs of AUX/IAAs, while the other patch engage the AUX/IAA PB1 domain. The latter is proposed to be positioned on TIR1 by the disordered degron tail that functions as a flexible joint. This interplay of IDRs and the PB1 domain facilitates specific lysines to be exposed for ubiquitin transfer. Following a detailed structural and

computational analysis of TIR1·auxin·AUX/IAA complex interfaces, we identified additional key residues in TIR1 (S201, R220, D481) that contribute to high-affinity receptor assemblies *via* auxin-independent interactions. Based on the identified residues, we created *tir1* mutant plants and showed that the putative KR-contacting D481, and the PB1 domain-interacting S201 in TIR1 are required for full auxin-responsiveness *in vivo*. We were also able to unveil a new hypersensitive TIR1 allele (R220A), which might act as a sentry close to the degron binding pocket in TIR1, facilitating the recruitment of distinct AUX/IAAs over others. My studies provided first-time evidence for a multivalent TIR1·AUX/IAA interaction model, in which a degradation signal (degron) drives auxin-mediated interaction, but it is not the sole contributor to auxin receptor formation.

Our results allow us to postulate a two-way model for TIR1·AUX/IAA complex assembly: On one side, IDRs in AUX/IAAs position them on TIR1 *via* auxin-independent interactions, followed by degron-driven TIR1·AUX/IAA interactions that seal off the auxin binding pocket in TIR1. Alternatively, auxin-dependent binding of the AUX/IAA degron to TIR1 initiate AUX/IAA recruitment, followed by IDR-driven, auxin-independent positioning of AUX/IAA degron flanking regions and the PB1 domain. In both cases, auxin binding is facilitated by IDRs in AUX/IAAs enabling correct positioning of ubiquitylation sites, and prolonged residency time of the AUX/IAAs on TIR1 for processive ubiquitylation.

2.2.2 Contributions

Own contributions:

Niemeyer *et al*, represents the pinnacle of my doctoral research project. This study based on previous work (Tan et al. (2007); Calderón Villalobos et al. (2012) and Winkler et al. (2017), see chapter 2.1) dwells with the structural and biochemical requirements for auxin-driven and IDR-tuned AUX/IAA recognition, and ubiquitylation by the SCF^{TIR1} E3 ligase. From a technical standpoint, I spearheaded the implementation of a chemical cross-linking/mass spectrometry (XL-MS) approach, as a powerful tool for 3D structure visualization of auxin receptor ensembles in action. As a result, we obtained the first topology model of an intrinsically disordered ubiquitylation target recruited by an SCF-type E3 ubiquitin ligase. Given the challenges for capturing structural

information of IDPs, the experimental set up I and my coauthors brought about in Niemeyer *et al.*, offers a unique opportunity, not only relevant for plant research. Niemeyer *et al.* evidenced it is technically possible to capture hormone receptors in action in order to obtain snapshots of the complex regulatory interplays during protein-protein and protein-small molecule interactions.

Estimated percentage-based author (M. Niemeyer) contribution to experimental work:

Biochemical and biophysical analyses: protein expressions and purification (100%), IVU assay (100%), yeast-two-hybrid analyses (60%), crosslinking (XL) experiments (100%) and sample preparation for LC-MS/MS (80%), size exclusion chromatography (SEC) (100%), circular dichroism (CD) spectroscopy (100%), radioligand (auxin) binding experiments (100%), sequence disorder analysis (100%), protein-protein docking (40%).

Molecular and *in vivo* analyses: cloning, mutagenesis and plant transformation (40%), auxin response root elongation assays (REAs) (30%).

Data analysis: CD, SEC, XL-coupled to LC/MS-MS, auxin binding kinetics, and REA assays (90%), analysis of *in silico* computational simulations (10%).

Estimated percentage-based author (M. Niemeyer) contribution to written manuscript:

Writing (40%), experimental design (70%), design and preparation of 7 of 8 main figures, 11 of 15 supplementary figures, and 3 tables (80%).

See "Author Contributions" section at the end of the manuscript for detailed description of input and experimental support from our scientific collaborators in this study.

2.2.3 Original publication

See next page. Supplementary Material in Chapter 7.2.

nature COMMUNICATIONS

ARTICLE

https://doi.org/10.1038/s41467-020-16147-2 OPEN

Flexibility of intrinsically disordered degrons in AUX/IAA proteins reinforces auxin co-receptor assemblies

Michael Niemeyer[1], Elena Moreno Castillo[1], Christian H. Ihling[2], Claudio Iacobucci[2], Verona Wilde[1], Antje Hellmuth[1], Wolfgang Hoehenwarter[3], Sophia L. Samodelov[4], Matias D. Zurbriggen[4], Panagiotis L. Kastritis[5], Andrea Sinz[2] & Luz Irina A. Calderón Villalobos[1✉]

Cullin RING-type E3 ubiquitin ligases $SCF^{TIR1/AFB1-5}$ and their AUX/IAA targets perceive the phytohormone auxin. The F-box protein TIR1 binds a surface-exposed degron in AUX/IAAs promoting their ubiquitylation and rapid auxin-regulated proteasomal degradation. Here, by adopting biochemical, structural proteomics and in vivo approaches we unveil how flexibility in AUX/IAAs and regions in TIR1 affect their conformational ensemble allowing surface accessibility of degrons. We resolve TIR1·auxin·IAA7 and TIR1·auxin·IAA12 complex topology, and show that flexible intrinsically disordered regions (IDRs) in the degron's vicinity, cooperatively position AUX/IAAs on TIR1. We identify essential residues at the TIR1 N- and C-termini, which provide non-native interaction interfaces with IDRs and the folded PB1 domain of AUX/IAAs. We thereby establish a role for IDRs in modulating auxin receptor assemblies. By securing AUX/IAAs on two opposite surfaces of TIR1, IDR diversity supports locally tailored positioning for targeted ubiquitylation, and might provide conformational flexibility for a multiplicity of functional states.

[1] Molecular Signal Processing Department, Leibniz Institute of Plant Biochemistry (IPB), Weinberg 3, 06120 Halle (Saale), Germany. [2] Department of Pharmaceutical Chemistry & Bioanalytics, Institute of Pharmacy, Martin Luther University Halle-Wittenberg, Charles Tanford Protein Center, Kurt-Mothes-Straße 3a, 06120 Halle (Saale), Germany. [3] Proteome Analytics, Leibniz Institute of Plant Biochemistry (IPB), Weinberg 3, 06120 Halle (Saale), Germany. [4] Institute of Synthetic Biology & Cluster of Excellence on Plant Science (CEPLAS), Heinrich-Heine University of Düsseldorf, Universitätsstrasse 1, 40225 Düsseldorf, Germany. [5] ZIK HALOMEM & Institute of Biochemistry and Biotechnology, Martin Luther University Halle-Wittenberg, Biozentrum, Weinbergweg 22, 06120 Halle (Saale), Germany. ✉email: LuzIrina.Calderon@ipb-halle.de

Proteolysis entails tight spatiotemporal regulation of cellular protein pools[1,2]. The ubiquitin-proteasome system (UPS) rules over protein turnover, and controls stimulation or attenuation of gene regulatory networks through transcriptional repressors or activators[2]. Typical E1-E2-E3 enzymatic cascades warrant specific ubiquitylation by catalyzing the ATP-dependent attachment of ubiquitin moieties to target proteins[3]. Directly and indirectly, every single aspect of cellular integrity and adaptation is impacted by protein ubiquitylation, e.g., cell cycle progression, apoptosis/survival, oxidative stress, differentiation, and senescence[4].

In SKP1/CULLIN1/F-BOX PROTEIN (SCF)-type E3 ubiquitin ligases, the interchangeable F-box protein (FBP) determines specificity to the E3 through direct physical interactions with the degradation targets[5,6]. These carry a short degradation signal or degron, located mostly within structurally disordered regions, which is recognized by cognate E3 ligases[7]. Primary degrons within a protein family, whose members share the same fate, behave as islands of sequence conservation surrounded by fast divergent intrinsically disordered regions (IDRs)[7]. Once a favorable E3-target association stage is accomplished, one or multiple lysine (Lys) residues in the target become accessible[8–10]. Conformational flexibility on the part of the E3-target ensemble permits then an E2-loaded with Ub (E2~Ub) to approach the bound target, such that a suitable microenvironment for catalytic Ub transfer is created[7]. Efficient degradation by the UPS requires the 26S proteasome to bind its protein target through a polyubiquitin chain with a specific topology, and subsequently engages the protein at a flexible initiation region for unfolding and degradation[11]. A primary degron for E3 recruitment, a ubiquitin chain on specific Lys residues, together with IDRs are the basic elements for efficient ubiquitin-mediated proteasomal degradation[7].

Biological active intrinsically disordered proteins (IDPs) and IDRs exist as structural non-uniform ensembles, due to dynamic back-bone movement[12]. Some functions of IDPs are entropic in nature and originate precisely from their lack of well-defined structure[13]. UPS targets often contain IDRs or are IDPs functioning, i.e., in plant signal transduction[14–17]. The auxin indole 3-acetic acid (IAA) promotes plant growth and development by triggering the degradation of auxin/indole-3-acetic-acid proteins (AUX/IAAs), which leads to changes in gene expression[18]. AUX/IAAs are mostly short-lived transcriptional repressors with half-lives varying from ~6 to 80 min, and the expression of most family members is rapidly (<15 min) induced by auxin[19]. The *Arabidopsis* genome encodes for 29 AUX/IAAs, and 23 of them carry a mostly conserved VGWPP-[VI]-[RG]-x(2)-R degron as recognition signal for an $SCF^{TIR1/AFB1-5}$ E3 ubiquitin ligase for auxin-mediated AUX/IAA ubiquitylation and degradation[20,21]. Under low auxin concentrations, AUX/IAAs are stabilized and repress type A ARF (auxin response factor) transcription factors via physical heterotypic interactions through their type I/II Phox/Bem1p (PB1) domain (formerly known as DIII-DIV) and recruitment of topless (TPL) co-repressors[21,22]. When auxin levels reach a certain threshold, FBPs transport inhibitor response 1 (TIR1)/auxin signaling F-box 1–5 (AFB1-5) gain affinity for the AUX/IAA degron by direct IAA binding[23,24]. The resulting AUX/IAA ubiquitylation and degradation ensues ARF derepression and auxin-induced transcriptional changes[25]. Since AUX/IAA transcripts are themselves auxin regulated, they act, once the intracellular AUX/IAA pool is replenished, in a negative feedback loop repressing ARF activity de novo[26,27].

These molecular interactions establish highly pleiotropic and complex physiological and morphological auxin responses during plant development[28]. During embryogenesis for instance, auxin controls normal organ formation, as evidenced by early developmental arrest in several auxin response mutants[29]. Loss of ARF5 function in the mutant *monopteros* (*mp*) prevents root formation[30,31]. Identical effects are seen in the *bodenlos* (*bdl*) mutant, in which aberrant AUX/IAA stabilization, due to a mutation in its degron, renders the protein resistant to degradation causing *iaa/bdl* gain-of-function mutants to die during embryogenesis[31,32]. Concomitantly, genetic experiments have shown that reducing the number of functional TIR1/AFBs in plants leads to a variety of auxin-related growth defects, and increased resistance to exogenous auxin, due to compromised AUX/IAA ubiquitylation and turnover[33].

Biochemical and structural analyses in the last two decades have revolutionized our understanding of the mechanisms of auxin sensing and signal transduction. Degron-carrying AUX/IAAs and TIR1/AFB1–5 form an auxin co-receptor system, where auxin occupies a binding pocket in TIR1 just underneath the AUX/IAA degron[23]. Auxin-binding kinetics of the receptor are mainly determined by the specific AUX/IAA binding to TIR1[24]. Hence, different combinations of TIR1/AFBs and AUX/IAAs have different auxin-sensing properties, becoming a versatile co-receptor system for tracing fluctuating intracellular auxin concentrations[24]. While the degron is absolutely necessary for AUX/IAA recruitment and degradation, it does not explain all auxin-binding properties of a TIR1·AUX/IAA receptor pair[24]. Flexible regions outside the primary degron, decorated with specific lysine residues that undergo ubiquitylation in vitro[34], contribute to differential co-receptor assembly[24], AUX/IAA destabilization[35,36], as well as basal protein accumulation[37].

The dynamic range of auxin sensitivity in plant cells, and by default plant growth and development, rely on efficient AUX/IAA processing by the UPS. Particularly in view of the close to 30 AUX/IAA family members, the mechanistic details of this process still remain to be fully understood. Despite their ubiquitous role in signal transduction, research on their singularity and their distinct contribution on auxin sensing, is still in its infancy. At the structural level, it is of outmost relevance to unveil spatial and structural constraints for TIR1·AUX/IAA auxin co-receptor formation. Despite the fact a well-resolved ASK1·TIR1·auxin (IAA)·IAA7 degron crystal structure is available[23], we lack information on how a full AUX/IAA is positioned on TIR1. Thus, there is knowledge gap on whether additional structural features in TIR1 or AUX/IAAs might restrict or facilitate receptor assembly, auxin binding, and AUX/IAA ubiquitylation and degradation.

Here, we study the structural properties of full TIR1·AUX/IAA auxin co-receptor systems, and report on the influence of IDRs in two representative AUX/IAA family members, IAA7 and IAA12 on TIR1·AUX/IAA interactions. Our data demonstrates how an extended AUX/IAA fold promotes recruitment by TIR1, by offering restrained conformational plasticity for correct positioning on TIR1. We also offer a model of how a potential allosteric effect, that fine-tunes TIR1·AUX/IAA interactions, influences AUX/IAA-regulated gene expression.

Results

AUX/IAAs exhibit intrinsic structural disorder. Regions flanking the canonical GWPPVR degron motif influence AUX/IAA protein recruitment by the SCF^{TIR1}, impact auxin binding, and AUX/IAA degradation[24,34–37]. A broader sequence context of the AUX/IAA degron might be crucial for the adequate regulation of AUX/IAA processing and turnover, including post-translational modifications (e.g., ubiquitylation), protein–protein interactions and protein–ligand interactions[24,35,36]. To evaluate whether structural flexibility is a common feature among AUX/IAAs, we predicted global structural disorder along the sequences of the 29 *Arabidopsis thaliana* AUX/IAAs in silico (IUPred2A) (Fig. 1a,

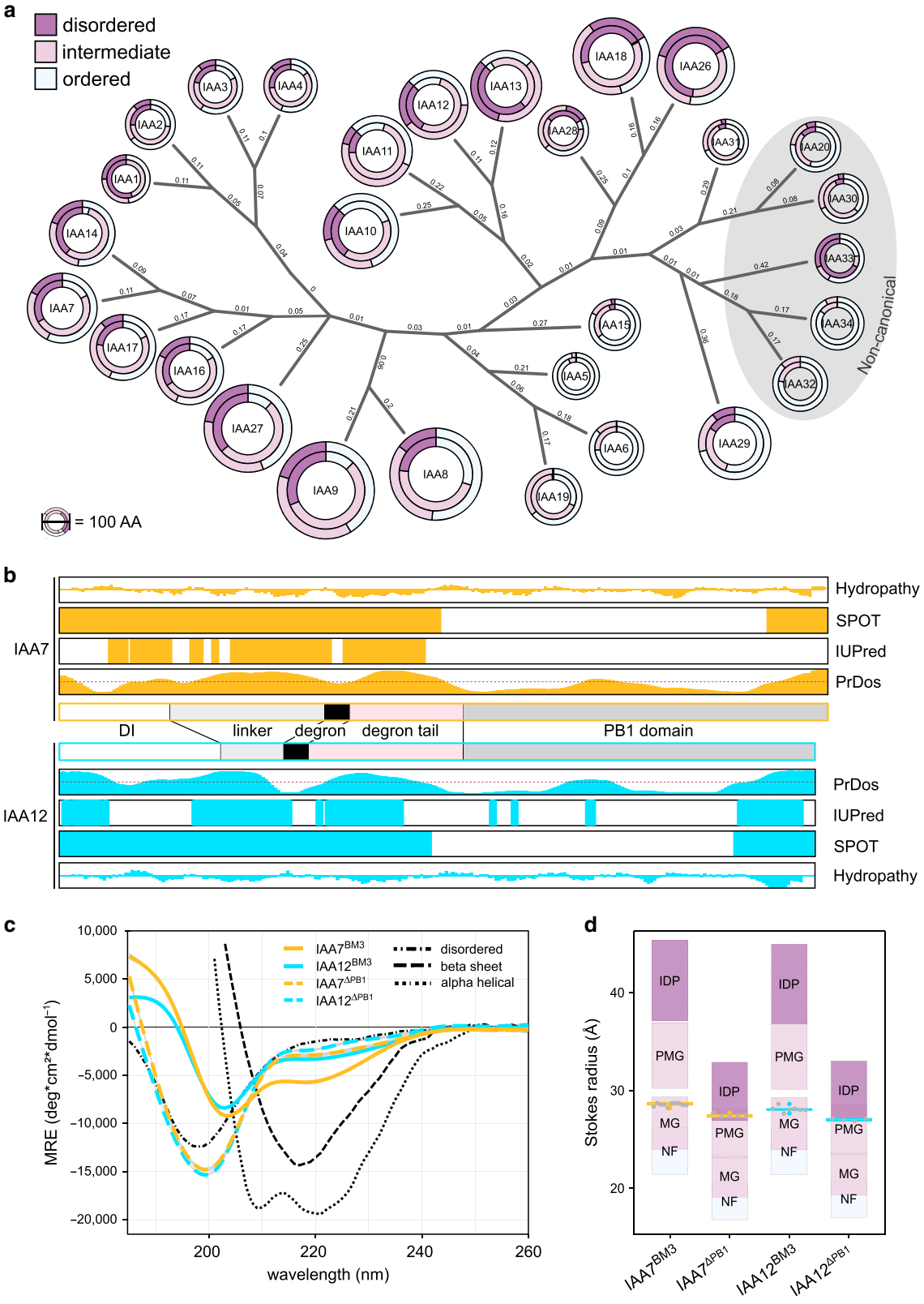

Supplementary Fig. 1, and Supplementary Data 1). We scored the probability of disorder for every amino acid residue in a context-dependent manner[38], and particularly focused on sequences flanking the well-structured PB1 domain (Fig. 1a and Supplementary Fig. 1). We defined scores for disorder probability as high (disordered, >0.6), intermediate (0.4–0.6), or low (ordered, <0.4). AUX/IAA sister pairs arrange in subclades with high sequence similarity, and almost all subclades contain IDRs distributed along their N-terminal halves (NTDs), and much less so, towards the end of their C-terminal PB1 domains (Fig. 1a and Supplementary Fig. 1). The lengths of the AUX/IAAs do not correlate with an enrichment of disorder segments because IAA1-4 or IAA28 (average length below 200 aa) exhibit features of disorder, while similarly small AUX/IAAs (e.g., IAA6, IAA15, IAA19, IAA32, or

Fig. 1 AUX/IAA proteins are intrinsically disordered outside the PB1 domain. a Simplified phylogenetic tree (with average branch length depicted) of 29 *Arabidopsis thaliana* AUX/IAAs showing their sequence composition based on IUPred2A prediction for disorder (score classification: disorder (dark lilac): >0.6; intermediate (light lilac): 0.4–0.6; ordered (white): <0.4). Outer circles correspond to full length proteins, inner circles represent disorder prediction excluding the PB1 domain (scale shows width per 100 AA). **b** In silico prediction maps of disorder along the IAA7 (orange) and IAA12 (aquamarine) sequence using SPOT, IUPRED1, and PrDos algorithms. AUX/IAA domain structure (Domain I (DI), a linker, a core degron, a degron tail and the Phox/Bem1p (PB1) domain) are displayed. Outer plots represent Kyte-Doolittle hydropathy (scale from −4 to +4). Dotted line in PrDos prediction represents a 0.5 threshold. **c** Circular dichroism spectra of IAA7 (orange) and IAA12 (aquamarine) oligomerization-deficient (solid lines) and PB1-less variants (dashed colored lines) show the lack of defined secondary structure elements outside of the PB1 domain. Reference spectra (black dotted lines) are depicted. Ellipticity is calculated as mean residual ellipticity (MRE). Shown is the mean of three independent experiments ($n = 3$). **d** IAA7 (orange) and IAA12 (aquamarine) exhibit an extended fold according to Stokes radii determination via size exclusion chromatography. Theoretical Stokes radii of known folds (lilac color gradient, labeled rectangles): intrinsically disordered protein (IDP, dark lilac), premolten globule (PMG, light lilac), molten globule (MG, light lilac), natively folded (NF, white) plus 10% outer limits, and experimental values (colored box plots with whiskers = ~25% (1.5*IQR) of the data points (gray dots); Outliers shown as colored dots; $n = 4$, 5, 7, and 10 correspondingly for $IAA12^{\Delta PB1}$, $IAA7^{\Delta PB1}$, $IAA12^{BM3}$, $IAA7^{BM3}$).

IAA34) are predicted to be well-structured. With the exception of IAA33, all non-canonical AUX/IAAs, which lack the core degron motif for interaction with TIR1, are rather ordered. IAA33 diverged early during the evolution from the rest of the AUX/IAAs[28], and it belongs, together with canonical IAA26 and IAA13, to the most disordered family members. Although IAA12 and IAA13 are close ohnologs, IAA13 entails comparatively more disordered segments. IAA7 and IAA12, which are members of a different AUX/IAA subclade[21], appear to have similar bias for IDRs (Fig. 1a and Supplementary Fig. 1).

IAA12 carries a GWPPIG degron that differs from the canonical GWPPVR degron in IAA7, and they equip TIR1·AUX/IAA complexes with distinct auxin binding affinities (TIR1·IAA7: $K_d = \sim 20$ nM and TIR1·IAA12: $K_d = \sim 250$ nM)[24]. Nevertheless, these differences cannot be solely attributed to the identity of the degron[24]. Therefore, IDRs flanking the degron could probably participate in interactions with TIR1, affecting auxin sensitivities. In order to investigate the distribution of disorder in IAA7 and IAA12 proteins, we performed in silico analyses using multiple disorder prediction algorithms (Fig. 1b). Consistently, all tested algorithms show that most of the disorder segments in IAA7 and IAA12 are located on their NTDs. We also observe an enrichment of hydrophilic residues in these IDRs based on the hydropathy index, indicating that these regions may be solvent exposed (Fig. 1b). Almost 50% of IAA7 and IAA12 amino acid content correspond to disordered regions. In IAA7, but most notably in IAA12, we observe a predominant "order-dip" corresponding to the core degron (Fig. 1b).

In order to obtain hints for IDR presence in IAA7 and IAA12 in solution, we used recombinantly expressed proteins, and further analyzed their secondary structure and overall shape via CD spectroscopy and size exclusion chromatography (Fig. 1c, d and Supplementary Figs. 2 and 3). We looked into a functionally relevant transient AUX/IAA fold, while considering different protein conformational classes (Fig. 1c). We included oligomerization-deficient variants $IAA7^{BM3}$, $IAA12^{BM3}$ (ref. [39]), and also IAA7 and IAA12 truncated variants lacking the compactly folded PB1 domain, $IAA7^{\Delta PB1}$ and $IAA12^{\Delta PB1}$. Both $IAA7^{BM3}$ and $IAA12^{BM3}$ exhibit a rather complex mix of secondary structure elements characteristic of premolten globule–like proteins, displaying a minimum at ~205 nm, and a shoulder near 220 nm in CD spectra[40]. CD spectra of $IAA7^{\Delta PB1}$ and $IAA12^{\Delta PB1}$ shifted toward a shorter wavelength with a minimum at just below 200 nm, which is characteristic for random coil proteins (Fig. 1c and Supplementary Fig. 2). We also measured the Stokes radii (R_S) for $IAA7^{BM3}$, $IAA12^{BM3}$ together with the theoretical values of IAA7 and IAA12 displaying specific folds, native fold (NF), molten globular (MG), premolten globule (PMG), and unfolded (IDP) (Fig. 1d). Since all measured Stokes radii are larger than the ones expected for their respective natively folded proteins, we conclude that $IAA7^{BM3}$ and $IAA12^{BM3}$ adopt extended structures mainly due to large proportions of intrinsically disordered segments outside of the PB1 domain.

Intrinsic disorder impacts auxin-driven receptor association. As IAA7 and IAA12 have distinct and contrasting TIR1-interaction properties, we reasoned generating IAA7 and IAA12 chimeric proteins could enable to pinpoint the contribution of IDRs flanking the degron to auxin-dependent TIR1·AUX/IAA associations. IAA7 and IAA12, as well as their sister proteins IAA14 and IAA13, respectively, exhibit differences in their disordered degron tail length and charge distribution (Supplementary Fig. 4). While IAA7 and IAA14 have in average a short degron tail (<30 aa), IAA12 and IAA13 have a longer degron tail (44 aa) linking the degron to the PB1 oligomerization domain (Supplementary Fig. 4). We defined five different modules flanked by motifs conserved throughout the AUX/IAA family: DI (N-terminus including KR motif), core degron (VGWPP-[VI]-[RG]-x(2)-R), the PB1 domain, and two variable IDRs connecting either the DI and degron (linker), or the degron and PB1 domain (degron tail) (Fig. 2a and Supplementary Fig. 4). We exchanged the modules between IAA7 and IAA12 and used the resulting seamless chimeras in the yeast two-hybrid system (Y2H) to assess their respective ability to interact with TIR1 (Fig. 2a, Supplementary Fig. 4, and Supplementary Data 1). As previously reported, we find native IAA7, denoted here 7-7-7-7-7, interacts with TIR1 in an auxin-dependent manner more strongly than native IAA12 (12-12-12-12-12). Mimicking degron mutants iaa7/axr2-1 (P87S) or iaa12/bdl (P74S) in the IAA7 or IAA12 chimeras (7-7-7m-7-7, 12-12-12m-12-12) abolishes, expectedly, their association with TIR1 (Fig. 2a). Exchanging the disordered degron tail of IAA7 for the one in IAA12 in the IAA(7-7-7-12-7) chimera does not affect interaction with TIR1. A IAA(12-12-12-7-12) chimera, however, associates with TIR1 much more efficiently than wild type IAA (12-12-12-12-12). Similarly, PB1 domain exchanges between IAA7 or IAA12 positively affect the ability of IAA(12-12-12-12-7) chimera to interact with TIR1. To investigate the interdependency of the degron tail and the PB1 domain, we exchanged the flexible degron tail of IAA12 together with its corresponding PB1 domain, and fused them to IAA7 (IAA(7-7-7-12-12)). In this case, TIR1·IAA(7-7-7-12-12) interaction is greatly affected, while TIR1·IAA(12-12-12-7-7) interaction, although weak, remains stronger than TIR1·IAA(12-12-12-12-12) association. Of note, independently of the specific core degron sequence, GWPPVR in IAA7 or GWPPIG in IAA12, the IAA7 degron tail, and PB1 combo of IAA7 favors auxin-dependent TIR1·AUX/IAA chimera interactions. Furthermore, alterations in the IAA7 domain structure interferes with its degradation. (Supplementary Fig. 5). Taken together, auxin-dependent and -independent interactions are influenced by the degron tail, as well as the PB1 domain, and these regions may act in concert.

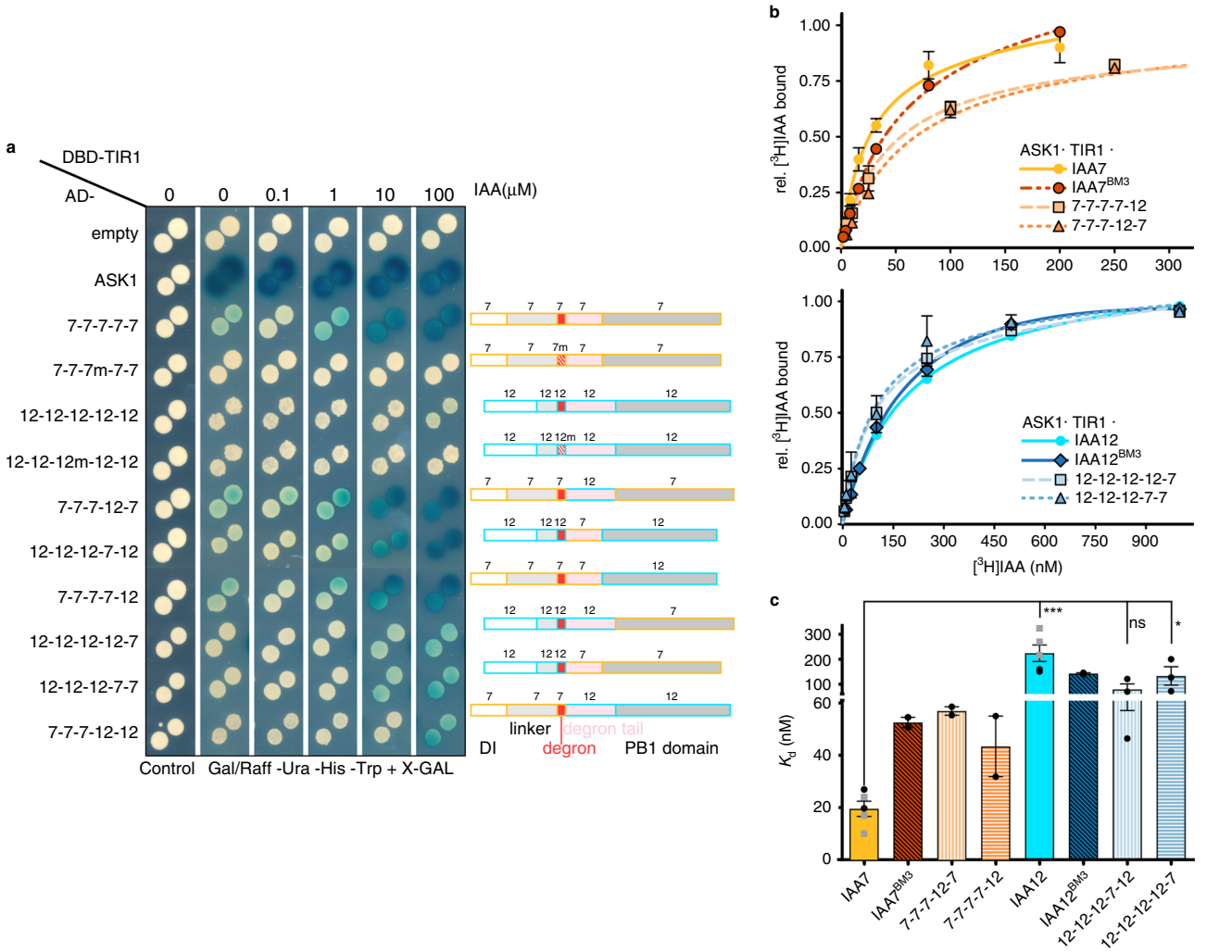

Fig. 2 Auxin-dependent TIR1·IAA7 and TIR1·IAA12 interactions rely on the interplay between the degron, degron tail and the PB1 domain. a Y2H interaction matrix (left) for TIR1 with ASK1, and ten chimeric proteins built by fusing IAA7 and IAA12 segments flanked by conserved motifs throughout the AUX/IAA family. Yeast diploids containing LexA DBD-TIR1 and AD-AUX/IAA chimeras were spotted to selective medium with increasing IAA concentrations, and β-galactosidase reporter expression indicated TIR1·AUX/IAA interactions. AD-empty vector as negative control. Domain organization and composition of seamless chimeric IAA7 (orange) and IAA12 (aquamarine) constructs depicted in boxes (right) with DI (white) (till KR motif), linker (light gray), core degron (red), degron tail (light pink), and PB1 domain (dark gray). **b** Saturation binding assays using [^{3}H]IAA and recombinant ASK1·TIR1·IAA7 (shades of orange) or ASK1·TIR1·IAA12 (shades of blue) ternary complexes. TIR1·IAA7 complex exhibits a high affinity (K_d = ~20 nM) for auxin, whereas IAA12-containing co-receptor complexes provide tenfold lower affinity for auxin (K_d = ~200 nM). Oligomerization-deficient IAA7^{BM3} and IAA12^{BM3} variants, and chimeric AUX/IAA proteins in complex with ASK1·TIR1 distinctly affect auxin bind capabilities of a co-receptor system. Shown are saturation binding curves for each co-receptor pair as relative [^{3}H]IAA binding normalized to the highest value of each curve. Each point reflects means of 2–3 independent experiments (n = 3 for 12-12-12-7-12 and 12-12-12-12-7; otherwise n = 2), each of them comprising of technical triplicates, and depicted as means ± SEM. **c** Comparison of dissociation constants (K_d) obtained in saturation-binding experiments for each ASK1·TIR1·AUX/IAA ternary complex. Shown are mean values from our experiments (black dots) combined with published[24] K_d values for IAA7 and IAA12 (gray squares) K_d values depicted as means ± SEM (n = 2 + 3 for IAA7 and IAA12; n = 3 for 12-12-12-7-12 and 12-12-12-12-7: otherwise n = 2). For $n \geq 3$, significant differences are indicated (Dunnett's multiple comparison test, IAA7 as reference; *p < 0.0322, ***p < 0.0002).

In order to address whether accessibility of IDRs and the PB1 domain in AUX/IAAs affect the outcome of TIR1·AUX/IAA interactions, that is auxin sensing, we performed in vitro radioligand binding assays with TIR1, IAA7, and IAA12 wild type, chimeric, as well as IAA7^{BM3} and IAA12^{BM3} mutant proteins. Thereby, we also indirectly assayed whether AUX/IAA homo- and hetero-dimers, through the PB1 domain, might impinge on auxin binding. While PB1-compromised IAA7 (IAA7^{BM3}) together with TIR1 shows diminished auxin binding affinity, IAA12^{BM3} does not interfere with the auxin binding properties of the receptor complex (Fig. 2c). We observed the general trend of reduced auxin binding affinities when altering IAA7 in TIR1·IAA7^{BM3} (K_d = ~53 ± 2 nM), TIR1·IAA (7-7-7-12-7) (K_d = 93 nM), and TIR1·IAA (7-7-7-7-12) (K_d = 86 ± 25 nM) complexes in comparison to TIR1·IAA(7-7-7-7-7) (K_d = ~20 ± 6 nM) (n = 2–5; ± indicates SEM). We, however, measured relatively similar auxin affinities of TIR1·IAA12^{BM3} (K_d = ~143 ± 3 nM), TIR1·IAA (12-12-12-7-12) (K_d = ~172 ± 76 nM), TIR1·IAA (12-12-12-12-7) (K_d = ~152 ± 63 nM), and TIR1·IAA12 (K_d = ~224 ± 66 nM); (n = 2–5; ± indicates SEM) (Fig. 2b, c and Supplementary Fig. 6). The decrease in the auxin binding affinity of TIR1·IAA7^{BM3} and TIR1·IAA (7-7-7-7-12) hints to a positive effect of the IAA7 PB1 domain to auxin sensing (Fig. 2c). The degron tail, as well as the PB1 domain of IAA12 in the IAA7 context, reduce the

auxin binding affinity by around fourfold (Fig. 2b, c). Conversely, we did not trace a significant effect of individual IAA7 modules when inserted in the IAA12 context (Fig. 2a). This is consistent with our Y2H interaction data, evidencing the specific interdependency of degron tails and their corresponding PB1 domains. It further points to additive and separate effects of each intrinsically disordered degron tail and the PB1 domain on auxin-independent and auxin-dependent TIR1 interaction.

IDRs in AUX/IAAs facilitate their ubiquitylation. To next examine the contribution of the AUX/IAA IDRs to their ubiquitylation by the SCF^{TIR1} complex, we recapitulated auxin-triggered and SCF^{TIR1}-dependent IAA7 and IAA12 ubiquitylation in vitro (IVU)[34]. We followed IAA7 and IAA12 ubiquitylation over time using IAA concentrations in the range of their auxin binding affinity (K_d) of TIR1·IAA7 and TIR1·IAA12 complexes (i.e., ~20 nM to ~200 nM) and beyond (Figs. 2c and 3, and Supplementary Fig. 7). In our IVUs, AUX/IAA ubiquitylation is detectable as early as 10 min after incubation, and accelerated in an auxin-dependent manner. In the absence of auxin, IAA12~ubiquitin conjugates are less abundant than IAA7~ubiquitin conjugates (Fig. 3a and Supplementary Fig. 7). Differences between IAA7 and IAA12 ubiquitylation are prominent at shorter incubation times, and especially at concentrations below 150 nM (Fig. 3). We figured IAA7 and IAA12 ubiquitylation occurs rapidly, and differences in their ubiquitylation dynamics depend on the auxin binding affinities of their respective TIR1·AUX/IAA receptor complex. This is possibly the result of an increased dwell-time of the AUX/IAA on TIR1, which facilitates efficient ubiquitin transfer to lysines.

Putative ubiquitin acceptor Lys residues along the IAA7 and IAA12 sequences are enriched in the degron tail of IAA12, and the linker of IAA7, both of which appear to lack a three-dimensional (3D) structure (Fig. 3b). We aimed at gaining experimental evidence of IAA7 and IAA12 ubiquitylation sites, after IVU reactions, tryptic digest and LC/MS analysis. We were able to map only few specific lysine residues on IAA7 and IAA12, which are differently distributed along their sequence (Fig. 3b and Supplementary Data 2). Although IAA7 and IAA12 contain 24 and 18 lysines, respectively, only 3 and 6 of them were ubiquitylated. While we observe only few ubiquitylated lysine residues at the AUX/IAA N-terminus, most of the mapped ubiquitylation sites are located in the region downstream of the degron, either in the PB1 domain in IAA7, or the degron tail in IAA12. Even though 4 lysines are conserved in the PB1 domain of IAA7 and IAA12, only the non-conserved residues appear to be ubiquitylated in IAA7. The flexible degron tail of IAA7 did not get ubiquitylated, whereas 4 out of 7 lysines in the slightly longer disordered IAA12 degron tail could be mapped as ubiquitylation sites (Fig. 3b and Supplementary Data 2).

To further investigate whether the apparent structural divergence of IAA7 and IAA12 imposes restrictions to lysine access for ubiquitylation, we used chimeric IAA7 and IAA12 proteins in our IVU assay (Fig. 3c). As we aimed at visualizing absolute differences in ubiquitin conjugation, we traced auxin-dependent ubiquitin conjugation of chimeric AUX/IAAs at a fixed IAA concentration of 1 µM after 1 h IVU reaction. Exchanging the degron tails or the PB1 domains between IAA7 and IAA12 leads to differences in ubiquitylation profiles of chimeric proteins compared to their wild type counterparts. This happens as we either added or subtracted regions that contain the ubiquitin acceptor sites in the IAA7 and IAA12 chimeric proteins (Fig. 3c and Supplementary Fig. 8). For instance, we detect an increase of ubiquitin conjugates on IAA(7-7-7-12-7), which gains ubiquitylation sites due to the exchange of the IAA7 degron tail. Deleting the AUX/IAA degron tail or the PB1 domain in the chimeric proteins results in an overall reduction of ubiquitin conjugates on targets. Versions of IAA7 or IAA12 missing a degron tail and containing the PB1 domain of IAA12, IAA(7-7-7-Δ-12) and IAA(12-12-12-Δ-12), do not undergo auxin-triggered ubiquitylation (Fig. 3c and Supplementary Fig. 8). Similarly, AUX/IAA versions containing the IAA7 degron, but lacking a PB1 domain (IAA(7-7-7-7-Δ), and IAA(12-12-12-7-Δ)) are not conjugated by ubiquitin, probably due to the loss of the mapped ubiquitin acceptor sites (Fig. 3b). Our IVU assays on AUX/IAA chimeras validate our findings showing that the IAA7 PB1 domain or the flexible IAA12 degron tail carry propitious ubiquitylation sites. Thus, we postulate AUX/IAA ubiquitylation favorably occurs in exposed regions in IAA7 and IAA12, when they are recruited by TIR1.

Degron-flanking regions tailor TIR1·AUX/IAA ensembles. Owing to the relative lack of a stable 3D conformation, IDPs or proteins enriched in IDRs, such as AUX/IAAs, represent a challenge for structural biology studies. During interactions with target proteins, IDPs, particularly their IDRs, may undergo conformational changes that cannot be traced easily, or captured while happening[41,42]. Although the ASK1·TIR1·auxin (IAA)·IAA7 degron crystal structure enlightened us on how auxin is perceived, we lack information on the contribution of regions flanking the AUX/IAA degron on auxin binding. Without being able to structurally resolve intrinsically disordered degron-flanking regions, we are hindered in our understanding of how AUX/IAAs are actually positioned on TIR1. This has evidently far-reaching implications on SCF^{TIR1} E3 ubiquitin ligase activity and ubiquitin transfer to AUX/IAAs by an E2 ubiquitin conjugating enzyme.

To elucidate the driving factors for ASK1·TIR1·AUX/IAA complex assembly, and to unveil how IDRs in AUX/IAAs influence positioning on TIR1, we pursued a structural proteomics approach using chemical cross-linking coupled to mass spectrometric analyses (XL-MS) (Fig. 4a). We assembled ASK1·TIR1·AUX/IAA complexes containing either $IAA7^{BM3}$ or $IAA12^{BM3}$ proteins in the absence or presence of auxin, and added the MS-cleavable crosslinker disuccinimidyl dibutyric urea (DSBU). Reaction products were processed for mass spectrometric analysis, which utilizes the characteristic fragmentation of DSBU to identify crosslinked residues within the AUX/IAAs and the ASK1·TIR1·-AUX/IAA complex[43–45]. Our data shows multiple intra- and inter-molecular crosslinks (XLs) for ASK1·TIR1 and $IAA7^{BM3}$ or $IAA12^{BM3}$ proteins when auxin was included (Fig. 4b, c, Supplementary Fig. 9, Supplementary Data 3 and 4). In the absence of auxin, we observe only few inter-protein and similar intra-protein XLs when compared to auxin-containing samples (Fig. 4c, Supplementary Fig. 10, and Supplementary Data 3 and 4). In the presence of auxin, we identify two distinct clusters in TIR1 harboring crosslinker-reactive amino acid side chains with IAA7 and IAA12 (Fig. 4b and Supplementary Fig. 9). Cluster 1 comprises amino acid residues in LRR4–7 (140–229 aa), while cluster 2 consists of residues toward the TIR1 C-terminus located in LRR17–18 (485–529 aa). The location of the clusters on two opposing surfaces of TIR1 suggests a rather extended fold of the AUX/IAA protein when bound to TIR1 (Fig. 4b). The crosslinked residues along the sequences of ASK1·TIR1·$IAA7^{BM3}$ or ASK1·TIR1·$IAA12^{BM3}$ show an enrichment of highly variable intramolecular XLs within the AUX/IAAs (Fig. 4c). A low number of intra-protein XLs along the TIR1 sequence were detected as a consequence of its rigid solenoid fold, which is in agreement with the ASK1·TIR1 crystal structure (PDB: 2P1Q [http://www.rcsb.org/structure/2P1Q][23]). Inter-protein XLs indicate that the crosslinker-reactive clusters in TIR1 mainly connect with only a specific subset of AUX/IAA residues (Fig. 4b, c). Multiple IAA7

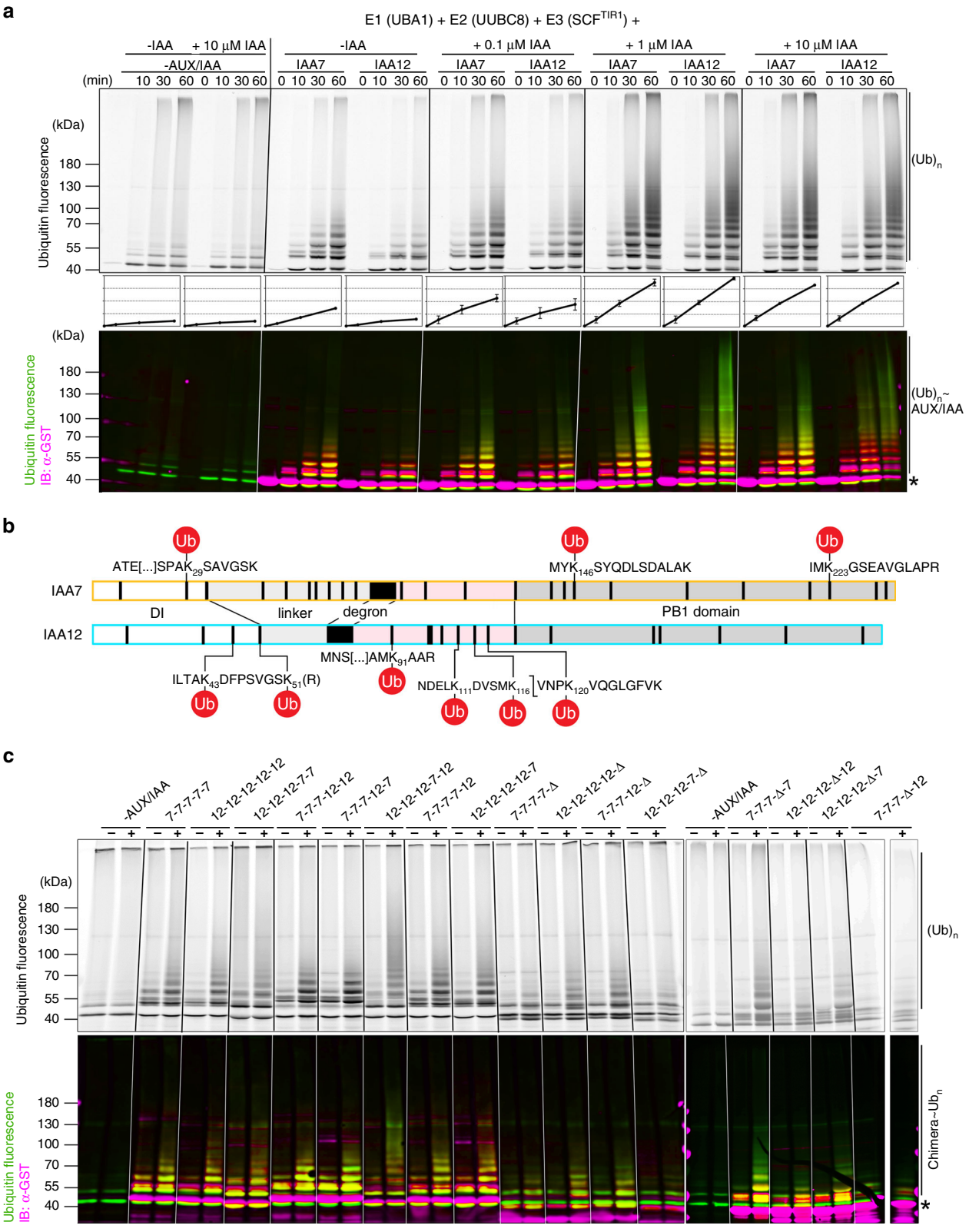

Fig. 3 Auxin-driven and SCF^{TIR1}-dependent ubiquitylation of IAA7 and IAA12 display distinct dynamics. a IVU assays with recombinant GST-IAA7 or GST-IAA12, E1 (*At*UBA1), E2 (*At*UBC8), reconstituted SCF^{TIR1} (*At*SKP1·TIR1, *Hs*Cul1 and *Mm*RBX1), fluorescein-labeled ubiquitin (Ub) and IAA (auxin). IAA7 and IAA12 ubiquitylation is auxin-driven and time-dependent. Ubiquitylation was monitored using the ubiquitin fluorescent signal (green), and anti-GST/Alexa Fluor 647-conjugated antibodies for detection of GST-AUX/IAAs (magenta). ImageQuantTL software was used for quantification (middle; means ± SEM, $n = 3$), and generation of merged image (bottom; overlapping Ub and GST signal: yellow). **b** IAA7 and IAA12 IVU samples were analyzed via LC-MS, and putative ubiquitylation sites, detected by the diGly (or LRGG) Ub remnant after tryptic digest, were mapped relative to the domain structure. IAA12 Ub sites agglomerate in the region upstream of the degron (white) and the degron tail (light pink). **c** Ubiquitin conjugation on chimeric IAA7 and IAA12 (colors as in **a**) proteins in the presence or absence of 1 μM IAA. IVU reaction time 1 h. (*) Asterisks depict unmodified AUX/IAAs.

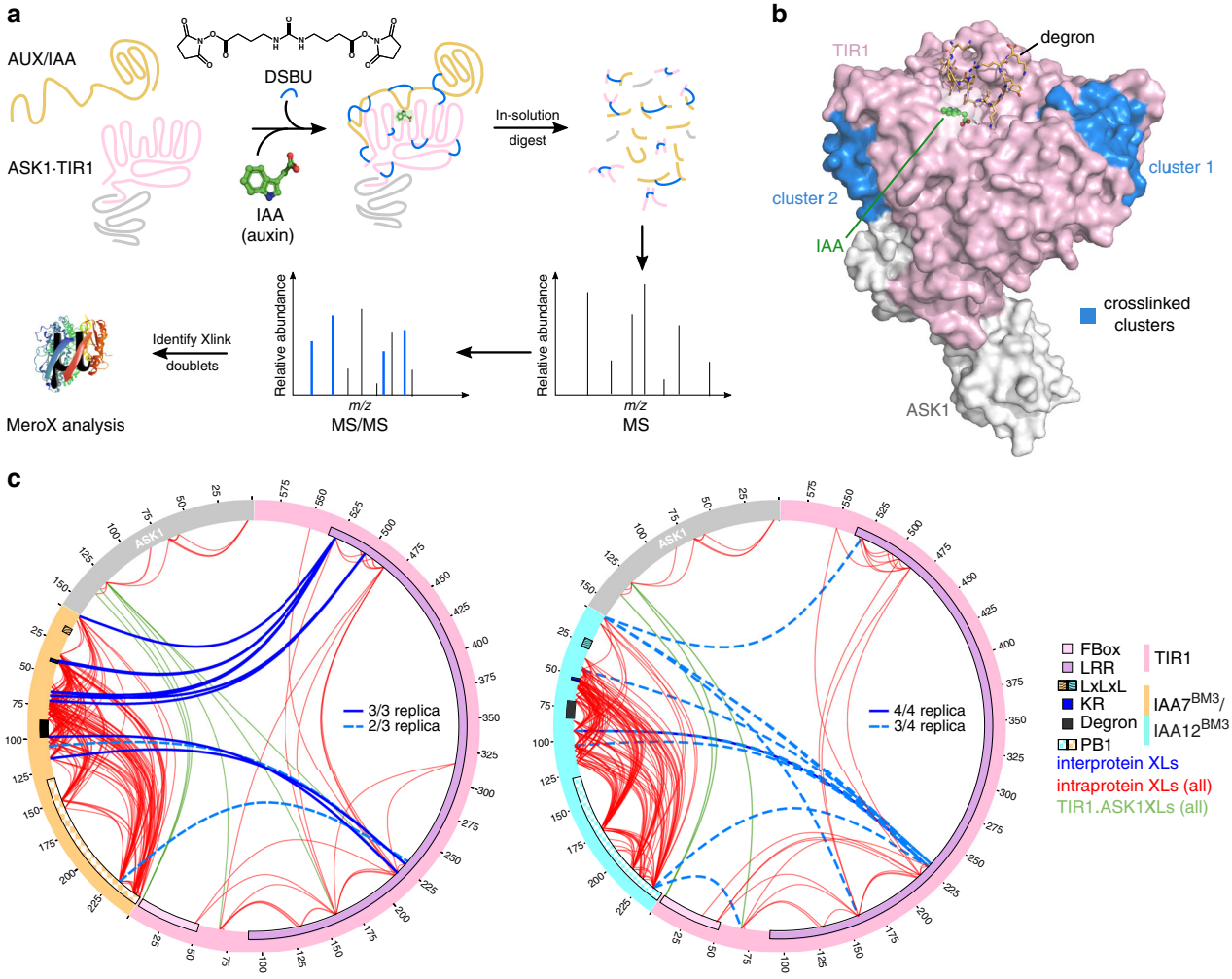

Fig. 4 Structural proteomics using an MS-cleavable crosslinker reveals TIR1·IAA7 and TIR1·IAA12 interaction interfaces. a Workflow for the cross-linking coupled to mass spectrometry (XL-MS) approach. Recombinant oligomerization-deficient IAA7 (orange) and IAA12 (aquamarine) proteins, and ASK1·TIR1 (gray and light pink, respectively) were incubated with the DSBU crosslinker, and samples were analyzed using LC/MS^2. Crosslinked peptides were identified using the MeroX software. **b** Interaction interfaces (blue) on TIR1 converge in two distinct patches around LRR4–7 (cluster 1) or LRR17–18 (cluster 2) revealing AUX/IAAs adopt an extended fold when in complex with TIR1. **c** Circular depiction of inter-protein (TIR1·AUX/IAAs) (blue) and intra-protein (red) crosslinks (XLs) along IAA7 (orange), IAA12 (aquamarine), TIR1 (light pink) and ASK1 (gray) protein sequence. XLs were identified in at least 2/3 or 3/4 independent experiments (dashed: 2/3 and 3/4; solid lines: 3/3 and 4/4). Specific XLs within TIR1 and between TIR1 and ASK1 (green) are in agreement with the crystal structure (PDB: 2P1Q [http://www.rcsb.org/structure/2P1Q]). Known motifs and protein domains are displayed.

residues upstream of the core degron, including the KR motif, preferably crosslinked to TIR1 cluster 2. While residues downstream of the core degron, including the PB1 domain, positioned towards TIR1 cluster 1 (Fig. 4c). Interestingly, degron-neighboring residues, populating the most stable part of TIR1·AUX/IAA complexes, are highly represented in the XL data sets (Supplementary Data 3 and 4). IAA12 is similarly positioned on TIR1, but exhibits even higher flexibility given the more diverse distribution of inter-protein XLs (Fig. 4c). This is also supported by the fact that we detect many more assemblies for ASK1·TIR1·IAA12^{BM3} across replicates, than for the ASK1·TIR1·IAA7^{BM3} complex (Fig. 4c). In conclusion, our structural proteomics approach confirms AUX/IAAs IAA7 and IAA12 exhibit flexible conformations in solution (intra-protein XLs), and adopt an extended fold when bound to TIR1.

As we gained a better understanding of the extended fold of IAA7 and IAA12 on TIR1, we wondered whether intrinsic disordered stretches flanking the degron might help to coordinate positioning of the AUX/IAA PB1 domain for ubiquitin transfer. An extended AUX/IAA configuration on TIR1 would be particularly relevant for allowing K146 and K223 in the PB1 domain of IAA7 to be readily available for ubiquitylation. In the case of IAA12, an assertive extension of the degron tail would expose K91, K111, K116, and K120 for ubiquitin attachment (Fig. 3b).

Conformational heterogeneity steers AUX/IAA interactions. To further investigate how intrinsic disorder in IAA7 and IAA12 influences their positioning on ASK1·TIR1, we combined our XL information with a molecular docking strategy (Fig. 5 and Supplementary Figs. 11 and 12). For that, we used available structures for the PB1 domains of AUX/IAAs and ARFs[39,46–48]. We docked homology-modeled PB1 domains of *Arabidopsis* IAA7 and IAA12 to the ASK1·TIR1 complex, applying distance restraints based on the XL data using HADDOCK (Supplementary Fig. 12 and Supplementary Tables 1 and 2). We also added an additional distance restraint reflecting the possible conformational space covered by the respective degron tails. We visualized the impact of the different restraints on the possible interaction interface of ASK1·TIR1·IAA7^{PB1} and ASK1·TIR1·IAA12^{PB1} by DisVis[49]

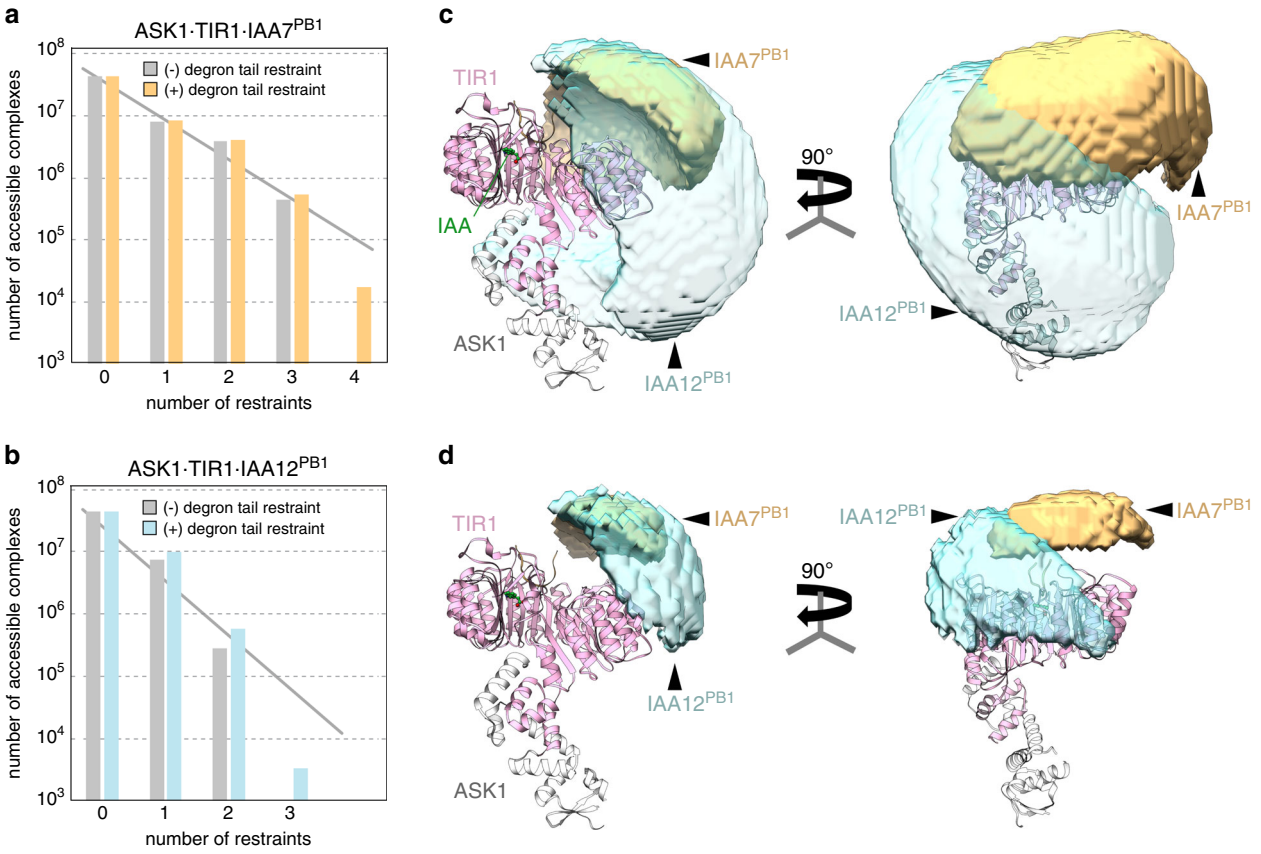

Fig. 5 XL-based docking substantiates the function of the AUX/IAA disordered degron tail positioning the PB1 domain on TIR1. Conformational space available for docking the PB1 domains of IAA7 (light orange) and IAA12 (aquamarine) on ASK1·TIR1 (gray, light pink) analyzed by DisVis based on the XL data restraints. **a**, **b** Including the length of the disordered degron tail of IAA7 (36 aa) or IAA12 (49 aa) as an additional restraint (colored bars) conspicuously reduces the conformational space, and the number of accessible TIR1·AUX/IAA^{PB1} complexes. **c**, **d** Visualization of the possible conformational space occupied by the PB1 domain on the ASK1·TIR1 protein complex without (**c**) or with (**d**) the degron tail length as distance restraint.

(Fig. 5). Evidently, by incorporating more distance restraints, we limit the number of ASK1·TIR1·AUX/IAA^{PB1} protein complexes, therefore reducing their explored interaction space (Fig. 5).

Intriguingly, the relationship between the accessible complexes vs. the number of restraints applied does not reveal a linear behavior, but shows a sharp drop when the degron tail restraint is added to all XL-based restraints (Fig. 5a, b). Comparing the groups of water-refined HADDOCK models leads to similar observations, and the best scoring groups are only sampled incorporating the degron tail restraint (Supplementary Tables 1 and 2). This indicates the disordered degron tail in AUX/IAAs restricts the conformational space explored by the PB1 domain on TIR1 (Supplementary Table 2 and Supplementary Fig. 12). The reduction of accessible ASK1·TIR1·IAA7^{PB1} and ASK1·TIR1·IAA12^{PB1} complexes for docking is also reflected by the decreased space that can be possibly occupied by the PB1 domain (Fig. 5c, d). Overall, XL-based docking of the PB1 domain of IAA12 on the ASK1·TIR1 complex is less-defined, and occupies a distinct conformational space than the ASK1·TIR1·IAA7^{PB1} complex.

In order to refine our docking data and identify the most energetically favored TIR1·AUX/IAA^{PB1} assemblies, we carried out molecular dynamic simulations coupled to free-binding energy calculations by MM/GBSA. We used as a starting structure ($t = 0$) the results from the HADDOCK simulations, including the degron tail restraint (cluster1_1; 2_1 (IAA7 and IAA12); 3_1(IAA12)), and performed 20 ns simulations for each TIR1·IAA7^{PB1} or TIR1·IAA12^{PB1}, resulting in stable complexes (Fig. 6a and Supplementary Fig. 12). We obtained the effective binding free-energy every 1 ps for each simulation, and observed distinct average effective energy (ΔG_{eff}) for the different groups in each system (TIR1·IAAx^{PB1} protein complex). Group 1 for TIR1·IAA7^{PB1} and groups 1 and 3 for TIR1·IAA12^{PB1} turn out to be energetically less favored, while groups 2 in each case show the lowest binding energy. This indicates groups 2 likely depict the most probable ensembles (Fig. 6a). We further carried out per-residue effective energy decomposition analysis (prEFED) followed by validation via computational alanine scanning (CAS) in order to identify relevant residues in groups 2 favoring TIR1·AUX/IAA^{PB1} interactions (Fig. 6b and Supplementary Table 3). We found residues in TIR1 that might engage in polar interactions with the AUX/IAA PB1 domain. D119, D170, V171, S172, H174, H178, S199, R220 along the LRR3–7 in TIR1 likely contribute to stabilization of the TIR1·IAA7^{PB1} complex. Residues H174, H178, S199 also stabilize TIR1·IAA12^{PB1} interactions together with R156, S177, S201, and R205 in TIR1 LRR4–6 (Fig. 6b, c and Supplementary Fig. 13).

A paradigm for TIR1·auxin·AUX/IAA interactions in vivo. To next determine whether the in silico identified TIR1 residues contribute to its function, and therefore auxin receptor formation, we first generated mutant proteins and evaluated their interaction potential in Y2H assays (Fig. 7a and Supplementary Fig. 14). Mutations S199A and R220A impair ASK1·TIR1, TIR1·IAA7, as

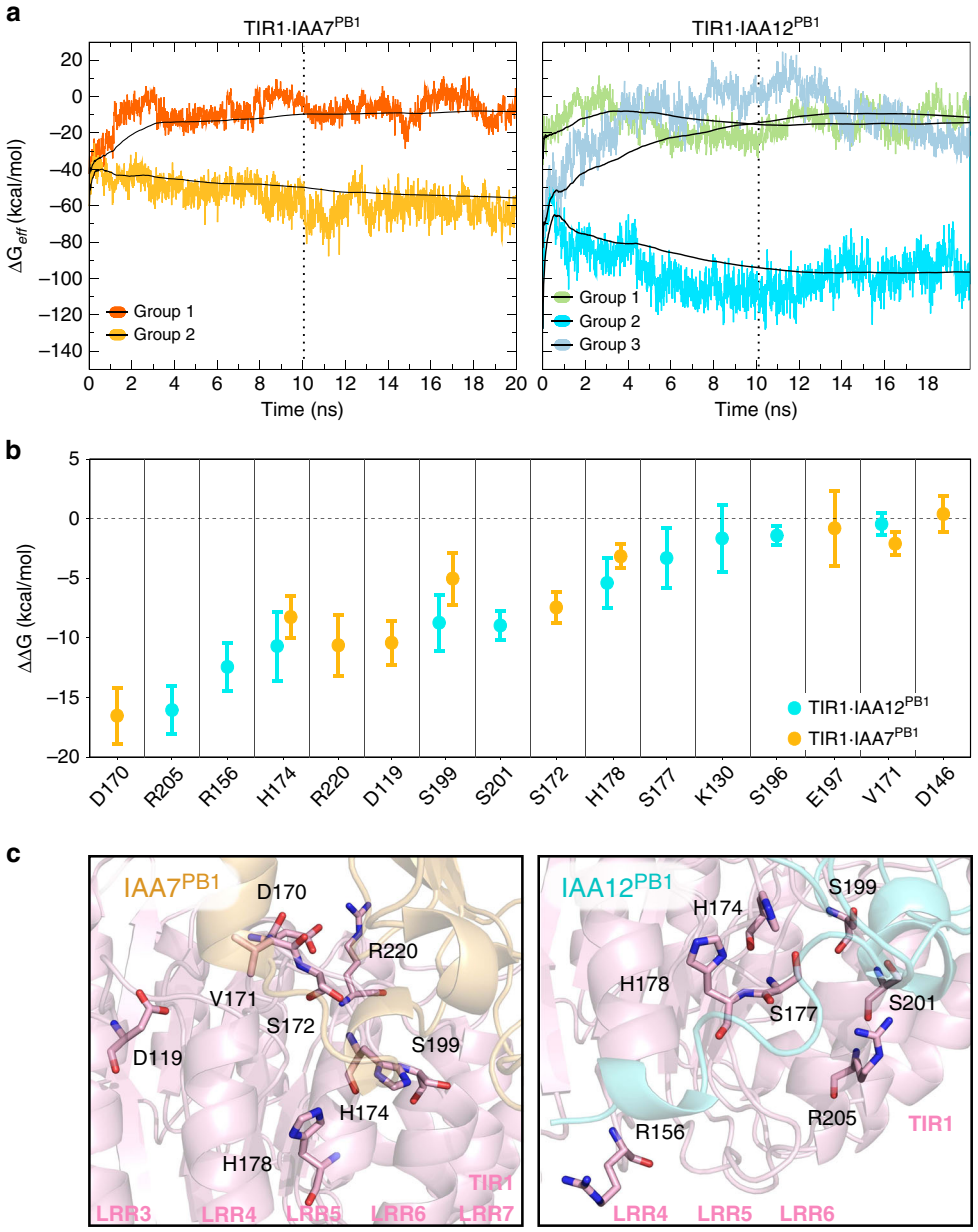

Fig. 6 Molecular dynamics simulations reveal energetically favorable TIR1·AUX/IAA^{PB1}-interacting moieties. a Time evolution of instantaneous ΔG_{eff} values over 20 ns identifying stable TIR1·AUX/IAA^{PB1} complexes from HADDOCK best scoring groups (IAA7: cluster1_1; 2_1; and IAA12: cluster1_1; 2_1; 3_1). Black lines indicate the accumulated mean values of ΔG_{eff} for each trajectory. One low energetic and stable complex (group 2, light orange (IAA7) or aquamarine (IAA12)) was identified for TIR1·IAA7^{PB1} (dark and light orange), and TIR1·IAA12^{PB1} (blues and green) systems. Dotted vertical line at 10 ns indicates the time point of equilibrium used as a reference for subsequent analysis. **b** Energetically relevant TIR1 residues for TIR1·AUX/IAA^{PB1} (TIR1·IAA7^{PB1}: orange; TIR1·IAA12^{PB1}: aquamarine) complex formation were identified by computational alanine scanning (CAS) using MD trajectories (in **a**) from the equilibration time point onwards (depicted as means ± SEM). **c** Stick representation of CAS-identified residues in TIR1 (light pink) localize to the LRR3–7 forming a polar patch that allows interaction with either IAA7^{PB1} (orange) or IAA12^{PB1} (aquamarine).

well as TIR1·IAA12 interactions. This implies these changes cause a long-range effect on TIR1 activity, and probably its overall conformational stability. Mutations S201A, D481R, and, to a lesser extent R156E drastically reduce basal TIR1·IAA7, and auxin-driven TIR1·IAA7 and TIR1·IAA12 associations (Fig. 7a). Importantly, at high auxin concentrations the effect of the TIR1 mutations S201A, D481R and R156E on TIR1·IAA7 associations, weakens. We envision a scenario in which in a high auxin environment, an intact AUX/IAA degron is glued and engaged by TIR1, which overrides and probably compensates for the loss of transient or milder interaction interfaces.

To further determine whether the new TIR1·AUX/IAA interfaces are required for biological function in planta, we transformed *tir1-1* mutant plants with constructs expressing mutant versions of *TIR1* under the control of the TIR1 promoter. We introduced single and double mutations in TIR1 affecting putative engagement sites for the PB1 domain and KR motif of AUX/IAAs, including R156E, S199A, S201A, R220A, or D481R, and tested their ability to rescue the auxin-resistant phenotype of *tir1-1* plants in root-elongation assays (Fig. 7b). If the newly identified TIR1 sites facilitate transient interactions with AUX/IAAs, we reasoned the more informative effects would be those traceable at low auxin

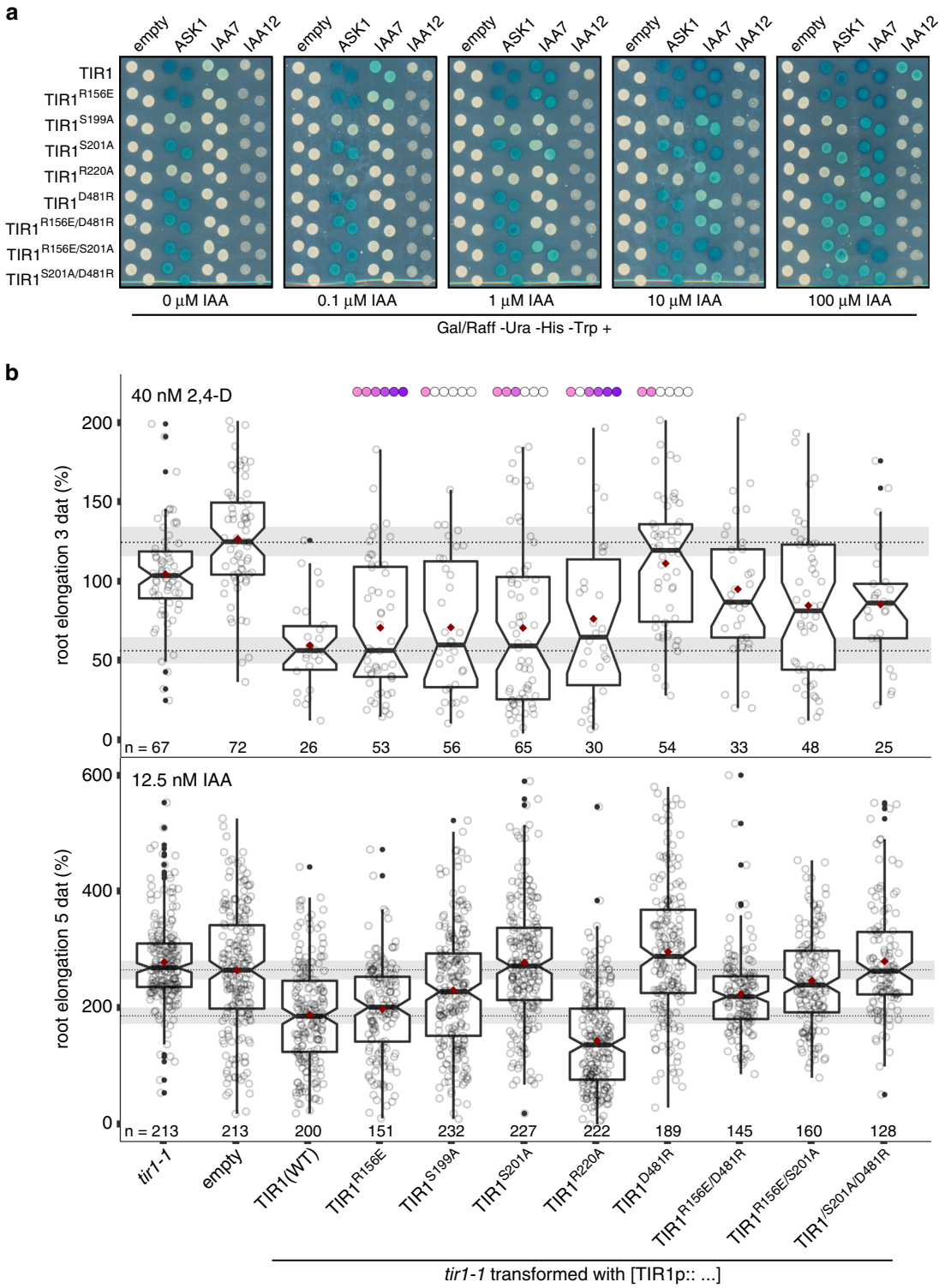

Fig. 7 Mutations on novel putative AUX/IAA-binding sites in TIR1 impair auxin responses in vivo. a Yeast two-hybrid (Y2H) interaction matrix for TIR1 wild type and TIR1-mutant versions carrying amino acid exchanges on relevant CAS-identified residues with ASK1, IAA7 and IAA12 at different auxin concentrations. **b** Box plots depicting root length of T1 *tir1-1* mutant plants carrying TIR1p:*tir1* mutant constructs. Transformed T1 seeds expressing RFP were selected by microscopy, and germinated in growth media. Five-day-old seedlings were transferred to growth medium containing either 40 nM 2,4-D or 12.5 nM IAA. Root elongation was traced on the day of transfer, and at days 3 and 5 after auxin treatment. *tir1-1* mutants are resistant to auxin treatment exhibiting long roots, and auxin sensitivity in *tir1-1* is restored by introducing a construct expressing wild type TIR1 under its own promoter. Numbers below the boxes correspond to the number of independent T1s (open circle's) analyzed per construct. Solid black horizontal lines represent median, dark red dots mean values and whiskers correspond to the upper and lower ~25% (1.5*IQR) of the data points. Outliers are shown as solid black dots. Shadow rectangles represent the notch size (~95% confidence interval) of the two reference data sets (empty vector and TIR1 wild type). Conservation of mutated residues in the TIR1/AFB1-5 F-box subclade is depicted as gradient colored circles above the plots (TIR1: light pink, AFB1-4: gradient of darker pink, AFB5: deep purple).

concentrations. Therefore, we transferred our transgenic lines to either a low concentration of natural IAA (12.5 nM), or a high concentration of synthetic auxin 2,4-D (40 nM). Compared to IAA, 2,4-D causes a sustained effect, as it accumulates over time in the cell[50]. As expected, a wild type version of TIR1 complements the auxin resistant *tir1-1* phenotype, while roots of *tir1-1* plants carrying the empty transformation vector, as a control, are blind to auxin, and continue elongating despite the treatment. Similarly, R156E and S199A restore wild type auxin sensitivity to seedlings treated with either 2,4-D or IAA for 3 to 5 days, respectively (Fig. 7b). This hints at those sites not having a prominent effect on TIR1 function in vivo. In contrast, S201A, D481R singles, and the double mutants R156E S201A and S201A D481R do not complement the root *tir1-1* phenotype of IAA treated plants (Fig. 7b). Although TIR1 S201 and R220 locate in the same cluster, they seem to affect TIR1 function differently. S201A complements the inhibitory effect of 2,4-D on root growth inhibition, indicating these plants might have been able to adapt to a sustained high auxin environment. R220A, on the other hand, confers dominant negative effects resulting in auxin hypersensitivity (Fig. 7b). In summary, we demonstrated the existence of two TIR1 amino acid clusters harboring S201, R220 and D481, essential for TIR1·AUX/IAA interaction interfaces, and TIR1 activity in vivo.

Discussion

Auxin is perceived by TIR1/AFBs and their ubiquitylation targets the AUX/IAA transcriptional repressors. While TIR1 adopts a compact solenoid fold, AUX/IAAs appear flexible and modular in nature as they engage in various protein interaction networks[26,51]. A 13-aa degron motif in AUX/IAAs seals a ligand-binding groove in TIR1, and is secured by auxin in place. To date, we lacked information on whether additional physical interactions between TIR1 and AUX/IAAs influence conformation and fate. We also did not know whether these interactions facilitate the formation of the final auxin receptor complex by a two-dimensional search on the part of TIR1 on the AUX/IAA surface or vice versa. We found IAA7 and IAA12 exhibit a highly dynamic conformation on account of IDRs along their sequence, which seems to favor recruitment by TIR1. Computational and experimental studies have shown IDRs, such as those in AUX/IAAs, act as inter-domain linkers contributing to protein–protein interactions by exclusively or partially forming binding interfaces[17,52,53]. Capturing TIR1·IAA7 and TIR1·IAA12 ensembles by XL-MS allowed us to visualize AUX/IAAs IDRs embracing TIR1 and expanding their, known so far, interaction interfaces. Although IAA7 and IAA12 show differences on IDR content and length, both embraced TIR1 in a similar manner. While the AUX/IAA degron drives auxin-mediated TIR1·AUX/IAA interactions, we found evidence for the IDR upstream of the degron and the PB1 domain to engage in transient interactions with two specific clusters of amino acids at the C-terminal domain (CTD), and the N-terminal domain (NTD) of TIR1, respectively (Fig. 8). A directional embrace of TIR1 by an open-armed AUX/IAA, strengthened by degron-flanking IDRs, might additionally secure a TIR1·auxin·degron "click" (Fig. 8).

From the AUX/IAA standpoint, their local flexibility evidently shapes their conformation and accessibility when in complex with TIR1. Flexible IDRs in AUX/IAAs, as shown for IAA7 and IAA12, serve as variable calipers that measure the available distance between the KR motif and the core degron, and the degron and the PB1 domain, to properly and, with the right orientation, dock on TIR1. Our data also provided evidence for dynamic allosteric modulation of a TIR1·AUX/IAA complex by the folded PB1 domain and IDRs in AUX/IAAs. We could track positive but also negative cooperativity, due to the degron tail and PB1 domain combination, fine-tuning conformational states of TIR1·IAA7 and TIR1·IAA12 pairs, respectively. Further long-range, probable allosteric, effects are reflected into AUX/IAA turnover, when PB1 domain and degron tail act as one element (Supplementary Fig. 5).

The effects of cooperative allostery driven by IDRs in AUX/IAA proteins might not be limited to the TIR1·AUX/IAA interaction, but rather influence the assembly into other complexes regulating auxin output signals[54]. It is therefore also possible that in response to fluctuating cellular auxin concentrations, transient TIR1·AUX/IAA interactions alter the energy landscape of AUX/IAA·TPL, AUX/IAA·ARF and AUX/IAA·AUX/IAA assemblies and/or possible decorations with PTMs. Future studies will tell whether IDRs in AUX/IAAs, and the recently described IDRs in ARFs, affect their protein assembly's localization or activity[55]. One can envision, IDR-driven cooperativity resulting in a multiplicity of allosterically regulated interactions within the auxin signaling pathway, where AUX/IAAs act as signaling hubs within the different complexes.

Within the *Arabidopsis* AUX/IAA protein family, nearly half of the degron tails are between 20 and 40 aa long and show high disorder probability (Supplementary Fig. 1). Seven of the 23 degron-containing AUX/IAAs (IAA19, IAA4, IAA6, IAA5, IAA1, IAA2, IAA15), however, carry a relatively ordered degron tail shorter than 20 amino acids (Supplementary Figs. 1 and 15). Is that specific length an evolutionary constraint for TIR1 association? Auxin-dependent gene regulation, and AUX/IAA proteins appear in the land plant lineage over 500 mya[28,56]. When comparing the proteins sequence of the ancestral AUX/IAAs in moss and *Marchantia*[57,58], we observed their degron tails are not much longer than the average degron tails (40 aa) of *Arabidopsis* AUX/IAAs, despite the overall length of these proteins being at least double that of angiosperm AUX/IAAs. It will be interesting to investigate whether degron tails length and disorder content are deeply conserved features for surface availability, and whether short degron tails (<20 aa) can still offer tailored positioning on TIR1. It remains also to be determined whether IDRs flanking the degron befit AUX/IAAs, particularly closely similar AUX/IAA ohnologs, with signatures that calibrate degron accessibility. Furthermore, the degron tail might generate an entropic force[59,60] that is fine-tuned, but also restricted, by IDR length, modulating binding of AUX/IAAs to TIR1. It remains to be established whether degron tails in different AUX/IAAs impact the interaction surface with TIR1, which we anticipate might translate into variability of binding kinetics.

Do structural features in TIR1 aid AUX/IAA positioning? Our data shows that is indeed the case. We found R220 located in cluster 1 to actively participate in TIR1·AUX/IAA associations in silico, in vitro, and in vivo. In fact, the TIR1 mutation R220A caused auxin hypersensitivity in *Arabidopsis* seedlings. Previously, D170E and M473L *tir1* mutant alleles showed faster AUX/IAA degradation, and increased transcription of auxin-responsive genes resulting also in auxin hypersensitivity[61]. Based on our biochemical and structural proteomics data, a few scenarios could explain the effect of R220A *TIR1* mutant allele. Thanks to its positive charge and size, R220 might play a sentry role for guiding the location of the disordered degron tail and the PB1 domain of AUX/IAAs on TIR1. Alanine-substituted R220 might result in a positional effect of the C-terminal portion of AUX/IAAs altering the exchange rates of different AUX/IAAs. Auxin-dependent, but also auxin-independent TIR1·AUX/IAA interactions could be expedited if the R220A conversion relaxes the positioning of the PB1, of at least a subset of AUX/IAAs. Most intriguingly, R220 is almost fully conserved among the members of the TIR1/AFB FBP subclade in *Arabidopsis* supporting its central role monitoring

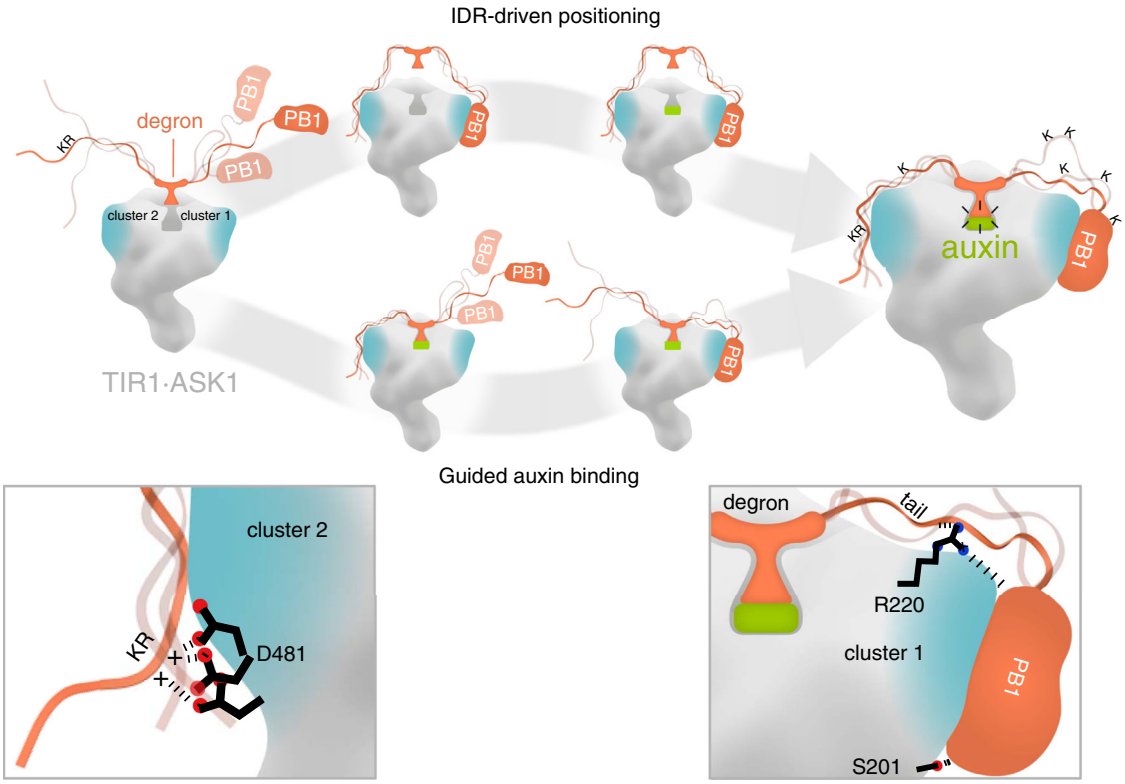

Fig. 8 Model for ASK1·TIR1·AUX/IAA complex assembly fine-tuned by IDRs flanking the AUX/IAA degron. The F-box protein TIR1 of the SCF^{TIR1} E3 ubiquitin ligase recruits AUX/IAA targets for their ubiquitylation and degradation. The phytohormone auxin and a core degron in AUX/IAAs are essential for AUX/IAA recognition. Intrinsically disordered regions (IDRs) flanking the degron provide high flexibility and an extended fold to AUX/IAAs, influencing TIR1·AUX/IAA complex formation. At least two different routes are possible for dynamic AUX/IAA recruitment and UPS-mediated degradation: (i) auxin-triggered association between TIR1 and the AUX/IAA degron paves the way for positioning adjacent IDRs, which exposes ubiquitin acceptor sites for efficient ubiquitylation; (ii) transient auxin-independent interactions between IDRs, as well as the PB1 domain in AUX/IAAs, and two patches (clusters 1 and 2) of residues at opposite sides of TIR1, assist on auxin binding and offer tailored positioning. Residues R220 and S201 from cluster 1 (right zoom in) and D481 from cluster 2 (left zoom in) in TIR1 play a major role in TIR1·AUX/IAA complex formation. The residency time of an AUX/IAA target on TIR1, enables processivity of AUX/IAA ubiquitylation, and impinges on availability of IDRs as initiation sites for degradation by the 26S proteasome.

target recruitment (Fig. 7b). This data allowed us to postulate that the right positioning of the degron tail and the PB1 domain of AUX/IAAs on cluster 1 in TIR1 might have a favorable effect on auxin sensing, as part of the target recruitment mechanism (Fig. 8).

Particular stretches of amino acids with increased evolutionary conservation within disordered segments have been found to determine interaction specificity, acting as functional sites[62–64]. This seems to precisely apply to the region in AUX/IAAs upstream of the degron containing the auxin-responsive Lys-Arg (KR) dipeptide motif[35,65]. The KR exhibits a high level of conservation, and in addition to being part of a bipartite nuclear localization signal (NLS), the KR contributes to assembly of a TIR1·AUX/IAA auxin receptor complex and, probably as a result, is required for basal proteolysis in planta and AUX/IAA degradation dynamics[24,35,36,65]. Interestingly, the ability of the KR to act as auxin-responsive rate motif influencing AUX/IAA turnover, and the magnitude of this effect could only be correlated with the proximity of the KR to the degron[35,36]. How mechanistically could the KR exert an effect on TIR1 recognition and further AUX/IAA processing? Our findings lead us to propose an answer to a more than 10 year's long-standing question. As part of the AUX/IAA embrace to TIR1, we found the KR motif embedded in the IDR upstream of the degron confers alternative, and probably, first binding contacts with TIR1 (Fig. 8). We predict a high-IDR flexibility in the NTD of AUX/IAAs warrants a necessary distance between the KR and the core degron for reaching distinct TIR1 contact sites, including D481 (Fig. 8). D481 is located in a negative charged patch in cluster 2 within the CTD of TIR1 (Fig. 8 and Supplementary Fig. 9). According to our XL data, the TIR1 exposed patch (incl., D481, S482, E459, or E506) comes into close proximity with the KR-containing IDR in AUX/IAAs making electrostatic interactions possible. We tested a reversed charge exchange for D481, and the resulting D481R abolished basal TIR1·IAA7 association, while weakening auxin-driven TIR1·IAA7 and TIR1·IAA12 interactions. Not only might a charge exchange lead to a repulsion of the AUX/IAA KR motif, but an Arg-replacement might displace and therefore slow down or prevent KR engagement. While TIR1 and AFB1 offer similar contact points to the KR in AUX/IAAs, AFB2, and AFB3 exhibit opposite charged residues (Lys) that however might still provide charge–charge interactions with a specific subset of AUX/IAAs. It remains to be determined whether this is an additional feature facilitating differential auxin sensing by distinct TIR1/AFBs·AUX/IAA co-receptor combinations[24].

The described interaction interfaces and structural disorder in AUX/IAAs appear also to be instrumental for processivity in ubiquitin transfer by the SCF^{TIR1} E3 ubiquitin ligase. This is crucial as once an active E2-E3-target assembly has formed, spatial and geometric constraints such as distance and orientation relative to the E3-bound primary degron limit ubiquitylation surface and lysine selection for degradation[7]. AUX/IAA sequence

harbors a number of putative ubiquitin acceptor lysines (~9% total sequence) (Supplementary Fig. 15). Our data showed that not all of these sites are favorable for ubiquitylation. Downstream of the core degron, AUX/IAAs likely lend an attractive region for ubiquitin conjugation. We envision either the PB1 or the degron tail facilitating the accessibility of residues that undergo ubiquitylation. Upon TIR1·AUX/IAA interaction, IDRs either orient the PB1 domain-located lysines (e.g. IAA7) or act themselves as ubiquitylation acceptor sites as ubiquitin acceptor sites (e.g. IAA12). Properly positioned ubiquitin moieties at the suitable distance of an IDR, and an IDR with unbiased sequence composition as an initiation site will certainly impact efficient AUX/IAA degradation by the proteasome[66–68]. Hence, it will be imperative to shed light on where AUX/IAAs are ubiquitylated in vivo, and where exactly the proteasome initiates degradation relative to the ubiquitylation sites.

In summary, we unveiled an expanded network of TIR1·AUX/IAA interactions modulated by intrinsically disordered regions flanking the degron, and identified key residues for co-receptor formation and auxin perception. Our biochemical studies combined with a structural proteomics approach demonstrated IDRs in IAA7 and IAA12 harbor specific features that support TIR1·-AUX/IAA interactions. In planta data confirmed these findings, and revealed a wider extent of TIR1·AUX/IAA interactions modulating auxin signaling, and likely enabling efficient ubiquitin transfer.

From a biological perspective, we evidenced that IDRs outside of a degron in ubiquitylation targets can participate, in particularly, basal interactions with an E3. We captured for the first time ensembles of a highly flexible ubiquitylation target and an SCF-type E3 ubiquitin ligase, identified novel interaction interfaces, and confirmed the relevance of specific interaction sites in vivo.

From a technical standpoint, XL-MS-based structural proteomics, which is yet to become widely regarded, offered a unique opportunity to visualize transient protein–protein interactions, otherwise difficult to capture. The gain in structural information, in combination with biochemical and in vivo validation opens up great opportunities to discover novel interaction interfaces and pinpoint new functional sites in a protein of interest. Additionally, our studies highlight the power of a combined experimental set-up for unraveling selection mechanisms in complex formation, and understanding how IDR-driven allostery might influence a complex signaling network.

Methods

Phylogenetic tree generation and secondary structure analysis. Phylogenetic tree construction was done using Clustal Omega[69] with standard settings (Neighbor-joining tree without distance corrections), and the full length protein sequences of all *Arabidopsis* AUX/IAAs deposited at uniprot[https://www.uniprot.org/] (Supplementary Data 1). The constructed tree was visualized by iTOL[70] and manually edited. In silico disorder analysis was performed with the web-based IUPred2A tool[38] utilizing AUX/IAA protein sequences. The resulting disorder probability was used to categorize each residue as either ordered (<0.4), intermediate (0.4–0.6), or disordered (>0.6). Same analysis was carried out for all AUX/IAA proteins excluding the PB1 domain (for reference, the conserved VKV motif was earmarked as the start of the PB1 domain). Residues of each category were plotted using R. IAA7 and IAA12 disorder predictions were additionally carried out using SPOT[71] and PrDOS[72] algorithms with standard settings. Hydropathy plots were generated via Expasy-linked ProtScale[73,74] using the Kyte-Doolittle method[75].

Protein purification. ASK1·TIR1 complex was purified from Sf9 cells as described earlier[23] with minor changes. In brief, ASK1 was co-purified with GST-TIR1 using GSH affinity chromatography (gravity flow) and anion chromatography (MonoQ) followed by tag-removal and a final size-exclusion chromatography (SEC) step (Superdex 200) using an ÄKTA FPLC system.

AUX/IAA proteins, including chimeric versions, were expressed as GST-tagged proteins in *E.coli* and purified using GSH affinity chromatography, including a high-salt wash (1 M NaCl) and gravity flow anion exchange chromatography (Sepharose Q). For circular dichroism, the GST-tag was removed on the GSH column matrix with thrombin, and fractions containing AUX/IAAs were briefly concentrated, passed over a benzamidine column, and further purified using a Sephacryl S-100 column (SEC) with an ÄKTA FPLC system. This step was carried out using the CD measurement buffer (see CD measurement section) for buffer exchange.

Size exclusion chromatography and size calculations. The last protein purification step was used to simultaneously determine the Stokes radii of AUX/IAAs in CD buffer (10 mM KPi pH 7.8; 150 mM KF; 0.2 mM TCEP). The HiPrep 16/60 Sephacryl S-100 high-resolution column was calibrated using gel filtration standards (Bio-Rad, Cat. #151-1901) with added bovine serum albumin (BSA) before the runs. Stokes radii for the globular known reference proteins were calculated as described[76]. The Stokes radii of AUX/IAA variants were calculated from the resulting calibration curve equation based on their retention volume ($n = 4–10$).

Circular dichroism (CD) measurements. After purification, including tag-removal and size-exclusion chromatography, AUX/IAAs were concentrated and adjusted to 2.5–5 µM in CD buffer. CD measurements were carried out on a Jasco CD J-815 spectrometer and spectra were recorded from 260 nm to 185 nm as 32 accumulations using a 0.1 nm interval and 100 nm/min scanning speed. Cell length was 1 mm and temperature was set to 25 °C. All spectra were buffer corrected using CD buffer as a control and converted to mean residual ellipticity (MRE). Reference spectra for a disordered (MEG-14; PCDDBID: CD0004055000 [https://pcddb.cryst.bbk.ac.uk/deposit/CD0004055000/?files=&dl]), a beta-sheet (BtuB; PCDDBID: CD0000102000 [https://pcddb.cryst.bbk.ac.uk/deposit/CD0000102000]) and an alpha-helical protein (amtB; PCDDBID: CD0000099000 [https://pcddb.cryst.bbk.ac.uk/deposit/CD0000099000]) were used.

[3H]-labeled auxin binding assay. Radioligand binding assays for determining dissociation constants of auxin receptors[77] were performed using purified ASK1·TIR1 protein complexes, GST-tagged AUX/IAAs (incl. chimeric AUX/IAAs) and [^{3}H]IAA with a specific activity of 25 Ci/mmol (Hartmann Analytic). Final protein concentrations in a 100 µL reaction were 0.01 µM ASK1·TIR1 complex and 0.3 µM AUX/IAAs. Complexes were allowed to form 1 h on ice, shaking. For non-specific binding controls, reactions contained additionally 2 mM cold IAA. Data was evaluated with GraphPad Prism v 5.04, and fitted using the "one site total and non-specific binding" preset.

LexA yeast two-hybrid assays. LexA-based yeast two-hybrid assays were performed using mated yeast strains EGY48 + pSH18-34 and YM4271 transformed with either LexA DBD-fusions of TIR1 or tir1 mutants in the pGILDA vector; or AD-fusions of ASK1, IAA7, IAA12, or iaa7/12 chimeras in the pB42AD vector (GoldenGate system, Supplementary Data 1). For each assay, same count of yeast cells ($OD_{600} = 0.4$ or 0.8 for IAA12(-like)) were spotted on selection media (Gal/Raff–Ura –His–Trp) containing BU salts (final: 7 g/L Na_2HPO_4, 3 g/L NaH_2PO_4, pH 7), X-Gal (final 80 mg/L) and the given auxin (IAA) concentration. Plates were incubated at 30 °C for several days and constantly monitored. Expression of chimeric AUX/IAAs and TIR1 mutants in yeast was confirmed using immunoblot analysis on lysates from haploid yeast. Fifty milliliters liquid selection medium (Gal/Raff -Ura -His or -Trp) were inoculated with an 1/25 volume overnight culture and grown to $OD_{600} \approx 0.6$. Cells were harvested, washed with distilled water and lysed in 200 µL lysis buffer (0.1 M NaOH, 2% β-mercaptoethanol, 2% sodium dodecyl sulfate, 0.05 M EDTA, 200 µM benzamidine, 1 mM PMSF, Roche protease inhibitor cocktail) at 90 °C for 10 min. After neutralization with 5 µL 4 M sodium acetate for 10 min at 90 °C, 50 µL 4X Laemmli was added and samples were separated via SDS-PAGE and immunoblotted (anti-HA(F-7): Santa Cruz Biotechnology (sc-7392; 1:1000), anti LexA: abcam (ab14553; 1:500), anti-Tubulin (YL1/2): abcam (ab6160; 1:5000), anti-rabbit-AP: Sigma-Aldrich (A3687; 1:10000), anti-mouse-AP: Sigma-Aldrich (A2179; 1:10000)).

In vitro reconstitution of Ub-conjugation (IVU). In vitro ubiquitylation (IVU) reactions[34] were prepared as follows: Two protein mixtures (mix A and mix B) were prepared in parallel. Mix A contained 50 µM ubiquitin (Ub; fluorescein-labeled Ub^{S20C}: Ub^{K0}; 4:1 mix), 0.2 µM 6xHis-UBA1 (E1) and 2 µM 6xHis-AtUBC8 (E2) in reaction buffer (30 mM Tris-HCl, pH 8.0, 100 mM NaCl, 2 mM DTT, 5 mM $MgCl_2$, 1 µM $ZnCl_2$, 2 mM ATP). Mix B contained 1 µM Cul1·RBX1, 1 µM ASK1·TIR1, and 5 µM AUX/IAA protein in reaction buffer. Mix B was aliquoted and supplemented with IAA to reach the indicated final concentration. Mixtures A and B were separately incubated for 5 or 10 min at 25 °C, respectively. Equal volumes of mix A and B were combined, aliquots were taken at specified time points, and reactions were stopped by denaturation in Laemmli buffer. IVUs with chimeric AUX/IAAs were carried out 1 h with 1 µM IAA. Immunodetection of Ub-conjugated proteins was performed using polyclonal anti-GST in rabbit (1:20,000; Sigma, G7781) antibodies combined with secondary anti-rabbit Alexa Fluor® Plus 647 antibody (1:20,000; Thermo Fischer Scientific, A32733). Detection was performed with a Typhoon FLA 9500 system (473 nm excitation wavelength and LPB filter for fluorescein-labeled ubiquitin signal detection and 635 nm excitation wavelength and LPR filter for GST signal).

Quantification of ubiquitylated AUX/IAAs was achieved by using ImageQuant TL software automatic lane detection of in-gel fluorescein signals above unmodified GST-IAA7 and GST-IAA12 proteins (~50 kDa). As the signal for ubiquitylated AUX/IAAs increase, the signal for unmodified GST-IAA7 and GST-IAA12 fusion proteins decreases. This was quantified after blotting and immunodetection using the Alexa Fluor 647 signal, and automatic band detection. All signals were background subtracted (rubberband method).

LC-MS analyses of IVU reactions. Three sets of IVUs, corresponding to three biological replicates, were performed on consecutive weeks using AUX/IAA proteins from different batch preparations. After 30 min, IVUs were stopped by denaturing with urea, reduced with DTT and alkylated with iodoacetamide. Trypsin digestion was carried out overnight at 37 °C. Upon quenching and desalting, peptides were separated using liquid chromatography C18 reverse phase chemistry and later electrosprayed on-line into a QExactive Plus mass spectrometer (Thermo Fisher Scientific). A Top20 DDA scan strategy with HCD fragmentation was used for MS/MS peptide sequencing. Ubiquitylated residues on identified peptides were mapped using GG and LRGG signatures (as tolerated variable modifications) from using both the Mascot software v2.5.0 (Matrix Science) linked to Proteome Discoverer v1.4 (Thermo Fisher Scientific), and the MaxQuant software v1.5.0.0.

Crosslinking (XL) reactions and LC-MS analyses. DSBU (ThermoFisher) XL reactions containing either 4–5 µM of ASK1·TIR1, and 5 µM IAA7^{BM3} or IAA12^{BM3} or 10 µM IAA7^{BM3} or IAA12^{BM3} alone were incubated for 1 h at 25 °C. Proteins were pre-incubated 15 min in the presence or absence of 10 µM auxin (IAA) before addition of 1 mM DSBU (100 molar excess). After TRIS quenching, samples were sonicated in the presence of sodium deoxycholate, reduced with DTT, and alkylated with iodoacetamide. Alkylation was further quenched by DTT, samples were incubated with trypsin overnight at 37 °C, and protein digestion was stopped with 10% TFA.

Upon centrifugation (5 min 14,000 x *g*), proteolytic peptide mixtures were analyzed by LC/MS/MS on an UltiMate 3000 RSLC nano-HPLC system coupled to an Orbitrap Q-Exactive Plus mass spectrometer (Thermo Fisher Scientific). Peptides were separated on reversed phase C18 columns (trapping column: Acclaim PepMap 100, 300 µm × 5 mm, 5 µm, 100 Å (Thermo Fisher Scientific); separation column: self-packed Picofrit nanospray C18 column, 75 µM × 250 mm, 1.9 µm, 80 Å, tip ID 10 µm (New Objective)) or µPAC™ 200 cm C18 (Pharmafluidics). After desalting the samples on the trapping column, peptides were eluted and separated using a linear gradient from 3% to 40% B (solvent A: 0.1% (v/v) formic acid in water, solvent B: 0.08% (v/v) formic acid in acetonitrile) with a constant flow rate of 300 nL/min over 90 min. Data were acquired in data-dependent MS/MS mode with stepped higher-energy collision-induced dissociation (HCD) and normalized collision energies of 27%, 30%, and 33%. Each high-resolution full scan (*m*/*z* 375 to 1799, $R = 140{,}000$ at *m*/*z* 200) in the orbitrap was followed by high-resolution product ion scans ($R = 17{,}500$) of the ten most intense signals in the full-scan mass spectrum (isolation window 2 Th); the target value of the automated gain control was set to 3,000,000 (MS) and 200,000 (MS/MS), maximum accumulation times were set to 100 ms (MS) and 250 ms (MS/MS) and the maximum cycle time was 5 s. Precursor ions with charge states <3+ and >8+ or were excluded from fragmentation. Dynamic exclusion was enabled (duration 60 s, window 3 ppm).

Data analysis of crosslinked (XL)-peptides. For XL analysis, mass spectrometric *.raw files were converted to mzML using Proteome Discoverer 2.0. MeroX analysis was performed with the following settings: Proteolytic cleavage: C-terminal at Lys (blocked as XL site) and Arg with max. 3 missed cleavages, peptides' length: 5 to 30, static modification: alkylation of Cys by IAA, variable modification: oxidation of M, crosslinker: DSBU with specificity towards Lys, Ser, Thr, Tyr, and N-termini, analysis mode: RISE-UP mode, precursor mass accuracy: 5 ppm, product ion mass accuracy: 10 pm (performing mass recalibration, average of deviations), signal-to-noise ratio: 1.5, precursor mass correction activated, prescore cutoff at 55% intensity, FDR cutoff: 5%, and minimum score cutoff: 70. All analyses included the cRAP database sequences. Decoy database was generated using shuffled sequences with kept protease sites. Shown in Fig. 4 are all detected intramolecular XL and all ASK1·TIR1 XLs. Sequences of IAA7 and IAA12 contain 5 or 2 additional amino acids at the N-terminus, respectively. Detailed results can be found in Supplementary Data 3 and 4. For further analysis only inter-protein XLs between TIR1 and AUX/IAAs found in at least 2/3 (IAA7) or 3/4 (IAA12) experiments were considered.

XL-based docking using HADDOCK and DisVis analysis. Comparative models of IAA7 and IAA12 PB1 domains were created using multi-sequence-structure-alignments (PIR formatted) as input for MODELLER 0.921[78]. Input files, alignment files and derived models are provided in the Supplementary Data 5 (modeller_files.tgz). In addition, the C-terminal helix of both IAA7 and IAA12 PB1 domains were modeled de novo and subsequently added to the structure (resulting pdb: C-ter). The generated models (ten C-terminal helix variants) were incorporated for the HADDOCK-based docking together with the available ASK1·TIR1 structure (PDB codehttps://www.rcsb.org/structure/code: 2P1Q [http://www.rcsb.org/structure/2P1Q], resolution: $R = 1.91$ Å)[23]. HADDOCK parameter files are provided in the Supplementary Data 6 (haddock_files).tgz. A detailed description on how to prepare pdb files and incorporate distance restraints can be found elsewhere[79]. Formatted pdb files were uploaded to the HADDOCK server[80,81] using guru access level. To incorporate restraints, we used known distances reported for DSBU and albumin XLs from our data sets (Supplementary Table 1 and Supplementary Data 3 and 4). Accordingly, we further added a distance restraint (degron tail restraint) corresponding to the degron tail length calculated as described in ref. [82]. Here, the theoretical Stokes radii of a given peptide for different folding states (min: folded; max: disordered) are calculated and used as restraints. For each complex docked, 10,000 rigid body docking structures were generated followed by a second iteration (400 best structures). Finally, 200 models/structures were water refined (explicit solvent) and clustered (FCC[83] at 0.6 RMSD cutoff).

Using the same restraints, the possible conformational docking space of the PB1 domains was searched, and visualized using DisVis[49,84,85] with standard parameters (Supplementary Data 7 (DisVis_only_files).tgz). In addition, in order to validate the derived models, we performed a docking with HADDOCK including both, the distance restraints shown in Supplementary Table 1, and active residues calculated by DisVis. In brief, the restraints were used to generate the possible conformational docking space of the PB1 domains, followed by calculation of active residues, based on their interaction propensities using DisVis. DisVis considers those residues as active most contacted in the solutions consistent with the provided distance restraints. Those residues with an interaction propensity higher than 1.0 were selected, and subsequently used as active residues for the docking with HADDOCK under the general definition of ambiguous interaction restraints[86]. Parameter files used for this docking and final structures are provided as Supplementary Data 8 (disvis_haddock).tgz. The combination of distance restraints and DisVis-calculated active residues showed high restraint violation energies and the results from this approach were not further used. PyMOL™ (Version 2.1) and UCSF Chimera[87] were implemented for image creation.

Molecular dynamic simulations of protein–protein complexes. One refined structure of each group, derived from the XL-based docking by HADDOCK incorporating the disorder restraint (two groups for TIR1·IAA7^{PB1}; three groups for TIR1·IAA12^{PB1}), was used as starting structure for MD simulations (cluster1_1 and cluster2_1 from haddock_files.tgz/haddock_files/IAA07/With_disorder_restraint/; cluster1_1, cluster2_1 and cluster3_1 from haddock_files.tgz/haddock_files/ IAA12/With_disorder_restraint/, both from Supplementary Data 6 (haddock_files).tgz). The five structures were prepared using structure preparation and protonate 3D (pH = 7.5) modules and subsequently minimized with AMBER10 force-field[88] in MOE 2019.0101 (Chemical Computing Group Inc., Montreal, Quebec, Canada).

Molecular dynamic simulations were performed with the GROMACS software package (version 4.6.5)[89]. The parameters corresponding to the proteins were generated with AMBER99SB-ILDN force-field[90] and TIP3P explicit solvation model[91]. Electro-neutrality was guaranteed by adding Na^+ and Cl^- ions into the unit cells at an appropriate ratio to reach a final NaCl concentration of 0.2 mol/L. The protocol employed here to perform MD simulations involves prior energy minimization (EM) and position-restrained equilibration, as outlined by Lindahl[92] for lysozyme in water. Newton's equation of motion for the position-restrained equilibration was solved using the leap-frog integrator[93], with a time step of $\Delta t = 2$ fs for a total time of 50 ps (25,000 integration steps). The system was simulated at constant temperature and pressure of 310 K and 1 atm, respectively. The Berendsen algorithm[94] for the pressure and Velocity rescaling[95] for the temperature with time constant (τ) of 3 ps and 0.1 ps, was respectively implemented[96]. Obeying the Maxwell–Boltzmann distribution from 50 to 310 K[96] random initial velocities were assigned to each atom prior to the MD simulations.

Once the system was equilibrated, we proceeded to the productive dynamic simulation without position restraint[97] for 20 ns. The system simulation was carried out at $T = 310$ K and $p = 1$ atm. The Parrinello-Rahman coupling algorithm[98,99] was used to keep pressure constant with a time constant (τ) of 1 ps[96]. The temperature, non-bonded interaction and time step were controlled or set up similarly as in the equilibration run. The snapshots of all runs were saved each 10 ps. Molecular dynamics parameter files (mdp), and the minimized and equilibrated starting structure for each run, are provided in the Supplementary Data 9 (MD).tgz. Detailed MD simulation method is included in Supplementary Methods.

Effective binding free-energy calculations using MM-GBSA. The effective binding free-energy (ΔG_{eff}) of the protein–protein complexes formation was calculated using MMPBSA.py from Amber18 package employing the MM-GBSA method[100]. We followed the single trajectory approach, in which the trajectories for the free proteins were extracted from that of the protein–protein complexes. GB^{OBC1} and GB^{OBC2} implicit solvation models were employed[100]. The ΔG_{eff} values were obtained every 10 ps from the productive MD simulation (20,000 ps). We calculated the cumulative mean (also referred to as accumulated mean) for each of the 2000 ΔG_{eff} values. We computed the accumulated mean for each position by summing over all previous values and dividing by their number.

Energetically relevant residues (hot-spots) at the interfaces of TIR1·AUX/IAA^{PB1} complexes were predicted by using the per-residue effective free-energy decomposition (prEFED) protocol implemented in MMPBSA.py[100]. Hot-spot residues were defined as those with a side-chain energy contribution (ΔG_{SC}) of ≤ −1.0 kcal/mol. We used computational alanine scanning (CAS)[100] to further assess per-residue free-energy contributions. Alanine single-point mutations were generated on previously identified hot-spots from the prEFED protocol. Both prEFED and CAS protocols were performed from the last 10 ns of the MD simulation.

Plant materials and root-elongation assays. Transgenic *Arabidopsis thaliana* plants expressing mutated TIR1 versions (tir1cds$^{(mut)}$) driven by the TIR1 promoter (TIR1p) were generated using Gateway cloning. A ~2.3 kB TIR1 promoter fragment was amplified and subcloned in a pUC57-based entry vector using *Xma*I and *Kpn*I sites. Similarly, TIR1 cDNA fragments, either wild type or carrying mutations in KR- or PB1-binding sites were amplified from the pGILDA-TIR1 or pGILDA- tir1cds$^{(mut)}$ yeast expression constructs[24]. A list of primers utilized in this study has been provided as Supplementary Data 1. Primers added Gateway *attB* recombination sites to clone inserts into pDONR221^{TM}/ZEO (Invitrogen). Final constructs were obtained using a double Gateway reaction of the respective Entry clones and pEN-4 entry vector containing the TIR1 promoter, into the destination vector pDEST (pEDO 097 (4 ccdb-2)) TIR1p:tir1cds$^{(mut)}$. Nine different TIR1p:tir1cds$^{(mut)}$ constructs and TIR1p:TIR1cds$^{(wt)}$, as a complementation control, were introduced by Agrobacterium-mediated transformation into *tir1-1* mutant plants. Transformed seeds (T1s) expressing red fluorescence protein (RFP) were selected by fluorescence microscopy, surface sterilized, and directly sowed in ½ MS medium with 1% sucrose. After seed stratification for 3 days at 4 °C, seedlings were grown at 22 °C under long day (LD) conditions (16 h light, 8 h dark) and 90 μE/m^2/s of light for 4 days. For auxin treatments, about 250 T1 seedlings per construct were transferred to vertical plates containing ½ MS growth medium (with 1% sucrose) supplemented with auxins, either 12.5 nM IAA (indole 3-acetic acid) or 40 nM 2,4-D synthetic analog (2,4-dichlorophenoxyacetic acid). Seedlings were grown at 22 °C under LD conditions, and root elongation was traced up to 5 days after transfer to auxin plates.

Reporting summary. Further information on research design is available in the Nature Research Reporting Summary linked to this article.

Data availability

All data generated in this study has been made available either in the Source Data File, via the respective repository entry, or is provided as separate files. Mass spectrometry proteomics data have been deposited to the ProteomeXchange Consortium via the PRIDE partner repository with the data sets identifiers: PXD015285 [https://www.ebi.ac.uk/pride/archive/projects/PXD015285] (XL-MS) and PXD015392 [https://www.ebi.ac.uk/pride/archive/projects/PXD015392] (ubiquitylation site identification data). All other information supporting the findings of this study is available from the corresponding author upon reasonable request.

Code availability

All code used in this manuscript is published and described in the corresponding parts of the manuscript.

Received: 2 October 2019; Accepted: 17 April 2020;
Published online: 08 May 2020

References

1. Chen, B., Retzlaff, M., Roos, T. & Frydman, J. Cellular strategies of protein quality control. *Cold Spring Harb. Perspect. Biol.* **3**, a004374 (2011).
2. Hershko, A. & Ciechanover, A. The ubiquitin system. *Annu. Rev. Biochem.* **67**, 425–479 (1998).
3. Komander, D. & Rape, M. The ubiquitin code. *Annu. Rev. Biochem.* **81**, 203–229 (2012).
4. Oh, E., Akopian, D. & Rape, M. Principles of ubiquitin-dependent signaling. *Annu. Rev. Cell Dev. Biol.* **34**, 137–162 (2018).
5. Hua, Z. & Vierstra, R. D. The cullin-RING ubiquitin-protein ligases. *Annu. Rev. Plant Biol.* **62**, 299–334 (2011).
6. Hao, B. et al. Structural basis of the Cks1-dependent recognition of p27(Kip1) by the SCF(Skp2) ubiquitin ligase. *Mol. Cell* **20**, 9–19 (2005).
7. Guharoy, M., Bhowmick, P., Sallam, M. & Tompa, P. Tripartite degrons confer diversity and specificity on regulated protein degradation in the ubiquitin-proteasome system. *Nat. Commun.* **7**, 10239 (2016).
8. Mattiroli, F. & Sixma, T. K. Lysine-targeting specificity in ubiquitin and ubiquitin-like modification pathways. *Nat. Struct. Mol. Biol.* **21**, 308–316 (2014).
9. Tang, X. et al. Suprafacial orientation of the SCFCdc4 dimer accommodates multiple geometries for substrate ubiquitination. *Cell* **129**, 1165–1176 (2007).
10. Guharoy, M., Bhowmick, P. & Tompa, P. Design principles involving protein disorder facilitate specific substrate selection and degradation by the ubiquitin-proteasome system. *J. Biol. Chem.* **291**, 6723–6731 (2016).
11. Prakash, S., Tian, L., Ratliff, K. S., Lehotzky, R. E. & Matouschek, A. An unstructured initiation site is required for efficient proteasome-mediated degradation. *Nat. Struct. Mol. Biol.* **11**, 830–837 (2004).
12. Uversky, V. N. & Dunker, A. K. Understanding protein non-folding. *Biochim. Biophys. Acta* **1231-64**, 2010 (**1804**).
13. Uversky, V. N. Intrinsic disorder, protein-protein interactions, and disease. *Adv. Protein Chem. Struct. Biol.* **110**, 85–121 (2018).
14. Pietrosemoli, N., Garcia-Martin, J. A., Solano, R. & Pazos, F. Genome-wide analysis of protein disorder in *Arabidopsis thaliana*: implications for plant environmental adaptation. *PLoS ONE* **8**, e55524 (2013).
15. Pazos, F., Pietrosemoli, N., Garcia-Martin, J. A. & Solano, R. Protein intrinsic disorder in plants. *Front. Plant Sci.* **4**, 363 (2013).
16. Covarrubias, A. A., Cuevas-Velazquez, C. L., Romero-Perez, P. S., Rendon-Luna, D. F. & Chater, C. C. C. Structural disorder in plant proteins: where plasticity meets sessility. *Cell Mol. Life Sci.* **74**, 3119–3147 (2017).
17. Staby, L. et al. Eukaryotic transcription factors: paradigms of protein intrinsic disorder. *Biochem. J.* **474**, 2509–2532 (2017).
18. Chapman, E. J. & Estelle, M. Mechanism of auxin-regulated gene expression in plants. *Annu. Rev. Genet.* **43**, 265–285 (2009).
19. Abel, S., Nguyen, M. D. & Theologis, A. The PS-IAA4/5-like family of early auxin-inducible mRNAs in *Arabidopsis thaliana*. *J. Mol. Biol.* **251**, 533–549 (1995).
20. Worley, C. K. et al. Degradation of Aux/IAA proteins is essential for normal auxin signalling. *Plant J.* **21**, 553–562 (2000).
21. Liscum, E. & Reed, J. W. Genetics of Aux/IAA and ARF action in plant growth and development. *Plant Mol. Biol.* **49**, 387–400 (2002).
22. Tiwari, S. B., Hagen, G. & Guilfoyle, T. J. Aux/IAA proteins contain a potent transcriptional repression domain. *Plant Cell* **16**, 533–543 (2004).
23. Tan, X. et al. Mechanism of auxin perception by the TIR1 ubiquitin ligase. *Nature* **446**, 640–645 (2007).
24. Calderón Villalobos, L. I. et al. A combinatorial TIR1/AFB-Aux/IAA co-receptor system for differential sensing of auxin. *Nat. Chem. Biol.* **8**, 477–485 (2012).
25. Gray, W. M., Kepinski, S., Rouse, D., Leyser, O. & Estelle, M. Auxin regulates SCF(TIR1)-dependent degradation of AUX/IAA proteins. *Nature* **414**, 271–276 (2001).
26. Vernoux, T. et al. The auxin signalling network translates dynamic input into robust patterning at the shoot apex. *Mol. Syst. Biol.* **7**, 508 (2011).
27. Tiwari, S. B., Wang, X. J., Hagen, G. & Guilfoyle, T. J. AUX/IAA proteins are active repressors, and their stability and activity are modulated by auxin. *Plant Cell* **13**, 2809–2822 (2001).
28. Mutte, S. K. et al. Origin and evolution of the nuclear auxin response system. *Elife* **7**, pii: e33399 (2018).
29. Mockaitis, K. & Estelle, M. Auxin receptors and plant development: a new signaling paradigm. *Annu. Rev. Cell Dev. Biol.* **24**, 55–80 (2008).
30. Berleth, T. & Jürgens, G. The role of the monopteros gene in organising the basal body region of the *Arabidopsis* embryo. *Development* **118**, 575–587 (1993).
31. Weijers, D. & Jürgens, G. Auxin and embryo axis formation: the ends in sight? *Curr. Opin. Plant Biol.* **8**, 32–37 (2005).
32. Hamann, T., Mayer, U. & Jürgens, G. The auxin-insensitive *bodenlos* mutation affects primary root formation and apical-basal patterning in the *Arabidopsis* embryo. *Development* **126**, 1387–1395 (1999).
33. Parry, G. et al. Complex regulation of the TIR1/AFB family of auxin receptors. *Proc. Natl Acad. Sci. USA* **106**, 22540–22545 (2009).
34. Winkler, M. et al. Variation in auxin sensing guides AUX/IAA transcriptional repressor ubiquitylation and destruction. *Nat. Commun.* **8**, 15706 (2017).
35. Dreher, K. A., Brown, J., Saw, R. E. & Callis, J. The *Arabidopsis* Aux/IAA protein family has diversified in degradation and auxin responsiveness. *Plant Cell* **18**, 699–714 (2006).
36. Moss, B. L. et al. Rate motifs tune auxin/indole-3-acetic acid degradation dynamics. *Plant Physiol.* **169**, 803–813 (2015).
37. Ramos, J. A., Zenser, N., Leyser, O. & Callis, J. Rapid degradation of auxin/indoleacetic acid proteins requires conserved amino acids of domain II and is proteasome dependent. *Plant Cell* **13**, 2349–2360 (2001).
38. Meszaros, B., Erdos, G. & Dosztanyi, Z. IUPred2A: context-dependent prediction of protein disorder as a function of redox state and protein binding. *Nucleic Acids Res.* **46**, W329–W337 (2018).
39. Dinesh, D. C. et al. Solution structure of the PsIAA4 oligomerization domain reveals interaction modes for transcription factors in early auxin response. *Proc. Natl Acad. Sci. USA* **112**, 6230–6235 (2015).
40. Uversky, V. N. Cracking the folding code Why do some proteins adopt partially folded conformations, whereas other don't?. *FEBS Lett.* **514**, 181–183 (2002).

41. Uversky, V. N. A decade and a half of protein intrinsic disorder: biology still waits for physics. *Protein Sci.* **22**, 693–724 (2013).
42. Sigalov, A. B. Structural biology of intrinsically disordered proteins: revisiting unsolved mysteries. *Biochimie* **125**, 112–118 (2016).
43. Iacobucci, C. et al. A cross-linking/mass spectrometry workflow based on MS-cleavable cross-linkers and the MeroX software for studying protein structures and protein-protein interactions. *Nat. Protoc.* **13**, 2864–2889 (2018).
44. Sinz, A. Divide and conquer: cleavable cross-linkers to study protein conformation and protein-protein interactions. *Anal. Bioanal. Chem.* **409**, 33–44 (2017).
45. Gotze, M., Iacobucci, C., Ihling, C. H. & Sinz, A. A simple cross-linking/mass spectrometry workflow for studying system-wide protein interactions. *Anal. Chem.* **91**, 10236–10244 (2019).
46. Korasick, D. A. et al. Molecular basis for AUXIN RESPONSE FACTOR protein interaction and the control of auxin response repression. *Proc. Natl Acad. Sci. USA* **111**, 5427–5432 (2014).
47. Nanao, M. H. et al. Structural basis for oligomerization of auxin transcriptional regulators. *Nat. Commun.* **5**, 3617 (2014).
48. Han, M. et al. Structural basis for the auxin-induced transcriptional regulation by Aux/IAA17. *Proc. Natl Acad. Sci. USA* **111**, 18613–18618 (2014).
49. van Zundert, G. C. & Bonvin, A. M. DisVis: quantifying and visualizing accessible interaction space of distance-restrained biomolecular complexes. *Bioinformatics* **31**, 3222–3224 (2015).
50. Eyer, L. et al. 2,4-D and IAA amino acid conjugates show distinct metabolism in *Arabidopsis*. *PLoS ONE* **11**, e0159269 (2016).
51. Luo, J., Zhou, J. J. & Zhang, J. Z. Aux/IAA gene family in plants: molecular structure, regulation, and function. *Int. J. Mol. Sci.* **19**, 259 (2018).
52. O'Shea, C. et al. Structures and short linear motif of disordered transcription factor regions provide clues to the interactome of the cellular hub protein radical-induced cell death1. *J. Biol. Chem.* **292**, 512–527 (2017).
53. Arai, M., Sugase, K., Dyson, H. J. & Wright, P. E. Conformational propensities of intrinsically disordered proteins influence the mechanism of binding and folding. *Proc. Natl Acad. Sci. USA* **112**, 9614–9619 (2015).
54. Ferreon, A. C. M., Ferreon, J. C., Wright, P. E. & Deniz, A. A. Modulation of allostery by protein intrinsic disorder. *Nature* **498**, 390 (2013).
55. Powers, S. K. et al. Nucleo-cytoplasmic partitioning of arf proteins controls auxin responses in *Arabidopsis thaliana*. *Mol. Cell* **76**, 177–190.e5 (2019).
56. Kato, H., Nishihama, R., Weijers, D. & Kohchi, T. Evolution of nuclear auxin signaling: lessons from genetic studies with basal land plants. *J. Exp. Bot.* **69**, 291–301 (2018).
57. Flores-Sandoval, E., Eklund, D. M. & Bowman, J. L. A simple auxin transcriptional response system regulates multiple morphogenetic processes in the Liverwort Marchantia polymorpha. *PLoS Genet.* **11**, e1005207 (2015).
58. Rensing, S. A. et al. The Physcomitrella genome reveals evolutionary insights into the conquest of land by plants. *Science* **319**, 64–69 (2008).
59. Csizmok, V. et al. An allosteric conduit facilitates dynamic multisite substrate recognition by the SCF(Cdc4) ubiquitin ligase. *Nat. Commun.* **8**, 13943 (2017).
60. Keul, N. D. et al. The entropic force generated by intrinsically disordered segments tunes protein function. *Nature* **563**, 584–588 (2018).
61. Yu, H. et al. Mutations in the TIR1 auxin receptor that increase affinity for auxin/indole-3-acetic acid proteins result in auxin hypersensitivity. *Plant Physiol.* **162**, 295–303 (2013).
62. Davey, N. E. et al. SLiMPrints: conservation-based discovery of functional motif fingerprints in intrinsically disordered protein regions. *Nucleic Acids Res.* **40**, 10628–10641 (2012).
63. Davey, N. E. et al. Attributes of short linear motifs. *Mol. Biosyst.* **8**, 268–281 (2012).
64. Zarin, T. et al. Proteome-wide signatures of function in highly diverged intrinsically disordered regions. *Elife* **8**, pii: e46883 (2019).
65. Abel, S., Oeller, P. W. & Theologis, A. Early auxin-induced genes encode short-lived nuclear proteins. *Proc. Natl Acad. Sci. USA* **91**, 326–330 (1994).
66. Bard, J. A. M., Bashore, C., Dong, K. C. & Martin, A. The 26S proteasome utilizes a kinetic gateway to prioritize substrate degradation. *Cell* **177**, 286–298 e15 (2019).
67. Fishbain, S. et al. Sequence composition of disordered regions fine-tunes protein half-life. *Nat. Struct. Mol. Biol.* **22**, 214–221 (2015).
68. Fishbain, S., Prakash, S., Herrig, A., Elsasser, S. & Matouschek, A. Rad23 escapes degradation because it lacks a proteasome initiation region. *Nat. Commun.* **2**, 192 (2011).
69. Madeira, F. et al. The EMBL-EBI search and sequence analysis tools APIs in 2019. *Nucleic Acids Res.* **47**, W636–W641 (2019).
70. Letunic, I. & Bork, P. Interactive Tree Of Life (iTOL) v4: recent updates and new developments. *Nucleic Acids Res.* **47**, W256–W259 (2019).
71. Hanson, J., Yang, Y., Paliwal, K. & Zhou, Y. Improving protein disorder prediction by deep bidirectional long short-term memory recurrent neural networks. *Bioinformatics* **33**, 685–692 (2017).
72. Ishida, T. & Kinoshita, K. PrDOS: prediction of disordered protein regions from amino acid sequence. *Nucleic Acids Res.* **35**, W460–W464 (2007).
73. Artimo, P. et al. ExPASy: SIB bioinformatics resource portal. *Nucleic Acids Res.* **40**, W597–W603 (2012).
74. Wilkins, M. R. et al. Protein identification and analysis tools in the ExPASy server. *Methods Mol. Biol.* **112**, 531–552 (1999).
75. Kyte, J. & Doolittle, R. F. A simple method for displaying the hydropathic character of a protein. *J. Mol. Biol.* **157**, 105–132 (1982).
76. Uversky, V. N. Use of fast protein size-exclusion liquid chromatography to study the unfolding of proteins which denature through the molten globule. *Biochemistry* **32**, 13288–13298 (1993).
77. Hellmuth, A. & Calderón Villalobos, L. I. Radioligand binding assays for determining dissociation constants of phytohormone receptors. *Methods Mol. Biol.* **1450**, 23–34 (2016).
78. Webb, B. & Sali, A. Protein structure modeling with MODELLER. *Methods Mol. Biol.* **1654**, 39–54 (2017).
79. de Vries, S. J., van Dijk, M. & Bonvin, A. M. The HADDOCK web server for data-driven biomolecular docking. *Nat. Protoc.* **5**, 883–897 (2010).
80. Dominguez, C., Boelens, R. & Bonvin, A. M. HADDOCK: a protein-protein docking approach based on biochemical or biophysical information. *J. Am. Chem. Soc.* **125**, 1731–1737 (2003).
81. van Zundert, G. C. P. et al. The HADDOCK2.2 web server: user-friendly integrative modeling of biomolecular complexes. *J. Mol. Biol.* **428**, 720–725 (2016).
82. Hamdi, K. et al. Structural disorder and induced folding within two cereal, ABA stress and ripening (ASR) proteins. *Sci. Rep.* **7**, 15544 (2017).
83. Rodrigues, J. P. et al. Clustering biomolecular complexes by residue contacts similarity. *Proteins* **80**, 1810–1817 (2012).
84. Nakikj, D. & Mamykina, L. DisVis: visualizing discussion threads in online health communities. *AMIA Annu. Symp. Proc.* **2016**, 944–953 (2016).
85. van Zundert, G. C. et al. The DisVis and powerfit web servers: explorative and integrative modeling of biomolecular complexes. *J. Mol. Biol.* **429**, 399–407 (2017).
86. Bonvin, A., Karaca, E., Kastritis, P. L. & Rodrigues, J. Defining distance restraints in HADDOCK. *Nat. Protoc.* **13**, 1503 (2018).
87. Pettersen, E. F. et al. UCSF Chimera-a visualization system for exploratory research and analysis. *J. Comput. Chem.* **25**, 1605–1612 (2004).
88. Case, D. A. et al. *AMBER10*. (University of California, San Francisco, 2008).
89. Pronk, S. et al. GROMACS 4.5: a high-throughput and highly parallel open source molecular simulation toolkit. *Bioinformatics* **29**, 845–854 (2013).
90. Hornak, V. et al. Comparison of multiple Amber force fields and development of improved protein backbone parameters. *Proteins* **65**, 712–725 (2006).
91. Jorgensen, W. L., Chandrasekhar, J., Madura, J. D., Impey, R. W. & Klein, M. L. Comparison of simple potential functions for simulating liquid water. *J. Chem. Phys.* **79**, 926–935 (1983).
92. Lindahl, E. Molecular dynamics simulations. *Methods Mol. Biol.* **1215**, 3–26 (2015).
93. Verlet, L. Computer "experiments" on classical fluids. I. Thermodynamical properties of lennard-jones. *Molecules Phys. Rev.* **159**, 98–103 (1967).
94. Berendsen, H. J. C., Postma, J. P. M., DiNola, A. & Haak, J. R. Molecular dynamics with coupling to an external bath. *J. Chem. Phys.* **81**, 3684 (1984).
95. Bussi, G., Donadio, D. & Parrinello, M. Canonical sampling through velocity rescaling. *J. Chem. Phys.* **126**, 014101 (2007).
96. Páll, S., Abraham, M. J., Kutzner, C., Hess, B. & Lindahl, E. Tackling exascale software challenges in molecular dynamics simulations with GROMACS. In: Markidis S, Laure E (eds) Solving Software Challenges for Exascale. EASC 2014. Lecture Notes in Computer Science 8759:3–7 (Springer, Cham, 2015).
97. Schneider, T. & Stoll, E. Molecular-dynamics study of a 3-dimensional one-component model for distortive phase-transitions. *Phys. Rev. B* **17**, 1302–1322 (1978).
98. Parrinello, M. & Rahman, A. Polymorphic transitions in single crystals: a new molecular dynamics method. *J. Appl. Phys.* **52**, 7182–7190 (1981).
99. Nosé, S. & Klein, M. L. Constant pressure molecular dynamics for molecular systems. *Mol. Phys.* **50**, 1055–1076 (1983).
100. Case, D. A. et al. *AMBER 2018*. (University of California, San Francisco, 2018).

Acknowledgements

We thank Wolfgang Brandt for initial in silico models of AUX/IAA PB1 domains, and Silvestre Marillonet for the design of constructs for Golden Gate Technology. Thanks to Steffen Abel, Elisabeth Chapman, and Claus Schwechheimer for providing input to the manuscript. This work was supported by the Deutsche Forschungsgemeinschaft (DFG: research project CA716/2-1, and Research Training Group RTG2467), and core funding of the Leibniz Institute of Plant Biochemistry (IPB).

Author contributions

M.N., E.M.C., and L.I.A.C.V. prepared the manuscript and designed experiments. M.N. performed biochemical experiments and analyzed the data. M.N., C.I., and C.H.I. carried out XL-MS experiments and data analysis. P.K. and M.N carried out all HADDOCK-based

approaches including DisVis, and E.M.C. computational calculation and simulations. M.N., A.H., and V.W. generated Y2H constructs and performed the assays. M.N. designed and executed ubiquitylation experiments, and together with W.H. analyzed mass spectral data of ubiquitylation sites. S.S. and M.Z. carried out ratiometric experiments and analyzed the data. M.N., E.M.C., V.W., and L.I.A.C.V. generated and analyzed *Arabidopsis* transgenic lines. E.M.C., C.I, C.I., P.K., and A.S. provided input to the manuscript. All authors approved the intellectual content.

Competing interests

The authors declare no competing interests.

Additional information

Supplementary information is available for this paper at https://doi.org/10.1038/s41467-020-16147-2.

Correspondence and requests for materials should be addressed to L.I.A.Cón.V.

Peer review information *Nature Communications* thanks Branimir Bertosa, Lucia Strader, and the other, anonymous reviewer(s) for their contribution to the peer review of this work. Peer review reports are available.

Reprints and permission information is available at http://www.nature.com/reprints

Publisher's note Springer Nature remains neutral with regard to jurisdictional claims in published maps and institutional affiliations.

2.3 Bagchi R, *et al.* The Arabidopsis ALF4 protein is a negative regulator of SCF E3 ligases.

Bagchi R, Melnyk CW, Christ G, Winkler M, Kirchsteiner K, Salehin M, Mergner J, **Niemeyer M**, Schwechheimer C, Calderón Villalobos LIA, Estelle M (**2018**) The Arabidopsis ALF4 protein is a negative regulator of SCF E3 ligases. **EMBO J.** Jan 17;37(2):255-268. doi: 10.15252/embj.201797159. Epub 2017 Dec 12.

2.3.1 Aims and summary

In this study, we characterized Arabidopsis ABERRANT LATERAL ROOT FORMATION4 (ALF4), and evaluated whether ALF4 acts as a functional ortholog of mammalian GLMN, a CUL-RING E3 ubiquitin ligase (CRL) regulator. As described in chapter 1.1.5, CRL-dependent protein ubiquitylation is regulated at the levels of CRL complex assembly, and ubiquitin transfer activity. In plants, mutations in genes regulating CRL activity result in auxin-related defects affecting *e.g.* overall root growth and root system architecture. *ALF4* mutant plants are affected in auxin-regulated traits, showing a strong reduction of lateral root formation, and reduced primary root elongation in combination with loss of apical dominance. Among three *alf4* mutant alleles we studied, two were lethal early in seedling development, and the weak allele *alf4-1* that carries a 12 bp deletion in the first intro/exon junction, displays reduced auxin responses. From a molecular perspective we found the ALF4 C-terminus interacts *via* its conserved residues K484 and R614 with the E2-binding CRL component RBX1, making ALF4 and E2 binding to RBX1 mutually exclusive. ALF4 directly competes for the E2 binding site, and reduces AUX/IAA ubiquitylation *in vitro*. This correlates with increased stability of SCF targets RGA and IAA17 in *alf4* mutant plants. In addition, *alf4-1* plants show elevated TIR1 levels, while CUL1 stability is reduced. The loss of ALF4 activity impact CUL1 stability, and likely reduces the overall level of functional SCF complexes, which explains the reduction of total ubiquitin conjugates in *alf4-1* mutants.

2.3.2 Contributions

Own contributions:

In Bagchi *et al.* I provided biochemical evidence for the influence of *At*ALF4 on auxin-mediated AUX/IAA ubiquitylation. I used the IVU assay developed in Winkler *et al.,* to reconstitute auxin- and SCF^{TIR1}-dependent AUX/IAA ubiquitylation in the presence of *At*ALF4 and *At*UBC8. A ratio-dependent competition between ALF4 and UBC8 evidenced the ALF4 inhibitory effect. I contributed to the experimental conception and execution of the study by directly supervising and mentoring Gideon Christ, a master student in the lab. In his master thesis, our biochemical approaches provided key clues for understanding ALF4 direct interaction with CRL components, and its inhibitory effect on AUX/IAA ubiquitylation *in vitro*. In this regard, I guided experiments involving protein expression, purification, IVU assays and interaction studies.

Estimated percentage-based author (M. Niemeyer) contribution to experimental work:

Protein expression and purification of IVU-related proteins (50%), *in vitro* ubiquitylation assays (IVU) (30%). Data analysis: IVU data (100%)

Estimated percentage-based author (M. Niemeyer) contribution to written manuscript:

Writing (5%), design and preparation of 1 main figure and 1 supplementary figure (10%).

Other contributions:

75% supervision of a master student (Gideon Christ) involved fulltime in this study.

See "Author Contributions" section at the end of the manuscript for detailed description of input and experimental support from our scientific collaborators in this study.

2.3.3 Original publication

See next page. Supplementary Material in Chapter 7.3.

Article

SOURCE DATA | TRANSPARENT PROCESS

THE EMBO JOURNAL

The *Arabidopsis* ALF4 protein is a regulator of SCF E3 ligases

Rammyani Bagchi[1], Charles W Melnyk[2,†], Gideon Christ[3], Martin Winkler[3,4], Kerstin Kirchsteiner[1], Mohammad Salehin[1], Julia Mergner[5,‡], Michael Niemeyer[3], Claus Schwechheimer[5], Luz Irina A Calderón Villalobos[3] & Mark Estelle[1,*]

Abstract

The cullin-RING E3 ligases (CRLs) regulate diverse cellular processes in all eukaryotes. CRL activity is controlled by several proteins or protein complexes, including NEDD8, CAND1, and the CSN. Recently, a mammalian protein called Glomulin (GLMN) was shown to inhibit CRLs by binding to the RING BOX (RBX1) subunit and preventing binding to the ubiquitin-conjugating enzyme. Here, we show that *Arabidopsis* ABERRANT LATERAL ROOT FORMATION4 (ALF4) is an ortholog of GLMN. The *alf4* mutant exhibits a phenotype that suggests defects in plant hormone response. We show that ALF4 binds to RBX1 and inhibits the activity of SCF^{TIR1}, an E3 ligase responsible for degradation of the Aux/IAA transcriptional repressors. *In vivo*, the *alf4* mutation destabilizes the CUL1 subunit of the SCF. Reduced CUL1 levels are associated with increased levels of the Aux/IAA proteins as well as the DELLA repressors, substrate of SCF^{SLY1}. We propose that the *alf4* phenotype is partly due to increased levels of the Aux/IAA and DELLA proteins.

Keywords auxin; cullin-RING E3 ligases; glomulin; plant development
Subject Categories Plant Biology; Post-translational Modifications, Proteolysis & Proteomics
DOI 10.15252/embj.201797159 | Received 26 April 2017 | Revised 10 November 2017 | Accepted 16 November 2017 | Published online 12 December 2017
The EMBO Journal (2018) 37: 255–268

Introduction

Ubiquitin–protein conjugation is a highly regulated process that involves ubiquitin-activating and conjugating enzymes (E1 and E2), as well as a ubiquitin ligase (E3). The E3 ligase coordinates with the E2 enzyme to conjugate ubiquitin to lysine residues in the substrate protein. The cullin-RING ligases (CRLs) are a large class of E3 ligases that consist of a cullin, a RING protein called RING BOX1 (RBX1), and a substrate adapter protein (Hua & Vierstra, 2011). In humans, CRLs have been implicated in a wide variety of cellular processes, including those related to cancer, while in plants they have a central role in diverse developmental and physiological processes (Hua & Vierstra, 2011; Kelley & Estelle, 2012; Zheng *et al*, 2016). The Skp1-Cullin1-F-box (SCF) E3s are a subclass of CRLs in which the substrate adapter consists of Skp1 (ASK in plants) and an F-box protein. Although there are many F-box proteins in all eukaryotes, the family has dramatically expanded in plants (~700 in *Arabidopsis*), suggesting that SCFs have been co-opted for many cellular and developmental programs (Gagne *et al*, 2002).

SCF regulation is a highly dynamic process that involves several proteins and protein complexes (Deshaies & Joazeiro, 2009; Hua & Vierstra, 2011; Lydeard *et al*, 2013). These E3s are activated by conjugation of the ubiquitin-related protein RELATED TO UBIQUITIN (RUB), or NEDD8 in animals, to the C-terminus of the cullin subunit. Neddylation causes dramatic conformational changes in CUL1 and RBX1 that allow the RING domain on RBX1 to interact with the E2 (Duda *et al*, 2008). On the other hand, SCFs are inhibited by the COP9 SIGNALOSOME (CSN) through its de-neddylating activity as well as by direct binding to the SCF (Enchev *et al*, 2012). Another protein, CULLIN-ASSOCIATED NEDD8-DISSOCIATED PROTEIN 1 (CAND1), binds to the cullin and is important for substrate adapter exchange (Pierce *et al*, 2013; Wu *et al*, 2013; Zemla *et al*, 2013).

The human disease glomuvenous malformation, characterized by cutaneous lesions, is caused by mutations in the *Glomulin* (*GLMN*) gene. In the familial form of this disease, affected individuals typically carry one loss-of-function *glmn* allele and experience a second somatic *glmn* mutation in the affected tissue (Duda *et al*, 2012; Tron *et al*, 2012). The *glmn* null mice die as embryos, suggesting that the gene is probably essential in humans (Tron *et al*, 2012). Recent studies indicate that GLMN regulates CRLs by binding to RBX1 and preventing the E2-conjugating enzyme from engaging the CRL (Duda *et al*, 2012; Tron *et al*, 2012). In human cells, one

1 Howard Hughes Medical Institute, University of California San Diego, La Jolla, CA, USA
2 Sainsbury Laboratory, University of Cambridge, Cambridge, UK
3 Department of Molecular Signal Processing, Leibniz Institute of Plant Biochemistry, Halle, Germany
4 Institute of Biology, Structural Biology/Biochemistry, Humboldt-University Berlin, Berlin, Germany
5 Plant Systems Biology, Technische Universität München, Freising, Germany
*Corresponding author. Tel: +1 858 246 0453; E-mail: mestelle@ucsd.edu
†Present address: Department of Plant Biology, Swedish University of Agricultural Sciences, Uppsala, Sweden
‡Present address: Proteomics and Bioanalytics, Technische Universität München, Freising, Germany

known consequence of *glmn* mutations is a decrease in the amount of the F-box protein Fbw7 and an increase in the level of Fbw7 substrates cyclin E and c-Myc (Tron *et al*, 2012).

There are several well-characterized SCFs in plants, including SCF^{TIR1} and SCF^{SLY1} (Schwechheimer & Willige, 2009; Salehin *et al*, 2015; Lavy & Estelle, 2016). SCF^{TIR1} promotes the degradation of transcriptional repressors called Aux/IAA proteins in response to the hormone auxin, while SCF^{SLY1} promotes degradation of another class of transcriptional regulators, the DELLA proteins, in response to the hormone gibberellic acid (GA). Strikingly, several SCF subunits, as well as regulators of SCF activity, were originally identified through screens for auxin-resistant mutants in *Arabidopsis* (Walker & Estelle, 1998).

The *Arabidopsis aberrant lateral root formation 4* (*alf4*) mutant exhibits a number of auxin-related defects but its role in auxin signaling is unknown. The mutant was isolated in a screen for defects in root architecture, particularly a dramatic reduction in lateral root formation (Celenza *et al*, 1995; DiDonato *et al*, 2004). In addition, *ALF4* is required for protoplast regeneration, callus formation, and efficient graft formation (Chupeau *et al*, 2013; Melnyk *et al*, 2015; Shang *et al*, 2016). Here, we demonstrate that ALF4 inhibits SCF ligases and is related to mammalian GLMN. Further, we show that Aux/IAA and DELLA proteins accumulate in the *alf4* mutant. These results suggest that the developmental defects ascribed to the mutant are at least partly due to defects in hormone signaling.

Results

The *alf4* mutants are resistant to auxin and display defects in root and shoot growth

Previous studies established that the *alf4-1* mutant has a normal primary root, but is deficient in lateral root initiation (Celenza *et al*, 1995; DiDonato *et al*, 2004). We confirmed this phenotype with three *alf4* alleles containing deletions or T-DNA insertions (Figs 1A and B, and EV1). All three lines had normal or near-normal primary root elongation but formed dramatically fewer lateral roots. In addition, all three alleles were affected in shoot development (Fig 1C and D). The rosettes of mutant plants were much smaller than the wild-type control and had distorted leaves and twisted petioles. Rarely did the *alf4-2* or *alf4-063* mutants survive long enough to flower on soil, but *alf4-1* produced a short and largely infertile inflorescence. Based on these results and previous observations, it is likely that *alf4-1,* a 12-bp deletion mutant, is not a null allele (DiDonato *et al*, 2004). To determine whether the effect of the mutation on the shoot was due to a reduced root system, we grafted *alf4* scions onto Col-0 wild-type root stocks. As shown in Fig 1C and D, the wild-type root stock enhanced growth of the mutant shoot and increased fertility of the *alf4-1* shoot. However, scions from *alf4-2* and *alf4-063* remained severely affected, indicating that ALF4 function was required in the shoot.

The phenotype of the *alf4* mutant suggests a defect in auxin signaling. To address this possibility, we examined the effects of auxin on primary root growth in *alf4-1* and Col-0 plants and found that the mutant was resistant to low concentrations of IAA (Fig 1E). Further, *alf4-1* plants exhibited a delayed gravitropic response, consistent with a defect in auxin signaling (Fig 1F). To determine whether ALF4 was required for the transcriptional response to auxin, we introduced the *pDR5:GFP* reporter into the *alf4*-1 mutant. We found that GFP signal was reduced in the mutant compared to the wild type in the absence and presence of the auxin 1-naphthyl acetic acid (NAA) (Fig 1G and H). In contrast, the response to the cytokinin N6-benzyladenine (BA) using the *pARR5:GFP* cytokinin reporter was largely unaffected in the *alf4* mutant (Fig EV2). These results suggest that the pleiotropic phenotype exhibited by the *alf4* mutants may be partly due to reduced auxin response.

Expression of ALF4 in the root

The *ALF4* gene is broadly expressed throughout the plant (DiDonato *et al*, 2004). To further examine expression of *ALF4* in the root, we analyzed the previously published *pALF4:ALF4-GFP* line (DiDonato *et al*, 2004). We found that ALF4 protein was present in the nuclei of cells in the primary root tip, particularly the epidermal cells, and in the vascular tissue (Fig 2A and F). Consistent with the lateral root defect, ALF4 protein begins to accumulate in the lateral root primordium and continues to increase in levels throughout formation of the lateral root meristem and emergence of the lateral root (Fig 2B–E). To determine whether the *ALF4* gene was regulated by auxin or cytokinin, we also treated the *pALF4:ALF4-GFP* line with NAA, the auxin transport inhibitor naphthylphthalamic acid (NPA), and BA. We did not observe a clear effect of these treatments on expression of the transgene (Fig EV2). In addition, publically available data show that *ALF4* is not regulated by GA (http://bar.utoronto.ca) (Winter *et al*, 2007).

Figure 1. The *alf4* mutants exhibit a pleiotropic phenotype.

A, B Primary root length (A) and lateral root number (B) of wild-type and mutant seedlings (different letters represent significant differences within a time point, mean ± SE, n = 34–49 roots/treatment, ANOVA with Tukey's *post hoc* test, $P < 0.01$).

C Wild-type and mutant plants 35 days after grafting. The top row are ungrafted, while the bottom row are mutant scion grafted onto a Col-0 root stock.

D Wild-type and mutant plants 70 days after grafting.

E Effect of auxin on wild-type and *alf4-1* root growth. Five-day-old seedlings were transferred to fresh medium ± IAA and allowed to grow for 3 days. Growth is presented as the percentage of the DMSO control treatment for each genotype. Each value represents the mean, and error bars represent standard deviation ($n \geq 10$).

F Gravitropic response in wild-type and *alf4-1* seedlings. Seedlings grown on agar medium were rotated 90 degrees at t = 0. The angle of curvature from the horizontal was measured at the times indicated. Each point represents the mean of six measurements. Error bars represent the standard deviation ($n \geq 10$).

G Expression of the auxin-responsive marker, *pDR5:GFP*, (green signal) imaged in the presence or absence of synthetic auxin NAA for 24 h. Roots were counterstained with propidium iodide (red signal).

H Quantification of GFP in (G) (different letters represent significant differences between groups, mean ± SE, n = 9–15 root tips/treatment, ANOVA with Tukey's *post hoc* test, $P < 0.01$).

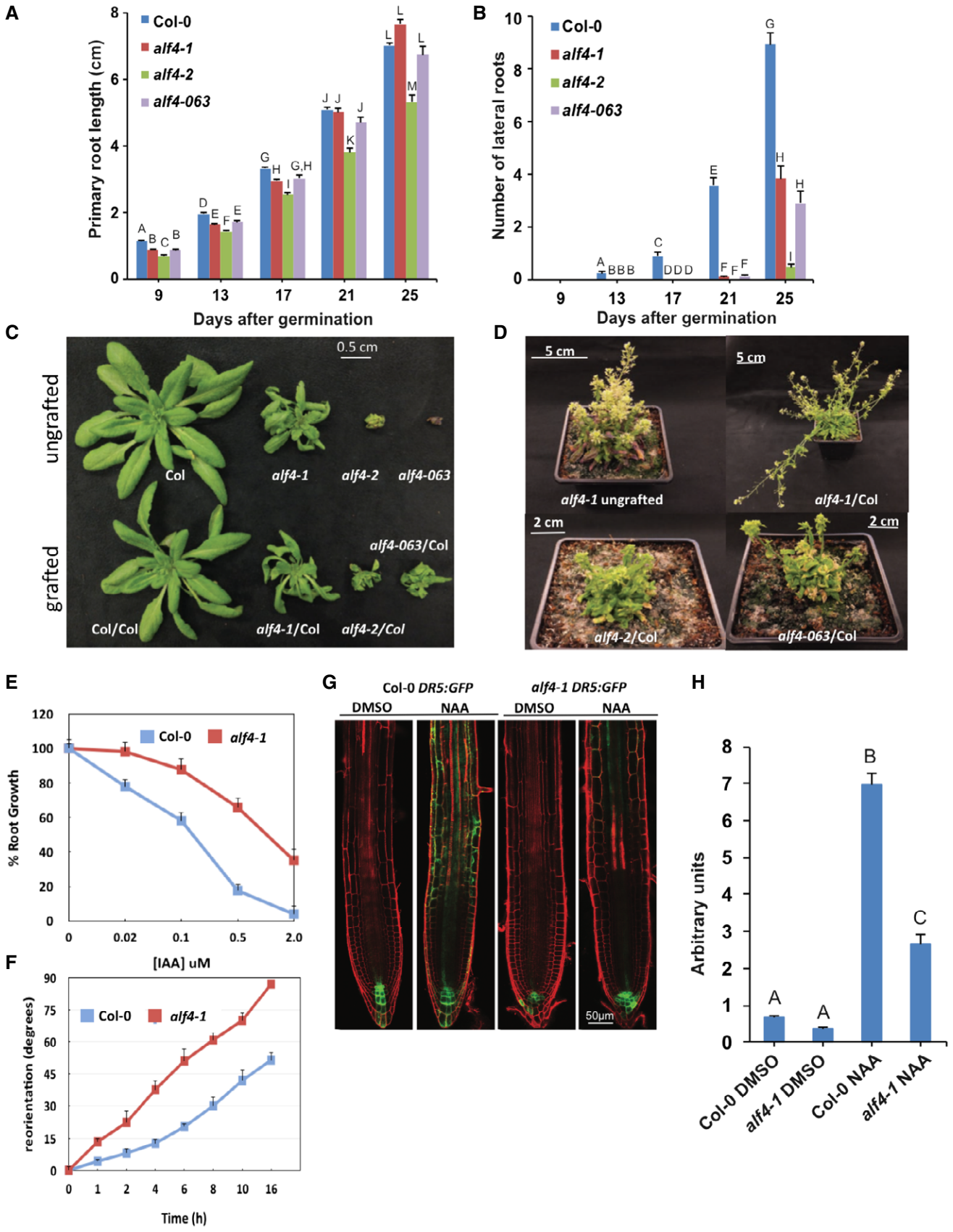
A
Primary root length (cm)
Col-0
alf4-1
alf4-2
alf4-063
Days after germination
B
Number of lateral roots
Days after germination
C
ungrafted
grafted
0.5 cm
Col
alf4-1
alf4-2
alf4-063
alf4-063/Col
Col/Col
alf4-1/Col
alf4-2/Col
D
5 cm
alf4-1 ungrafted
alf4-1/Col
2 cm
alf4-2/Col
alf4-063/Col
E
% Root Growth
F
[IAA] uM
reorientation (degrees)
Time (h)
G
Col-0 DR5:GFP
alf4-1 DR5:GFP
DMSO
NAA
50µm
H
Arbitrary units
Col-0 DMSO
alf4-1 DMSO
Col-0 NAA
alf4-1 NAA

Figure 1.

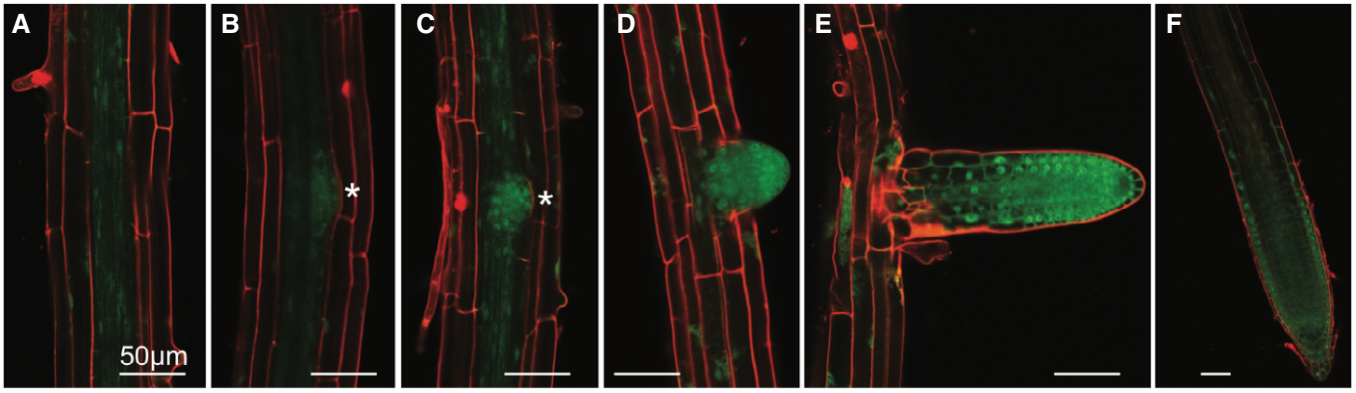

Figure 2. ALF4 protein accumulates during lateral root formation.
pALF4:ALF4-GFP seedlings display ALF4-GFP (green signal) and are counterstained with propidium iodide (red signal). Scale bar is 50 μm.

A *ALF4* is expressed in the vasculature.

B–E ALF4 protein accumulates in the lateral root primordium and the emerging lateral root. Asterisks highlight the location of the emerging lateral root.

F ALF4 protein is also present throughout the primary root tip.

The ALF4 protein is related to GLMN and interacts with RBX1

The GLMN protein was recently shown to be an important regulator of cullin-RING E3 ligases in mammals (Duda *et al*, 2012; Tron *et al*, 2012). GLMN interacts with RBX1 and prevents binding of the E2 protein. Structural studies showed that GLMN consists of a series of helical repeats similar to HEAT repeats (Duda *et al*, 2012). The protein has two such domains, bisected by a single helix that is perpendicular to the other helices, while the RBX1-binding domain is in the C-terminal HEAT repeat domain. An amino acid alignment of GLMN and ALF4 revealed that the two proteins are ~25% identical along their entire length. Importantly, several key residues known to contribute to the interaction between GLMN and RBX1 are conserved in ALF4 (Fig EV3). In addition, the Phyre2 protein structure prediction server predicted that ALF4 was a helical repeat protein with an overall organization that is very similar to GLMN (Fig EV4) (Kelley *et al*, 2015).

To determine whether ALF4 interacted with *Arabidopsis* RBX1, we performed a series of *in vitro* and *in vivo* experiments. Yeast two-hybrid assays demonstrated a strong interaction between the two proteins in this assay (Fig 3A). To further assess this interaction, we generated two ALF4 protein variants where the conserved K484 and R614 amino acids were replaced with alanine. Both residues contribute to the interaction between GLMN and RBX1 (Duda *et al*, 2012). In addition, we generated a mutant lacking the C-terminal 94 amino acids ($ALF4^{1\text{-}532stop}$). In the yeast assay, the strength of the interaction between $ALF4^{A484A614}$ and RBX1 was similar to that of wild-type ALF4. In contrast, $ALF4^{1\text{-}532stop}$ did not interact with RBX1, indicating that the C-terminal region of ALF4 is, as in the case of GLMN, important for RBX1 binding (Fig 3A).

To confirm the interaction between ALF4 and RBX1, we performed a co-immunoprecipitation experiment using the *pALF4:ALF4-GFP* line and an antibody directed against a peptide from human RBX1 that recognizes *Arabidopsis* RBX1 (Xu *et al*, 2002; Gilkerson *et al*, 2009). The results in Fig 3B show that RBX1 is recovered in an immunoprecipitation of ALF4-GFP, indicating that these two proteins are interacting in the plant extract. We extended this finding using an *in vitro* pulldown experiment. As expected, wild-type ALF4 clearly interacted with RBX1 *in vitro*. However, neither $ALF4^{A484A614}$ nor $ALF4^{1\text{-}532stop}$ were recovered in this GST-RBX1 pulldown assay, confirming that K484 and R614 are important for RBX1 binding (Fig 3C).

To demonstrate an interaction *in vivo,* we performed a BiFC (bimolecular fluorescence complementation) experiment using RBX1 with wild-type and mutant ALF4. Similar to the yeast two-hybrid and pulldown experiments, only the wild-type ALF4 protein displayed a robust interaction with RBX1 (Fig 3D). The mutant variants interacted weakly ($ALF4^{A484A614}$) or not at all ($ALF4^{1\text{-}532stop}$).

Finally, to quantify ALF4–RBX1 interaction when RBX1 is associated with cullin in solution, we carried out microscale thermophoresis (MST) (Fig 3E). For this experiment, recombinant, purified MmRBX1–HsCUL1 (Li *et al*, 2005) was fluorescently labeled and incubated with ALF4 at a range of concentrations. We used the mouse RBX1 and human CUL1 proteins for this experiment because their expression had been optimized (Li *et al*, 2005). Within the concentration range 7 μM to 0.21 nM, ALF4 exhibited an affinity for MmRBX1–HsCUL1 with a K_d of 346.04 ± 77.05 nM (Figs EV5 and EV6). ALF4 clearly interacted with Cul1–RBX1, and given their structural similarities, the ALF4–RBX1 interaction likely resembles that of GLMN-RBX1.

The *alf4* mutant stabilizes the SCF^{TIR1} and SCF^{SLY} substrates IAA17 and RGA

Since ALF4 may regulate CRL assembly or activity, we examined the levels of SCF^{TIR1} and SCF^{SLY1} substrates, the Aux/IAA and DELLA repressors of the auxin and gibberellin pathways, respectively. To determine the effects of *alf4* on DELLA proteins, we examined the turnover of the DELLA protein REPRESSOR OF GA1-3 (RGA) in the wild type and *alf4-063* mutant after inhibition of protein biosynthesis with cycloheximide (CHX). Immunoblots showed that RGA strongly accumulated in the *alf4* background (Fig 4A). In addition, RGA levels in *alf4* plants were not reduced

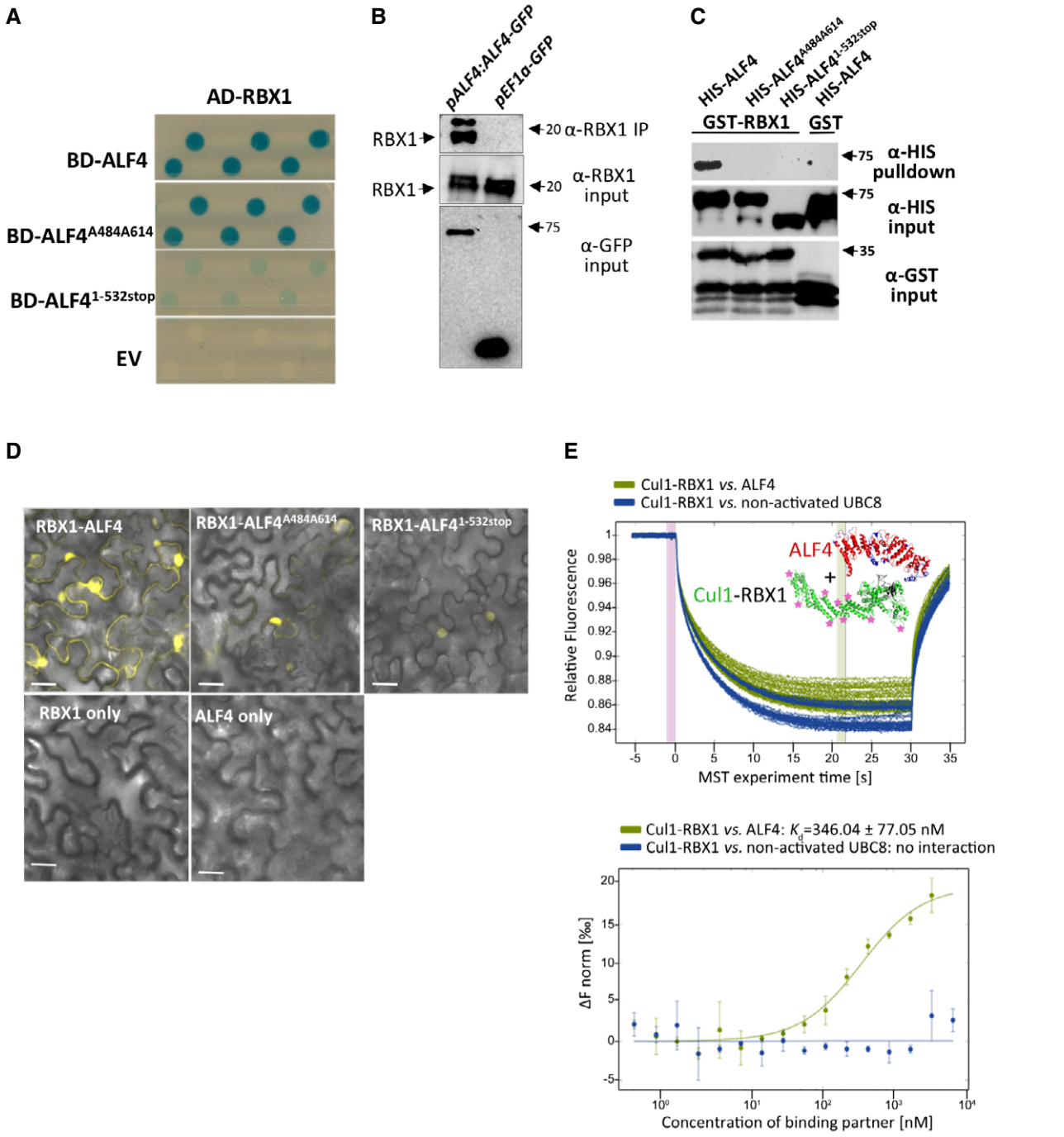

Figure 3. ALF4 interacts with RBX1.

A The ALF4$^{1\text{-}532stop}$ mutant displays reduced interaction with RBX1 in comparison with full-length ALF4 protein in a yeast two-hybrid assay. Blue color represents X-GAL staining. EV, empty vector.

B RBX1 co-immunoprecipitates with ALF4 in extracts prepared from 14-day-old *pALF4:ALF4-GFP* plants. The *pEF1α-GFP* line serves as a control.

C *In vitro* pulldown of HIS-ALF4 and ALF4 mutants with GST-tagged RBX1 or GST alone. ALF4 variants do not interact with RBX1.

D BIFC assay testing the interaction of ALF4 or ALF4 mutants in pCYCE(R) vector with RBX1 cloned in pVYNE(R). Scale bars are 50 μm.

E Microscale thermophoresis (MST) analysis of ALF4 binding to Cul1–RBX. Thermophoresis curves for protein binding over a temperature gradient and over time (upper panel), and fitted curves plotting normalized fluorescence against concentration of ligands (lower panel). HsCul1–RBX1 interacts with ALF4 with a K_d = 346.04 ± 77.05 nM. Measurements were performed with a dilution series of ALF4 concentrations from 7 μM to 0.21 nM, and constant levels of fluorescently labeled Cul1–RBX1 (10 nM). Dissociation constant was calculated from three independent biological replicates. Binding of Cul1–RBX1 to not-charged E2 (UBC8) (without ubiquitin) serves as a negative control (blue). In the upper panel start (0 s) and end (21 s) of the temperature gradient were indicated with pink and green boxes, respectively. Error bars to correspond s.e.m. of three independently collected MST traces. See Figs EV5 and EV6 for MST raw data.

Source data are available online for this figure.

within 30 min of CHX treatment in *alf4*, whereas the protein was degraded to 60% of its initial levels in the wild type (Fig 4A and B).

To determine the role of ALF4 in Aux/IAA degradation, we used a *pDEX:IAA17-GFP* construct to examine IAA17 levels after auxin treatment in *alf4-1* compared to wild-type controls. After a 4-h dexamethasone treatment, the amount of IAA17-GFP was clearly higher in the root tip of *alf4-1* plants compared to the wild type (Fig 4C and D). Examination of IAA17-GFP levels after auxin treatment revealed that the protein was relatively stable in *alf4-1* plants compared to the wild type. Importantly, *IAA7-GFP* transcript abundance was similar in the two lines. Because accumulation of Aux/IAA proteins results in auxin resistance, these results are consistent with reduced auxin response observed in the *alf4* mutant (Salehin *et al*, 2015).

If ALF4 functions like GLMN and inhibits CRL activity, it is counterintuitive that SCF substrates should be stabilized in the *alf4* mutant. One possibility is that loss of ALF4 leads to changes in the abundance of SCF subunits. To assess this possibility, we first examined CUL1 levels in wild-type and *alf4-1* plants, in the absence and presence of the proteasome inhibitor MG132. The immunoblot in Fig 5A shows that the levels of unmodified and neddylated CUL1 are reduced in the mutant compared to the wild type. Treatment with MG132 increased the amount of both forms in the mutant and wild type, indicating that CUL1 is a substrate for the proteasome. However, we note that CUL1 levels in *alf4* plants are not restored to wild-type levels by MG132. To determine whether CUL1 stability is affected in the mutant, we treated

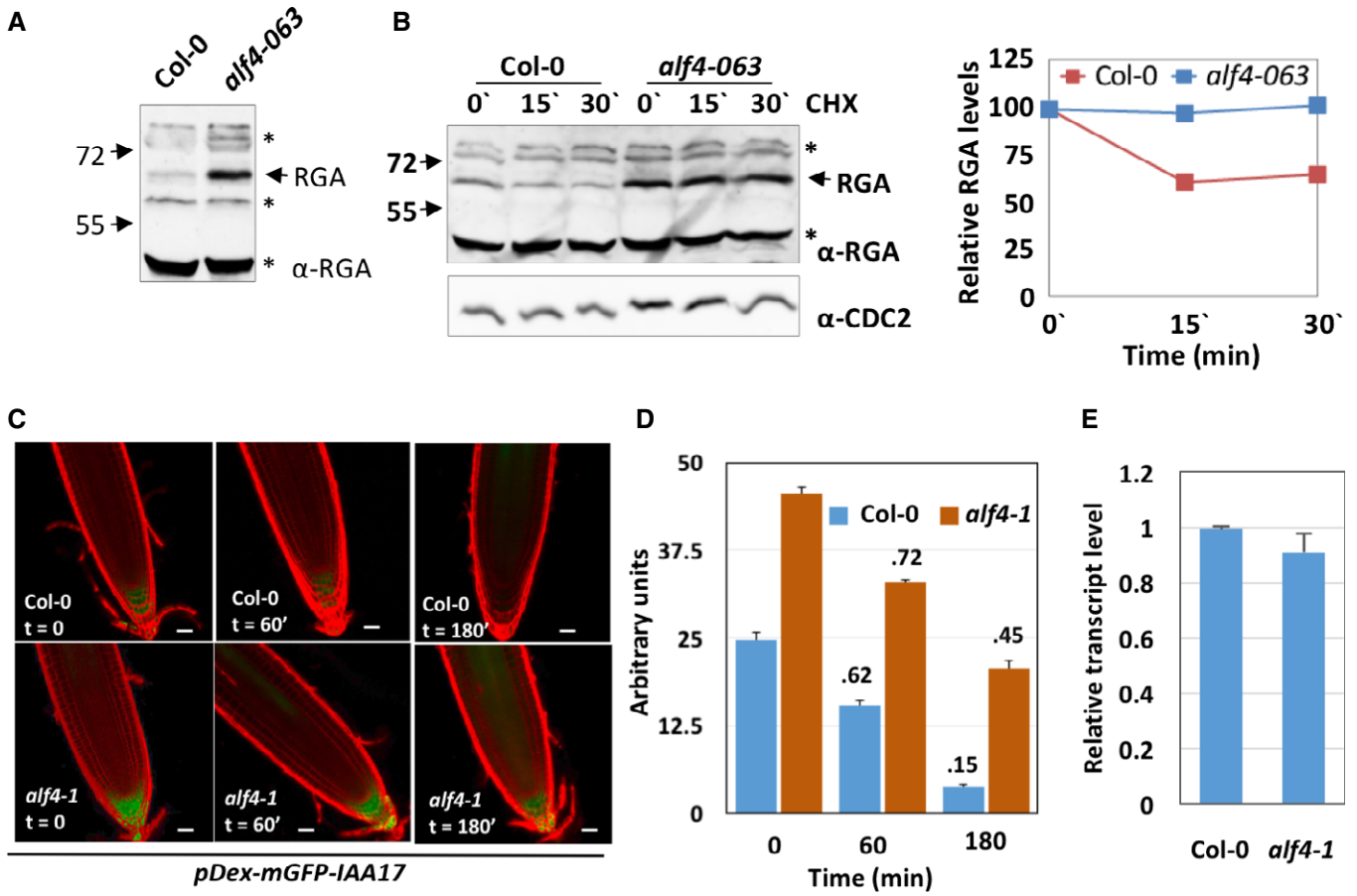

Figure 4. SCF substrates accumulate in the *alf4* mutant.

A Total protein extracts prepared from 13-day-old wild-type and *alf4-063* seedlings, separated by SDS–PAGE, and probed with anti-RGA antibody. Background cross-reacting bands are indicated by asterisks.

B 8-day-old wild-type and mutant seedlings were treated with 50 μM cycloheximide (CHX) for up to 30 min as indicated in the figure. Total protein extracts were separated by SDS–PAGE and probed with anti-RGA antibody. Asterisks indicate background cross-reacting bands. The anti-CDC2 immunoblot serves as loading control. Relative RGA signal intensity was measured using MultiGAUGE and plotted on the right.

C Confocal images showing IAA17-GFP levels in wild-type and *alf4-1* roots. Seedlings were treated with 5 μM dexamethasone for 4 h followed by treatment with 10 μM IAA for the indicated time. Scale bars are 50 μm.

D IAA17-GFP levels measured using ImageJ software. Data were collected from 4 roots for each time point. Error bars represent standard deviation. The difference between Col-0 and *alf4-1* is significant $P < 0.001$, Student's *t*-test (two-tailed) for each of the time points (t = 0, t = 60′ and t = 180′). Values above the bar are the fraction of IAA17-GFP remaining relative to time zero.

E Relative *IAA17-GFP* transcript levels in 7-day-old seedlings after treatment with dexamethasone for 4 h. Data shown are from three biological replicates. Error bars represent standard deviation. Differences are not significant, Student's *t*-test (two-tailed).

Source data are available online for this figure.

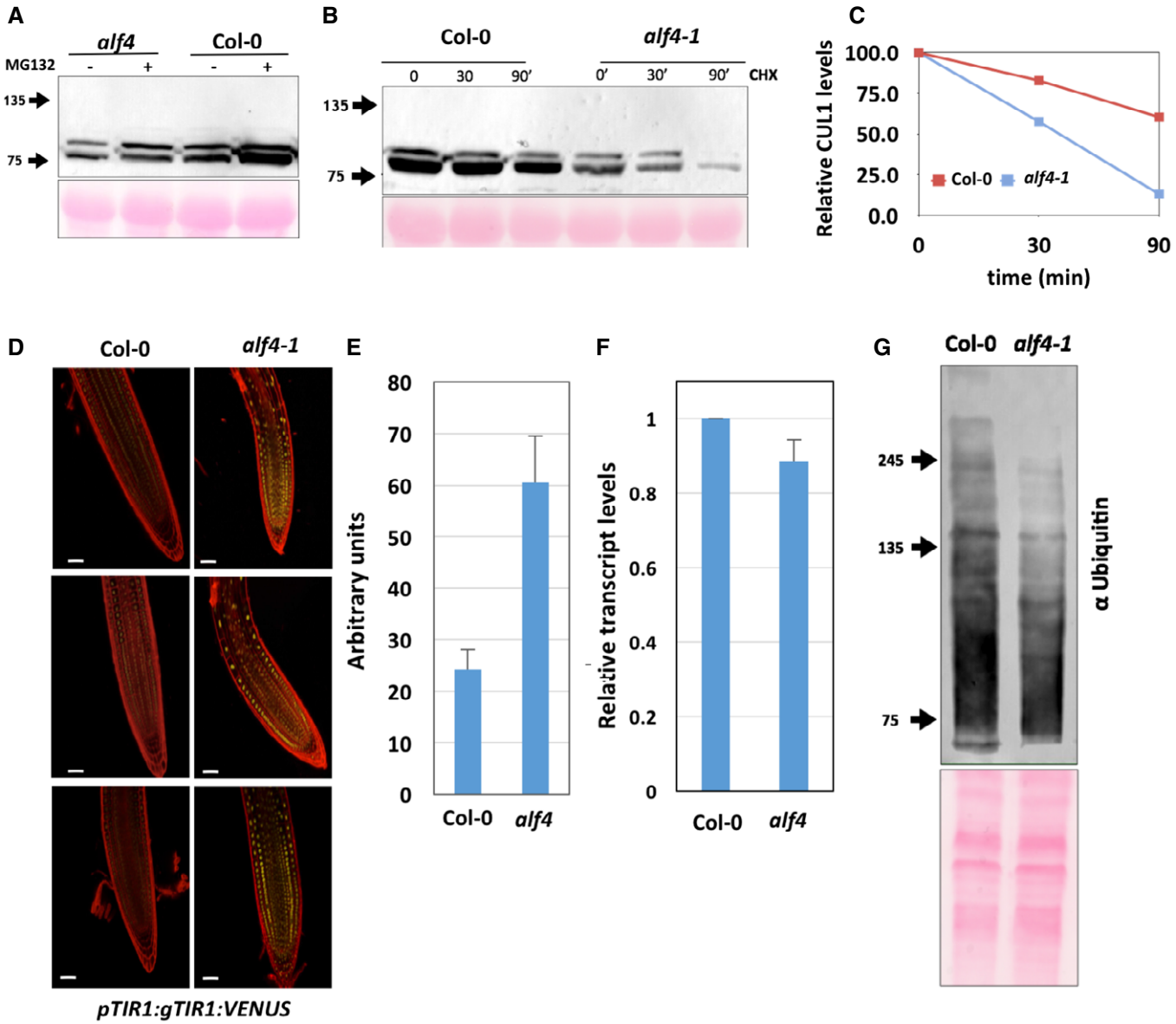

Figure 5. Stability of SCF subunits of the *alf4* mutant.

A Total protein extracts prepared from 7-day-old wild-type and *alf4-1* seedlings treated or untreated with 100 μM MG132 were separated by SDS–PAGE and probed with anti-CUL1 antibody. The bands are CUL1 and CUL1 modified with NEDD8.

B 7-day-old wild-type and *alf4*-1 mutant seedlings were treated with 200 μM cycloheximide (CHX) for up to 90 min as indicated. Total protein extracts were separated by SDS–PAGE and probed with anti-CUL1 antibody. Total protein stained with Ponceau S served as loading control.

C Immunoblot was used to quantify CUL1 protein levels in wild-type and mutant plants using ImageJ. The levels of unmodified CUL1 are expressed relative to Ponceau S-stained Rubisco large subunit.

D Confocal images showing root tip regions of representative 7-day-old *pTIR1:gTIR1-VENUS* and *alf4-1 pTIR1:gTIR1-VENUS* seedlings. Scale bars are 50 μm.

E TIR1-VENUS protein levels in wild-type and mutant plants measured with ImageJ. Error bars represent standard deviation (n = 7 plants). Difference between Col-0 and *alf4-1* is significant $P < 0.001$, Student's t-test (two-tailed).

F Relative transcript level of *TIR1-Venus* was measured in wild-type and *alf4-1* lines by qRT–PCR. Data are from three biological replicates. Error bars represent standard deviation. Differences are not significant, Student's t-test (two-tailed).

G Immunoblot of total protein from 7-day-old wild type and *alf4-1* probed with anti-ubiquitin antibody. The experiment was repeated twice with similar results.

Source data are available online for this figure.

seedlings with CHX and collected samples at time intervals thereafter. The data in Fig 5B and C show that CUL1 stability is substantially reduced in the mutant. In contrast, we find that TIR1 abundance, as detected by examining a fusion of TIR1 to the fluorescent protein VENUS, are increased in the mutant (Fig 5D and E). Since *TIR1-VENUS* transcript accumulation is not affected in the mutant (Fig 5F), the increase in protein levels is probably due to increased stability.

Since RBX1 functions in all CRL E3 ligases, it is possible that the *alf4* mutants have a broad defect in ubiquitin–protein conjugation. To assess this possibility, we performed an immunoblot of total cellular proteins with an anti-ubiquitin antibody. Indeed, the results in Fig 5G show a general decrease in the amount of ubiquitinated proteins in the *alf4-1* mutant.

SCF^{TIR1}-dependent degradation of Aux/IAA proteins is inhibited by ALF4

Based on the known function of the GLMN protein, we hypothesized that the ALF4–RBX1 interaction may influence the access of ubiquitin-charged E2s (E2~Ub) to RBX1, and therefore the ubiquitination of SCF targets. To determine whether this was the case, we established an *in vitro* assay utilizing human ubiquitin-activating enzyme (UBE1), the *Arabidopsis* conjugating enzyme AtUBC8, ubiquitin, and the RING domain of RBX1 ($RBX1^{RING}$). Previous studies have shown that the RING domain is sufficient to promote protein ubiquitination in these conditions (Hardtke *et al*, 2002; Voiniciuc *et al*, 2013). The data in Fig 6A demonstrate this activity and show that the reaction is E2- and $RBX1^{RING}$-dependent. The introduction of wild-type ALF4 strongly inhibited the ubiquitination reaction (Fig 6A). Further, and consistent with our earlier results, neither $ALF4^{A484A614}$ nor $ALF4^{1\text{-}532stop}$ had a significant effect on the reaction.

To further explore the impact of ALF4 on SCF activity, we reconstituted E1-E2-SCF^{TIR1}-mediated ubiquitination of Aux/IAAs in an *in vitro* ubiquitination system (IVU) as previously described (Winkler *et al*, 2017). All the components of the enzyme cascade are included in this assay including E1 (UBA1), the E2 AtUBC8, the E3 SCF^{TIR1}, and the substrate GST-IAA7 (Fig EV7A). As expected, we found that GST-IAA7 ubiquitination is mediated by SCF^{TIR1} in an auxin- and time-dependent manner (Fig 6B and D). The addition of excess ALF4 to the IVU reactions prevented the formation of IAA7–ubiquitin conjugates (Fig 6B). Further, the addition of increasing amounts of ALF4 resulted in a concentration-dependent decrease in the levels of ubiquitinated IAA7 (Fig 6C).

In human cells, GLMN inhibits the activity of SCF^{FBW7} by masking the E2 binding face of RBX1 (Duda *et al*, 2012). To determine whether ALF4 acted in a similar way, we examined the effects of increased E2 protein on SCF^{TIR1} activity (Fig 6D). In the absence of ALF4, the addition of higher levels of E2 stimulated the formation of IAA7–ubiquitin. This effect was also observed in the presence of ALF4, indicating that E2 and ALF4 exert counteracting effects on IAA7 ubiquitination. Taken together with our other results, these findings indicate that ALF4 probably inhibits SCF activity by competing with the E2 for binding to RBX1.

Discussion

The ubiquitin-proteasome system is a complex and highly regulated network that mediates the degradation of thousands of proteins (Vierstra, 2009). In general, degradation of specific substrates is regulated at the level of substrate recognition. However, the activities of E3 ligases are also directly regulated in a number of ways (Vittal *et al*, 2015). In the case of the CRLs, the E3 is activated by neddylation of the cullin subunit and inhibited by the CSN and CAND1 proteins. Typical for the ubiquitin system, these components are highly conserved and their loss can result in lethality in plants and animals. Here, we show that the *Arabidopsis* ALF4 protein, similar to human GLMN, inhibits SCF E3 ligases. Like GLMN, ALF4 binds to the RBX1 subunit of the SCF likely preventing the interaction between the E2 and RBX1.

Although the similarity between ALF4 and GLMN is low at the sequence level, several key residues required for interaction with RBX1 are conserved. In addition, modeling of the ALF4 structure indicates that ALF4 consists of a series of helical repeats similar to the HEAT repeats of GLMN. By analogy with the published GLMN structure, the C-terminus of ALF4 probably interacts with RBX1. Indeed, a truncated ALF4 lacking 94 amino acids at the C-terminus of the protein is deficient in RBX1 binding. Further, substitution of the conserved residues K484 and K614 with alanine greatly reduces both RBX1 binding and activity *in vitro.* MST also demonstrates that ALF4 binds to RBX1. Although the affinity constant for ALF4–MmRBX1–HsCUL1 binding is about ten times higher than that previously found for the GLMN–MmRBX1–HsCul1 interaction, this difference is likely due to the cross-species nature of the proteins we used for MST (Duda *et al*, 2012). Finally, the proposed activity of ALF4 is supported by our demonstration that ALF4 inhibits general RBX1-dependent ubiquitination as well as TIR1-dependent ubiquitination of the SCF^{TIR1} substrate IAA7.

We find that the SCF substrates RGA and IAA17 are stabilized in the *alf4* mutant compared to the wild-type control. This is counterintuitive since loss of an SCF inhibitor should result in decreased substrate levels. However, this result is consistent with previous studies of CRL regulators. For example, in *Arabidopsis*, a decrease in abundance of the CSN results in accumulation of NEDD8-modified CUL1 relative to the wild type, consistent with the de-neddylating activity of the CSN. This change is associated with a decrease in the amount of TIR1, probably because of increased autocatalytic degradation of the F-box protein, and a corresponding increase in SCF substrates (Schwechheimer *et al*, 2001; del Pozo *et al*, 2002; Stuttmann *et al*, 2009a,b). In the case of the *alf4* mutants, we also find that the levels of CUL1 are decreased. However, in this case, and unlike the *csn* mutants, both modified and unmodified CUL1 abundance is reduced. Paradoxically, we find that the level of TIR1 is increased in the *alf4* mutant. We speculate that this may be because neddylated CUL1 is limiting in the mutant so that a larger fraction of the TIR1 pool is not assembled into an SCF and therefore not subject to autocatalytic degradation. This idea is supported by our earlier studies showing that TIR1 is unstable when assembled into an SCF complex (Yu *et al*, 2015). One important question is why CUL1 is less stable in *alf4* plants. This may be because the loss of ALF4 results in an increase in autocatalytic ubiquitination and degradation. However, our results with MG132 are not consistent with this idea. CUL1 is clearly degraded by the proteasome but if decreased CUL1 stability in *alf4* is proteasome dependent, we would expect MG132 treatment would restore CUL1 amounts to near wild-type levels. The fact that it does not leaves open the possibility that another protease is involved. Further experiments will be required to resolve this issue.

Accumulation of IAA17 and RGA, as well as other members of the DELLA and Aux/IAA families, may be responsible for many aspects of the *alf4* growth phenotype. However, since CUL1 is found in all SCF complexes, it is likely that most, perhaps all, SCFs are affected by the loss of ALF4. This is consistent with our observation

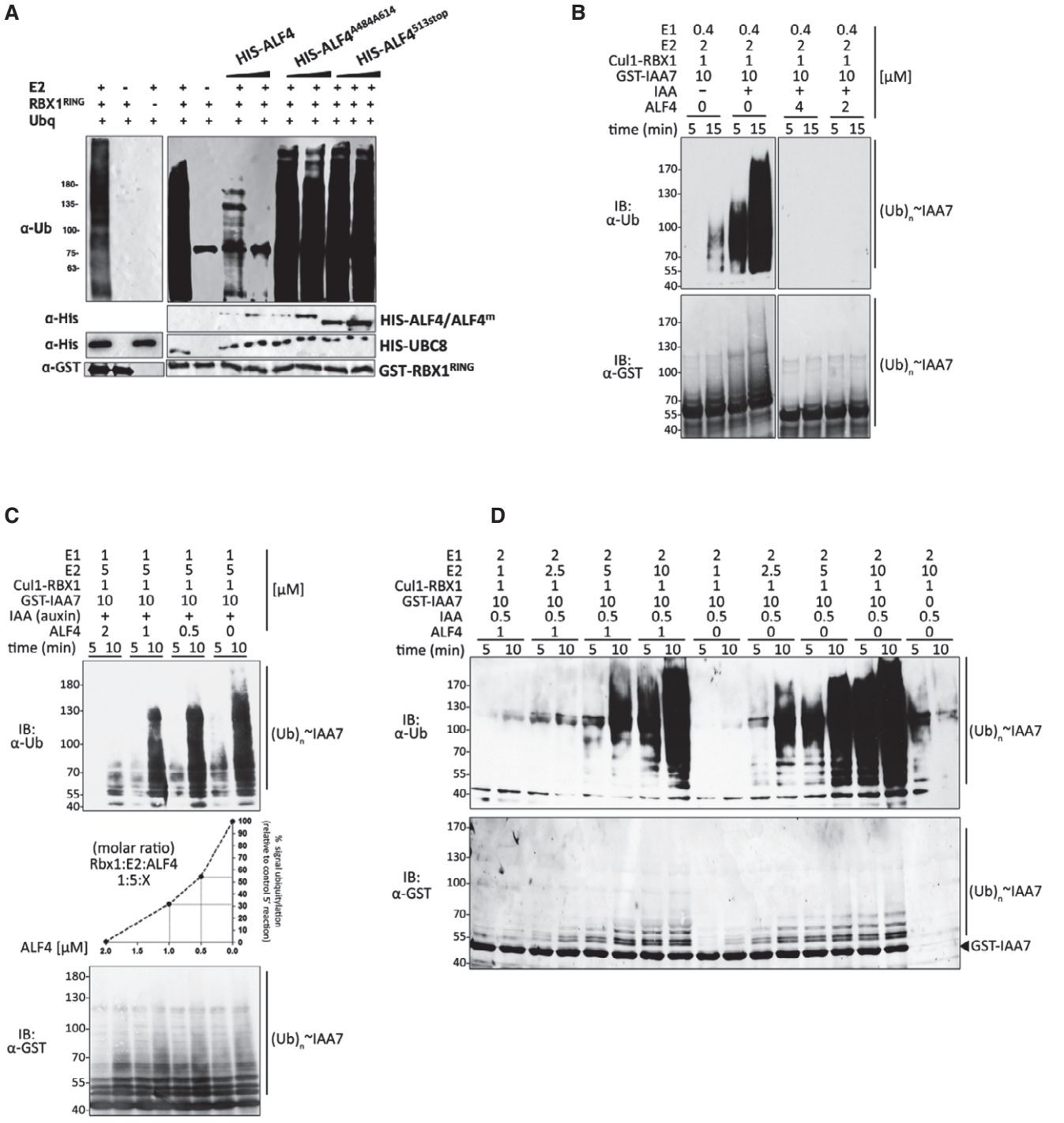

Figure 6. ALF4 inhibits SCF^{TIR1} E3 ligase activity.

A Ubiquitination assays including 6xHis-At-UBA1 (E1), 6xHis-At-UBC8 (E2), GST-RBX1^{RING}, and ubiquitin (Ub) in the presence and absence of 6xHIS-ALF4 protein were performed. The reactions were separated by SDS–PAGE and probed with anti-ubiquitin antibody.

B–D SCF^{TIR1}- and auxin-dependent transfer of ubiquitin to GST-IAA7 protein. Each reaction consists of UBA1 (E1), UBC8 (E2), ubiquitin, Cul1–RBX1, TIR1-ASK1, GST-IAA7, and various amounts of ALF4. Immunoblots with either anti-ubiquitin or anti-GST antibodies show IAA7–ubiquitin conjugates. Numbers to the left of the blots indicate protein size (in kDa). (B) Rapid (5 and 15 min) inhibition of GST-IAA7 ubiquitination occurs in the presence of ALF4. (C) ALF4 inhibits GST-IAA7 ubiquitination in a concentration-dependent manner. The levels of ubiquitin–protein conjugates are expressed relative to the 5-min reaction without ALF4 control. (D) Increasing levels of E2 reduce the effects of ALF4 on ubiquitination of IAA7. Ubiquitin conjugates on target proteins were detected as above, while anti-GST and anti-mouse-Alexa 647 antibodies were used for the detection of specific ubiquitin species on GST-IAA7. The last two lanes in the immunoblots correspond to reactions (5–10 min) containing all IVU components and GST (instead of GST-IAA7) as a control.

Source data are available online for this figure.

that the *alf4* mutation causes a general decrease in the level of ubiquitinated proteins. Whether ALF4 regulates CUL3- and CUL4-based CRLs remains to be explored. Surprisingly, the *glmn* mutation in human cells appears to have a somewhat specific effect on SCF^{Fbw7} (Tron *et al*, 2012). The basis for this specificity is currently unknown. One possibility is that GLMN regulates the activity of a specific pool of CRLs, perhaps defined by its subcellular distribution.

Previous reports demonstrated that the *alf4* mutants are deficient in the early divisions of pericycle cells during lateral root formation. Although auxin is required at this stage of the process, it was proposed that ALF4 functions independently of auxin (DiDonato *et al*, 2004). Here, we show that *alf4* is resistant to auxin and displays reduced *pDR5:GFP* activity, suggesting that reduced auxin response contributes to the lateral root defect. We also observe a strong rosette and inflorescence phenotype in *alf4-1*. The *alf4-2* and *alf4-063* mutants are extremely small and slow-growing and rarely survive to flower. Grafting experiments suggest that a reduced root system contributes to the aerial phenotype, but nevertheless, the ALF4 protein is clearly required in the rosette and inflorescence. Thus, like GLMN in mouse, ALF4 appears to be essential for viability.

Although CRLs are activated or inhibited by several factors including NEDD8, the CSN, and now ALF4/GLMN, how these factors are regulated remains an open question. The CSN is released from the SCF by the presence of substrate, at least *in vitro* (Enchev *et al*, 2012). Presumably ALF4 is released from the SCF under appropriate conditions, perhaps in response to increased E2 levels or by an increase in substrate levels. A recent report also demonstrated that *ALF4* transcription is regulated by very long-chain fatty acids (Shang *et al*, 2016). These molecules are thought to restrict the ability of pericycle cells to form callus tissue, possibly by repressing transcription of *ALF4*. In the future, it will be interesting to determine whether *ALF4* is regulated by other signaling pathways.

Materials and Methods

Plant material, growth conditions, and microscopy

Previously published *alf4-1* (Celenza *et al*, 1995), *alf4-063* (SALK_063183) (DiDonato *et al*, 2004), *pALF4:ALF4-GFP* (DiDonato *et al*, 2004), and *pDR5rev:GFP-ER* (Friml *et al*, 2003) are in the Col-0 background. *pARR5:GFP* (Yanai *et al*, 2005) is in the Ws background. *alf4-2* (SALK_089074) is a newly described allele in the Col-0 background and was obtained from the Nottingham *Arabidopsis* Seed Centre. *Alf4* allele mutation sites were mapped using the primers in Table EV1. Further information on *alf4* alleles is shown in Fig EV1. For grafting, root growth assays, and confocal imaging, plants were grown vertically on MS plates with 1% bacto agar (no sucrose) under short day conditions (8 h of 80–100 $\mu mol/m^2/s$ light) at 20°C. Seven days after germination, plants were grafted according to a previously published protocol (Melnyk *et al*, 2015). Ten days after grafting, grafted plants and non-grafted controls were moved into soil under long day conditions (16 h of 120 $\mu mol/m^2/s$ light) at 20°C. Care was taken to select successful grafts, indicated by the presence of lateral root growth and the absence of adventitious root formation at 10 days. For hormone treatment of *pDR5:GFP* and *pARR5:GFP* lines, 8-day-old plants were transferred onto MS media containing DMSO, 0.08 μM BA, or 1 μM NAA. After 24 h, plants were stained with propidium iodide and imaged on a Zeiss LSM-700 laser confocal scanning microscope. For ALF4-GFP imaging, 10-day-old plants were stained with propidium iodide and imaged on a LSM-700 microscope. For *pALF4:ALF4-GFP* hormone treatments, 5-day-old plants were transferred onto 1/2MS media containing DMSO, 0.08 μM BA, 1 μM NAA, or 5 μM NPA and after 48 h imaged on an LSM-700 microscope. Image quantifications for *pDR5:GFP* and *pARR5:GFP* lines were done on the entire image using the mean function on FIJI (fiji.sc). Brightness was adjusted for controls and samples equally. For immunoblot analysis of RGA, seedlings were grown on full MS media for 8 or 13 days. CHX treatment was performed in liquid GM supplemented with 50 μM CHX. To generate *pDex:IAA17-GFP* plants, *IAA17* CDs was PCR-amplified and cloned into Sfi1A and Sfi1B sites of pENTR-D-GFP vector and subsequently cloned into binary vector *pDexSalkOne* using LR Gateway reaction (Invitrogen 11791). The resulting *pDex-mGFP-IAA17* clone was transformed into Agrobacterium GV3101 strain and transformed into Col-0 plants by floral dip (Clough & Bent, 1998). Independent T3 lines were obtained by hygromycin selection.

Plasmid construction

Two *ALF4* isoforms were used in this study. The majority of the data were generated using UniProt isoform 1 (Q84VX3-1) which is 626 amino acids. The data in Figs 6B and C, and EV7A were generated using a shorter isoform (F4JWD6), which lacks exon 9 and an N-terminal extension. The two isoforms generated similar results in biochemical studies. cDNAs were cloned into *pENTRdTOPO* vector (Invitrogen K2400). Full-length *ALF4* cDNA was amplified by polymerase chain reaction using primers *ALF4_FL/GW-F* and *ALF4_FL-R*. $ALF4^{A484,A614}$ cDNA was amplified using *ALF4 K484A_F* and *ALF4 K484A_R* followed by *ALF4R614A_F* and *ALF4R614A_R*. $ALF4^{1\text{-}532stop}$ was generated with primers *ALF4_FL/GW-F* and $ALF4FL^{532stop}$*-R*. Similarly, RBX1 cDNA was amplified using primers RBX1_F/GW and RBX1_REV. The RBX1 ring domain ($RBX1^{RING}$) was amplified using primer set RBX1-142F and RBX1_REV. These entry clones were then further subcloned into different destination vectors using Gateway® LR technology (Invitrogen 11791).

Auxin root growth assay

The effects of exogenous auxin IAA on root growth were determined as described in Prigge *et al* (2016). Surface-sterilized wild-type and *alf4-1* seeds were placed on vertically oriented 1/2 strength MS plates with 1% bacto agar under long day conditions (16-h light and 8-h dark) in a growth chamber (80 $\mu mol/m^2/s$, 22°C). Five-day-old seedlings of similar size were then transferred to new plates supplemented with various concentrations of auxin. After 3 days, the amount of new root growth was measured and the percentage root growth inhibition was calculated relative to root growth on minimal medium minus hormone.

Gravitropic assay

To determine the response of roots to gravity, wild-type and *alf4-1* seedlings were germinated and grown for 3 days on MS medium

under long day conditions. Plants of similar size were selected and transferred to square petri dish containing the same media and grown for a day before being rotated by 90°. To measure root re-orientation, the plates were scanned at regular time intervals. Root angle was measured using ImageJ.

Yeast two-hybrid assay

For yeast two-hybrid assays, full-length *ALF4* cDNA as well as mutant versions were ligated into the *pGILDA* vector (Clontech), while the *RBX1* cDNA was inserted into the *pB42AD* plasmid (Clontech) and transformed into *Escherichia coli* competent cells. Bait and prey constructs were co-transformed into *Saccharomyces cerevisae* strain EGY48 (Clontech), and transformants were selected on SD supplemented with –Ura/–His/–Trp drop-out solution (BD Biosciences) and glucose medium. To test the interaction between ALF4 or ALF4 mutants with RBX1, yeast colonies that grew fastest were plated on SD-galactose/raffinose inducing medium containing –Ura/–His/–Trp drop-out supplement containing 80 μg/ml X-Gal (5-bromo-4-chloro-indolyl-b-D-galactopyranoside).

Bimolecular fluorescence complementation (BiFC)

For the BiFC assay, *ALF4* or *ALF4* mutant cDNAs were cloned into destination vectors pDEST–VYCE(R) (Gehl *et al*, 2009), while *RBX1* cDNA was cloned into pDEST–VYNE(R) (Gehl *et al*, 2009). These binary vectors were transferred into *Agrobacterium tumefaciens* strain GV3101 (pMP90). For transient expression, *A. tumefaciens* strains carrying the BiFC constructs were used together with the p19 strain for infiltration of 5- to 6-week-old *Nicotiana benthamiana* leaves. Fluorescence of the lower epidermis of leaf disks 2–5 days after infiltration was visualized with the confocal laser scanning microscope.

Confocal microscopy

Confocal imaging of plant roots shown in Figs 4C and 5D was performed using a Zeiss LSM 710 microscope. To visualize primary root tips, they were counterstained in 10 mg/l propidium iodide for 1–2 min, rinsed, and mounted in water. ImageJ was used to quantify the intensity of YFP or GFP fluorescence signal.

qRT–PCR

RNA was extracted from 7-day-old seedlings using the RNeasy plant mini kit (Qiagen), and the yield was quantified using a NanoDrop spectrophotometer. A total of 500 ng of total RNA was used for DNase I treatment (Ambion) and then reverse-transcribed using a poly-dT primer and the Superscript III First Strand cDNA Synthesis System for RT–PCR (Invitrogen). Quantitative PCR was performed on a CFX96 Real-Time System (Bio-Rad). RNA levels were normalized against transcripts of the GAPC2 gene (AT1G13440). The oligos used for PCR are listed in Table EV1.

Protein expression, purification, and analysis

Using the Gateway® cloning technology, coding sequences of *At*ALF4 (Q84VX3-1 and F4JWD6) were cloned into the pDEST™17 vector (ThermoFisher Scientific) as an N-terminal 6× histidine fusion. The ALF4 fusion protein was expressed in *E. coli* BL21 (DE3) cells grown in 2× YT medium. *Escherichia coli* cells with an OD600 = 0.8–1 were induced with 0.6 mM IPTG after a 20-min cold shock. After 6-h incubation at 25°C, cells were harvested by centrifugation (6,000 × *g*, 20 min, 4°C). For lysis, 5 ml lysis buffer (50 mM Tris–HCl pH 8.0, 200 mM NaCl, 10 mM imidazole, complete EDTA-free protease inhibitor cocktail (Roche), 2 mM DTT, 1 PMSF) per gram pellet was added and the cell suspension was sonicated (3 × 2 min, 1 s pulse/1 s pause). The lysate was clarified by centrifugation at 50,000 × *g* for 20 min at 4°C and applied to an Äkta pure FPLC system (GE Healthcare) for purification. As a first affinity purification step, the lysate was loaded to a pre-equilibrated (50 mM Tris–HCl pH 8.0, 200 mM NaCl, 10 mM imidazole, 2 mM DTT) 1 ml Protino® Ni-NTA (Macherey-Nagel) column, and eluted via a 10–400 mM imidazole gradient. ALF4 protein peaks were combined, and for an anion exchange (anIEX) purification step, a buffer exchange was carried out to 50 mM Tris–HCl pH 8.0, 50 mM NaCl, 2 mM DTT, with a 30-kDa cut-off centricon (Amicon). AnIEX purification was performed with a MonoQ 5/50 GL (GE Healthcare) column, and the protein was eluted by a gradient from 50 to 500 mM NaCl. All ALF4-containing fractions were combined, concentrated to a volume of 2–3 ml, and applied directly into a HiLoad S200 16/60 PG size exclusion chromatography (SEC) column. ALF4 protein was eluted with 50 mM Tris–HCl pH 8.0, 200 mM NaCl, 2 mM DTT at a flow rate of 1 ml/min. Upon SEC, two species of ALF4 eluted: one at a retention volume of ~45 ml and second one around 65 ml. All ALF4-containing fractions were combined, concentrated, and stored in storage buffer (50 mM Tris–HCl pH 8.0, 200 mM NaCl, 2 mM DTT, 10% (v/v) glycerol) at −80°C after being flash-frozen in liquid nitrogen. Preparation of recombinant expressed GST-tagged ASK1–TIR1 protein complex from SF9 insect cells, GST-tagged HsCul1–MmRBX1 (split'n coexpress system), 6xHis-UBA1, and 6xHis-UBC8 from *E. coli* was performed as previously published (Tan *et al*, 2007; Calderon Villalobos *et al*, 2012; Winkler *et al*, 2017).

Plant protein extraction and analysis

Seedlings of the indicated age were harvested and ground to a fine powder in liquid nitrogen followed by extraction in plant buffer containing 50 mM Tris pH 7.5, 150 mM NaCl, 10% glycerol, 0.1% NP-40, complete protease inhibitor (Roche), and 20 μM MG-132. Cellular debris was removed by centrifugation and total protein concentration was quantified by BCA (Thermo scientific) or Bradford assay. Samples were separated by SDS–PAGE followed by transfer to nitrocellulose membrane (Amersham). Blots were then incubated with anti-ASK antibody (1:1,000), anti-ubiquitin antibody (1:1,000; VWR International), anti-RGA antibody (1:1,000; Willige *et al*, 2007), and anti-CDC2 antibody (1:5,000; Santa Cruz Biotechnology), to detect the recovered proteins. Membranes were visualized using ECL Plus or Super Signal Western Blot Detection System (GE healthcare).

For the immunoprecipitation assays, total proteins were extracted from 2-week-old seedlings expressing *pALF4:ALF4-GFP* and *pEF1a:GFP* (Meckfessel *et al*, 2012). 15 μl of anti-GFP polyclonal antibody (Invitrogen) was crosslinked by BS3 (Thermo Scientific Pierce, P121580) to Protein G Dynabeads (Life Technologies,

10004D) and incubated with 10 mg of total proteins for 4 h at 4°C. The complexes were washed several times and then applied to SDS–PAGE for immunoblot detection. Rabbit anti-RBX1/ROC1 polyclonal antibody (Thermo Fisher AHO0402), raised against the synthetic peptide CysPLDNREWEFQKYGH, was used at 1:1,000 dilution to detect RBX1 protein.

RBX1-based *in vitro* ubiquitination assay

RBX1-dependent ubiquitination assays were performed in 30 μl reactions containing 50 mM Tris–HCl, pH 7.5, 10 mM $MgCl_2$, 1 mM ATP, 0.05 mM $ZnCl_2$, 0.2 mM DTT, 10 mM phosphocreatine, phosphocreatine kinase (0.1 units), 100 ng 6xHis-UBE1 (E1) (BostonBiochem), 250 ng 6xHis-UBC8 (E2), 2 μg ubiquitin (BostonBiochem), 250 ng GST-$RBX1^{RING}$, in the presence or absence of 100 ng of ALF4. Similar reactions without the E2 enzyme or RBX1 were used as controls. RBX1 was synthesized as previously described (Voiniciuc *et al*, 2013). The reactions were incubated at 30°C for 2 h or at different time interval. The reaction was stopped by the addition of reducing loading buffer. Samples were then loaded and separated by SDS–PAGE, blotted onto nitrocellulose membrane, and analyzed using anti-ubiquitin antibody (VWR International) at a dilution of 1:1,000. Membranes were visualized using the ECL Plus Western Blot Detection System (GE healthcare).

SCF^{TIR1}-dependent ubiquitination assay

In vitro ubiquitination assays (IVUs) were carried out as recently described (Winkler *et al*, 2017). In brief, UBA1 (E1) and UBC8 (E2) were incubated with different concentrations of highly purified ALF4, and mixed with pre-assembled SCF^{TIR1} (E3) and GST-IAA7 with or without IAA (auxin). IVU samples were incubated at 25°C, 500 rpm, aliquots were taken at specified time points, and ubiquitin chain formation was stopped by the addition of 4× Laemmli buffer and denaturation 5 min 95°C. Either 8% or 5–15% acrylamide gradient gels were used for separation of ubiquitinated samples. For the detection of ubiquitinated species, immunoblotting was performed using primary anti-ubiquitin in mouse (1:500 or 1:2,000, P4D1, Santa Cruz), and anti-GST in rabbit (1:20,000, G7781, SIGMA) antibodies, followed by anti-mouse HRP (1:10,000, Thermo Fischer Scientific), and anti-rabbit AP (1:10,000, Sigma-Aldrich) or anti-rabbit Alexa Fluor Plus 647 (1:35,000, A32733, Thermo Fischer Scientific) secondary antibodies. Nitrocellulose membranes were scanned using a Typhoon FLA9500 system (473-nm excitation wavelength and LPB filter) or incubated with either alkaline phosphatase or ECL substrates.

Microscale thermophoresis

5 μM HsCul1–MmRbx1 was labeled using the Monolith NTTM Protein Labeling Kit RED-NHS (Nanotemper Technologies) according to the manufacturer's protocol. The dye/protein ratio used was 10:1. Free dye was removed with the supplied buffer exchange column using MST analysis buffer (50 mM Tris–HCl pH 7.5, 150 mM NaCl, 10 mM $MgCl_2$, 0.05% (v/v) Tween-20). Labeling efficiency was determined by measuring absorbance at 280 and 650 nm and using Beer–Lambert law for concentration determination. Labeled Cul1–RBX1 protein sample was adjusted to 20 nM with the MST analysis buffer (see above). ALF4 was centrifuged for 10 min (21,000 × *g*, 4°C) and used in a 16 step 1:1 dilution series in MST analysis buffer containing 1 mg/ml BSA. ALF4 concentrations from 14 μM to 0.42 nM were set up and included in the MST experiment. For thermophoresis measurements, Cul1–RBX1-labeled protein sample was mixed 1:1 with each of the ALF4 dilution series which results in 10 nM labeled Cul1–RBX1, and 7 μM–0.21 nM ALF4 concentrations. After 5-min incubation at room temperature, each dilution was filled into Monolith NTTM MST Premium-coated capillaries (Nanotemper Technologies). A capillary scan was performed with 20% LED power, while MST measurements for affinity were performed at 20 and 40% LED power in a Monolith NT.115 (Nanotemper Technologies). For analysis, the data of three independently generated measurements with different protein preparations (biological replicates) at 40% LED power were used, applying the signal from Thermophoresis + T-Jump in the NT Affinity Analysis software version 2.0.2.

Expanded View for this article is available online.

Acknowledgements
We thank John Celenza for providing *alf4-1* and *pALF4:ALF4-GFP* seeds. Work in the authors' laboratories was supported by grants from NIH (GM43644 to ME), the Gordon and Betty Moore Foundation (to ME), and the Howard Hughes Medical Institute (ME). CWM was supported by a Clare College Junior Research Fellowship and Gatsby Charitable Trust grants GAT3272/C and GAT3273-PR1. JM and CS were supported by a grant from the Deutsche Forschungsgemeinschaft through the Sonderforschungsbereich 924.

Author contributions
RB and CWM characterized the mutant. CWM examined *ALF4* gene expression. RB performed Y2H, *in vitro* pulldown and BiFC experiments. GC and MW performed MST experiments. GC, MW, and MN carried out SCF^{TIR1}-based ubiquitination assays. RB and JM examined the levels of SCF subunits and substrates. KK and MS provided reagents. RB, CWM, GC, MW, CS, LIACV, and ME designed the experiments. RB, CWM, CS, LIACV, and ME wrote the paper.

Conflict of interest
The authors declare that they have no conflict of interest.

References

Calderon Villalobos LI, Lee S, De Oliveira C, Ivetac A, Brandt W, Armitage L, Sheard LB, Tan X, Parry G, Mao H, Zheng N, Napier R, Kepinski S, Estelle M (2012) A combinatorial TIR1/AFB-Aux/IAA co-receptor system for differential sensing of auxin. *Nat Chem Biol* 8: 477 – 485

Celenza JL Jr, Grisafi PL, Fink GR (1995) A pathway for lateral root formation in *Arabidopsis thaliana*. *Genes Dev* 9: 2131 – 2142

Chupeau MC, Granier F, Pichon O, Renou JP, Gaudin V, Chupeau Y (2013) Characterization of the early events leading to totipotency in an *Arabidopsis* protoplast liquid culture by temporal transcript profiling. *Plant Cell* 25: 2444 – 2463

Clough SJ, Bent AF (1998) Floral dip: a simplified method for *Agrobacterium*-mediated transformation of *Arabidopsis thaliana*. *Plant J* 16: 735 – 743

Deshaies RJ, Joazeiro CA (2009) RING domain E3 ubiquitin ligases. *Annu Rev Biochem* 78: 399 – 434

DiDonato RJ, Arbuckle E, Buker S, Sheets J, Tobar J, Totong R, Grisafi P, Fink GR, Celenza JL (2004) *Arabidopsis* ALF4 encodes a nuclear-localized protein required for lateral root formation. *Plant J* 37: 340 – 353

Duda DM, Borg LA, Scott DC, Hunt HW, Hammel M, Schulman BA (2008) Structural insights into NEDD8 activation of cullin-RING ligases: conformational control of conjugation. *Cell* 134: 995 – 1006

Duda DM, Olszewski JL, Tron AE, Hammel M, Lambert LJ, Waddell MB, Mittag T, DeCaprio JA, Schulman BA (2012) Structure of a glomulin-RBX1-CUL1 complex: inhibition of a RING E3 ligase through masking of its E2-binding surface. *Mol Cell* 47: 371 – 382

Enchev RI, Scott DC, da Fonseca PC, Schreiber A, Monda JK, Schulman BA, Peter M, Morris EP (2012) Structural basis for a reciprocal regulation between SCF and CSN. *Cell Rep* 2: 616 – 627

Friml J, Vieten A, Sauer M, Weijers D, Schwarz H, Hamann T, Offringa R, Jurgens G (2003) Efflux-dependent auxin gradients establish the apical-basal axis of *Arabidopsis*. *Nature* 426: 147 – 153

Gagne JM, Downes BP, Shiu SH, Durski AM, Vierstra RD (2002) The F-box subunit of the SCF E3 complex is encoded by a diverse superfamily of genes in *Arabidopsis*. *Proc Natl Acad Sci USA* 99: 11519 – 11524

Gehl C, Waadt R, Kudla J, Mendel RR, Hansch R (2009) New GATEWAY vectors for high throughput analyses of protein-protein interactions by bimolecular fluorescence complementation. *Mol Plant* 2: 1051 – 1058

Gilkerson J, Hu J, Brown J, Jones A, Sun TP, Callis J (2009) Isolation and characterization of cul1-7, a recessive allele of CULLIN1 that disrupts SCF function at the C terminus of CUL1 in *Arabidopsis thaliana*. *Genetics* 181: 945 – 963

Hardtke CS, Okamoto H, Stoop-Myer C, Deng XW (2002) Biochemical evidence for ubiquitin ligase activity of the *Arabidopsis* COP1 interacting protein 8 (CIP8). *Plant J* 30: 385 – 394

Hua Z, Vierstra RD (2011) The cullin-RING ubiquitin-protein ligases. *Annu Rev Plant Biol* 62: 299 – 334

Kelley DR, Estelle M (2012) Ubiquitin-mediated control of plant hormone signaling. *Plant Physiol* 160: 47 – 55

Kelley LA, Mezulis S, Yates CM, Wass MN, Sternberg MJ (2015) The Phyre2 web portal for protein modeling, prediction and analysis. *Nat Protoc* 10: 845 – 858

Lavy M, Estelle M (2016) Mechanisms of auxin signaling. *Development* 143: 3226 – 3229

Li T, Pavletich NP, Schulman BA, Zheng N (2005) High-level expression and purification of recombinant SCF ubiquitin ligases. *Methods Enzymol* 398: 125 – 142

Lydeard JR, Schulman BA, Harper JW (2013) Building and remodelling Cullin-RING E3 ubiquitin ligases. *EMBO Rep* 14: 1050 – 1061

Meckfessel MH, Blancaflor EB, Plunkett M, Dong Q, Dickstein R (2012) Multiple domains in MtENOD8 protein including the signal peptide target it to the symbiosome. *Plant Physiol* 159: 299 – 310

Melnyk CW, Schuster C, Leyser O, Meyerowitz EM (2015) A developmental framework for graft formation and vascular reconnection in *Arabidopsis thaliana*. *Curr Biol* 25: 1306 – 1318

Pierce NW, Lee JE, Liu X, Sweredoski MJ, Graham RL, Larimore EA, Rome M, Zheng N, Clurman BE, Hess S, Shan SO, Deshaies RJ (2013) Cand1 promotes assembly of new SCF complexes through dynamic exchange of F box proteins. *Cell* 153: 206 – 215

del Pozo JC, Dharmasiri S, Hellmann H, Walker L, Gray WM, Estelle M (2002) AXR1-ECR1-dependent conjugation of RUB1 to the *Arabidopsis* Cullin AtCUL1 is required for auxin response. *Plant Cell* 14: 421 – 433

Prigge MJ, Greenham K, Zhang Y, Santner A, Castillejo C, Mutka AM, O'Malley RC, Ecker JR, Kunkel BN, Estelle M (2016) The *Arabidopsis* auxin receptor F-box proteins AFB4 and AFB5 are required for response to the synthetic auxin picloram. *G3 (Bethesda)* 6: 1383 – 1390

Salehin M, Bagchi R, Estelle M (2015) SCFTIR1/AFB-based auxin perception: mechanism and role in plant growth and development. *Plant Cell* 27: 9 – 19

Schwechheimer C, Serino G, Callis J, Crosby WL, Lyapina S, Deshaies RJ, Gray WM, Estelle M, Deng XW (2001) Interactions of the COP9 signalosome with the E3 ubiquitin ligase SCFTIRI in mediating auxin response. *Science* 292: 1379 – 1382

Schwechheimer C, Willige BC (2009) Shedding light on gibberellic acid signalling. *Curr Opin Plant Biol* 12: 57 – 62

Shang B, Xu C, Zhang X, Cao H, Xin W, Hu Y (2016) Very-long-chain fatty acids restrict regeneration capacity by confining pericycle competence for callus formation in *Arabidopsis*. *Proc Natl Acad Sci USA* 113: 5101 – 5106

Stuttmann J, Lechner E, Guérois R, Parker JE, Nussaume L, Genschik P, Noël LD (2009a) COP9 signalosome- and 26S proteasome-dependent regulation of SCFTIR1 accumulation in *Arabidopsis*. *J Biol Chem* 284: 7920 – 7930

Stuttmann J, Parker JE, Noël LD (2009b) Novel aspects of COP9 signalosome functions revealed through analysis of hypomorphic csn mutants. *Plant Signal Behav* 4: 896 – 898

Tan X, Calderon-Villalobos LI, Sharon M, Zheng C, Robinson CV, Estelle M, Zheng N (2007) Mechanism of auxin perception by the TIR1 ubiquitin ligase. *Nature* 446: 640 – 645

Tron AE, Arai T, Duda DM, Kuwabara H, Olszewski JL, Fujiwara Y, Bahamon BN, Signoretti S, Schulman BA, DeCaprio JA (2012) The glomuvenous malformation protein Glomulin binds Rbx1 and regulates cullin RING ligase-mediated turnover of Fbw7. *Mol Cell* 46: 67 – 78

Vierstra RD (2009) The ubiquitin-26S proteasome system at the nexus of plant biology. *Nat Rev Mol Cell Biol* 10: 385 – 397

Vittal V, Stewart MD, Brzovic PS, Klevit RE (2015) Regulating the regulators: recent revelations in the control of E3 ubiquitin ligases. *J Biol Chem* 290: 21244 – 21251

Voiniciuc C, Dean GH, Griffiths JS, Kirchsteiger K, Hwang YT, Gillett A, Dow G, Western TL, Estelle M, Haughn GW (2013) Flying saucer1 is a transmembrane RING E3 ubiquitin ligase that regulates the degree of pectin methyl esterification in *Arabidopsis* seed mucilage. *Plant Cell* 25: 944 – 959

Walker L, Estelle M (1998) Molecular mechanisms of auxin action. *Curr Opin Plant Biol* 1: 434 – 439

Willige BC, Ghosh S, Nill C, Zourelidou M, Dohmann EM, Maier A, Schwechheimer C (2007) The DELLA domain of GA INSENSITIVE mediates the interaction with the GA INSENSITIVE DWARF1A gibberellin receptor of Arabidopsis. *Plant Cell* 19: 1209 – 1220

Winkler M, Niemeyer M, Hellmuth A, Janitza P, Christ G, Samodelov SL, Wilde V, Majovsky P, Trujillo M, Zurbriggen MD, Hoehenwarter W, Quint M, Calderón Villalobos LIA (2017) Variation in auxin sensing guides AUX/IAA transcriptional repressor ubiquitylation and destruction. *Nat Commun* 8: 15706

Winter D, Vinegar B, Nahal H, Ammar R, Wilson GV, Provart NJ (2007) An "Electronic Fluorescent Pictograph" browser for exploring and analyzing large-scale biological data sets. *PLoS One* 2: e718

Wu S, Zhu W, Nhan T, Toth JI, Petroski MD, Wolf DA (2013) CAND1 controls *in vivo* dynamics of the cullin 1-RING ubiquitin ligase repertoire. *Nat Commun* 4: 1642

Xu L, Liu F, Lechner E, Genschik P, Crosby WL, Ma H, Peng W, Huang D, Xie D (2002) The SCF(COI1) ubiquitin-ligase complexes are required for jasmonate response in *Arabidopsis*. *Plant Cell* 14: 1919 – 1935

Yanai O, Shani E, Dolezal K, Tarkowski P, Sablowski R, Sandberg G, Samach A, Ori N (2005) *Arabidopsis* KNOXI proteins activate cytokinin biosynthesis. *Curr Biol* 15: 1566 – 1571

Yu H, Zhang Y, Moss BL, Bargmann BO, Wang R, Prigge M, Nemhauser JL, Estelle M (2015) Untethering the TIR1 auxin receptor from the SCF complex increases its stability and inhibits auxin response. *Nat Plants* 1: pii: 14030

Zemla A, Thomas Y, Kedziora S, Knebel A, Wood NT, Rabut G, Kurz T (2013) CSN- and CAND1-dependent remodelling of the budding yeast SCF complex. *Nat Commun* 4: 1641

Zheng N, Zhou Q, Wang Z, Wei W (2016) Recent advances in SCF ubiquitin ligase complex: clinical implications. *Biochim Biophys Acta* 1866: 12 – 22

3. Discussion and future perspectives

In the next section, I aim to expand on and connect the topics discussed in the three publications. I further seek to connect my findings with recent advances in the field of auxin signaling in particular, and ubiquitylation in general. In this manner I strived to present new concepts and ideas to be explored in further studies. Findings from Winkler *et al.* (2017) will be discussed in light of the structural proteomics results reported in Niemeyer *et al.* (2020). In addition, theories connecting some of the novel identified AUX/IAA features (*e.g.* intrinsic disorder) with open questions in the auxin field, such as non-canonical and fast auxin responses, will be presented. I also hypothesize on how ALF4 functions can be integrated in the SCF regulatory cycle.

3.1 New insights into multivalent complex formation based on the auxin receptor

Since the crystal structure of ASK1·TIR1·auxin·IAA7^{degron} was published, a few studies have proposed an extensive tunability in the auxin co-receptor system, which depends on the diversity, and biochemical and structural features of the single protein components (Tan et al., 2007; Havens et al., 2012; Shimizu-Mitao and Kakimoto, 2014). The AUX/IAA family expansion, and its diversity along non-conserved domains, particularly outside the core degron have been proposed to drive auxin receptor tunability and divergent auxin binding co-receptor properties (Calderón Villalobos et al., 2012; Guseman et al., 2015; Moss et al., 2015). Degron flanking regions escaped detailed structural investigations, due to their first postulated and now shown by us, intrinsic disorder (Dinesh et al., 2016; Winkler et al., 2017; Niemeyer et al., 2020). Solving the topology of two full auxin receptor systems, ASK1·TIR1·IAA7 and ASK1·TIR1·IAA12, represents a significant advancement in our current knowledge of how TIR1 engages full-length AUX/IAA during auxin perception. Also, these studies advanced our understanding of how IDRs in signaling proteins exert critical functions, despite lacking a defined three-dimensional structure (Niemeyer et al., 2020). IDRs are under less selective evolutionary pressure, and can occupy a spearheading role fine-tuning auxin signaling during land plant evolution, explaining also why so many AUX/IAA genes were retained (Ahrens et al., 2017; Winkler et al., 2017; Mutte et al., 2018).

Since the functional output of auxin-dependent TIR1/AFBs·AUX/IAA associations is AUX/IAA ubiquitylation, sufficient high, receptor-specific, auxin concentrations would lead to fast and processive Ub conjugation to AUX/IAAs. Steady-state intracellular auxin concentrations are proposed to fluctuate in the nM range, while high auxin spikes might reach low µM concentrations (Band et al., 2012; Kramer and Ackelsberg, 2015; Fendrych et al., 2018). Based on the auxin binding affinity of specific co-receptors, auxin concentrations lower than the corresponding K_d, do not facilitate AUX/IAA ubiquitylation efficiently (Winkler et al., 2017; Niemeyer et al., 2020). The system is rather threshold-based with sigmoidal behavior: As soon as a certain auxin concentration is reached, rapid AUX/IAA ubiquitylation follows. In other words, at very high intracellular auxin concentrations (*e.g.* > 1 µM) it would not be possible to observe a difference in the ubiquitylation of different AUX/IAAs incorporated in either high or low affinity auxin co-receptor systems (**Figure 7c**).

The threshold-based behavior suggests a certain AUX/IAA dwell time on TIR1/AFBs is needed for precise recruitment, and especially, subsequent ubiquitylation. Upon auxin-triggered degron binding, an AUX/IAA multisite association including cooperative PB1 and degron tail engagement on one site, and N-terminal, KR motif-related interactions on the other site of TIR1, facilitates prolonged dwell times.

The engagement of the folded PB1 domain with TIR1 is a rather surprising finding from our work, as it was often excluded from previous analysis or showed a negative effect on auxin responsiveness (Havens et al., 2012; Moss et al., 2015). The negative effect of the AUX/IAA PB1 domain on their degradation rates, is explainable by the longer processing time at the proteasome due to the stable PB1 fold (Havens et al., 2012; Moss et al., 2015; Bard et al., 2019). Focusing on the PB1 domain has the potential to reveal additional modulating functions of extended, and specialized interaction interfaces, as seen in a recent study comparing ARF and AUX/IAA PB1 domain interactions (Kim et al., 2020). The additionally identified contacting PB1 residues reside in the very C-terminus of AUX/IAA PB1 domains, which contribute also to TIR1 binding (see **chapter 7.2, Supp. Fig. 13**). This C-terminal PB1 domain extension is variable among the AUX/IAAs, and holds the potential for specificity, similarly to the flexible loop connecting the two faces of the PB1 fold, formerly known as DIII and DIV AUX/IAA domains.

During auxin receptor formation, PB1 positioning can modulate an entropic force relying on IDRs, such as the degron tail (dT), further contributing to TIR1/AFBs·AUX/IAA associations (Keul et al., 2018). Intrinsic disorder in AUX/IAAs in the PB1 domain-connecting dT, and in their N-terminus provide sufficient flexibility for multivalent or avidity-based interactions (Fung et al., 2018; Bugge et al., 2020). Compared to IAA7 and IAA12, IAA6 and IAA19 appear to be more ordered (see **chapter 7.2, Supp. Fig. 1**), while covering a similar range of auxin binding capabilities when in complex with TIR1 (Winkler et al., 2017; Niemeyer et al., 2020). In this context, intrinsic disorder is rather indirectly responsible for different affinities by allowing and/or restricting other receptor-stabilizing interactions. AUX/IAA degron flanking regions enable typical disorder-mediated context-driven TIR1·auxin·degron interactions (Bugge et al., 2020). Specifically, the distinct distribution of charges on the surface of TIR1/AFBs and along the AUX/IAA degron flanking sequences is likely the basis for disorder-mediated context-based interactions during TIR1/AFB·AUX/IAA co-receptor pairing (see **Appendix, Figure 12**). Fluctuating conformational states of AUX/IAA degron flanking regions allow the flexible positioning of *e.g.* the charged residues on the TIR1 surface. The overall interaction with TIR1 (auxin-dependent and independent) is then based on the pairing of disordered regions with the connected PB1 domain (Niemeyer et al., 2020).

The newly identified TIR1·AUX/IAA interaction sites, including one for the degradation-relevant KR motif, might regulate complex assembly and disassembly, *e.g.* by exposing and occupying AUX/IAA binding motifs and ubiquitylation sites (next section) (Dreher et al., 2006). The diversity in the AUX/IAA protein family in combination with the six TIR1/AFB1-5, acting as versatile docking surfaces, results in an ideal model system to study the interplay of small molecule-triggered association and IDR-modulated protein-protein and protein-small molecule interactions. The common layout of small-molecule (*e.g.* phytohormone)-triggered ubiquitylation target recruitment by SCF-type E3 ligases, allows us to draw conclusions beyond auxin signaling. It is possible that other co-receptors systems *e.g.* the COI1-JAZ receptor for jasmonate-perception, function in a similar fashion. IDRs in JAZs (see **Appendix**, **Figure 13**) might enable correct positioning of JAZs on COI1, supporting a multivalency or avidity-driven interaction mechanism. The concept of disorder as a functional factor ensuing proper auxin sensing has just emerged, and future studies will lead us to further insights into how IDRs affect complex formation in phytohormone signaling pathways and beyond. Given the multisite interactions of AUX/IAAs with TIR1, auxin-driven co-

receptor formation potentially drives AUX/IAAs out of other complexes as will be discussed in the following section.

3.2 Do multivalent interactions facilitate assembly & disassembly of AUX/IAA-containing complexes?

Since AUX/IAAs contribute to many cellular processes, engage in numerous PPIs and carry regions of intrinsic disorder, one can postulate they act as hub proteins (Vandereyken et al., 2018; Covarrubias et al., 2020; Niemeyer et al., 2020). The following chapter describes AUX/IAA interactions, with emphasis on domain specific effects, and AUX/IAA-containing complexes beyond the auxin co-receptor, such as the transcriptional repressor complex (see chapter 1.5), and possible complexes located in non-canonical auxin signaling pathways. The regulatory potential of IDR-located PTMs shifting AUX/IAAs from one to another complex is also discussed.

Multivalency of TIR1·AUX/IAA interactions facilitates repressors complex disassembly

We described TIR1·AUX/IAA^{PB1} contacts, which may alter additional PB1-driven interactions AUX/IAAs engage in, *e.g.* with ARFs. The highly conserved PB1 domain is a versatile interaction module, and functions also at the core of auxin signaling, as it ensues AUX/IAA·ARF heteromer formation (Sumimoto et al., 2007; Korasick et al., 2014; Kim et al., 2020). Auxin-triggered AUX/IAA^{degron} recruitment by TIR1 allows TIR1·AUX/IAA^{PB1} contacts to be established. These extra contacts likely support AUX/IAA dislodgement from the transcriptional repressor complex, where strong ARF^{PB1}·AUX/IAA^{PB1} heteromeric binding dominates. Additionally, competition between ARF^{PB1}·AUX/IAA^{PB1} and TIR1· AUX/IAA^{PB1} interactions can act as a lever to tune repressor strength and repressor complex disassembly, explaining differences in repressor strength of IAA12 and IAA3 (Maraschin et al., 2009). The before-mentioned C-terminal extension in AUX/IAA PB1 domains, which also contribute to co-receptor formation, could also play a role during repressor complex disassembly (Ferreon et al., 2013; Niemeyer et al., 2020). A recent study showed that these extension carries residues, which partially expand the previously described basic patch of the PB1 domain (*e.g.* K125 and R205 in IAA17), and enhance the formation of AUX/IAA-specific

AUX/IAA·ARF heteromers (Korasick et al., 2014; Dinesh et al., 2015; Kim et al., 2020). The consideration of the extra residues in the PB1·PB1 interface explains some of the specificity seen for AUX/IAA and /or ARF containing complexes (Vernoux et al., 2011; Piya et al., 2014).

The KR motif surrounding residues in IAA7 establish flexible contacts with the TIR1 cluster 2 (LRR17-18), and probably enhance or modulate auxin co-receptor assembly (Niemeyer et al., 2020). The TPL-recruiting EAR motif, probably not directly involved in TIR1·AUX/IAA interactions, might be still restricted in its TPL-binding function upon receptor formation (Ke et al., 2015). As a result, rising auxin concentrations drive the recruitment of AUX/IAAs to TIR1, and the additional contacts, between TIR1 and AUX/IAAs (Niemeyer et al., 2020), liberate AUX/IAAs from other binding partners, such as ARFs and TPL.

Except from the canonical nuclear auxin signaling cascade (**Figure 4**), the new TIR1 interaction interfaces can influence other AUX/IAAs interactions in the same manner. AUX/IAAs are incorporated in many non-auxin phytohormone-driven processes *via* extensive crosstalk, and interact with an array of other proteins, such as transcriptional regulators, and controlling thereby the expression of a number of nuclear genes (Altmann et al., 2020). For instance, AUX/IAAs directly interact with cryptochrome 1 (CRY1) and phytochrome B (phyB) during light sensing, RGA-LIKE (RGL) proteins upon salt stress-induced GA signaling, and *Os*IPK2 during *Os*IAA11-dependent LR formation in rice (Chen et al., 2017; Shi et al., 2017; Luo et al., 2018; Xu et al., 2018). CRY1·AUX/IAA associations depend on the disordered N-terminal half of the AUX/IAAs, and therefore might competes with the newly identified TIR1 interaction interfaces during auxin co-receptor formation. CRY1·AUX/IAA interaction further could hinder TPL recruitment. The influence of other AUX/IAA-containing complexes on the formation of canonical auxin co-receptor complexes, and the ARF-bound repressor complex remains to be studied in the future.

Are multivalent AUX/IAA interactions key for non-canonical auxin responses?

The multivalency in TIR1·AUX/IAA interactions, and the hub protein-like behavior of AUX/IAAs imply their putative involvement in fast transcription-independent (auxin) signaling events. Non-canonical auxin signaling refers to a variety of physiological auxin responses, which are either too fast (less than 5 minutes) to rely on canonical transcriptional responses, or they involve non-

canonical components, such as degron-less AUX/IAAs (Kubeš and Napier, 2019). Some non-canonical auxin responses share components with the inherent canonical pathway, while others seem to involve the activity of atypical players *e.g.* the PB1 domain-less ARF3 (ETTIN) or transmembrane kinase 1 (TMK1) (Simonini et al., 2016; Dindas et al., 2018; Fendrych et al., 2018; Simonini et al., 2018; Cao et al., 2019; Kuhn et al., 2020; Lv et al., 2020). The former was recently examined during very fast auxin responses in roots and root hairs (Dindas et al., 2018; Fendrych et al., 2018). Surprisingly, fast auxin-triggered root growth inhibition depends on TIR1, and occurs within a few minutes uncoupled from protein synthesis (Fendrych et al., 2018). The fast auxin-mediated root growth inhibition could be explained by IAA-triggered rapid membrane depolarization accompanied by changes in calcium fluxes, as reported for root hairs (Dindas et al., 2018).

How TIR1/AFBs activity impinge on these fast responses remains elusive. It is not difficult to imagine that the multivalency of TIR1/AFBs·AUX/IAA interactions might exclude additional TIR1 and AUX/IAA PPIs, for instance recruitment or heteromerization with non-canonical AUX/IAAs (**Figure 10**). Non-canonical AUX/IAAs, which lack a core degron, play an important role in other hormone signaling pathways, as shown for OsIAA26 during ethylene signaling. Thus, intriguingly non-canonical AUX/IAAs can influence auxin-driven traits such as, IAA33 in root stem cell identity, and IAA32/34 during apical hook maintenance (Chen et al., 2018; Cao et al., 2019; Lv et al., 2020). Intriguingly, those processes are unlikely to happen in the nucleus, and Dindas et al. (2018) and Fendrych et al. (2018) both propose a cytoplasmic auxin sensing by TIR1/AFBs, and possibly AUX/IAAs, as the AUX/IAA-mimicking DII-Venus signal was correlating with rapid

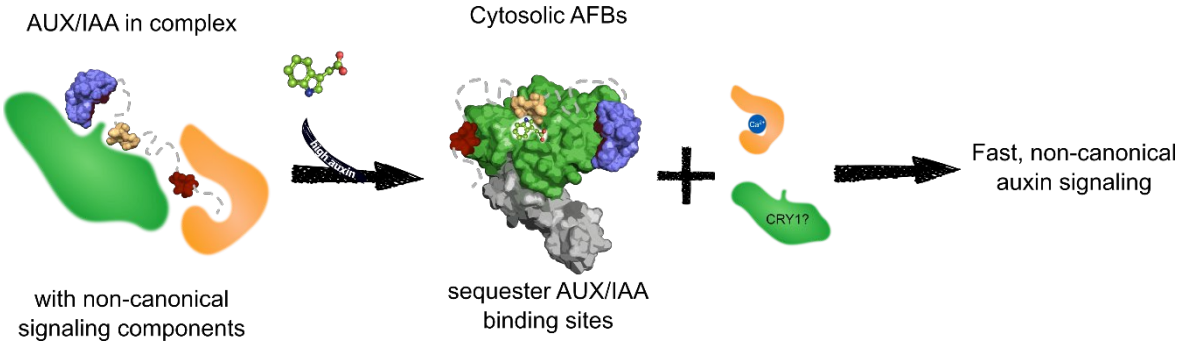

Figure 10: One possible mechanism for the contribution of AUX/IAAs on non-canonical auxin signaling events. Cytosolic complexes containing non-canonical auxin signaling components, such as CRY1 or ETTIN, might be sequestered by AUX/IAAs. Upon auxin influx, AUX/IAAs might be recruited to cytosolic non-SCF assembled AFBs, *e.g.* AFB1, and non-canonical signaling components are free to exert their function. This might prompt fast auxin responses, during root growth inhibition, and calcium-mediated membrane depolarization.

auxin responses (Fendrych et al., 2018). Recently, it has been shown that TIR1/AFBs nuclear localization is rather unusual, and only TIR1 is mainly localized to the nucleus (90-95%), while AFB1-5 primarily localize in the cytoplasm (Prigge et al., 2020). Non-nuclear localization of the *At*AUX/IAAs is less described, but there are some indications of cytoplasmic localization of non-canonical *At*AUX/IAAs, and even *At*IAA8 and degron-containing maize AUX/IAAs (Arase et al., 2012; Ludwig et al., 2014; Cao et al., 2019; Lv et al., 2020). This opens up the possibility for AUX/IAAs and TIR1/AFBs participating in cytosolic, fast auxin-dependent responses. Cooperativity of multiple regions in AUX/IAAs and the additional interaction interfaces with TIR1, and likely AFBs, can help to assemble and disassemble those, so far unknown, fast signaling complexes (**Figure 10**) (Ferreon et al., 2013; Niemeyer et al., 2020). Particularly, AFB1 may play a crucial role in those unexplored cytosolic AUX/IAA-containing complexes, as it highly accumulates in the cytoplasm (Prigge et al., 2020). Since AFB1 is unable to properly assemble in an SCF complex (Yu et al., 2015), a non-degradative outcome of AFB1·AUX/IAA complex formation is plausible, and can explain the reversibility of auxin-dependent fast root growth inhibition (Fendrych et al., 2018). Putative AFB1·AUX/IAA complexes could also retain AUX/IAAs in the cytosol after synthesis, to prolong or modulate auxin responses. The agglomeration of interaction interfaces in AUX/IAAs, such as the degron & the EAR motif in IDRs, and the cooperativity of the degron tail and the PB1 domain makes AUX/IAAs versatile signaling integrators of canonical and non-canonical auxin signaling events. Future studies will contribute to uncovering the basis of complex nuclear and non-nuclear auxin signaling mechanisms.

Do competitive PTMs regulate AUX/IAAs association with proteins?

PTMs can influence protein binding to specific sites, and shape the conformational landscape of IDRs, for instance in AUX/IAAs, and thereby shift functionality and association behavior (Darling and Uversky, 2018). Multivalency-driven competition allows fast and regulated remodeling of AUX/IAA-containing complexes, and can function independent from the canonical transcriptional auxin signaling cascade (see above section). For AUX/IAAs, mainly two PTMs have been described so far: ubiquitylation and phosphorylation (Colón-Carmona et al., 2000; Maraschin et al., 2009; Winkler et al., 2017; Mergner et al., 2020; Niemeyer et al., 2020). In addition, peptidyl-prolyl isomerases modulate the conformers of AUX/IAA degrons to enhance auxin-dependent AUX/IAA

degradation (Jing et al., 2015; Ramans Harborough et al., 2019). Concerted PTMs, often occurring in IDRs have been described as a characteristic feature of hub proteins (Vandereyken et al., 2018). AUX/IAA IDRs might exert a dual function carrying binding motifs to associate with other proteins (*e.g.* TPL and TIR1/AFBs), and harboring PTM sites for their regulation (Haynes et al., 2006; Darling and Uversky, 2018; Vandereyken et al., 2018).

We identified ubiquitylation sites in AUX/IAAs in degron-flanking IDRs and the PB1 domain, which contribute to TIR1·AUX/IAA, AUX/IAA·ARF, and AUX/IAA·TPL complex formation (Korasick et al., 2014; Dinesh et al., 2015; Winkler et al., 2017; Niemeyer et al., 2020). Ubiquitylation sites accumulate around the KR motif, which is important for normal auxin-responsive AUX/IAA degradation (Dreher et al., 2006; Winkler et al., 2017; Niemeyer et al., 2020). We could also show that residues surrounding the KR motif of AUX/IAAs contact TIR1, and ubiquitylation in these regions could potentially weaken TIR1·AUX/IAA binding (Niemeyer et al., 2020). Close proximity of KR and EAR motifs (depending on the AUX/IAA ~10 amino acids), and the ubiquitylation in between both motifs (IAA6$^{K32/33}$, IAA7^{K29}, IAA12^{K43}, IAA19^{K25}) allows not only TIR1·AUX/IAA^{KR} interactions to be modulated, but ubiquitylation could also keep AUX/IAAs from recruiting TPL (Winkler et al., 2017; Niemeyer et al., 2020). So, ubiquitylation may not only trigger AUX/IAA degradation by its inherent function, but it might shift AUX/IAA associations towards their proteasomal degradation pathway, and away from other interactions, such as the repressor complex.

Phosphorylation has been also described for AUX/IAAs (Mergner et al., 2020). Phospho-degrons in SCF substrates in animal systems are highly common, but much less so often described in plant UPS targets, so far (Spoel et al., 2009; Skaar et al., 2013). Although not so far evidenced for AUX/IAAs, their phosphorylation could impinge on their binding by TIR1/AFBs, or their degradation (Hao et al., 2007; Spoel et al., 2009). The opposite, a phosphorylation-dependent inhibition of ubiquitylation, has been shown in *e.g.* cancer-related pathways or the regulation of synaptic proteins (Nalavadi et al., 2012; Moeller et al., 2014; Du et al., 2020). A rapport between phosphorylation and ubiquitylation on AUX/IAAs, is plausible, especially where phospho-sites coincide with ubiquitylation sites. Specifically, in IAA7 both PTMs were detected close to the KR motif, and only three amino acids apart, on S26 and K29, while in the case of IAA12 ubiquitylation and phosphorylation were described in the region downstream of the degron (S83 and K91)

(Mergner et al., 2020; Niemeyer et al., 2020). Although it is unclear so far, whether phosphorylation and ubiquitylation inhibit each other, for instance, sterically, and change the affinity for TIR1/AFBs. The accumulation of PTMs and binding motifs in regions upstream of the AUX/IAA degron could also facilitate the regulated shift of AUX/IAAs from one complex to another, *e.g.* from an ARF·AUX/IAA·TPL repressor complex to an $SCF^{TIR1/AFB1-5}$·AUX/IAA auxin co-receptor complex. Future biochemical studies will certainly shed light into the relationship of ubiquitylation and phosphorylation on AUX/IAAs and their influence on activity and stability.

3.3 AUX/IAA ubiquitylation signals rely on auxin receptor assembly

Ubiquitylation of UPS targets, such as AUX/IAAs, on specific sites is determined by the controlled recruitment of targets by the E3 ubiquitin ligase and target positioning during ubiquitin transfer. The AUX/IAA degron is crucial for recruitment by the $SCF^{TIR1/AFB1-5}$ E3 ubiquitin ligase, but little has been known, before this work, regarding the mechanistic and dynamics of ubiquitin transfer to AUX/IAAs. Initial studies exploring AUX/IAA ubiquitylation focused on the auxin-inducibility of Ub conjugation, and their resulting proteasomal degradation (Maraschin et al., 2009). *In vivo*, ubiquitylation-dependent degradation of AUX/IAAs is of such importance (Worley et al., 2000; reviewed in: Reed, 2001), that alternative non-lysine sites seem to be used for ubiquitylation, if no lysine residues are available (Gilkerson et al., 2015). My studies enabled us to unveil, where AUX/IAA ubiquitylation occurs, and to expose the structural constraints guiding Ub conjugation of $SCF^{TIR1/AFB1-5}$ targets.

Fast-evolving IDRs drive the variability in the AUX/IAA family, and harbor ubiquitin acceptor sites (Winkler et al., 2017; Niemeyer et al., 2020). We clearly identified ubiquitylation on lysine residues, and found those to be promiscuous, which indicates some flexibility for which residues undergo covalent attachment of ubiquitin (Winkler et al., 2017; Niemeyer et al., 2020). Nevertheless, the clustering of ubiquitylated lysines in specific AUX/IAA regions, particularly downstream of the degron is indicative of some preference for certain locations along the AUX/IAA sequence. These favored locations might undergo ubiquitylation *in vivo* even after genetically engineering lysine-less AUX/IAAs (see Chapter 1.4) (Gilkerson et al., 2015). Proper positioning of AUX/IAA substrates on the E3 Ub ligase during ubiquitin transfer likely ensures this partial Ub site selectivity.

As the TIR1/AFBs are an integral part of the SCF E3 ligase, the formed E3-ligase·substrate complex topology greatly determines where ubiquitylation on AUX/IAAs will take place. While AUX/IAA ubiquitylation occurs in specific regions downstream of the degron, it remains flexible regarding the precise residues. This promiscuity likely resides in the typical multimeric organization of $SCF^{TIR1/AFBs}$ and is a rather widespread feature among CUL-containing RING E3 Ub ligases. CUL1-type CRLs or SCFs carry some intrinsic flexibility in itself, which is provided at the C-terminal WHB domain of the CUL1 subunit and the bound RBX1. This SCF flexibility is primarily enhanced through NEDD8 conjugation to CUL1, as part of the SCF activation mechanism (Duda et al., 2008; Baek et al., 2020).

In general terms, SCF flexibility is needed to promote ubiquitylation of possibly hundreds of different targets, recruited by several hundred FBPs (~700 FBPs) in *Arabidopsis* (Gagne et al., 2002; Walton et al., 2016). The flexible nature of SCF-type E3 ligases counteracts structure-driven residue selectivity *e.g.* seen in Ub chain formation. This also explains the promiscuous site selection for ubiquitylation, while maintaining preference for ubiquitylation hotpots in target proteins (Mattiroli and Sixma, 2014; Walton et al., 2016). Recently, a human SCF-type E3 ligase, $SCF^{\beta TRCP}$, was captured in action during ubiquitin transfer to a substrate mimic, the IκBα phospho-degron, by creating a stabilized SCF-substrate intermediate (Baek et al., 2020). In silico testing of this published structure on our resolved ASK1·TIR1·AUX/IAA^{PB1} system (generated by molecular dynamics simulations based on XL-MS data), allowed us to rationalize the ubiquitylation sites we detected. Superimposition of the structures revealed the close positioning of ubiquitylated lysines in AUX/IAAs towards the Ub~E2 intermediate (**Figure 11**, unpublished).

The distance between the activated C-terminus of Ub and ubiquitylated lysines in AUX/IAAs is less than 20 Å, which explains the preferential ubiquitylation of some PB1- and dT-located lysines over others. The superimposed structures also explain the shift towards dT-located lysines (Lys120) in IAA12, as, compared to the $IAA7^{PB1}$, fewer PB1 domain-located lysines are accessible (**Figure 11, right insets**). The explanation also applies for IAA6 and IAA19, as their ubiquitylation sites we identified are similarly distributed in the dT and PB1 domains (Winkler et al., 2017).

In the future, site-specific quantification of AUX/IAA ubiquitylation, for instance by Ub-PSAQ, a specifically modified LC-MS/MS method (Ub protein standard absolute quantification (Kaiser et al., 2011)) could reveal whether some lysines are preferred for ubiquitylation over others.

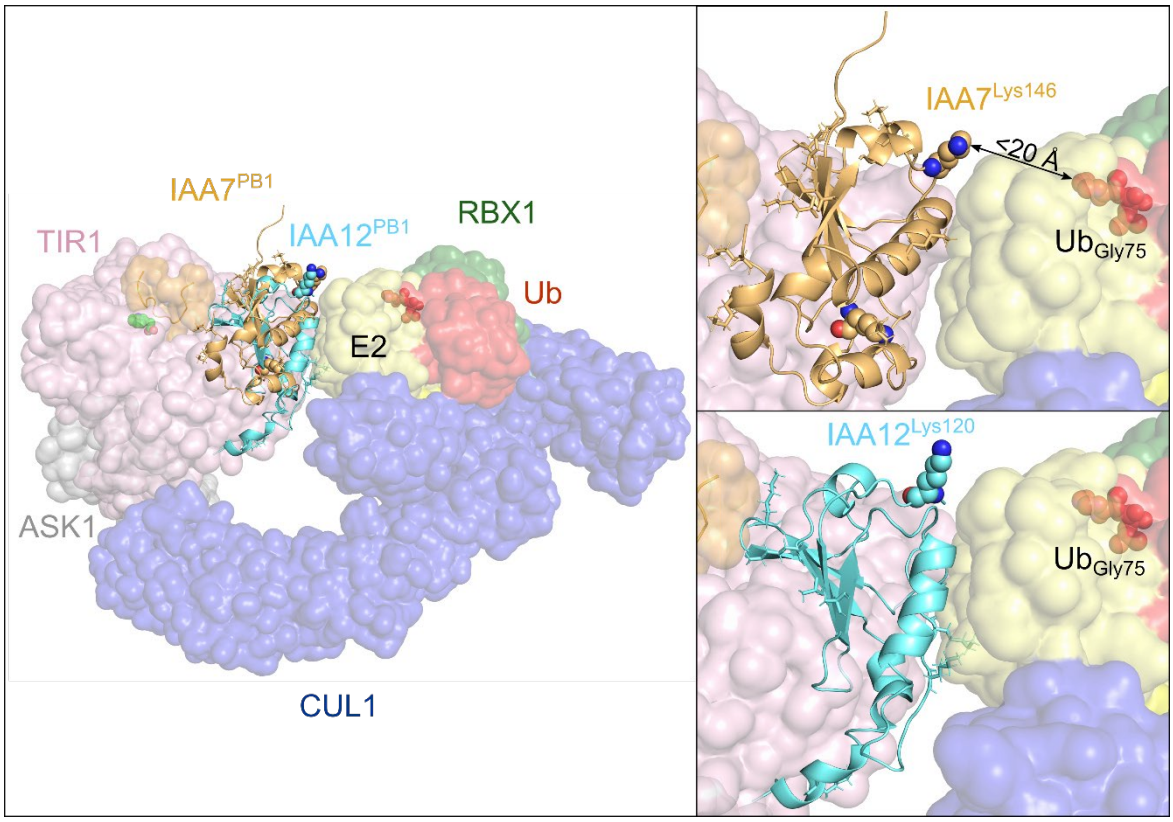

Figure 11: Postulated Ub transfer mechanism on AUX/IAA substrates upon recruitment by SCF-type E3 ligases SCF$^{TIR1/AFBs}$. Superimposition of our MD-simulated TIR1·IAA7^{PB1} (orange) and TIR1·IAA12^{PB1} (aquamarine) complexes on SCF$^{\beta TRCP}$ during UBE2D (E2)-mediated Ub transfer to the phospho-degron mimic derived from IκBα (PDB: 6TTU). Insets (right) show the activated C-terminus of E2-bound (yellow) ubiquitin (red) pointing towards PB1-located lysine residues, which we found to be ubiquitylated (spheres). Lys120 of IAA12 is located outside of the PB1 fold in the IAA12 degron tail. Additional IAA12 lysines (sticks) are located on the opposite PB1 surface, pointing away from Ub, and unlikely serve as ubiquitylation sites (unpublished).

A recent wide-scoped analysis of the *Arabidopsis* proteome (Mergner et al., 2020), likely includes *in vivo* ubiquitylation sites in their raw data. An in-depth analysis of this data taking into account the Ub remnant (diGly or LRGG modification of peptides), might help to draw a picture of specific SCF-mediated ubiquitylation of proteins.

My findings while dissecting AUX/IAA regions and determining their ubiquitylation likelihood are in agreement with observations for multiple UPS targets. Animal proteins targeted for proteasomal degradation possess predominantly an unstructured (disordered) initiation region of ≥30 amino acids, and its terminus being separated from ubiquitylation site(s) by ~25 amino acids (Prakash et al., 2004; Inobe et al., 2011; Bard et al., 2019). Simultaneous ubiquitylation on multiple sites facilitates substrate degradation, and allows turnover of substrates ubiquitylated at the terminus of the initiation site, which otherwise interferes with proteasome engagement (Braten et al., 2016; Bard et al., 2019). This might be especially relevant for IAA6 and IAA19, as both proteins are ubiquitylated at the N-terminal K3, which is likely their disordered initiation site. Such a Ub

position is likely inhibiting proteasome engagement and subsequent degradation (Bard et al., 2019). Nevertheless, the other identified ubiquitylation sites in IAA6 and IAA19 fulfill the distance requirements, and might counteract the K3 ubiquitylation, if happening simultaneously (Winkler et al., 2017; Bard et al., 2019). Based on AUX/IAA sequence composition, it is probable that additional features make some AUX/IAAs better UPS substrates than others. This is intriguing, as it allow us to speculate there is also substrate prioritization directly at the proteasome (Fishbain et al., 2015). A possible scenario for such prioritization might be relevant at high auxin concentrations *e.g.* in the root stem cell niche or during LR formation (Olatunji et al., 2017), where multiple AUX/IAAs might simultaneously be recruited to and ubiquitylated by $SCF^{TIR1/AFBs}$ E3 ligases.

The aforementioned distance and length requirements in disordered initiation regions of UPS targets are complemented by ubiquitin chain type preferences by the proteasome (Inobe et al., 2011; Guharoy et al., 2016; Bard et al., 2019; Martinez-Fonts et al., 2020). Likely K48-linked ubiquitin chains attached to an AUX/IAA protein determine its fate at the proteasome, as being recognized by Ub receptors, Rpn1, Rpn10 and Rpn13 at the proteasome (Finley, 2009; Ciechanover and Stanhill, 2014; Martinez-Fonts et al., 2020). Although our *in vitro* ubiquitylation assay (IVU) serves to determines the dynamics of ubiquitin chain formation on AUX/IAAs, it also comes with some limitations. The ubiquitin chain type formed on targets of SCF-type E3 ligases, such as $SCF^{TIR1/AFB1-5}$, is highly dependent on the E2 used in the assay (Stewart et al., 2016; Winkler et al., 2017; Deol et al., 2019). In our IVU, we predominantly used the widely expressed, chain type-wise rather promiscuous UBC8, which has shown activity with H2 RING-type E3s (Kraft et al., 2005; Ramadan et al., 2015). We have also tested UBC1 and UBC4 E2s in our assay, but they were not able to assist in the formation of multimeric ubiquitin chains on AUX/IAAs in our assay. We showed that UBC8 preferentially forms K11, K48 and K63 chains on AUX/IAAs, but we currently lacking information on UBC8's interaction with $SCF^{TIR1/AFB1-5}$ E3 ligases *in planta* (Winkler et al., 2017). While K48 Ub chains canonically flag substrates for proteasomal degradation, K63 Ub chains lead to reduced degradation of model substrates by yeast proteasomes *in vitro*, and K11 Ub chains do not seem to prompt proteins to the proteasome *in vitro* (Reichard et al., 2016; Winkler et al., 2017; Martinez-Fonts et al., 2020).

To date, only E2 UBC13 has been connected to auxin signaling, but its role has been rather proposed to be the formation K63-linked Ub chains on the auxin transporter PIN2 for its endocytosis. If

UBC13 aids AUX/IAA ubiquitylation is less probable. Thus, the effect of UBC13 compromised activity on AUX/IAA levels is most likely indirect (Leitner et al., 2012; Wen et al., 2014). It remains therefore to be established, which E2(s) specifically associate with $SCF^{TIR1/AFB1-5}$ for AUX/IAA ubiquitylation and degradation *in vivo*. Because of the multimeric nature of SCF-type E3 ligases, and the fast exchange of E2s on RBX1, an approach based on protein-protein crosslinking and mass spectrometric identification has the potential to capture transient E2-E3 interactions in the future (Ding et al., 2016; Chojnacki et al., 2017; Braxton et al., 2019; Gotze et al., 2019; Graaf et al., 2019). It is possible, so far unknown, factors contribute to E2 selectivity for specific SCF complexes and their targets. For instance, ALF4/GLMN bind RBX1 directly and competes with Ub chain type-determining E2s. Some selectivity towards a subset of SCF complexes has been shown to be affected by the loss of GLMN (see following section) (Duda et al., 2012; Tron et al., 2012; Bagchi et al., 2018). Such a selectivity could be auxin-induced and ALF4-dependent, and lead to a specific subset of E2s interacting with $SCF^{TIR1/AFB1-5}$ during auxin signaling.

3.4 ALF4 integrates into SCF regulation through ratio-based competition with E2s

We have shown that ALF4 strongly influences CRL-mediated ubiquitylation in general, and SCF^{TIR1}-dependent AUX/IAA ubiquitylation, in particular (Bagchi et al., 2018). ALF4, alike its human ortholog GLMN, acts as a broad positive regulator of ubiquitylation *in vivo*, while inhibiting single target ubiquitylation *in vitro* (Bagchi et al., 2018). Previously studied SCF complex regulators, CAND1 and CSN behave similarly, and together enable rapid assembly and activation of specific SCF-type E3 ligases on demand (**Figure 3**) (Zhang et al., 2008; Enchev et al., 2012; Liu et al., 2018; Wang et al., 2020). Structural studies on GLMN have shown, that GLMN binds a CUL1·RBX1 complex, competing for the E2 docking site of RBX1. Our studies show ALF4 functions similarly to GLMN (Duda et al., 2012; Tron et al., 2012; Bagchi et al., 2018). This supports our hypothesis that GLMN in animals and ALF4 in plants may function as a general ubiquitylation inhibitor, through E2 competition, without SCF-type E3 ligase preferences.

For a true competition to occur between E2s and ALF4/GLMN for RBX1 binding, comparable binding affinities are a prerequisite. Indeed, the E2 CDC34 and GLMN, both interact with CUL1·RBX1 in a low nanomolar range, promoting an active exchange under certain conditions

(compare: Kleiger et al., 2009b; Duda et al., 2012). This allows us to postulate that once above a threshold, ALF4/GLMN stabilization or increased protein levels might hinder substrate ubiquitylation. Decisive for ubiquitylation will be, in this case, the ratio between active SCF complex, E2s and ALF4/GLMN (Duda et al., 2012; Bagchi et al., 2018). In *Arabidopsis*, CUL1 and RBX1 levels are rather stable, while ALF4 accumulates under certain developmental conditions, *e.g.* during LR formation (Gray et al., 2002; Shen et al., 2002; DiDonato et al., 2004; Bagchi et al., 2018; Kim et al., 2018). By controlling cellular ALF4 levels, plants might have retained a mechanism to control ALF4-dependent inhibition of SCF complexes, and avoid, in this manner, their permanent inactivation. The controlled availability of ALF4/GLMN pools might explain the specific stabilization of some SCF targets over others as seen in *glmn* mutant cell lines (Tron et al., 2012). Rising the active ALF4 pool might allow ALF4 to compete with similarly or lower concentrated E2s, while higher concentrated E2s may still be able to bind RBX1. In this way, a collateral ALF4 selectivity towards similarly abundant E2s can be achieved, and the potential ALF4/GLMN role as an E2 exchange factor might be narrowed down to a subset of E2s. This evidently has a direct influence on initiation of ubiquitylation, or ubiquitin chain extension on SCF-type E3 ligase substrates.

A sufficiently high concentrated E2 (~5-fold ALF4) can overcome ALF4 inhibition (Bagchi et al., 2018), and lead to preference for specific E2s. Protein concentration determination in mouse embryonic fibroblasts (MEF) showed GLMN being 11-times less abundant than the N8-conjugating E2 UBC12, and only five active ubiquitin-specific E2s being more abundant than UBC12 (Schwanhäusser et al., 2011). Thereby, GLMN could be integrated into the neddylation machinery or prioritize specific E2s, as the ratios of the components would allow certain E2s to efficiently compete with ALF4/GLMN (Duda et al., 2012; Bagchi et al., 2018). ALF4 is likely behaving in a similar manner, as the ratio between ALF4 and RCE1 (UBC12 ortholog) is comparable with the ratio of mammalian orthologs. A ratio-dependent competition between UBC12/RCE1 and ALF4 for RBX1 binding, might result in a positive regulation of NEDD8-conjugation to CRLs, as ALF4 hinders lower abundant E2s to bind CRLs. Of note, five E2s conjugating ubiquitin (not UbL) occur in similar ratios as RCE1 in plant cells, it would be interesting to determine whether they have the capability to compete with ALF4 for interaction with RBX1 (Mergner et al., 2020). Thus, it results intriguing, that GLMN does not seem to discriminate

on the basis neddylation status of CUL1 (Duda et al., 2012). Whether this is also the case for ALF4, it remains to be established. Superimposing RBX1-bound GLMN (PDB: 4F52) on the recent $SCF^{\beta TRCP}$ structure (used in **Figure 11**; PDB: 6TTU) suggests that N8~CUL1 is not able to switch to the fully active conformation while GLMN is bound to RBX1. This occurs as GLMN would clash with N8 in this conformation (Duda et al., 2012; Baek et al., 2020). ALF4/GLMN binding to N8~CUL1 is likely possible due to the conformational flexibility of N8~CUL1·RBX1 (Duda et al., 2008; Baek et al., 2020). Inhibition of SCF-type E3 ligases by ALF4/GLMN could be the result of a dual mechanism: restricting the conformational flexibility of N8~CUL1; and competing for E2 binding to RBX1. Although GLMN bind CUL1, neddylated or not, it appears to inhibit de-neddylation *per se*, by blocking CSN binding to a N8~CUL1·RBX1 (Enchev et al., 2012). If this is the case in plants, and only a specific subset of neddylated SCFs become affected by ALF4 action, ALF4 might sustain the activation status these SCFs. By extending the activation window for a specific SCF, its unique substrates would be continuously recruited for ubiquitylation and degradation. Other concurrent SCFs, on the other hand, might be displaced due to limited access to the main scaffold components, which would probably explain the reduction in overall substrate ubiquitylation.

Even though the basic principles of SCF, and probably general CRL regulation seem to apply similarly to plant and mammalian systems, the vast expansion of FBPs in plants suggests an adaption of the SCF regulatory cycle, and the ratio of its components to support its versatility (**Figure 3**). This is especially noticeable when comparing the ratios between CUL1, RBX1 and CAND1 proteins. In plants, relative CUL1 levels are higher than in animal cells (Schwanhäusser et al., 2011; Mergner et al., 2020). While in animal (MEF) cells, RBX1 levels are twice as high as CUL1 levels, the opposite seems to be the case in plants (Schwanhäusser et al., 2011; Mergner et al., 2020). Additionally, compared to what has been observed in mammalian systems where CAND1 levels are almost equivalent to CUL1 (CAND1 ≈ 1.6x CUL1), plant CAND1 levels are low (~1% of CUL1). In fact, after calculating the minimal amount of CAND1 necessary for an efficient SCF activation cycle, on could conclude that plant CAND1 levels are only just enough to prompt efficient SCF assembly (Liu et al., 2018). One could postulate the expansion of FBPs and relative high levels of CUL1 available in plants, could give rise to a high number of active *e.g.* SCF^{X}, SCF^{Y}, SCF^{Z} complexes at a given time point. If that is the case, preformed SCF complexes would require less CAND1 for SR

exchange, which might explain the overall low levels of CAND1 present in plants. The role of ALF4, reducing SCF activity by E2 competition, might be important to keep the increased number of active SCF E3 ligases in check. Whether CUL1, E2 and ALF4/GLM protein levels equal active functional CUL1, E2 and ALF4/GLMN protein pools remain uncertain and is rather variable across cells. Posttranslational control of ALF4/GLMN, E2s, RBX1, CAND1 and CUL1 might directly impinge on their balance and interdependence.

This conceptual framework will require detailed biochemical studies in the future, which will hopefully deepen our understanding of CUL1 and ALF4 equilibrium, as well as ALF4- and E2-competition for the RBX1 docking site, and ALF4 regulation. A detailed structural characterization of ALF4 will be fascinating, and will provide a deeper understanding of CRL-dependent ubiquitylation dynamics, and E3-E2 preferences *in vivo*. The pleiotropic growth and developmental defects caused by the loss of ALF4 protein in *alf4* mutant plants, are likely an indication of misregulated transcriptional control (Bagchi et al., 2018). Given the pivotal role of numerous SCFs guiding phytohormone signaling pathways, it remains to be established, how ALF4 integrates into a variety of SCF's assembly cycles (**Figure 3**) (Tal et al., 2020).

3.5 Future perspectives

My studies and others suggest that fine-tuned hormone receptor assembly involves multivalent interactions of its components, which go beyond the short motif (degron)-driven small molecule (auxin) binding (Fung et al., 2018; Niemeyer et al., 2020). The flexibility of IDRs in a receptor component, such as AUX/IAA IDRs, in the TIR1·AUX/IAA auxin co-receptor system allows the context-dependent binding of multiple interaction surfaces (Csizmok et al., 2017; Bugge et al., 2020). The fast divergence in IDRs likely facilitated the role of AUX/IAA degron-flanking regions as affinity modulators in the protein family (Brown et al., 2002; Brown et al., 2011; Ferreon et al., 2013). The integration of these ideas beyond auxin signaling will surely yield new insights into other phytohormone signaling pathways, where hormones prompt substrate receptor (SR)-target interactions for hormone sensing and target ubiquitylation. Deciphering the presumably competitive (or allosteric) binding mechanisms of signal integrating hub proteins, such as

AUX/IAAs, might help to disentangle hormonal crosstalk. Finally allowing us, to identify general concepts for receptor assemblies and their influence on signaling complex composition.

On a different note, it would be intriguing to transfer and expand the knowledge of SCF (and CRL) regulatory cycles gained in mammals to the plant field and investigate its adaptation, given the vastness of FBPs present in plants (Gagne et al., 2002; Jin et al., 2004; Liu et al., 2018). The 6-membered TIR1/AFB FBP subclade can act as a model to study triggered, likely competitive assembly of different ASK·FBPs modules on a CUL1·RBX1 scaffold. The expansion of FBPs in plants led probably to an adapted SCF assembly regulation, and a shifted ratio of CRL components (Schwanhäusser et al., 2011; Mergner et al., 2020). How this influences SCF-dependent ubiquitylation and degradation is yet unknown and an exciting topic in the future. Investigating the precise integration of the new regulator ALF4 into the CRL regulatory cycle can provide hints to understand the complexity of CRLs and their ubiquitylation activity on proteins, which are deeply embedded in numerous life-defining processes such as cell cycle control.

4. Summary

Tuned ubiquitylation and subsequent degradation of AUX/IAA transcriptional repressor proteins shape plant growth and development. A combinatorial co-receptor system consisting any of six TIR1/AFBs and 23 degron-containing AUX/IAAs perceives auxin. Auxin-triggered associations increase the dwell time of AUX/IAAs on an $SCF^{TIR1/AFBs}$ E3 ubiquitin ligase, enabling Ub transfer to the AUX/IAAs, and their subsequent proteasomal degradation. Regions flanking the degradation signal, or degron, in AUX/IAAs modulate binding affinities of auxin co-receptors, and therefore tune AUX/IAA turnover. In this work, we reconstituted the SCF^{TIR1}-dependent ubiquitylation of two pairs of AUX/IAAs (IAA6 & IAA19; IAA7 & IAA12) to study the mechanistic basis of AUX/IAA ubiquitin conjugation. We showed that processive ubiquitylation on AUX/IAAs occurs in accordance with auxin binding capabilities of the respective TIR1·AUX/IAA auxin co-receptors. We identified ubiquitylation sites in fast-diverging, highly variable and flexible IDRs adjacent to the core degron in AUX/IAAs. These IDRs appear to modulate not only auxin binding of the corresponding co-receptor system, but also AUX/IAA ubiquitylation. IDRs lay therefore the foundation for functional diversification within the AUX/IAA protein family. In order to elucidate how IDRs in degron-flanking regions impact ASK1·TIR1·AUX/IAA complex formation, we combined an XL-MS approach with extensive computational modelling. A predominant extended fold of IAA7 and IAA12, while in complex with TIR1, facilitates accessibility of lysine residues during ubiquitin transfer, either by direct exposure of IDR-located lysines, or by positioning of a folded AUX/IAA PB1 domain. The association of AUX/IAA^{PB1} and ARF^{PB1} is crucial for the repression of genes, which are regulated by ARF transcription factors. Contacts between TIR1 and the PB1 domain, and ubiquitylation on or near the PB1 domain of AUX/IAAs likely hinder PB1-dependent repressor complex sustainment or formation. The combination of XL-MS and computational modeling led to the identification of AUX/IAA PB1 and KR contact residues in TIR1 contributing to its function *in vivo*.

This thesis included the biochemical characterization of the ALF4 protein, which binds to RBX1 in SCF-type E3 ubiquitin ligases, thereby competing with E2s for E3 associations. *In vitro*, ALF4 competition for an E2 docking site inhibits SCF^{TIR1}-dependent ubiquitylation of AUX/IAAs. *In vivo*, loss of ALF4 function reduces overall ubiquitylation, stabilizes SCF targets and, at the same time, destabilizes CUL1. As a general regulator of ubiquitylation, ALF4 action impacts multiple SCF-

regulated phytohormone signaling pathways, such as auxin signaling and GA (gibberellic acid) signaling, which likely explains the strong pleiotropic phenotypes in loss-of-function *alf4* mutants. Taken together, this thesis provided novel insights into auxin-triggered, IDR-assisted auxin co-receptor assembly, the dynamics of AUX/IAA ubiquitylation, and the biochemical function of ALF4, a novel SCF E3 ligase regulator. From a broader perspective, the findings of this work have implications for the functionalization of IDRs during hormone receptor formation and modulated hub protein-dependent complex assembly. Furthermore, the work delivers complementary ideas regarding the cross-kingdom adaptation of CRL activity regulation, and the ubiquitylation-driven adaptation of protein pools in response to developmental cues or triggered by small molecules, such as hormones.

5. Zusammenfassung

Die regulierte Ubiquitylierung und der anschließende Abbau von AUX/IAA Transkriptionsrepressoren bestimmen das Wachstum und die Entwicklung von Pflanzen. Das kombinatorische Co-Rezeptor System, bestehend aus 23 degronhaltigen AUX/IAAs und jedem der sechs TIR1/AFB Proteinen, nimmt Auxin wahr. Der Prozess der Auxinwahrnehmung erhöht die Verweildauer von AUX/IAAs auf einer $SCF^{TIR1/AFBs}$ E3 Ubiquitinligase und ermöglicht den Ub-Transfer auf die AUX/IAAs, sowie den darauffolgenden Abbau vermittels des Proteasoms. Sequenzabschnitte, welche das Abbausignal, auch Degron genannt, der AUX/IAAs umgeben, modulieren die Bindeaffinitäten der jeweiligen Co-Rezeptoren und bestimmen dadurch den Umsatz der AUX/IAAs. In dieser Dissertation rekonstituierten wir SCF^{TIR1}-abhängige Ubiquitylierung von zwei AUX/IAA-Paaren (IAA6 & IAA19; IAA7 & IAA12), um den zu Grunde liegenden Mechanismus der AUX/IAA Ubiquitin-Konjugation zu studieren. Wir zeigten, dass eine prozessive Ubiquitylierung der jeweiligen AUX/IAAs mit der Auxin-Bindefähigkeit des zugehörigen TIR1·AUX/IAA Auxin Co-Rezeptors einhergeht. Außerdem identifizierten wir Ubiquitylierungsstellen in den sich schnell entwickelnden und hochvariablen, sowie flexiblen IDRs, welche das Degron der AUX/IAAs umgeben. IDRs scheinen nicht nur die Auxinbindung des zugehörigen Co-Rezeptors zu modulieren, sondern sogleich die Ubiquitylierung des AUX/IAA Proteins, wodurch IDRs die Grundlage für die funktionelle Diversifikation in der AUX/IAA

Proteinfamilie legen. Um aufzuklären, wie sich IDRs in degronflankierenden Regionen auf die Komplexbildung von ASK1·TIR1·AUX/IAA auswirken, kombinierten wir eine XL-MS Methode mit umfangreichen computerbasierten Modellierungen. Die überwiegend gestreckte Struktur von IAA7 und IAA12 in Komplex mit TIR1 scheint den freien Zugang zu Lysinresten, während des Ubiquitintransfers, zu ermöglichen, indem IDRs diese Lysine selbst beinhalten oder die IDRs die gefaltete AUX/IAA PB1 Domäne entsprechend positionieren. Die Assoziation von AUX/IAA^{PB1} und ARF^{PB1} ist unabdingbar für die Repression von Genen, welche durch ARF Transkriptionsfaktoren reguliert werden. Sowohl Interaktionen zwischen TIR1 und der PB1-Domäne der AUX/IAAs, sowie die Ubiquitylierung nahe oder auf dieser, destabilisieren oder behindern die Bildung des PB1-abhängigen Repressorkomplexes. Die Kombination von XL-MS mit computerbasierter Modellierung, führte außerdem zur Identifikation von *in vivo* funktionsrelevanten Aminosäuren in TIR1, welche die AUX/IAA PB1 Domäne und das KR-Motiv kontaktieren. Diese Dissertation beinhalten außerdem die biochemische Beschreibung des Proteins ALF4, welches die RBX1 Untereinheit von SCF-E3-Ligasen bindet und somit mit den E2s um E3 Bindung konkurriert. *In vitro* hemmt diese Kompetition für die E2-Bindestelle, die die SCF^{TIR1}-abhängige Ubiquitylierung der AUX/IAA Proteine. *In vivo*, allerdings, führt der Verlust der ALF4-Funktion zur Reduktion des allgemeinen Ubiquitylierungslevels, stabilisiert SCF-Zielproteine und destabilisiert zugleich CUL1. Die Aktivität von ALF4, als allgemeiner Regulator der Ubiquitylierung, wirkt sich auf SCF-regulierte Phytohormonsignalwege, wie die Auxin- und GA (Gibberellinsäure)-Signaltransduktion, aus. Dies ist wahrscheinlich der Grund für die ausgeprägten pleiotropen Phänotypen von auf ALF4-Funktionsverlust basierenden *alf4*-Mutanten. Zusammengefasst, ermöglichte diese Dissertation neue Einsichten in die durch Auxin ausgelöste und von IDRs unterstützte Bildung des Auxin Co-Rezeptors, die Dynamik der AUX/IAA Ubiquitylierung und die biochemische Funktion von ALF4, einem neuartigen Regulator von SCF-E3-Ligasen. Im weiteren Sinn, ermöglichen die Ergebnisse eine genauere Sicht auf die Funktionsweise von IDRs im Rahmen der Rezeptorausprägung und der modulierten, Hubprotein-abhängigen Komplexbildung. Außerdem liefert diese Dissertation ergänzende Ideen bezüglich der Pflanzen- und Tierwelt übergreifenden Anpassung der Regulierung von CRL-Aktivität und die Ubiquitylierungs-basierte Anpassung von Proteinpools während des Wachstums oder ausgelöst durch kleine Moleküle, z.B. Hormone.

6. References

Abd-Hamid, N.-A., Ahmad-Fauzi, M.-I., Zainal, Z., and Ismail, I. (2020). Diverse and dynamic roles of F-box proteins in plant biology. Planta *251*, 68.

Aguilar-Hernández, V., Kim, D.-Y., Stankey, R.J., Scalf, M., Smith, L.M., and Vierstra, R.D. (2017). Mass Spectrometric Analyses Reveal a Central Role for Ubiquitylation in Remodeling the Arabidopsis Proteome during Photomorphogenesis. Molecular plant *10*, 846-865.

Ahrens, J.B., Nunez-Castilla, J., and Siltberg-Liberles, J. (2017). Evolution of intrinsic disorder in eukaryotic proteins. Cellular and molecular life sciences : CMLS *74*, 3163-3174.

Akutsu, M., Dikic, I., and Bremm, A. (2016). Ubiquitin chain diversity at a glance. Journal of cell science *129*, 875-880.

Altmann, M., Altmann, S., Rodriguez, P.A., Weller, B., Elorduy Vergara, L., Palme, J., La Marín-de Rosa, N., Sauer, M., Wenig, M., and Villaécija-Aguilar, J.A., et al. (2020). Extensive signal integration by the phytohormone protein network. Nature.

Arase, F., Nishitani, H., Egusa, M., Nishimoto, N., Sakurai, S., Sakamoto, N., and Kaminaka, H. (2012). IAA8 involved in lateral root formation interacts with the TIR1 auxin receptor and ARF transcription factors in Arabidopsis. Plos One *7*, e43414.

Bachmair, A., Novatchkova, M., Potuschak, T., and Eisenhaber, F. (2001). Ubiquitylation in plants: a post-genomic look at a post-translational modification. Trends in plant science *6*, 463-470.

Baek, K., Krist, D.T., Prabu, J.R., Hill, S., Klügel, M., Neumaier, L.-M., Gronau, S. von, Kleiger, G., and Schulman, B.A. (2020). NEDD8 nucleates a multivalent cullin-RING-UBE2D ubiquitin ligation assembly. Nature *578*, 461-466.

Bagchi, R., Melnyk, C.W., Christ, G., Winkler, M., Kirchsteiner, K., Salehin, M., Mergner, J., Niemeyer, M., Schwechheimer, C., and Calderón Villalobos, L.I.A., et al. (2018). The Arabidopsis ALF4 protein is a regulator of SCF E3 ligases. The EMBO journal *37*, 255-268.

Band, L.R., Wells, D.M., Larrieu, A., Sun, J., Middleton, A.M., French, A.P., Brunoud, G., Sato, E.M., Wilson, M.H., and Péret, B., et al. (2012). Root gravitropism is regulated by a transient lateral auxin gradient controlled by a tipping-point mechanism. Proc Natl Acad Sci U S A *109*, 4668-4673.

Bard, J.A.M., Bashore, C., Dong, K.C., and Martin, A. (2019). The 26S Proteasome Utilizes a Kinetic Gateway to Prioritize Substrate Degradation. Cell *177*, 286-298 e15.

Berg, J.M., Tymoczko, J.L., and Stryer, L. (2012). Biochemistry. This edition is for use outside the USA and Canada (New York, NY: Freeman Palgrave Macmillan).

Blázquez, M.A., Nelson, D.C., and Weijers, D. (2020). Evolution of Plant Hormone Response Pathways. Annu Rev Plant Biol.

Boughton, A.J., Krueger, S., and Fushman, D. (2020). Branching via K11 and K48 Bestows Ubiquitin Chains with a Unique Interdomain Interface and Enhanced Affinity for Proteasomal Subunit Rpn1. Structure (London, England : 1993) *28*, 29-43.e6.

Branigan, E., Carlos Penedo, J., and Hay, R.T. (2020). Ubiquitin transfer by a RING E3 ligase occurs from a closed E2~ubiquitin conformation. Nat Commun *11*, 2846.

Braten, O., Livneh, I., Ziv, T., Admon, A., Kehat, I., Caspi, L.H., Gonen, H., Bercovich, B., Godzik, A., and Jahandideh, S., et al. (2016). Numerous proteins with unique characteristics are degraded by the 26S proteasome following monoubiquitination. Proc Natl Acad Sci U S A *113*, E4639-47.

Braxton, C.N., Quartner, E., Pawloski, W., Fushman, D., and Cropp, T.A. (2019). Ubiquitin Chains Bearing Genetically Encoded Photo-Cross-Linkers Enable Efficient Covalent Capture of (Poly)ubiquitin-Binding Domains. Biochemistry *58*, 883-886.

Bremm, A., Freund, S.M., and Komander, D. (2010). Lys11-linked ubiquitin chains adopt compact conformations and are preferentially hydrolyzed by the deubiquitinase Cezanne. Nature structural & molecular biology *17*, 939-947.

Brouillard, P., Boon, L.M., Mulliken, J.B., Enjolras, O., Ghassibé, M., Warman, M.L., Tan, O.T., Olsen, B.R., and Vikkula, M. (2002). Mutations in a novel factor, glomulin, are responsible for glomuvenous malformations ("glomangiomas"). American journal of human genetics *70*, 866-874.

Brouillard, P., Boon, L.M., Revencu, N., Berg, J., Dompmartin, A., Dubois, J., Garzon, M., Holden, S., Kangesu, L., and Labrèze, C., et al. (2013). Genotypes and phenotypes of 162 families with a glomulin mutation. Molecular syndromology *4*, 157-164.

Brown, C.J., Johnson, A.K., Dunker, A.K., and Daughdrill, G.W. (2011). Evolution and disorder. Current opinion in structural biology *21*, 441-446.

Brown, C.J., Takayama, S., Campen, A.M., Vise, P., Marshall, T.W., Oldfield, C.J., Williams, C.J., and Dunker, A.K. (2002). Evolutionary rate heterogeneity in proteins with long disordered regions. Journal of molecular evolution *55*, 104-110.

Brown, N.G., VanderLinden, R., Watson, E.R., Weissmann, F., Ordureau, A., Wu, K.-P., Zhang, W., Yu, S., Mercredi, P.Y., and Harrison, J.S., et al. (2016). Dual RING E3 Architectures Regulate Multiubiquitination and Ubiquitin Chain Elongation by APC/C. Cell *165*, 1440-1453.

Bugge, K., Brakti, I., Fernandes, C.B., Dreier, J.E., Lundsgaard, J.E., Olsen, J.G., Skriver, K., and Kragelund, B.B. (2020). Interactions by Disorder – A Matter of Context. Frontiers in molecular biosciences *7*.

Calderón Villalobos, L.I., Lee, S., Oliveira, C. de, Ivetac, A., Brandt, W., Armitage, L., Sheard, L.B., Tan, X., Parry, G., and Mao, H., et al. (2012). A combinatorial TIR1/AFB-Aux/IAA co-receptor system for differential sensing of auxin. Nat Chem Biol *8*, 477-485.

Calderon-Villalobos, L.I., Tan, X., Zheng, N., and Estelle, M. (2010). Auxin perception--structural insights. Cold Spring Harbor perspectives in biology *2*, a005546.

Callis, J. (2014). The ubiquitination machinery of the ubiquitin system. The Arabidopsis book *12*, e0174.

Cao, M., Chen, R., Li, P., Yu, Y., Zheng, R., Ge, D., Zheng, W., Wang, X., Gu, Y., and Gelová, Z., et al. (2019). TMK1-mediated auxin signalling regulates differential growth of the apical hook. Nature *568*, 240-243.

Celenza, J.L., Grisafi, P.L., and Fink, G.R. (1995). A pathway for lateral root formation in Arabidopsis thaliana. Genes & development *9*, 2131-2142.

Černý, M., Novák, J., Habánová, H., Cerna, H., and Brzobohatý, B. (2016). Role of the proteome in phytohormonal signaling. Biochimica et biophysica acta *1864*, 1003-1015.

Chapman, E.J., and Estelle, M. (2009). Mechanism of auxin-regulated gene expression in plants. Annu Rev Genet *43*, 265-285.

Chen, H., Ma, B., Zhou, Y., He, S.-J., Tang, S.-Y., Lu, X., Xie, Q., Chen, S.-Y., and Zhang, J.-S. (2018). E3 ubiquitin ligase SOR1 regulates ethylene response in rice root by modulating stability of Aux/IAA protein. Proc Natl Acad Sci U S A *115*, 4513-4518.

Chen, Y., Yang, Q., Sang, S., Wei, Z., and Wang, P. (2017). Rice Inositol Polyphosphate Kinase (OsIPK2) Directly Interacts with OsIAA11 to Regulate Lateral Root Formation. Plant & cell physiology *58*, 1891-1900.

Chojnacki, M., Mansour, W., Hameed, D.S., Singh, R.K., El Oualid, F., Rosenzweig, R., Nakasone, M.A., Yu, Z., Glaser, F., and Kay, L.E., et al. (2017). Polyubiquitin-Photoactivatable Crosslinking Reagents for Mapping Ubiquitin Interactome Identify Rpn1 as a Proteasome Ubiquitin-Associating Subunit. Cell chemical biology *24*, 443-457.e6.

Chuang, H.-w., Zhang, W., and Gray, W.M. (2004). Arabidopsis ETA2, an apparent ortholog of the human cullin-interacting protein CAND1, is required for auxin responses mediated by the SCF(TIR1) ubiquitin ligase. The Plant cell *16*, 1883-1897.

Ciechanover, A., and Stanhill, A. (2014). The complexity of recognition of ubiquitinated substrates by the 26S proteasome. Biochimica et biophysica acta *1843*, 86-96.

Colón-Carmona, A., Chen, D.L., Yeh, K.C., and Abel, S. (2000). Aux/IAA proteins are phosphorylated by phytochrome in vitro. Plant Physiol *124*, 1728-1738.

Cope, G.A., Suh, G.S.B., Aravind, L., Schwarz, S.E., Zipursky, S.L., Koonin, E.V., and Deshaies, R.J. (2002). Role of predicted metalloprotease motif of Jab1/Csn5 in cleavage of Nedd8 from Cul1. Science (New York, N.Y.) *298*, 608-611.

Covarrubias, A.A., Romero-Pérez, P.S., Cuevas-Velazquez, C.L., and Rendón-Luna, D.F. (2020). The functional diversity of structural disorder in plant proteins. Archives of biochemistry and biophysics *680*, 108229.

Csizmok, V., Orlicky, S., Cheng, J., Song, J., Bah, A., Delgoshaie, N., Lin, H., Mittag, T., Sicheri, F., and Chan, H.S., et al. (2017). An allosteric conduit facilitates dynamic multisite substrate recognition by the SCF(Cdc4) ubiquitin ligase. Nat Commun *8*, 13943.

Darling, A.L., and Uversky, V.N. (2018). Intrinsic Disorder and Posttranslational Modifications: The Darker Side of the Biological Dark Matter. Frontiers in genetics *9*, 158.

Deol, K.K., Lorenz, S., and Strieter, E.R. (2019). Enzymatic Logic of Ubiquitin Chain Assembly. Frontiers in physiology *10*, 835.

Dharmasiri, N., Dharmasiri, S., and Estelle, M. (2005a). The F-box protein TIR1 is an auxin receptor. Nature *435*, 441-445.

Dharmasiri, N., Dharmasiri, S., Weijers, D., Lechner, E., Yamada, M., Hobbie, L., Ehrismann, J.S., Jürgens, G., and Estelle, M. (2005b). Plant development is regulated by a family of auxin receptor F box proteins. Developmental cell *9*, 109-119.

Dharmasiri, S., Dharmasiri, N., Hellmann, H., and Estelle, M. (2003). The RUB/Nedd8 conjugation pathway is required for early development in Arabidopsis. The EMBO journal *22*, 1762-1770.

DiDonato, R.J., Arbuckle, E., Buker, S., Sheets, J., Tobar, J., Totong, R., Grisafi, P., Fink, G.R., and Celenza, J.L. (2004). Arabidopsis ALF4 encodes a nuclear-localized protein required for lateral root formation. The Plant journal : for cell and molecular biology *37*, 340-353.

Dindas, J., Scherzer, S., Roelfsema, M.R.G., Meyer, K. von, Müller, H.M., Al-Rasheid, K.A.S., Palme, K., Dietrich, P., Becker, D., and Bennett, M.J., et al. (2018). AUX1-mediated root hair auxin influx governs SCFTIR1/AFB-type Ca2+ signaling. Nat Commun *9*.

Dinesh, D.C., Kovermann, M., Gopalswamy, M., Hellmuth, A., Calderon Villalobos, L.I., Lilie, H., Balbach, J., and Abel, S. (2015). Solution structure of the PsIAA4 oligomerization domain reveals interaction modes for transcription factors in early auxin response. Proc Natl Acad Sci U S A.

Dinesh, D.C., Villalobos, Luz Irina A. Calderon, and Abel, S. (2016). Structural Biology of Nuclear Auxin Action. Trends in plant science *21*, 302-316.

Ding, Y.-H., Fan, S.-B., Li, S., Feng, B.-Y., Gao, N., Ye, K., He, S.-M., and Dong, M.-Q. (2016). Increasing the Depth of Mass-Spectrometry-Based Structural Analysis of Protein Complexes through the Use of Multiple Cross-Linkers. Analytical chemistry *88*, 4461-4469.

Dissmeyer, N. (2019). Conditional Protein Function via N-Degron Pathway-Mediated Proteostasis in Stress Physiology. Annu Rev Plant Biol *70*, 83-117.

Dohmann, E.M., Levesque, M.P., Isono, E., Schmid, M., and Schwechheimer, C. (2008). Auxin responses in mutants of the Arabidopsis CONSTITUTIVE PHOTOMORPHOGENIC9 signalosome. Plant physiology *147*, 1369-1379.

Dreher, K.A., Brown, J., Saw, R.E., and Callis, J. (2006). The Arabidopsis Aux/IAA protein family has diversified in degradation and auxin responsiveness. The Plant cell *18*, 699-714.

Du, R., Huang, C., Chen, H., Liu, K., Xiang, P., Yao, N., Yang, L., Zhou, L., Wu, Q., and Zheng, Y., et al. (2020). SDCBP/MDA-9/syntenin phosphorylation by AURKA promotes esophageal squamous cell carcinoma progression through the EGFR-PI3K-Akt signaling pathway. Oncogene.

Dubeaux, G., Neveu, J., Zelazny, E., and Vert, G. (2018). Metal Sensing by the IRT1 Transporter-Receptor Orchestrates Its Own Degradation and Plant Metal Nutrition. Mol Cell *69*, 953-964.e5.

Duda, D.M., Borg, L.A., Scott, D.C., Hunt, H.W., Hammel, M., and Schulman, B.A. (2008). Structural insights into NEDD8 activation of cullin-RING ligases. conformational control of conjugation. Cell *134*, 995-1006.

Duda, D.M., Olszewski, J.L., Tron, A.E., Hammel, M., Lambert, L.J., Waddell, M.B., Mittag, T., DeCaprio, J.A., and Schulman, B.A. (2012). Structure of a glomulin-RBX1-CUL1 complex. inhibition of a RING E3 ligase through masking of its E2-binding surface. Molecular cell *47*, 371-382.

Eddins, M.J., Varadan, R., Fushman, D., Pickart, C.M., and Wolberger, C. (2007). Crystal structure and solution NMR studies of Lys48-linked tetraubiquitin at neutral pH. Journal of molecular biology *367*, 204-211.

Emberley, E.D., Mosadeghi, R., and Deshaies, R.J. (2012). Deconjugation of Nedd8 from Cul1 is directly regulated by Skp1-F-box and substrate, and the COP9 signalosome inhibits deneddylated SCF by a noncatalytic mechanism. The Journal of biological chemistry *287*, 29679-29689.

Enchev, R.I., Schulman, B.A., and Peter, M. (2015). Protein neddylation: beyond cullin-RING ligases. Nature reviews. Molecular cell biology *16*, 30-44.

Enchev, R.I., Scott, D.C., da Fonseca, Paula C. A., Schreiber, A., Monda, J.K., Schulman, B.A., Peter, M., and Morris, E.P. (2012). Structural basis for a reciprocal regulation between SCF and CSN. Cell reports *2*, 616-627.

Farcot, E., Lavedrine, C., and Vernoux, T. (2015). A modular analysis of the auxin signalling network. Plos One *10*, e0122231.

Fendrych, M., Akhmanova, M., Merrin, J., Glanc, M., Hagihara, S., Takahashi, K., Uchida, N., Torii, K.U., and Friml, J. (2018). Rapid and reversible root growth inhibition by TIR1 auxin signalling. Nature plants *4*, 453-459.

Feng, S., Shen, Y., Sullivan, J.A., Rubio, V., Xiong, Y., Sun, T.-P., and Deng, X.W. (2004). Arabidopsis CAND1, an unmodified CUL1-interacting protein, is involved in multiple developmental pathways controlled by ubiquitin/proteasome-mediated protein Degradation. The Plant cell *16*, 1870-1882.

Ferreon, A.C.M., Ferreon, J.C., Wright, P.E., and Deniz, A.A. (2013). Modulation of allostery by protein intrinsic disorder. Nature *498*, 390-+.

Finley, D. (2009). Recognition and processing of ubiquitin-protein conjugates by the proteasome. Annual review of biochemistry *78*, 477-513.

Finley, D., Chen, X., and Walters, K.J. (2016). Gates, Channels, and Switches: Elements of the Proteasome Machine. Trends in biochemical sciences *41*, 77-93.

Fishbain, S., Inobe, T., Israeli, E., Chavali, S., Yu, H., Kago, G., Babu, M.M., and Matouschek, A. (2015). Sequence composition of disordered regions fine-tunes protein half-life. Nat Struct Mol Biol *22*, 214-221.

Fukaki, H., Tameda, S., Masuda, H., and Tasaka, M. (2002). Lateral root formation is blocked by a gain-of-function mutation in the SOLITARY-ROOT/IAA14 gene of Arabidopsis. The Plant journal : for cell and molecular biology *29*, 153-168.

Fung, H.Y.J., Birol, M., and Rhoades, E. (2018). IDPs in macromolecular complexes: the roles of multivalent interactions in diverse assemblies. Current opinion in structural biology *49*, 36-43.

Gagne, J.M., Downes, B.P., Shiu, S.-H., Durski, A.M., and Vierstra, R.D. (2002). The F-box subunit of the SCF E3 complex is encoded by a diverse superfamily of genes in Arabidopsis. Proceedings of the National Academy of Sciences of the United States of America *99*, 11519-11524.

Gilkerson, J., Kelley, D.R., Tam, R., Estelle, M., and Callis, J. (2015). Lysine Residues Are Not Required for Proteasome-Mediated Proteolysis of the Auxin/Indole Acidic Acid Protein IAA1. Plant Physiology *168*, 708-720.

Goldenberg, S.J., Cascio, T.C., Shumway, S.D., Garbutt, K.C., Liu, J., Xiong, Y., and Zheng, N. (2004). Structure of the Cand1-Cul1-Roc1 complex reveals regulatory mechanisms for the assembly of the multisubunit cullin-dependent ubiquitin ligases. Cell *119*, 517-528.

Gotze, M., Iacobucci, C., Ihling, C.H., and Sinz, A. (2019). A Simple Cross-Linking/Mass Spectrometry Workflow for Studying System-wide Protein Interactions. Anal Chem *91*, 10236-10244.

Graaf, S.C. de, Klykov, O., van den Toorn, H., and Scheltema, R.A. (2019). Cross-ID: Analysis and Visualization of Complex XL-MS-Driven Protein Interaction Networks. Journal of proteome research *18*, 642-651.

Gray, W.M., Hellmann, H., Dharmasiri, S., and Estelle, M. (2002). Role of the Arabidopsis RING-H2 protein RBX1 in RUB modification and SCF function. The Plant cell *14*, 2137-2144.

Gray, W.M., Kepinski, S., Rouse, D., Leyser, O., and Estelle, M. (2001). Auxin regulates SCF(TIR1)-dependent degradation of AUX/IAA proteins. Nature *414*, 271-276.

Guharoy, M., Bhowmick, P., Sallam, M., and Tompa, P. (2016). Tripartite degrons confer diversity and specificity on regulated protein degradation in the ubiquitin-proteasome system. Nat Commun *7*, 10239.

Guilfoyle, T.J., Ulmasov, T., and Hagen, G. (1998). The ARF family of transcription factors and their role in plant hormone-responsive transcription. Cellular and molecular life sciences : CMLS *54*, 619-627.

Gundogdu, M., and Walden, H. (2019). Structural basis of generic versus specific E2-RING E3 interactions in protein ubiquitination. Protein science : a publication of the Protein Society *28*, 1758-1770.

Guo, J., Liu, J., Wei, Q., Wang, R., Yang, W., Ma, Y., Chen, G., and Yu, Y. (2017). Proteomes and Ubiquitylomes Analysis Reveals the Involvement of Ubiquitination in Protein Degradation in Petunias. Plant Physiology *173*, 668-687.

Guseman, J.M., Hellmuth, A., Lanctot, A., Feldman, T.P., Moss, B.L., Klavins, E., Calderon Villalobos, L.I., and Nemhauser, J.L. (2015). Auxin-induced degradation dynamics set the pace for lateral root development. Development *142*, 905-909.

Haas, A.L., and Rose, I.A. (1982). The mechanism of ubiquitin activating enzyme. A kinetic and equilibrium analysis. The Journal of biological chemistry *257*, 10329-10337.

Hamann, T., Benkova, E., Baurle, I., Kientz, M., and Jurgens, G. (2002). The Arabidopsis BODENLOS gene encodes an auxin response protein inhibiting MONOPTEROS-mediated embryo patterning. Genes & development *16*, 1610-1615.

Hamann, T., Mayer, U., and Jürgens, G. (1999). The auxin-insensitive bodenlos mutation affects primary root formation and apical-basal patterning in the Arabidopsis embryo. Development (Cambridge, England) *126*, 1387-1395.

Han, M., Park, Y., Kim, I., Kim, E.H., Yu, T.K., Rhee, S., and Suh, J.Y. (2014). Structural basis for the auxin-induced transcriptional regulation by Aux/IAA17. Proceedings of the National Academy of Sciences of the United States of America *111*, 18613-18618.

Hann, Z.S., Ji, C., Olsen, S.K., Lu, X., Lux, M.C., Tan, D.S., and Lima, C.D. (2019). Structural basis for adenylation and thioester bond formation in the ubiquitin E1. Proceedings of the National Academy of Sciences of the United States of America *116*, 15475-15484.

Hao, B., Oehlmann, S., Sowa, M.E., Harper, J.W., and Pavletich, N.P. (2007). Structure of a Fbw7-Skp1-cyclin E complex. multisite-phosphorylated substrate recognition by SCF ubiquitin ligases. Molecular cell *26*, 131-143.

Havens, K.A., Guseman, J.M., Jang, S.S., Pierre-Jerome, E., Bolten, N., Klavins, E., and Nemhauser, J.L. (2012). A synthetic approach reveals extensive tunability of auxin signaling. Plant physiology *160*, 135-142.

Haynes, C., Oldfield, C.J., Ji, F., Klitgord, N., Cusick, M.E., Radivojac, P., Uversky, V.N., Vidal, M., and Iakoucheva, L.M. (2006). Intrinsic disorder is a common feature of hub proteins from four eukaryotic interactomes. PLoS computational biology *2*, e100.

Hellmuth, A. (2017). Dynamics of auxin sensing by SCFTIR1/AFB-AUX/IAA co-receptor complexes in Arabidopsis (Universitäts- und Landesbibliothek Sachsen-Anhalt).

Heyman, J., and Veylder, L. de (2012). The anaphase-promoting complex/cyclosome in control of plant development. Molecular plant *5*, 1182-1194.

Hobbie, L., McGovern, M., Hurwitz, L.R., Pierro, A., Liu, N.Y., Bandyopadhyay, A., and Estelle, M. (2000). The axr6 mutants of Arabidopsis thaliana define a gene involved in auxin response and early development. Development (Cambridge, England) *127*, 23-32.

Holt, L.J. (2012). Regulatory modules: Coupling protein stability to phopshoregulation during cell division. FEBS letters *586*, 2773-2777.

Hua, Z., and Vierstra, R.D. (2011). The cullin-RING ubiquitin-protein ligases. Annu Rev Plant Biol *62*, 299-334.

Huang, D.T., Miller, D.W., Mathew, R., Cassell, R., Holton, J.M., Roussel, M.F., and Schulman, B.A. (2004). A unique E1-E2 interaction required for optimal conjugation of the ubiquitin-like protein NEDD8. Nature structural & molecular biology *11*, 927-935.

Husnjak, K., and Dikic, I. (2012). Ubiquitin-binding proteins: decoders of ubiquitin-mediated cellular functions. Annu Rev Biochem *81*, 291-322.

Inobe, T., Fishbain, S., Prakash, S., and Matouschek, A. (2011). Defining the geometry of the two-component proteasome degron. Nat Chem Biol *7*, 161-167.

Jin, J., Cardozo, T., Lovering, R.C., Elledge, S.J., Pagano, M., and Harper, J.W. (2004). Systematic analysis and nomenclature of mammalian F-box proteins. Genes & development *18*, 2573-2580.

Jing, H., Yang, X., Zhang, J., Liu, X., Zheng, H., Dong, G., Nian, J., Feng, J., Xia, B., and Qian, Q., et al. (2015). Peptidyl-prolyl isomerization targets rice Aux/IAAs for proteasomal degradation during auxin signalling. Nat Commun *6*, 7395.

Kagale, S., and Rozwadowski, K. (2011). EAR motif-mediated transcriptional repression in plants: an underlying mechanism for epigenetic regulation of gene expression. Epigenetics *6*, 141-146.

Kaiser, S.E., Riley, B.E., Shaler, T.A., Trevino, R.S., Becker, C.H., Schulman, H., and Kopito, R.R. (2011). Protein standard absolute quantification (PSAQ) method for the measurement of cellular ubiquitin pools. Nature methods *8*, 691-696.

Kato, H., Mutte, S.K., Suzuki, H., Crespo, I., Das, S., Radoeva, T., Fontana, M., Yoshitake, Y., Hainiwa, E., and van den Berg, W., et al. (2020). Design principles of a minimal auxin response system. Nature plants *6*, 473-482.

Ke, J., Ma, H., Gu, X., Thelen, A., Brunzelle, J.S., Li, J., Xu, H.E., and Melcher, K. (2015). Structural basis for recognition of diverse transcriptional repressors by the TOPLESS family of corepressors. Science Advances *1*.

Kelley, D.R., and Estelle, M. (2012). Ubiquitin-mediated control of plant hormone signaling. Plant physiology *160*, 47-55.

Kepinski, S., and Leyser, O. (2005). The Arabidopsis F-box protein TIR1 is an auxin receptor. Nature *435*, 446-451.

Keul, N.D., Oruganty, K., Schaper Bergman, E.T., Beattie, N.R., McDonald, W.E., Kadirvelraj, R., Gross, M.L., Phillips, R.S., Harvey, S.C., and Wood, Z.A. (2018). The entropic force generated by intrinsically disordered segments tunes protein function. Nature *563*, 584-588.

Kim, D.-Y., Scalf, M., Smith, L.M., and Vierstra, R.D. (2013). Advanced proteomic analyses yield a deep catalog of ubiquitylation targets in Arabidopsis. Plant Cell *25*, 1523-1540.

Kim, S.-H., Woo, O.-G., Jang, H., and Lee, J.-H. (2018). Characterization and comparative expression analysis of CUL1 genes in rice. Genes & genomics *40*, 233-241.

Kim, Y., Park, C., Cha, S., Han, M., Ryu, K.-S., and Suh, J.-Y. (2020). Determinants of PB1 Domain Interactions in Auxin Response Factor ARF5 and Repressor IAA17. Journal of molecular biology.

Kleiger, G., Hao, B., Mohl, D.A., and Deshaies, R.J. (2009a). The acidic tail of the Cdc34 ubiquitin-conjugating enzyme functions in both binding to and catalysis with ubiquitin ligase SCFCdc4. J Biol Chem *284*, 36012-36023.

Kleiger, G., Saha, A., Lewis, S., Kuhlman, B., and Deshaies, R.J. (2009b). Rapid E2-E3 assembly and disassembly enable processive ubiquitylation of cullin-RING ubiquitin ligase substrates. Cell *139*, 957-968.

Kliza, K., and Husnjak, K. (2020). Resolving the Complexity of Ubiquitin Networks. Frontiers in molecular biosciences *7*, 21.

Komander, D., and Rape, M. (2012). The ubiquitin code. Annual review of biochemistry *81*, 203-229.

Korasick, D.A., Westfall, C.S., Lee, S.G., Nanao, M.H., Dumas, R., Hagen, G., Guilfoyle, T.J., Jez, J.M., and Strader, L.C. (2014). Molecular basis for AUXIN RESPONSE FACTOR protein interaction and the control of auxin response repression. Proceedings of the National Academy of Sciences of the United States of America *111*, 5427-5432.

Kowarschik, K., Hoehenwarter, W., Marillonnet, S., and Trujillo, M. (2018). UbiGate: a synthetic biology toolbox to analyse ubiquitination. The New phytologist *217*, 1749-1763.

Kraft, E., Stone, S.L., Ma, L., Su, N., Gao, Y., Lau, O.-S., Deng, X.-W., and Callis, J. (2005). Genome analysis and functional characterization of the E2 and RING-type E3 ligase ubiquitination enzymes of Arabidopsis. Plant Physiology *139*, 1597-1611.

Kramer, E.M., and Ackelsberg, E.M. (2015). Auxin metabolism rates and implications for plant development. Frontiers in plant science *6*, 150.

Kubeš, M., and Napier, R. (2019). Non-canonical auxin signalling: fast and curious. J Exp Bot *70*, 2609-2614.

Kuhn, A., Ramans Harborough, S., McLaughlin, H.M., Natarajan, B., Verstraeten, I., Friml, J., Kepinski, S., and Østergaard, L. (2020). Direct ETTIN-auxin interaction controls chromatin states in gynoecium development. eLife *9*.

Lavy, M., and Estelle, M. (2016). Mechanisms of auxin signaling. Development (Cambridge, England) *143*, 3226-3229.

Lavy, M., Prigge, M.J., Tao, S., Shain, S., Kuo, A., Kirchsteiger, K., and Estelle, M. (2016). Constitutive auxin response in Physcomitrella reveals complex interactions between Aux/IAA and ARF proteins. eLife *5*.

Lechner, E., Achard, P., Vansiri, A., Potuschak, T., and Genschik, P. (2006). F-box proteins everywhere. Current opinion in plant biology *9*, 631-638.

Lee, B.-H., Lu, Y., Prado, M.A., Shi, Y., Tian, G., Sun, S., Elsasser, S., Gygi, S.P., King, R.W., and Finley, D. (2016). USP14 deubiquitinates proteasome-bound substrates that are ubiquitinated at multiple sites. Nature *532*, 398-401.

Lee, S., Sundaram, S., Armitage, L., Evans, J.P., Hawkes, T., Kepinski, S., Ferro, N., and Napier, R.M. (2014). Defining binding efficiency and specificity of auxins for SCF(TIR1/AFB)-Aux/IAA co-receptor complex formation. ACS chemical biology *9*, 673-682.

Leitner, J., Petrasek, J., Tomanov, K., Retzer, K., Parezova, M., Korbei, B., Bachmair, A., Zazimalova, E., and Luschnig, C. (2012). Lysine63-linked ubiquitylation of PIN2 auxin carrier protein governs

hormonally controlled adaptation of Arabidopsis root growth. Proceedings of the National Academy of Sciences of the United States of America *109*, 8322-8327.

Leyser, H.M., Lincoln, C.A., Timpte, C., Lammer, D., Turner, J., and Estelle, M. (1993). Arabidopsis auxin-resistance gene AXR1 encodes a protein related to ubiquitin-activating enzyme E1. Nature *364*, 161-164.

Leyser, O. (2018). Auxin Signaling. Plant Physiology *176*, 465-479.

Lincoln, C., Britton, J.H., and Estelle, M. (1990). Growth and development of the axr1 mutants of Arabidopsis. The Plant cell *2*, 1071-1080.

Ling, R., Colón, E., Dahmus, M.E., and Callis, J. (2000). Histidine-tagged ubiquitin substitutes for wild-type ubiquitin in Saccharomyces cerevisiae and facilitates isolation and identification of in vivo substrates of the ubiquitin pathway. Analytical biochemistry *282*, 54-64.

Liscum, E., and Reed, J.W. (2002). Genetics of Aux/IAA and ARF action in plant growth and development. Plant Mol Biol *49*, 387-400.

Liu, J., Furukawa, M., Matsumoto, T., and Xiong, Y. (2002). NEDD8 Modification of CUL1 Dissociates p120CAND1, an Inhibitor of CUL1-SKP1 Binding and SCF Ligases. Molecular cell *10*, 1511-1518.

Liu, X., Reitsma, J.M., Mamrosh, J.L., Zhang, Y., Straube, R., and Deshaies, R.J. (2018). Cand1-Mediated Adaptive Exchange Mechanism Enables Variation in F-Box Protein Expression. Mol Cell *69*, 773-786.e6.

Liu, X., Yang, S., Zhao, M., Luo, M., Yu, C.-W., Chen, C.-Y., Tai, R., and Wu, K. (2014). Transcriptional repression by histone deacetylases in plants. Molecular plant *7*, 764-772.

Lo, S.-C., and Hannink, M. (2006). CAND1-mediated substrate adaptor recycling is required for efficient repression of Nrf2 by Keap1. Molecular and Cellular Biology *26*, 1235-1244.

Ludwig, Y., Berendzen, K.W., Xu, C., Piepho, H.-P., and Hochholdinger, F. (2014). Diversity of stability, localization, interaction and control of downstream gene activity in the Maize Aux/IAA protein family. Plos One *9*, e107346.

Luo, J., Zhou, J.J., and Zhang, J.Z. (2018). Aux/IAA Gene Family in Plants. Molecular Structure, Regulation, and Function. Int J Mol Sci *19*.

Lv, B., Yu, Q., Liu, J., Wen, X., Yan, Z., Hu, K., Li, H., Kong, X., Li, C., and Tian, H., et al. (2020). Non-canonical AUX/IAA protein IAA33 competes with canonical AUX/IAA repressor IAA5 to negatively regulate auxin signaling. The EMBO journal *39*, e101515.

Ma, H., Duan, J., Ke, J., He, Y., Gu, X., Xu, T.-H., Yu, H., Wang, Y., Brunzelle, J.S., and Jiang, Y., et al. (2017). A D53 repression motif induces oligomerization of TOPLESS corepressors and promotes assembly of a corepressor-nucleosome complex. Science Advances *3*.

Maraschin, F.d.S., Memelink, J., and Offringa, R. (2009). Auxin-induced, SCF(TIR1)-mediated poly-ubiquitination marks AUX/IAA proteins for degradation. The Plant journal : for cell and molecular biology *59*, 100-109.

Martin-Arevalillo, R., Nanao, M.H., Larrieu, A., Vinos-Poyo, T., Mast, D., Galvan-Ampudia, C., Brunoud, G., Vernoux, T., Dumas, R., and Parcy, F. (2017). Structure of the Arabidopsis TOPLESS corepressor provides insight into the evolution of transcriptional repression. Proc Natl Acad Sci U S A *114*, 8107-8112.

Martinez-Fonts, K., Davis, C., Tomita, T., Elsasser, S., Nager, A.R., Shi, Y., Finley, D., and Matouschek, A. (2020). The proteasome 19S cap and its ubiquitin receptors provide a versatile recognition platform for substrates. Nature communications *11*, 477.

Mattiroli, F., and Sixma, T.K. (2014). Lysine-targeting specificity in ubiquitin and ubiquitin-like modification pathways. Nature structural & molecular biology *21*, 308-316.

Meas, R., and Mao, P. (2015). Histone ubiquitylation and its roles in transcription and DNA damage response. DNA repair *36*, 36-42.

Medvar, B., Raghuram, V., Pisitkun, T., Sarkar, A., and Knepper, M.A. (2016). Comprehensive database of human E3 ubiquitin ligases: application to aquaporin-2 regulation. Physiological Genomics *48*, 502-512.

Mendes, M.L., Fougeras, M.R., and Dittmar, G. (2020). Analysis of ubiquitin signaling and chain topology cross-talk. Journal of proteomics *215*, 103634.

Mergner, J., Frejno, M., List, M., Papacek, M., Chen, X., Chaudhary, A., Samaras, P., Richter, S., Shikata, H., and Messerer, M., et al. (2020). Mass-spectrometry-based draft of the Arabidopsis proteome. Nature *579*, 409-414.

Mergner, J., Heinzlmeir, S., Kuster, B., and Schwechheimer, C. (2015). DENEDDYLASE1 deconjugates NEDD8 from non-cullin protein substrates in Arabidopsis thaliana. The Plant cell *27*, 741-753.

Mergner, J., Kuster, B., and Schwechheimer, C. (2017). DENEDDYLASE1 counters automodification of neddylating enzymes to maintain NEDD8 homeostasis in Arabidopsis. The Journal of biological chemistry.

Mergner, J., and Schwechheimer, C. (2014). The NEDD8 modification pathway in plants. Frontiers in plant science *5*, 103.

Metzger, M.B., Pruneda, J.N., Klevit, R.E., and Weissman, A.M. (2014). RING-type E3 ligases: master manipulators of E2 ubiquitin-conjugating enzymes and ubiquitination. Biochimica et biophysica acta *1843*, 47-60.

Meyer, H.-J., and Rape, M. (2014). Enhanced protein degradation by branched ubiquitin chains. Cell *157*, 910-921.

Middleton, A.J., and Day, C.L. (2015). The molecular basis of lysine 48 ubiquitin chain synthesis by Ube2K. Scientific reports *5*, 16793.

Miricescu, A., Goslin, K., and Graciet, E. (2018). Ubiquitylation in plants: signaling hub for the integration of environmental signals. J Exp Bot *69*, 4511-4527.

Mockaitis, K., and Estelle, M. (2008). Auxin receptors and plant development. a new signaling paradigm. Annu Rev Cell Dev Biol *24*, 55-80.

Moeller, H.B., Aroankins, T.S., Slengerik-Hansen, J., Pisitkun, T., and Fenton, R.A. (2014). Phosphorylation and ubiquitylation are opposing processes that regulate endocytosis of the water channel aquaporin-2. Journal of cell science *127*, 3174-3183.

Morreale, F.E., and Walden, H. (2016). Types of Ubiquitin Ligases. Cell *165*, 248-248.e1.

Moss, B.L., Mao, H., Guseman, J.M., Hinds, T.R., Hellmuth, A., Kovenock, M., Noorassa, A., Lanctot, A., Villalobos, Luz Irina A. Calderon, and Zheng, N., et al. (2015). Rate Motifs Tune Auxin/Indole-3-Acetic Acid Degradation Dynamics. Plant Physiology *169*, 803-813.

Mutte, S.K., Kato, H., Rothfels, C., Melkonian, M., Wong, G.K., and Weijers, D. (2018). Origin and evolution of the nuclear auxin response system. eLife *7*.

Nagpal, P., Walker, L.M., Young, J.C., Sonawala, A., Timpte, C., Estelle, M., and Reed, J.W. (2000). AXR2 encodes a member of the Aux/IAA protein family. Plant Physiol *123*, 563-574.

Nakasone, M.A., Livnat-Levanon, N., Glickman, M.H., Cohen, R.E., and Fushman, D. (2013). Mixed-linkage ubiquitin chains send mixed messages. Structure (London, England : 1993) *21*, 727-740.

Nalavadi, V.C., Muddashetty, R.S., Gross, C., and Bassell, G.J. (2012). Dephosphorylation-induced ubiquitination and degradation of FMRP in dendrites: a role in immediate early mGluR-stimulated translation. The Journal of neuroscience : the official journal of the Society for Neuroscience *32*, 2582-2587.

Nanao, M.H., Vinos-Poyo, T., Brunoud, G., Thevenon, E., Mazzoleni, M., Mast, D., Laine, S., Wang, S., Hagen, G., and Li, H., et al. (2014). Structural basis for oligomerization of auxin transcriptional regulators. Nat Commun *5*, 3617.

Nielsen, C.P., and MacGurn, J.A. (2020). Coupling Conjugation and Deconjugation Activities to Achieve Cellular Ubiquitin Dynamics. Trends in biochemical sciences.

Niemeyer, M., Moreno Castillo, E., Ihling, C.H., Iacobucci, C., Wilde, V., Hellmuth, A., Hoehenwarter, W., Samodelov, S.L., Zurbriggen, M.D., and Kastritis, P.L., et al. (2020). Flexibility of intrinsically disordered degrons in AUX/IAA proteins reinforces auxin co-receptor assemblies. Nat Commun *11*.

Niu, K., Fang, H., Chen, Z., Zhu, Y., Tan, Q., Di Wei, Li, Y., Balajee, A.S., and Zhao, Y. (2019). USP33 deubiquitinates PRKN/parkin and antagonizes its role in mitophagy. Autophagy, 1-11.

Ohtake, F., Saeki, Y., Ishido, S., Kanno, J., and Tanaka, K. (2016). The K48-K63 Branched Ubiquitin Chain Regulates NF- κ B Signaling. Molecular cell *64*, 251-266.

Ohtake, F., Tsuchiya, H., Saeki, Y., and Tanaka, K. (2018). K63 ubiquitylation triggers proteasomal degradation by seeding branched ubiquitin chains. Proc Natl Acad Sci U S A *115*, E1401-E1408.

Olatunji, D., Geelen, D., and Verstraeten, I. (2017). Control of Endogenous Auxin Levels in Plant Root Development. International journal of molecular sciences *18*.

Pan, Z.Q., Kentsis, A., Dias, D.C., Yamoah, K., and Wu, K. (2004). Nedd8 on cullin. building an expressway to protein destruction. Oncogene *23*, 1985-1997.

Pierce, N.W., Lee, J.E., Liu, X., Sweredoski, M.J., Graham, R.L.J., Larimore, E.A., Rome, M., Zheng, N., Clurman, B.E., and Hess, S., et al. (2013). Cand1 promotes assembly of new SCF complexes through dynamic exchange of F box proteins. Cell *153*, 206-215.

Piya, S., Shrestha, S.K., Binder, B., Stewart, C.N., and Hewezi, T. (2014). Protein-protein interaction and gene co-expression maps of ARFs and Aux/IAAs in Arabidopsis. Frontiers in plant science *5*, 744.

Plechanovová, A., Jaffray, E.G., Tatham, M.H., Naismith, J.H., and Hay, R.T. (2012). Structure of a RING E3 ligase and ubiquitin-loaded E2 primed for catalysis. Nature *489*, 115-120.

Prakash, S., Tian, L., Ratliff, K.S., Lehotzky, R.E., and Matouschek, A. (2004). An unstructured initiation site is required for efficient proteasome-mediated degradation. Nat Struct Mol Biol *11*, 830-837.

Prigge, M.J., Greenham, K., Zhang, Y., Santner, A., Castillejo, C., Mutka, A.M., O'Malley, R.C., Ecker, J.R., Kunkel, B.N., and Estelle, M. (2016). The Arabidopsis Auxin Receptor F-Box Proteins AFB4 and AFB5 Are Required for Response to the Synthetic Auxin Picloram. G3 (Bethesda, Md.) *6*, 1383-1390.

Prigge, M.J., Platre, M., Kadakia, N., Zhang, Y., Greenham, K., Szutu, W., Pandey, B.K., Bhosale, R.A., Bennett, M.J., and Busch, W., et al. (2020). Genetic analysis of the Arabidopsis TIR1/AFB auxin receptors reveals both overlapping and specialized functions. eLife *9*.

Pruneda, J.N., Littlefield, P.J., Soss, S.E., Nordquist, K.A., Chazin, W.J., Brzovic, P.S., and Klevit, R.E. (2012). Structure of an E3:E2~Ub complex reveals an allosteric mechanism shared among RING/U-box ligases. Mol Cell *47*, 933-942.

Pu, Y., Walley, J.W., Shen, Z., Lang, M.G., Briggs, S.P., Estelle, M., and Kelley, D.R. (2019). Quantitative Early Auxin Root Proteomics Identifies GAUT10, a Galacturonosyltransferase, as a Novel Regulator of Root Meristem Maintenance. Molecular & cellular proteomics : MCP *18*, 1157-1170.

Ramadan, A., Nemoto, K., Seki, M., Shinozaki, K., Takeda, H., Takahashi, H., and Sawasaki, T. (2015). Wheat germ-based protein libraries for the functional characterisation of the Arabidopsis E2 ubiquitin conjugating enzymes and the RING-type E3 ubiquitin ligase enzymes. BMC Plant Biol *15*, 275.

Ramans Harborough, S., Kalverda, A.P., Thompson, G.S., Kieffer, M., Kubes, M., Quareshy, M., Uzunova, V., Prusinska, J.M., Hayashi, K.-I., and Napier, R., et al. (2019). A fuzzy encounter complex precedes formation of the fully-engaged TIR1-Aux/IAA auxin co-receptor system.

Ramos, J.A., Zenser, N., Leyser, O., and Callis, J. (2001a). Rapid degradation of auxin/indoleacetic acid proteins requires conserved amino acids of domain II and is proteasome dependent. The Plant cell *13*, 2349-2360.

Ramos, J.A., Zenser, N., Leyser, O., and Callis, J. (2001b). Rapid degradation of auxin/indoleacetic acid proteins requires conserved amino acids of domain II and is proteasome dependent. The Plant cell *13*, 2349-2360.

Ravid, T., and Hochstrasser, M. (2008). Diversity of degradation signals in the ubiquitin-proteasome system. Nature reviews. Molecular cell biology *9*, 679-690.

Reed, J.W. (2001). Roles and activities of Aux/IAA proteins in Arabidopsis. Trends Plant Sci *6*, 420-425.

Reichard, E.L., Chirico, G.G., Dewey, W.J., Nassif, N.D., Bard, K.E., Millas, N.E., and Kraut, D.A. (2016). Substrate Ubiquitination Controls the Unfolding Ability of the Proteasome. J Biol Chem *291*, 18547-18561.

Rinaldi, M.A., Liu, J., Enders, T.A., Bartel, B., and Strader, L.C. (2012). A gain-of-function mutation in IAA16 confers reduced responses to auxin and abscisic acid and impedes plant growth and fertility. Plant molecular biology *79*, 359-373.

Romero-Barrios, N., Monachello, D., Dolde, U., Wong, A., San Clemente, H., Cayrel, A., Johnson, A., Lurin, C., and Vert, G. (2020). Advanced Cataloging of Lysine-63 Polyubiquitin Networks by Genomic, Interactome, and Sensor-Based Proteomic Analyses. The Plant cell *32*, 123-138.

Romero-Barrios, N., and Vert, G. (2018). Proteasome-independent functions of lysine-63 polyubiquitination in plants. The New phytologist *217*, 995-1011.

Rusnac, D.-V., and Zheng, N. (2020). Structural Biology of CRL Ubiquitin Ligases. Advances in experimental medicine and biology *1217*, 9-31.

Santner, A., and Estelle, M. (2010). The ubiquitin-proteasome system regulates plant hormone signaling. The Plant journal : for cell and molecular biology *61*, 1029-1040.

Saracco, S.A., Hansson, M., Scalf, M., Walker, J.M., Smith, L.M., and Vierstra, R.D. (2009). Tandem affinity purification and mass spectrometric analysis of ubiquitylated proteins in Arabidopsis. Plant J *59*, 344-358.

Schwanhäusser, B., Busse, D., Li, N., Dittmar, G., Schuchhardt, J., Wolf, J., Chen, W., and Selbach, M. (2011). Global quantification of mammalian gene expression control. Nature *473*, 337-342.

Scott, D.C., Rhee, D.Y., Duda, D.M., Kelsall, I.R., Olszewski, J.L., Paulo, J.A., Jong, A., Ovaa, H., Alpi, A.F., and Harper, J.W., et al. (2016). Two Distinct Types of E3 Ligases Work in Unison to Regulate Substrate Ubiquitylation. Cell *166*, 1198-1214.e24.

Shen, W.-H., Parmentier, Y., Hellmann, H., Lechner, E., Dong, A., Masson, J., Granier, F., Lepiniec, L., Estelle, M., and Genschik, P. (2002). Null mutation of AtCUL1 causes arrest in early embryogenesis in Arabidopsis. Molecular biology of the cell *13*, 1916-1928.

Shi, H., Liu, W., Wei, Y., and Ye, T. (2017). Integration of auxin/indole-3-acetic acid 17 and RGA-LIKE3 confers salt stress resistance through stabilization by nitric oxide in Arabidopsis. J Exp Bot *68*, 1239-1249.

Shimizu-Mitao, Y., and Kakimoto, T. (2014). Auxin sensitivities of all Arabidopsis Aux/IAAs for degradation in the presence of every TIR1/AFB. Plant & cell physiology *55*, 1450-1459.

Simonini, S., Deb, J., Moubayidin, L., Stephenson, P., Valluru, M., Freire-Rios, A., Sorefan, K., Weijers, D., Friml, J., and Østergaard, L. (2016). A noncanonical auxin-sensing mechanism is required for organ morphogenesis in Arabidopsis. Genes & development *30*, 2286-2296.

Simonini, S., Mas, P.J., Mas, C.M.V.S., Østergaard, L., and Hart, D.J. (2018). Auxin sensing is a property of an unstructured domain in the Auxin Response Factor ETTIN of Arabidopsis thaliana. Scientific reports *8*, 13563.

Skaar, J.R., Pagan, J.K., and Pagano, M. (2013). Mechanisms and function of substrate recruitment by F-box proteins. Nature reviews. Molecular cell biology *14*, 369-381.

Spoel, S.H., Mou, Z., Tada, Y., Spivey, N.W., Genschik, P., and Dong, X. (2009). Proteasome-mediated turnover of the transcription coactivator NPR1 plays dual roles in regulating plant immunity. Cell *137*, 860-872.

Spratt, D.E., and Shaw, G.S. (2011). Association of the disordered C-terminus of CDC34 with a catalytically bound ubiquitin. Journal of molecular biology *407*, 425-438.

Stefanowicz, K., Lannoo, N., and van Damme, E.J.M. (2015). Plant F-box Proteins – Judges between Life and Death. Critical Reviews in Plant Sciences *34*, 523-552.

Stewart, M.D., Ritterhoff, T., Klevit, R.E., and Brzovic, P.S. (2016). E2 enzymes: more than just middle men. Cell research *26*, 423-440.

Stolz, A., and Dikic, I. (2018). Heterotypic Ubiquitin Chains: Seeing is Believing. Trends in cell biology *28*, 1-3.

Straube, R., Shah, M., Flockerzi, D., and Wolf, D.A. (2017). Trade-off and flexibility in the dynamic regulation of the cullin-RING ubiquitin ligase repertoire. PLoS computational biology *13*, e1005869.

Sumimoto, H., Kamakura, S., and Ito, T. (2007). Structure and function of the PB1 domain, a protein interaction module conserved in animals, fungi, amoebas, and plants. Science's STKE : signal transduction knowledge environment *2007*, re6.

Sun, Y., Wei, W. and Jin, J. (2020). Cullin-RING Ligases and Protein Neddylation. Biology and Therapeutics (Singapore: Springer Singapore).

Svozil, J., Gruissem, W., and Baerenfaller, K. (2015). Proteasome targeting of proteins in Arabidopsis leaf mesophyll, epidermal and vascular tissues. Frontiers in plant science *6*, 376.

Swatek, K.N., and Komander, D. (2016). Ubiquitin modifications. Cell research *26*, 399-422.

Swatek, K.N., Usher, J.L., Kueck, A.F., Gladkova, C., Mevissen, T.E.T., Pruneda, J.N., Skern, T., and Komander, D. (2019). Insights into ubiquitin chain architecture using Ub-clipping. Nature *572*, 533-537.

Tal, L., Gil, M.X.A., Guercio, A.M., and Shabek, N. (2020). Structural Aspects of Plant Hormone Signal Perception and Regulation by Ubiquitin Ligases1OPEN. Plant Physiol *182*, 1537-1544.

Tan, X., Calderon-Villalobos, L.I.A., Sharon, M., Zheng, C., Robinson, C.V., Estelle, M., and Zheng, N. (2007). Mechanism of auxin perception by the TIR1 ubiquitin ligase. Nature *446*, 640-645.

Tanaka, K. (2009). The proteasome: overview of structure and functions. Proceedings of the Japan Academy. Series B, Physical and biological sciences *85*, 12-36.

Tao, S., and Estelle, M. (2018). Mutational studies of the Aux/IAA proteins in Physcomitrella reveal novel insights into their function. The New phytologist *218*, 1534-1542.

Thomann, A., Dieterle, M., and Genschik, P. (2005). Plant CULLIN-based E3s. phytohormones come first. FEBS Lett *579*, 3239-3245.

Tian, Q., Nagpal, P., and Reed, J.W. (2003). Regulation of Arabidopsis SHY2/IAA3 protein turnover. The Plant journal : for cell and molecular biology *36*, 643-651.

Tiwari, S.B., Hagen, G., and Guilfoyle, T.J. (2004). Aux/IAA proteins contain a potent transcriptional repression domain. Plant Cell *16*, 533-543.

Tiwari, S.B., Wang, X.J., Hagen, G., and Guilfoyle, T.J. (2001). AUX/IAA proteins are active repressors, and their stability and activity are modulated by auxin. Plant Cell *13*, 2809-2822.

Tron, A.E., Arai, T., Duda, D.M., Kuwabara, H., Olszewski, J.L., Fujiwara, Y., Bahamon, B.N., Signoretti, S., Schulman, B.A., and DeCaprio, J.A. (2012). The glomuvenous malformation protein Glomulin binds Rbx1 and regulates cullin RING ligase-mediated turnover of Fbw7. Molecular cell *46*, 67-78.

Tsuchiya, H., Ohtake, F., Arai, N., Kaiho, A., Yasuda, S., Tanaka, K., and Saeki, Y. (2017). In Vivo Ubiquitin Linkage-type Analysis Reveals that the Cdc48-Rad23/Dsk2 Axis Contributes to K48-Linked Chain Specificity of the Proteasome. Mol Cell *66*, 488-502.e7.

Turek, I., Tischer, N., Lassig, R., and Trujillo, M. (2018). Multi-tiered pairing selectivity between E2 ubiquitin-conjugating enzymes and E3 ligases. The Journal of biological chemistry *293*, 16324-16336.

Ulmasov, T., Murfett, J., Hagen, G., and Guilfoyle, T.J. (1997). Aux/IAA proteins repress expression of reporter genes containing natural and highly active synthetic auxin response elements. The Plant cell *9*, 1963-1971.

Uzunova, V.V., Quareshy, M., Del Genio, C.I., and Napier, R.M. (2016). Tomographic docking suggests the mechanism of auxin receptor TIR1 selectivity. Open biology *6*.

Vandereyken, K., van Leene, J., Coninck, B. de, and Cammue, B.P.A. (2018). Hub Protein Controversy: Taking a Closer Look at Plant Stress Response Hubs. Frontiers in plant science *9*, 694.

Vernoux, T., Brunoud, G., Farcot, E., Morin, V., van den Daele, H., Legrand, J., Oliva, M., Das, P., Larrieu, A., and Wells, D., et al. (2011). The auxin signalling network translates dynamic input into robust patterning at the shoot apex. Molecular systems biology *7*, 508.

Walton, A., Stes, E., Cybulski, N., van Bel, M., Iñigo, S., Durand, A.N., Timmerman, E., Heyman, J., Pauwels, L., and Veylder, L. de, et al. (2016). It's Time for Some "Site"-Seeing: Novel Tools to Monitor the Ubiquitin Landscape in Arabidopsis thaliana. Plant Cell *28*, 6-16.

Wang, K., Deshaies, R.J., and Liu, X. (2020). Assembly and Regulation of CRL Ubiquitin Ligases. In Cullin-RING Ligases and Protein Neddylation. Biology and Therapeutics, Y. Sun, W. Wei and J. Jin, eds. (Singapore: Springer Singapore), pp. 33–46.

Wang, Y.-C., Wang, N., Xu, H.-F., Jiang, S.-H., Fang, H.-C., Su, M.-Y., Zhang, Z.-Y., Zhang, T.-L., and Chen, X.-S. (2018). Auxin regulates anthocyanin biosynthesis through the Aux/IAA-ARF signaling pathway in apple. Horticulture research *5*, 59.

Watson, E.R., Brown, N.G., Peters, J.-M., Stark, H., and Schulman, B.A. (2019). Posing the APC/C E3 Ubiquitin Ligase to Orchestrate Cell Division. Trends in cell biology *29*, 117-134.

Weijers, D., and Wagner, D. (2016). Transcriptional Responses to the Auxin Hormone. Annual review of plant biology *67*, 539-574.

Wen, R., Wang, S., Xiang, D., Venglat, P., Shi, X., Zang, Y., Datla, R., Xiao, W., and Wang, H. (2014). UBC13, an E2 enzyme for Lys63-linked ubiquitination, functions in root development by affecting auxin signaling and Aux/IAA protein stability. The Plant journal : for cell and molecular biology *80*, 424-436.

Wend, S., Dal Bosco, C., Kampf, M.M., Ren, F., Palme, K., Weber, W., Dovzhenko, A., and Zurbriggen, M.D. (2013). A quantitative ratiometric sensor for time-resolved analysis of auxin dynamics. Scientific reports *3*, 2052.

Wickliffe, K.E., Lorenz, S., Wemmer, D.E., Kuriyan, J., and Rape, M. (2011). The mechanism of linkage-specific ubiquitin chain elongation by a single-subunit E2. Cell *144*, 769-781.

Winkler, M., Niemeyer, M., Hellmuth, A., Janitza, P., Christ, G., Samodelov, S.L., Wilde, V., Majovsky, P., Trujillo, M., and Zurbriggen, M.D., et al. (2017). Variation in auxin sensing guides AUX/IAA transcriptional repressor ubiquitylation and destruction. Nat Commun *8*, 15706.

Worley, C.K., Zenser, N., Ramos, J., Rouse, D., Leyser, O., Theologis, A., and Callis, J. (2000). Degradation of Aux/IAA proteins is essential for normal auxin signalling. The Plant journal : for cell and molecular biology *21*, 553-562.

Wu, K., Kovacev, J., and Pan, Z.-Q. (2010). Priming and extending: a UbcH5/Cdc34 E2 handoff mechanism for polyubiquitination on a SCF substrate. Mol Cell *37*, 784-796.

Wu, M.-F., Yamaguchi, N., Xiao, J., Bargmann, B., Estelle, M., Sang, Y., and Wagner, D. (2015). Auxin-regulated chromatin switch directs acquisition of flower primordium founder fate. eLife *4*, e09269.

Xing, M., and Xue, H. (2012). A proteomics study of auxin effects in Arabidopsis thaliana. Acta biochimica et biophysica Sinica *44*, 783-796.

Xu, F., He, S., Zhang, J., Mao, Z., Wang, W., Li, T., Hua, J., Du, S., Xu, P., and Li, L., et al. (2018). Photoactivated CRY1 and phyB Interact Directly with AUX/IAA Proteins to Inhibit Auxin Signaling in Arabidopsis. Molecular plant *11*, 523-541.

Xu, P., Duong, D.M., Seyfried, N.T., Cheng, D., Xie, Y., Robert, J., Rush, J., Hochstrasser, M., Finley, D., and Peng, J. (2009). Quantitative proteomics reveals the function of unconventional ubiquitin chains in proteasomal degradation. Cell *137*, 133-145.

Yan, F., Huang, C., Wang, X., Tan, J., Cheng, S., Wan, M., Wang, Z., Wang, S., Luo, S., and Li, A., et al. (2020). Threonine ADP-Ribosylation of Ubiquitin by a Bacterial Effector Family Blocks Host Ubiquitination. Mol Cell.

Yan, J., Zhang, C., Gu, M., Bai, Z., Zhang, W., Qi, T., Cheng, Z., Peng, W., Luo, H., and Nan, F., et al. (2009). The Arabidopsis CORONATINE INSENSITIVE1 protein is a jasmonate receptor. The Plant cell *21*, 2220-2236.

Yang, X., Lee, S., So, J.-H., Dharmasiri, S., Dharmasiri, N., Ge, L., Jensen, C., Hangarter, R., Hobbie, L., and Estelle, M. (2004). The IAA1 protein is encoded by AXR5 and is a substrate of SCF(TIR1). The Plant journal : for cell and molecular biology *40*, 772-782.

Ye, X., Nalepa, G., Welcker, M., Kessler, B.M., Spooner, E., Qin, J., Elledge, S.J., Clurman, B.E., and Harper, J.W. (2004). Recognition of phosphodegron motifs in human cyclin E by the SCF(Fbw7) ubiquitin ligase. The Journal of biological chemistry *279*, 50110-50119.

Yu, H., Kago, G., Yellman, C.M., and Matouschek, A. (2016). Ubiquitin-like domains can target to the proteasome but proteolysis requires a disordered region. EMBO J *35*, 1522-1536.

Yu, H., and Matouschek, A. (2017). Recognition of Client Proteins by the Proteasome. Annual review of biophysics *46*, 149-173.

Yu, H., Zhang, Y., Moss, B.L., Bargmann, B.O., Wang, R., Prigge, M., Nemhauser, J.L., and Estelle, M. (2015). Untethering the TIR1 auxin receptor from the SCF complex increases its stability and inhibits auxin response. Nature plants *1*.

Zenser, N., Ellsmore, A., Leasure, C., and Callis, J. (2001). Auxin modulates the degradation rate of Aux/IAA proteins. Proceedings of the National Academy of Sciences of the United States of America *98*, 11795-11800.

Zhang, W., Ito, H., Quint, M., Huang, H., Noel, L.D., and Gray, W.M. (2008). Genetic analysis of CAND1-CUL1 interactions in Arabidopsis supports a role for CAND1-mediated cycling of the SCFTIR1 complex. Proceedings of the National Academy of Sciences of the United States of America *105*, 8470-8475.

Zheng, J., Yang, X., Harrell, J.M., Ryzhikov, S., Shim, E.-H., Lykke-Andersen, K., Wei, N., Sun, H., Kobayashi, R., and Zhang, H. (2002). CAND1 Binds to Unneddylated CUL1 and Regulates the Formation of SCF Ubiquitin E3 Ligase Complex. Molecular cell *10*, 1519-1526.

Zimmerman, E.S., Schulman, B.A., and Zheng, N. (2010). Structural assembly of cullin-RING ubiquitin ligase complexes. Current opinion in structural biology *20*, 714-721.

7. Appendix

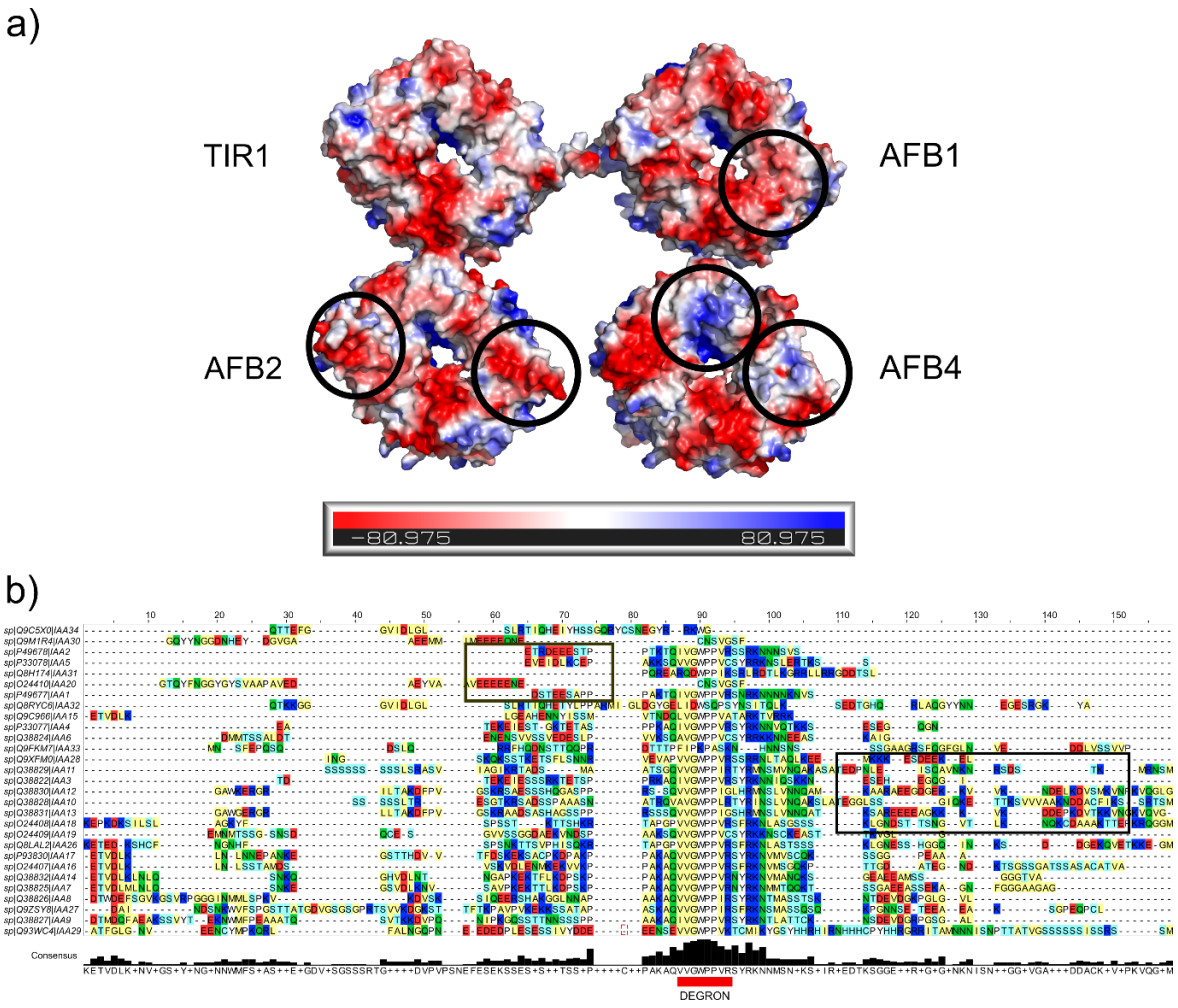

Figure 12: Charge distributions in TIR1/AFBs might influence selective auxin co-receptor formation. a) Vacuum electrostatics generated with Pymol on the surface of TIR1 (PDB: 2p1m) homology-modelled AFBs. **b)** Alignment (ClustlO) of degron-flanking regions in AUX/IAA proteins with amino acids colored according to their features.

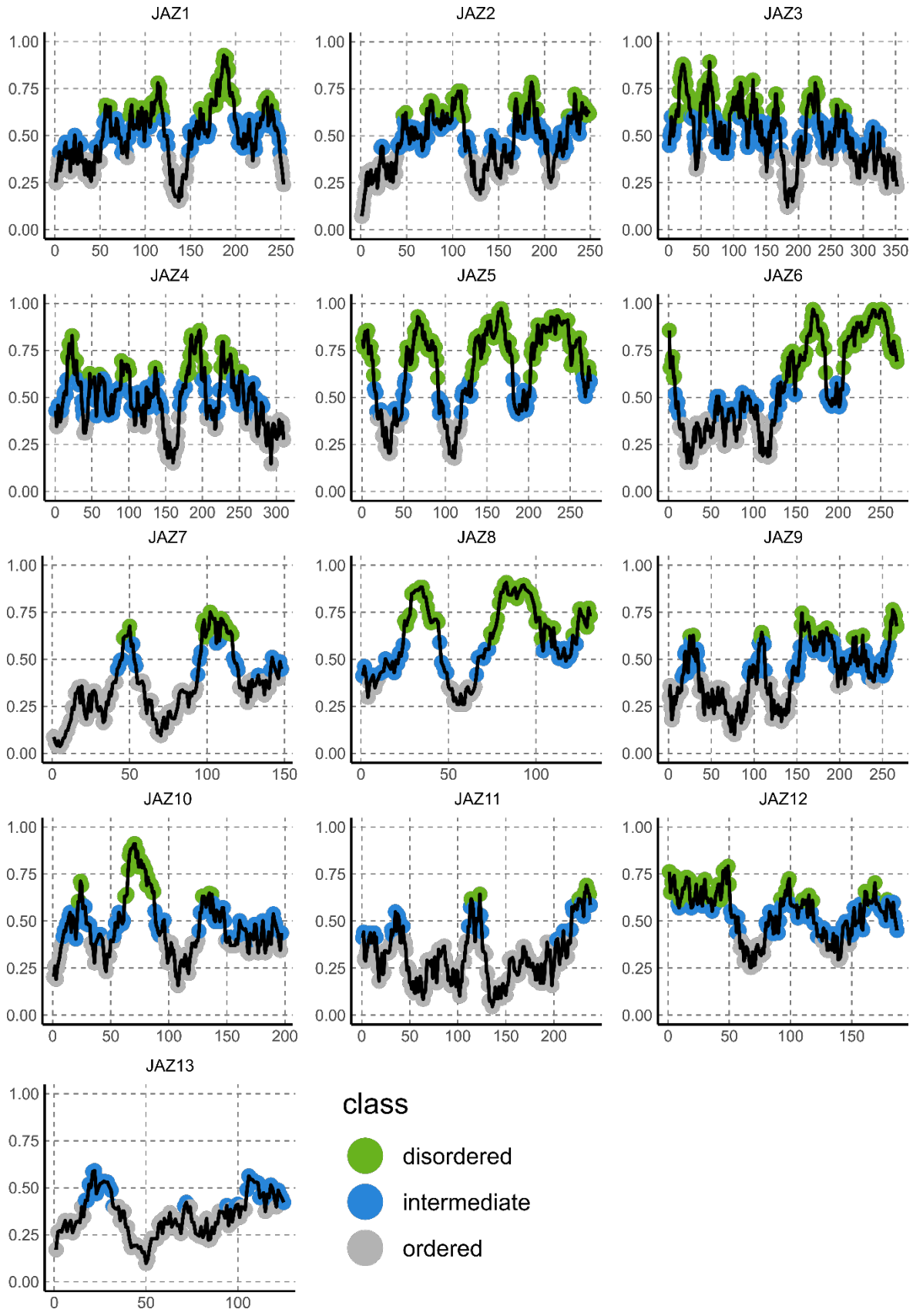

Figure 13: IUPred2A disorder prediction along the sequence of *Arabidopsis thaliana* JAZ proteins. The x-axis corresponds to the full-length amino acid sequence of each JAZ protein, and the y-axis depicts the IUPred2A score for each residue (probability for disorder 0-1). Residues are colored according to their disorder probability (disordered: ≥ 0.6, green; intermediate: 0.4-0.6, blue and ordered: ≤ 0.4, gray).

7.1 Supplementary Information for 2.1 Winkler M. *et al.* (2017)

Supplementary Information

Variation in auxin sensing guides AUX/IAA transcriptional repressor ubiquitylation and destruction

Winkler *et al.*

Supplementary Figures 1-16

Supplementary Tables 1-2

Supplementary Note 1

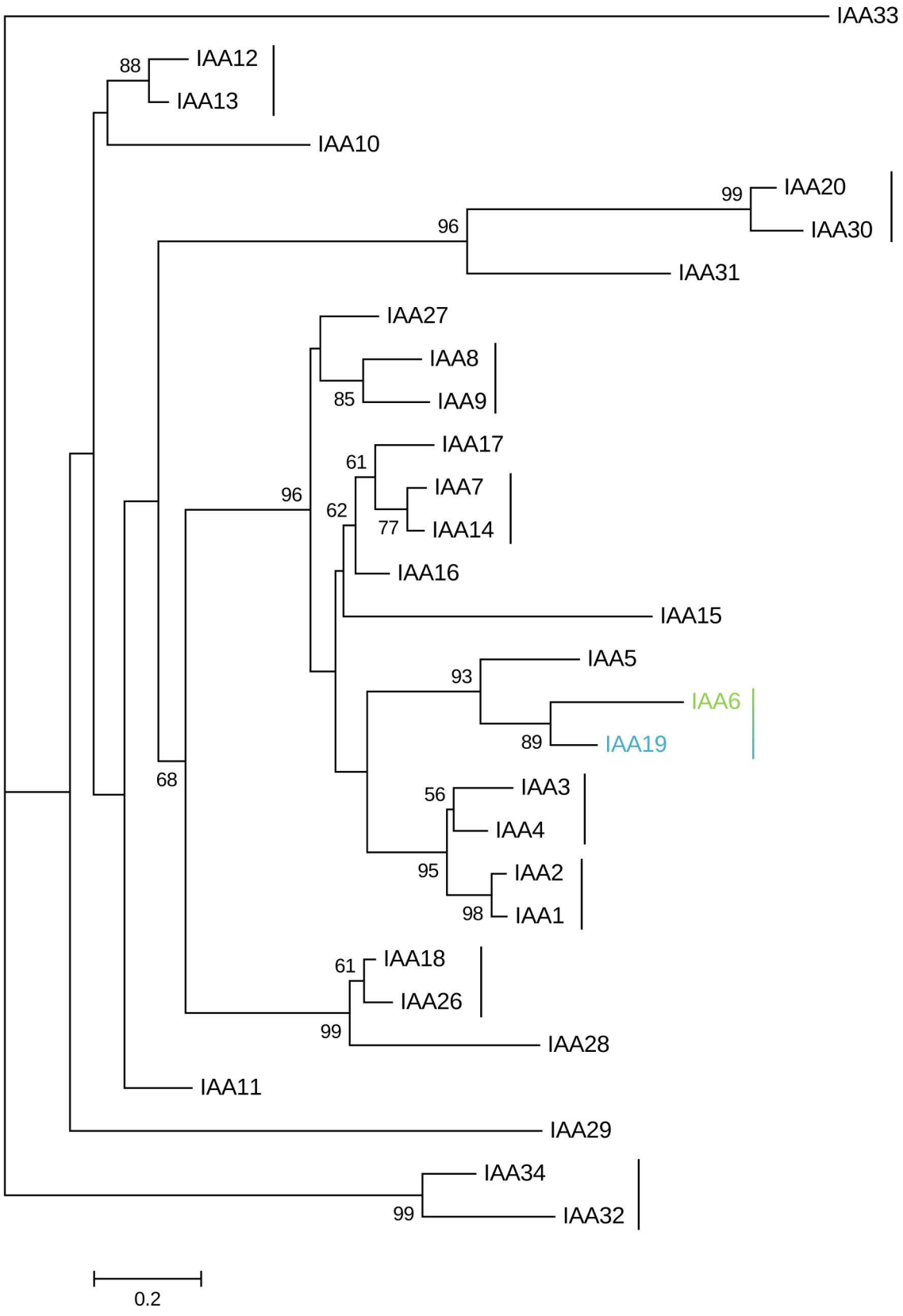

Supplementary Figure 1. Phylogeny of *A. thaliana* AUX/IAA proteins. The unrooted phylogenetic tree was created with the full-length protein sequences of 29 AUX/IAA proteins based on maximum likelihood. Vertical bars correspond to AUX/IAA sister pairs (ohnologs). IAA6 (green) and IAA19 (blue) ohnologs are highlighted. Bootstrap values greater than 50% are shown at the corresponding node. Scale bar 0.2 denotes 0.2 amino acid substitution per site.

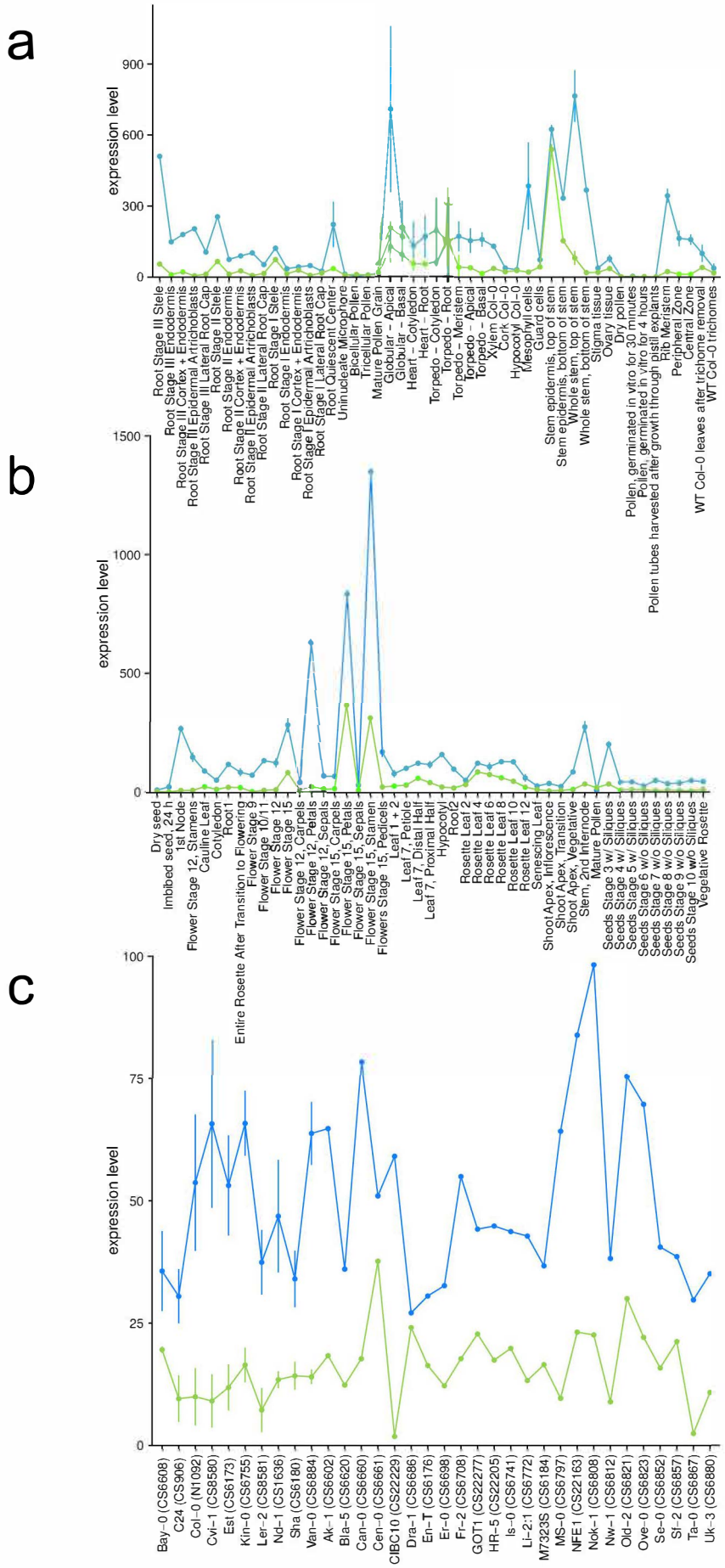

Supplementary Figure 2. Comparison of *IAA6* (green) and *IAA19* (blue) expression values for three different datasets: (**a**) Tissue specific/cell type, (**b**) AtGenExpress – development, and (**c**) AtGenExpress – natural variation, obtained from the Arabidopsis eFP browser (Schmidt, et al. 2005, Winter, et al. 2007). Error bars, s.d. See **Supplementary Note 1** for details and references

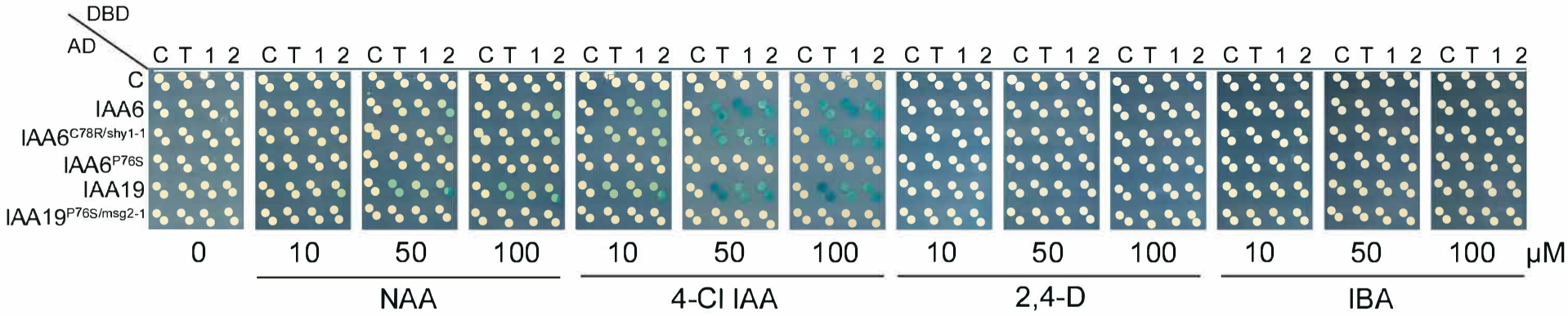

Supplementary Figure 3. LexA yeast two-hybrid interaction experiments of empty control (C), TIR1(T), AFB1 (1), or AFB2 (2) against IAA6, IAA6$^{C78R/shy1-1}$, IAA6^{P76S}, IAA19 and IAA19$^{P76S/msg2-1}$ on 10, 50 or 100 µM 1-naphthaleneacetic acid (NAA), 4-chloroindole-3-acetic acid (4-Cl IAA), 2,4-dichlorophenoxyacetic acid (2,4-D), or indole-3-butyric acid (IBA). β-galactosidase reporter expression indicates auxin-induced TIR1/AFB1/AFB2-AUX/IAA interactions.

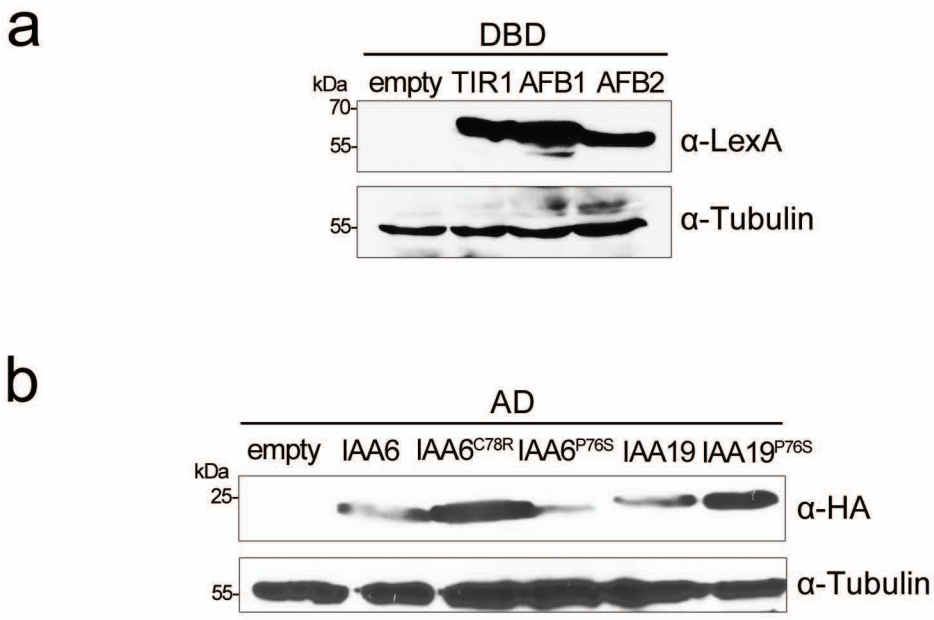

Supplementary Figure 4. (**a**) Immunoblots of LexA tagged -TIR1, -AFB1, -AFB2; and (**b**) HA tagged -IAA6, -IAA6$^{C78R/shy1-1}$, -IAA6^{P76S}, -IAA19, and -IAA19$^{P76S/msg2-1}$ proteins. TIR1, AFB1, AFB2, as well as AUX/IAA fusion proteins screened for auxin dependent interactions in yeast diploids are well expressed, and repetitive experiments (n>4) consistently showed that interactions (see **Fig. 1c and Supplementary Fig. 3**) are unlikely to be dependent upon fusion protein expression levels in yeast. Total proteins were extracted from yeast diploids grown on Gal/Raff -Ura-His-Trp and detected using either anti-HA (F-7) (Santa Cruz, SC7392) or anti-LexA (Abcam, AB14553) antibodies. Yeast α-Tubulin was detected with anti-Tubulin antibody (Abcam, AB6160) and used as loading control.

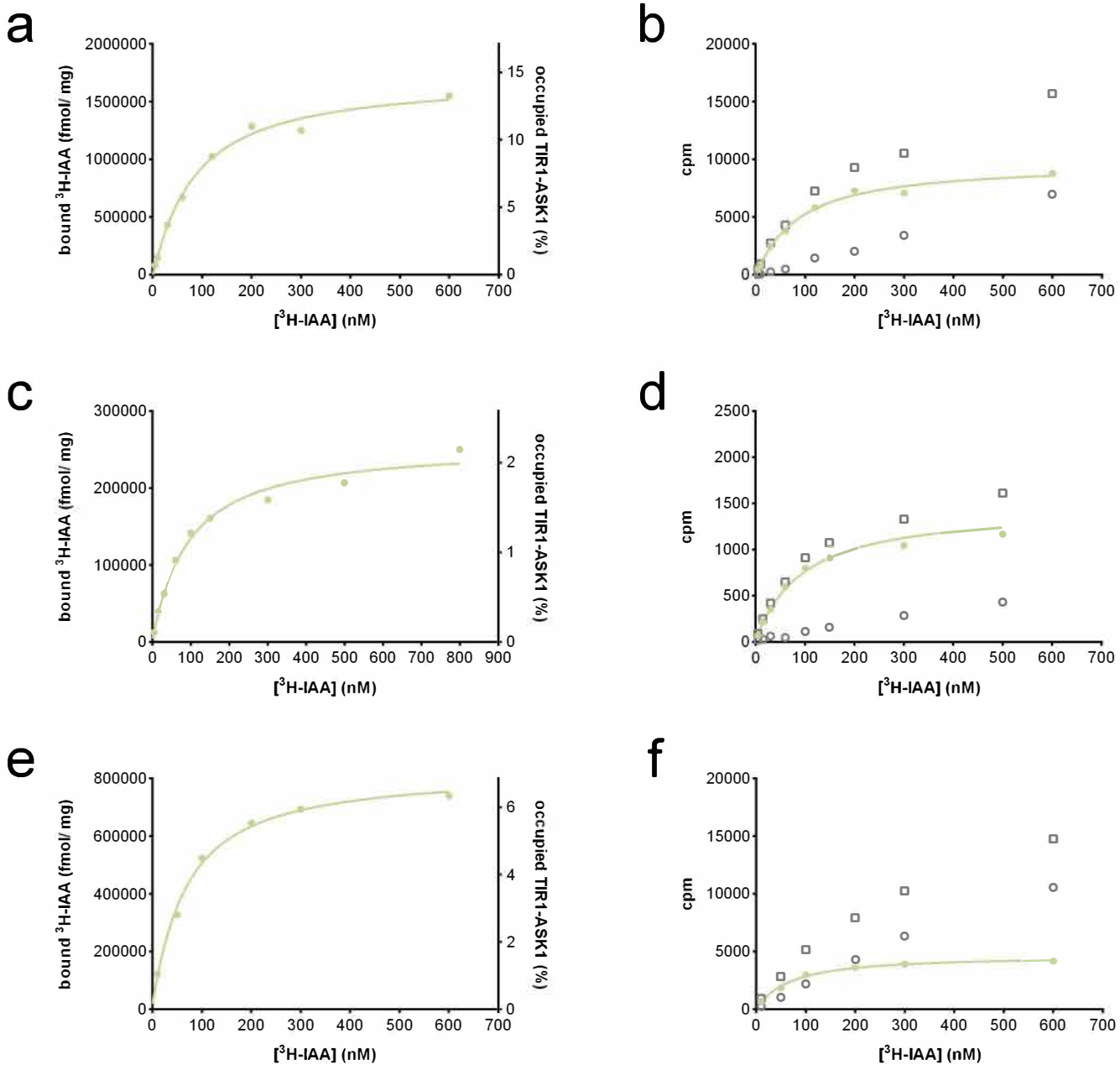

Supplementary Figure 5. Individual saturation binding experiments for the TIR1-IAA6 auxin co-receptor system. (**a, c, e**) Specific binding of IAA to TIR1-ASK1, expressed as either femtomol IAA bound per one milligram TIR1-ASK1 (left Y-axis) or fraction of TIR1 stably binding IAA (right Y-axis), was calculated assuming a 60% efficiency of the liquid scintillation counter and a molecular weight of 85.0 kDa for TIR1-ASK1. (**b, d, f**) Total, non-specific and specific binding (empty squares, empty circles and dots) shown as mean raw cpm data from two technical replicates. Specific binding was fitted to the Morrison model (**a-f**). Obtained K_d values are (74.0 ± 19.2) nM (**a, b**), (83.7 ± 18.3) nM (**c, d**) and (58.2 ± 13.6) nM (**e, f**).

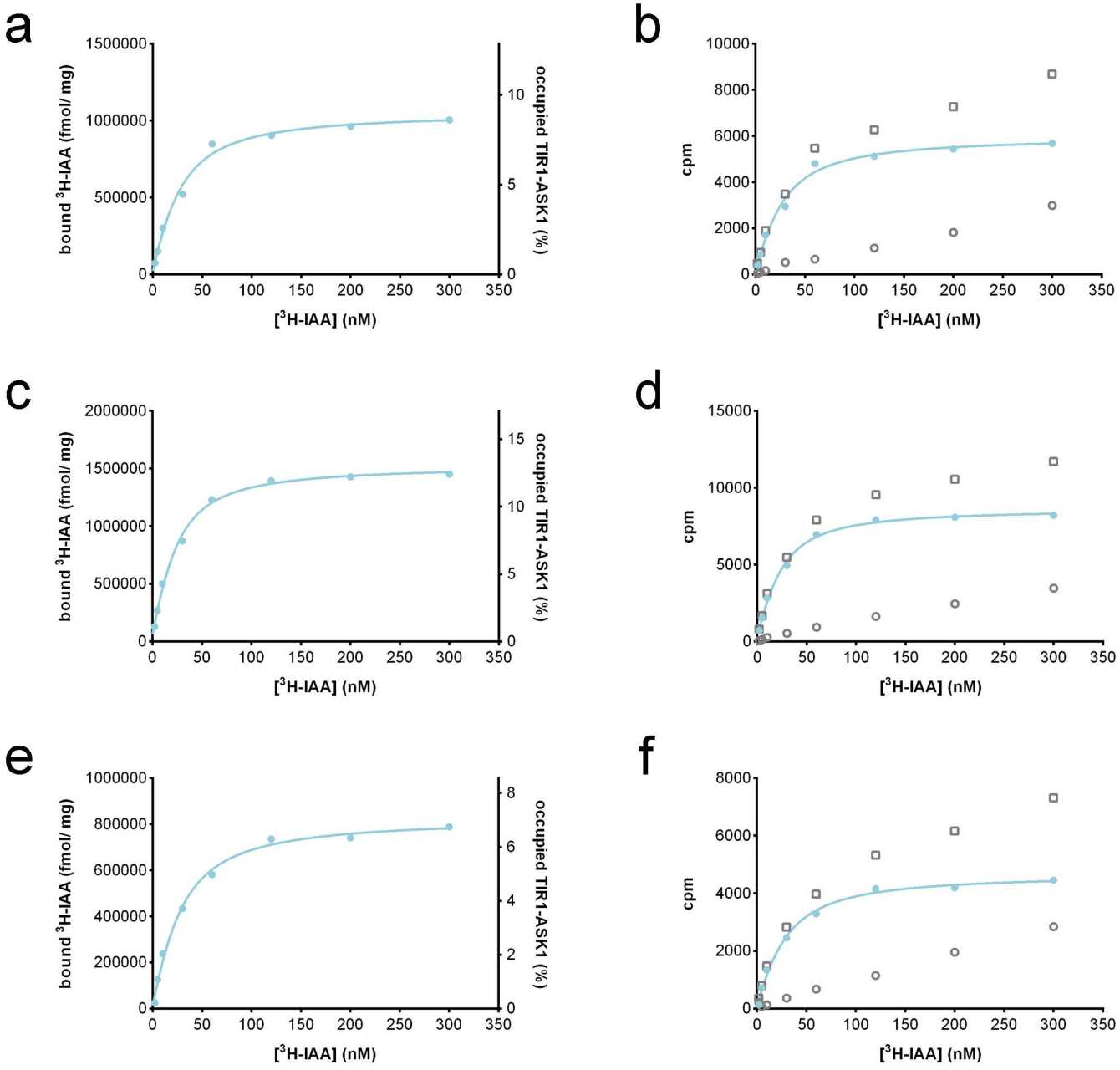

Supplementary Figure 6. Individual saturation binding experiments for the TIR1-IAA19 auxin co-receptor system. (**a, c, e**) Specific binding of IAA to TIR1-ASK1, expressed as either femtomol IAA bound per one milligram TIR1-ASK1 (left Y-axis), or fraction of TIR1 stably binding IAA (right Y-axis), was calculated assuming a 60% efficiency of the liquid scintillation counter and a molecular weight of 85.0 kDa for TIR1-ASK1. (**b, d, f**) Total, non-specific and specific binding (empty squares, empty circles and dots, respectively) shown as mean raw cpm data from two technical replicates. Specific binding was fitted to the Morrison model (**a-f**). Obtained K_d values are (16.4 ± 4.4) nM (**a, b**), (12.8 ± 3.0) nM (**c, d**) and (17.6 ± 2.9) nM (**e, f**).

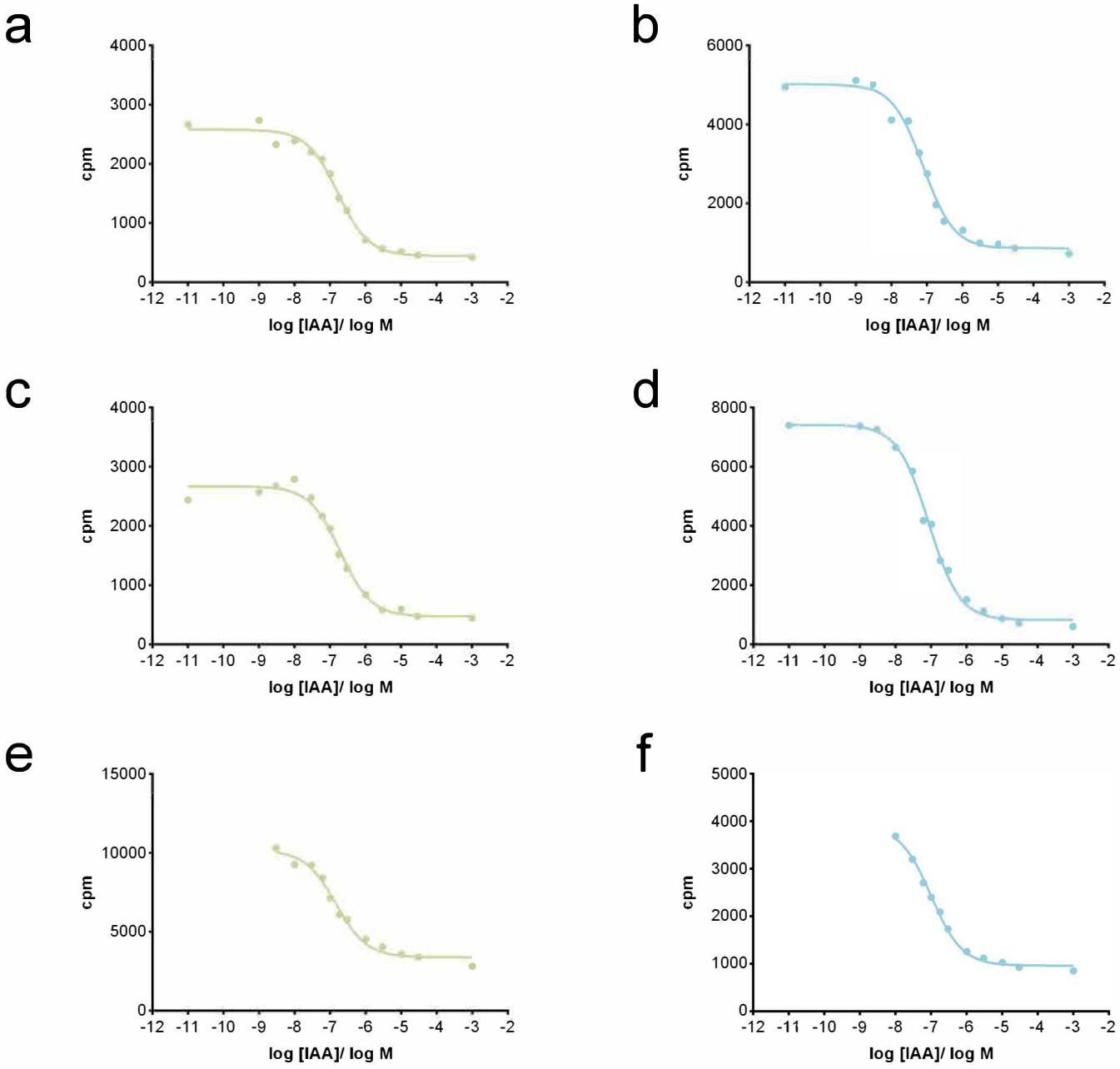

Supplementary Figure 7. Individual homologous competition binding experiments for TIR1-IAA6 and TIR1-IAA19 auxin co-receptors. Non-radioactive IAA was titrated to pre-formed TIR1-IAA6 (**a, c, e**) or TIR1-IAA19 (**b, d, f**) co-receptors bound to radioactive IAA. Resulting data are depicted as mean raw cpm data from two technical replicates were fitted to the built-in one site - logIC_{50} equation (GraphPad, Prism). K_i values were calculated according to the Cheng-Prusoff equation. K_i values for TIR1-IAA6 (**a**,**c**,**e**), and TIR1-IAA19 (**b**,**d**,**f**) are: 98.0 nM (**a**), 114.5 nM (**c**), 85.4 nM (**e**); and 29.7 nM (**b**), 32.3 nM (**d**), 38.5 nM (**f**).

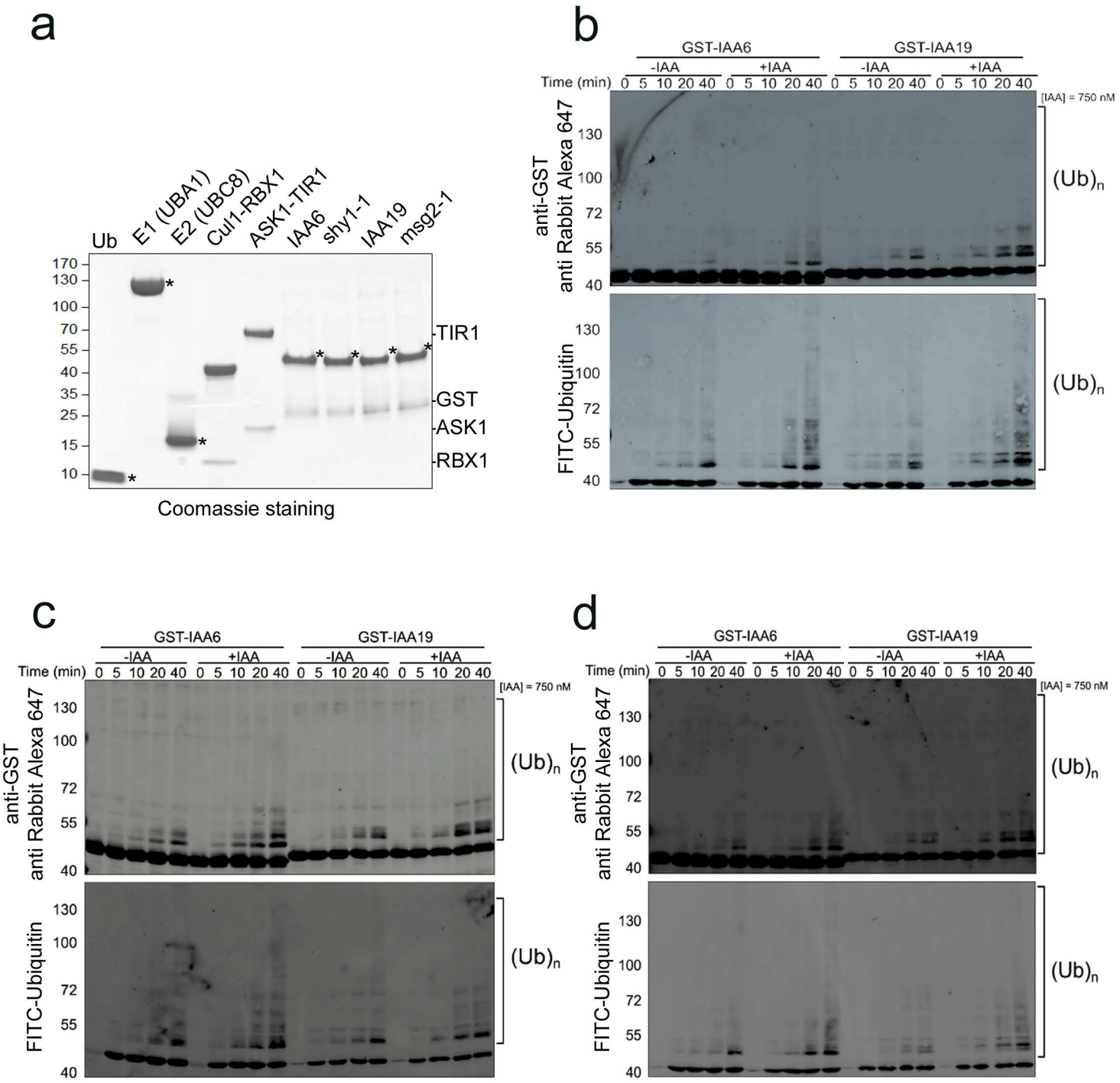

Supplementary Figure 8. (**a**) Coomassie staining of an SDS-gradient 4-12% gel depicting quality of proteins (~5 µg) incorporated in IVU reactions. (**b-d**) Replicate blots from 3 independent IVUs used for quantification in **Figure 2c**. Fluorescein-labeled ubiquitin signals of individual lanes were quantified using ImageQuant TL software. Shown are immunoblots for either direct ubiquitin detection (bottom) or AUX/IAA detection using α-GST and α-rabbit Alexa Fluor Plus 647 antibodies (see **Methods** for additional information). (**d**) Immunoblots correspond to **Figure 2c** in gray scale. (**e and f**) continued in next page.

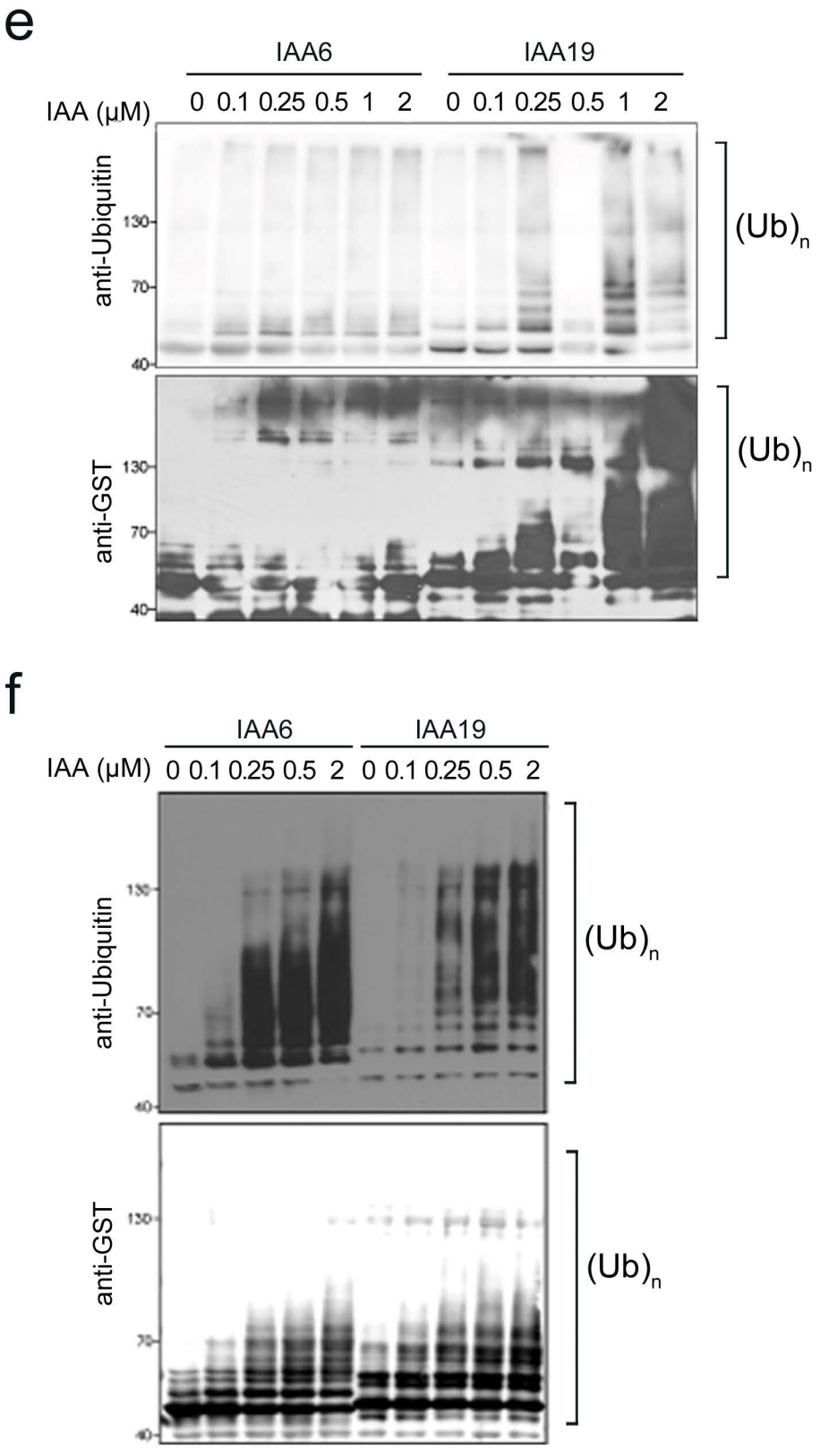

Supplementary Figure 8 continued. (**e and f**) Replicates showing auxin induced ubiquitylation of GST-IAA6 and GST-IAA19 (**see Figure 2d**). AUX/IAA ubiquitylated species were detected using α-Ub (P4D1) antibody and α-GST antibody.

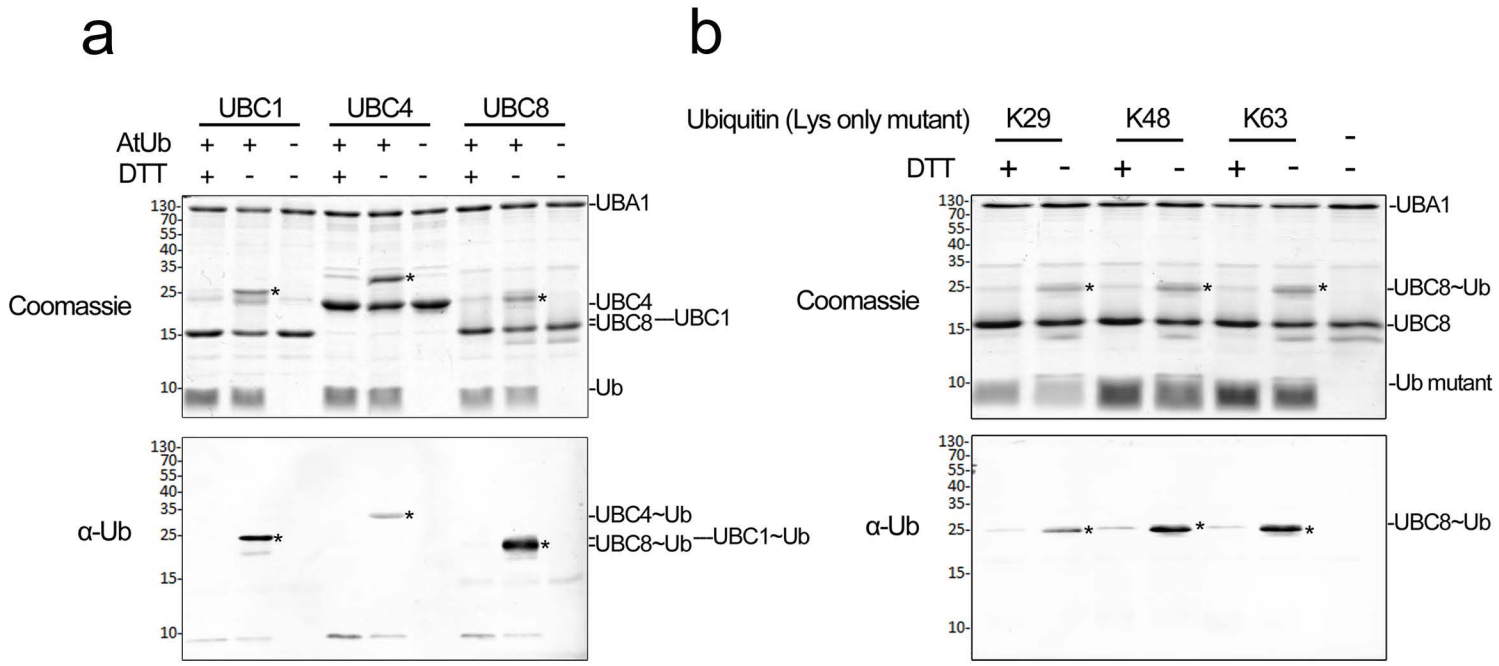

Supplementary Figure 9. ATP-dependent ubiquitin charging assays of Arabidopsis E2-ubiquitin conjugating enzymes used in this study. (**a**) UBC1, UBC4, and UBC8 charging assays show recombinantly expressed AtE2s are functional and can be Ub-charged *in vitro*. Asterisks indicate Ub-charged E2s (UBCx~Ub). (**b**) UBC8 can form a thioester bond with *Hs*Ubiquitin mutants containing only one lysine (Lys) residue available, namely K29, K48 or K63, while other Lys have been mutated to Arg. E2 (UBC8)-charging reactions were performed as described in the **Methods** section.

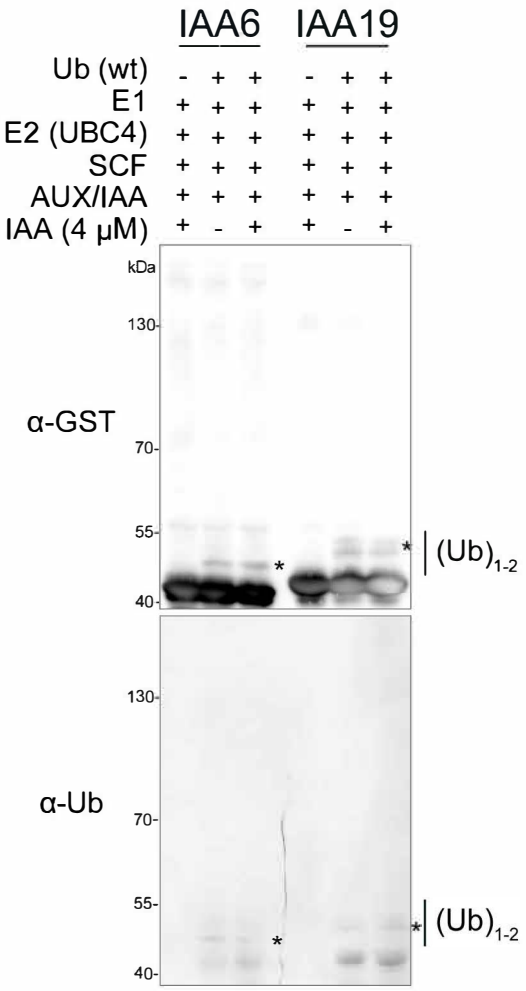

Supplementary Figure 10. UBC4 Ub-conjugating enzyme (E2) does not mediate poly-Ub-conjugation of IAA6 or IAA19 *in vitro*. As a result of 30 min IVU assays for IAA6 and IAA19, only low molecular ubiquitin conjugates, possibly monoubiquitin or diubiquitin (Ub_{1-2}), have been consistently detected with anti-GST and anti-Ub antibodies (*).

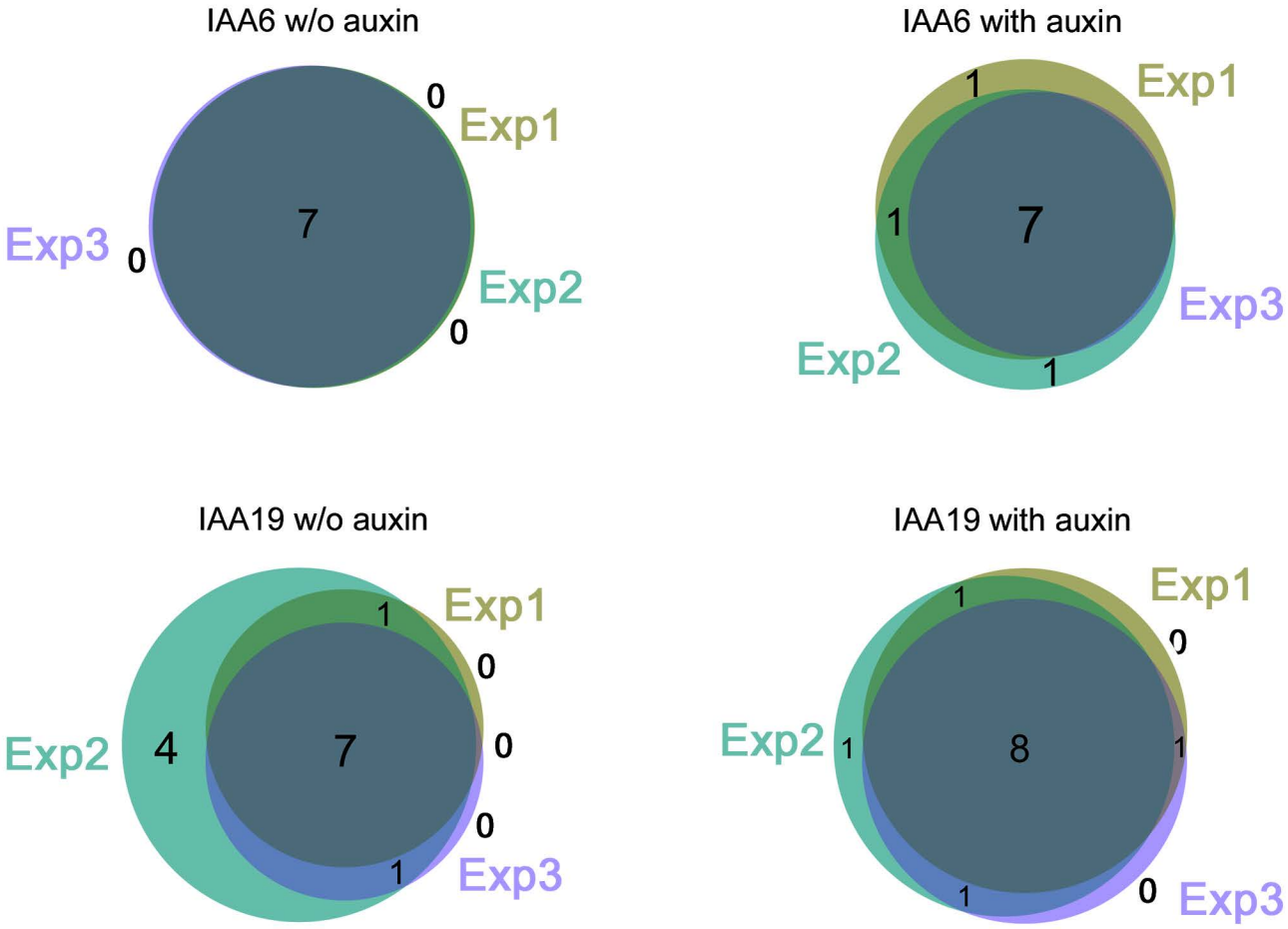

Supplementary Figure 11. Venn diagrams indicating the reproducibility in the identification of IAA6 and IAA19 ubiquitylated peptides upon three independent biological IVU reactions (Exp 1-3) with or without auxin followed by LC-MS analyses.

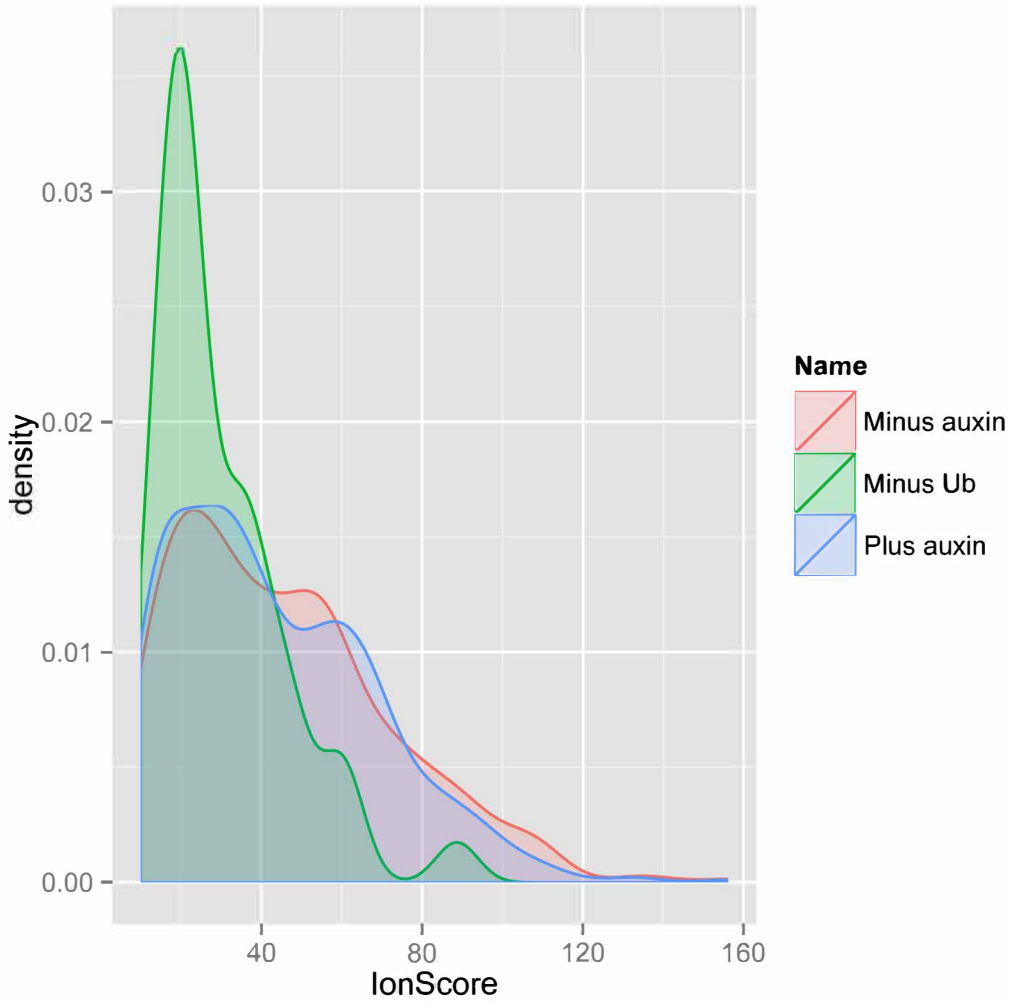

Supplementary Figure 12. Calculated false discovery rate (FDR) for IAA6 or IAA19 ubiquitylated peptides identified via LC-MS. Kernel density estimation of the PSMs (see **Supplementary Tables 1-2**) with a GG- modification identified in IVUs lacking Ub (Minus Ub), or containing Ub (supplemented with AUX/IAA or not, Plus Auxin, Minus Auxin respectively). FDR was calculated as described in the Methods section. An ion score of below 20 corresponded to an FDR threshold of 0.05 ($q<0.05$) for IVUs containing Ub and supplemented with auxin. The same ion score corresponded to an FDR threshold of 0.07 for IVUs containing Ub and not supplemented with auxin.

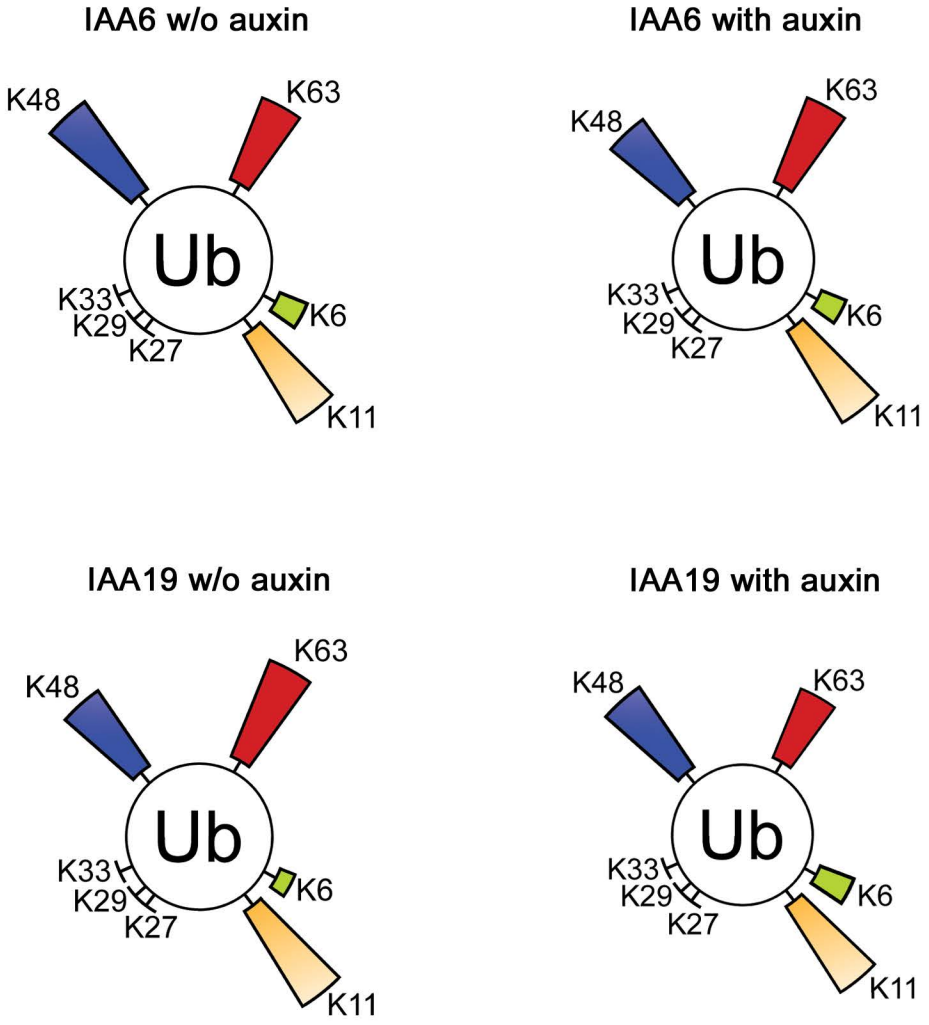

Supplementary Figure 13. Distribution of identified ubiquitin linkage types. *In vitro* ubiquitylation reactions for IAA6 (top) and IAA19 (bottom) were analyzed via LC-MS, and ubiquitin peptides corresponding to different ubiquitin linkage types were identified. A comparison of the number of peptide spectrum matches (PSMs) (see **Supplementary Tables 1-2** and PRIDE repository via ProteomeXchange with identifier PXD004027) for each of the ubiquitylated lysine residues in ubiquitin was used as a semi-quantitative index for determining the abundance of each linkage type in the reactions without or with auxin (4 μM IAA). Depicted values for a specific linkage type were calculated as the percentage of the total number of PSMs corresponding to diGly-/LRGG-modified ubiquitin peptides. All peptides assigned to contain the Ub remnant (diGly or LRGG) on non-canonical residues were excluded. No K27, K29 nor K33 linkages were detected in these reactions using UBC8 as E2-ubiquitin conjugating enzyme.

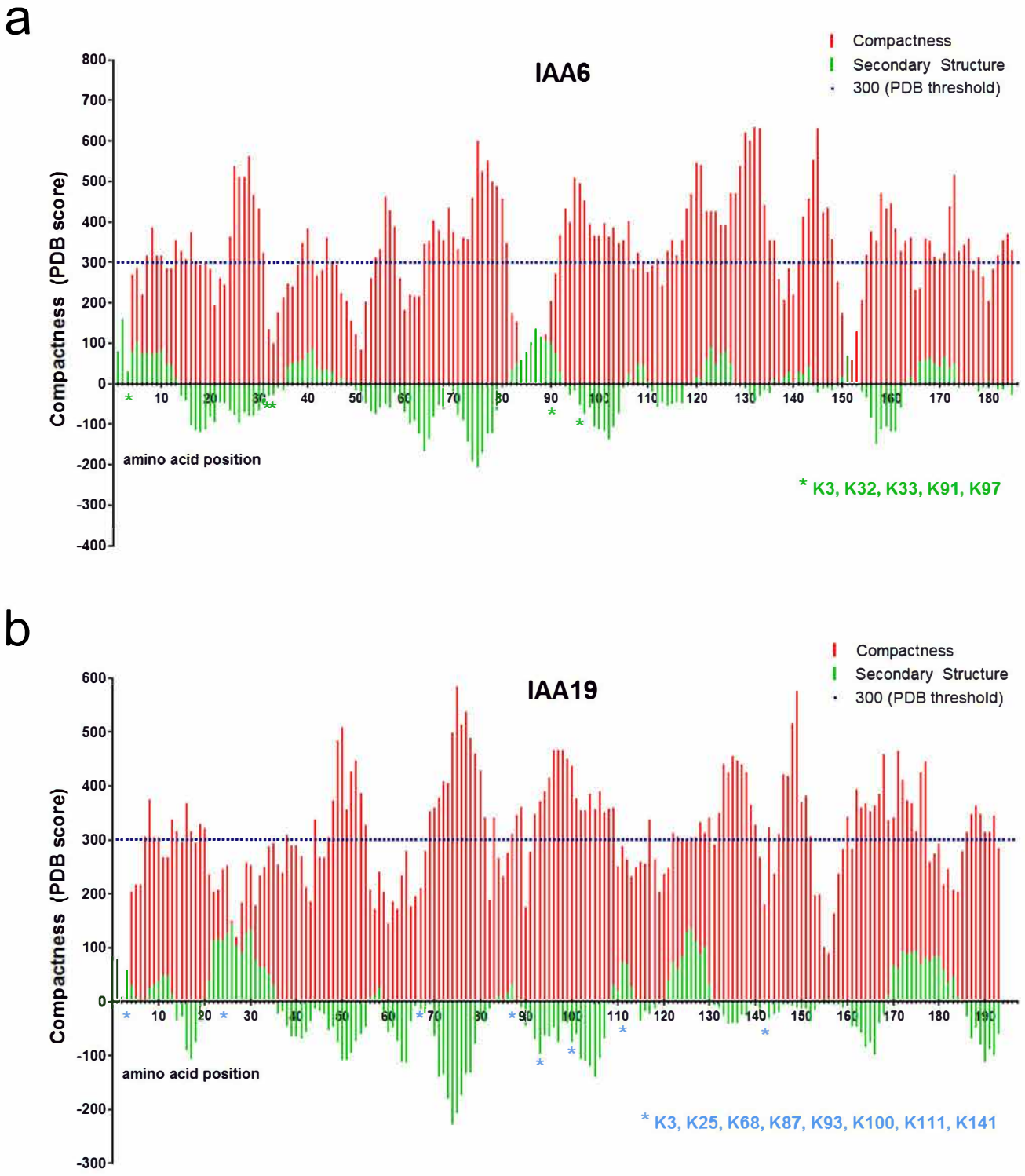

Supplementary Figure 14. (a-b) Meta structure analyses for Arabidopsis IAA6 **(a)** and IAA19 **(b)**, exhibiting features of intrinsically disordered proteins (IDPs) with regions of lower compactness. The threshold level in compactness is 300 (DisProt data base), while sequence regions that are significantly lower are flexible and open, amino acid segments above threshold can be considered classically folded. In secondary structure positive values denote alpha-helical regions, negative values beta sheets. Asterisks depict ubiquitylated sites identified via MS upon IVU reactions (for reference see **Supplementary Tables 1-2**).

c

d

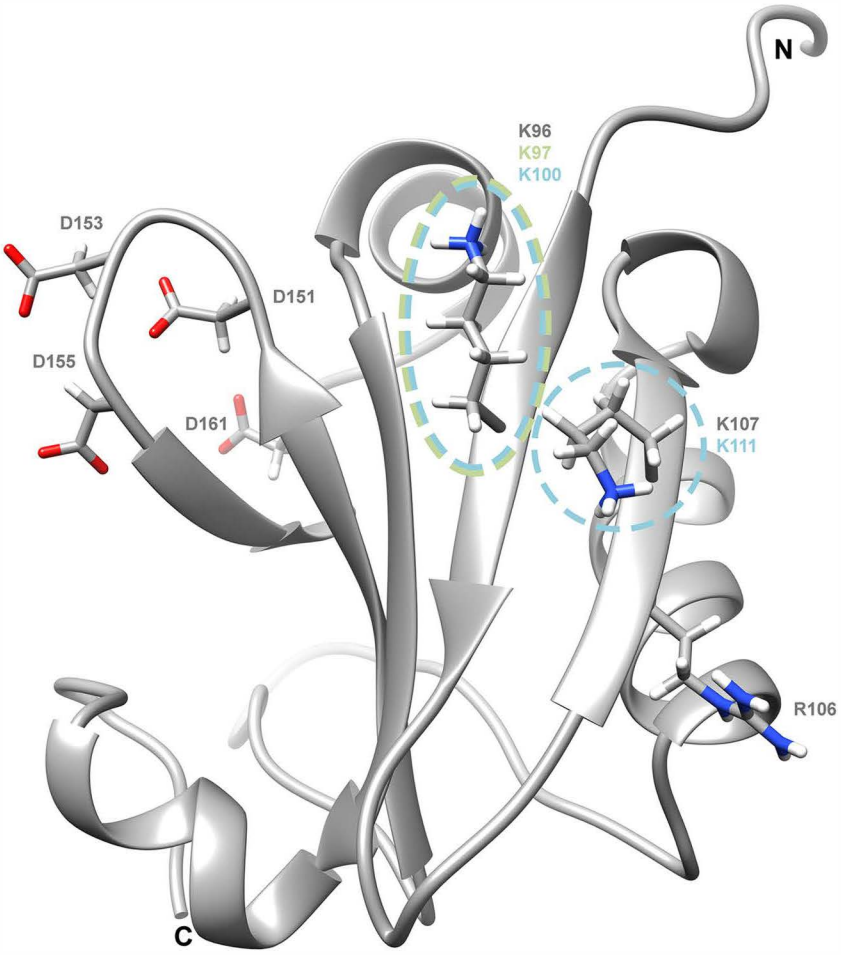

Supplementary Figure 14 continued. **(c-d)** Interface residues crucial for AUX/IAA and ARF homo- and hetero-dimerization are targeted for ubiquitylation *in vitro*. (**c**) MAFFT alignment of *A. thaliana At*IAA6, *At*IAA19 and *Pisum sativum Ps*IAA4. IAA6 and IAA19 residues found to be ubiquitylated by UBC8 in vitro are highlighted in green and blue, respectively. K97 of IAA6, and K100 as well as K111 of IAA19 are part of the basic patch in the AUX/IAA PB1 domain (Dinesh et al. PNAS 2015). (**d**) Structural representation of the acidic (D151, D153, D155, D161) and basic (K96, R106, K107) patches in the PB1 domain of PsIAA4, PDB: 2M1M). Ubiquitylation of K97 of IAA6 (green ellipse) and K100 and K111 of IAA19 (blue ellipses) could interfere with proper dimerization of IAA6 and IAA19 with other AUX/IAAs and/or ARFs.

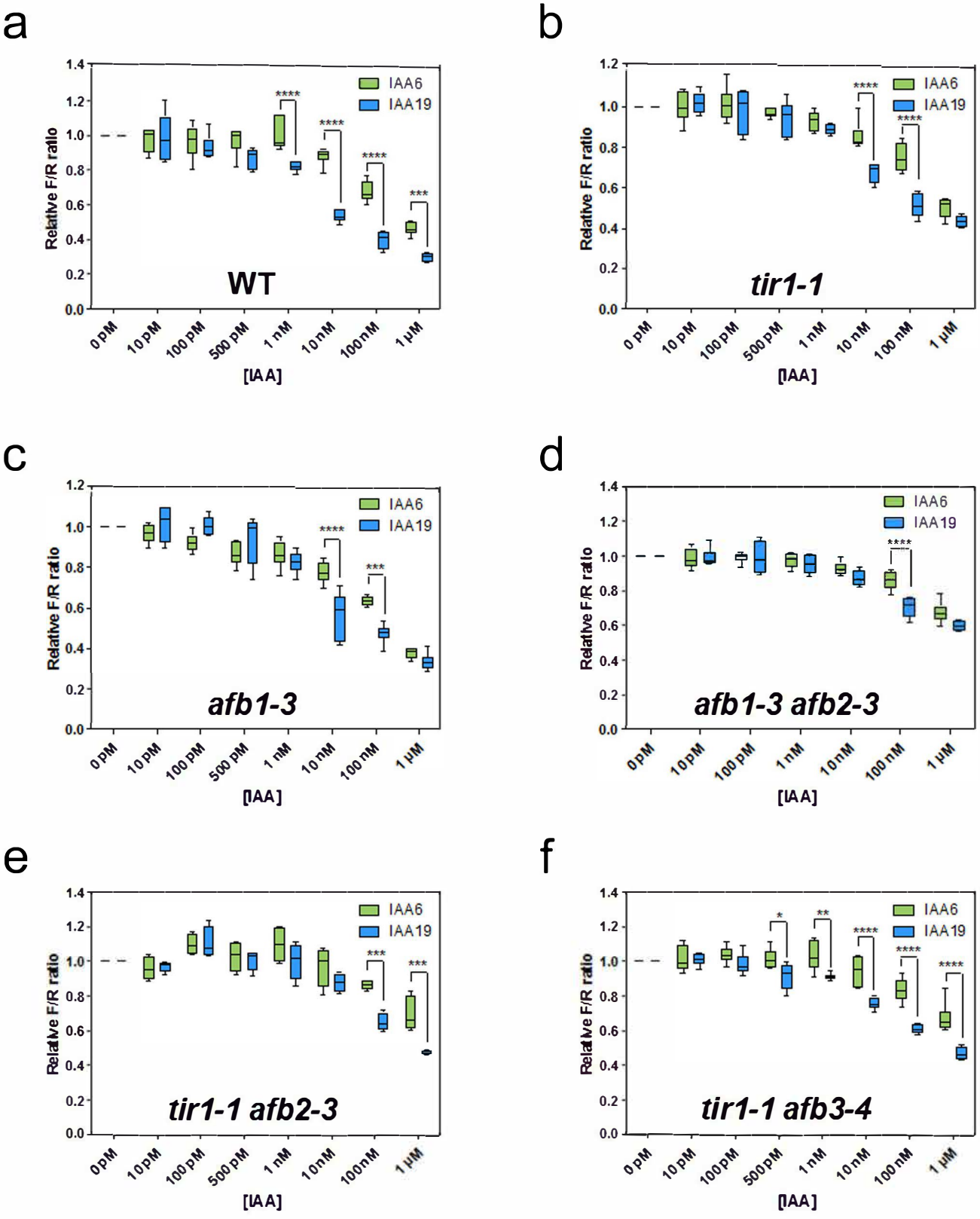

Supplementary Figure 15. Quantitative characterization of IAA6 and IAA19 sensor variants in different genetic backgrounds of *Arabidopsis* leaf protoplasts, namely from *Col-0 (WT)* (**a**), as well as *tir1-1* (**b**), *afb1-3* (**c**), *afb1-3 afb2-3* (**d**), *tir1-1 afb2-3* (**e**), and *tir1-1 afb3-4* (**f**) mutant plants. Decrease in F/R ratios is a measure of sensor degradation after 30 min incubation with various IAA concentrations. Results are means +/- s.e.m. of biological replicates (n=6). Statistical significances were calculated via two-way ANOVA with P<0.05 (*), P<0.01(**), P<0.001 (***), and P<0.0001 (****).

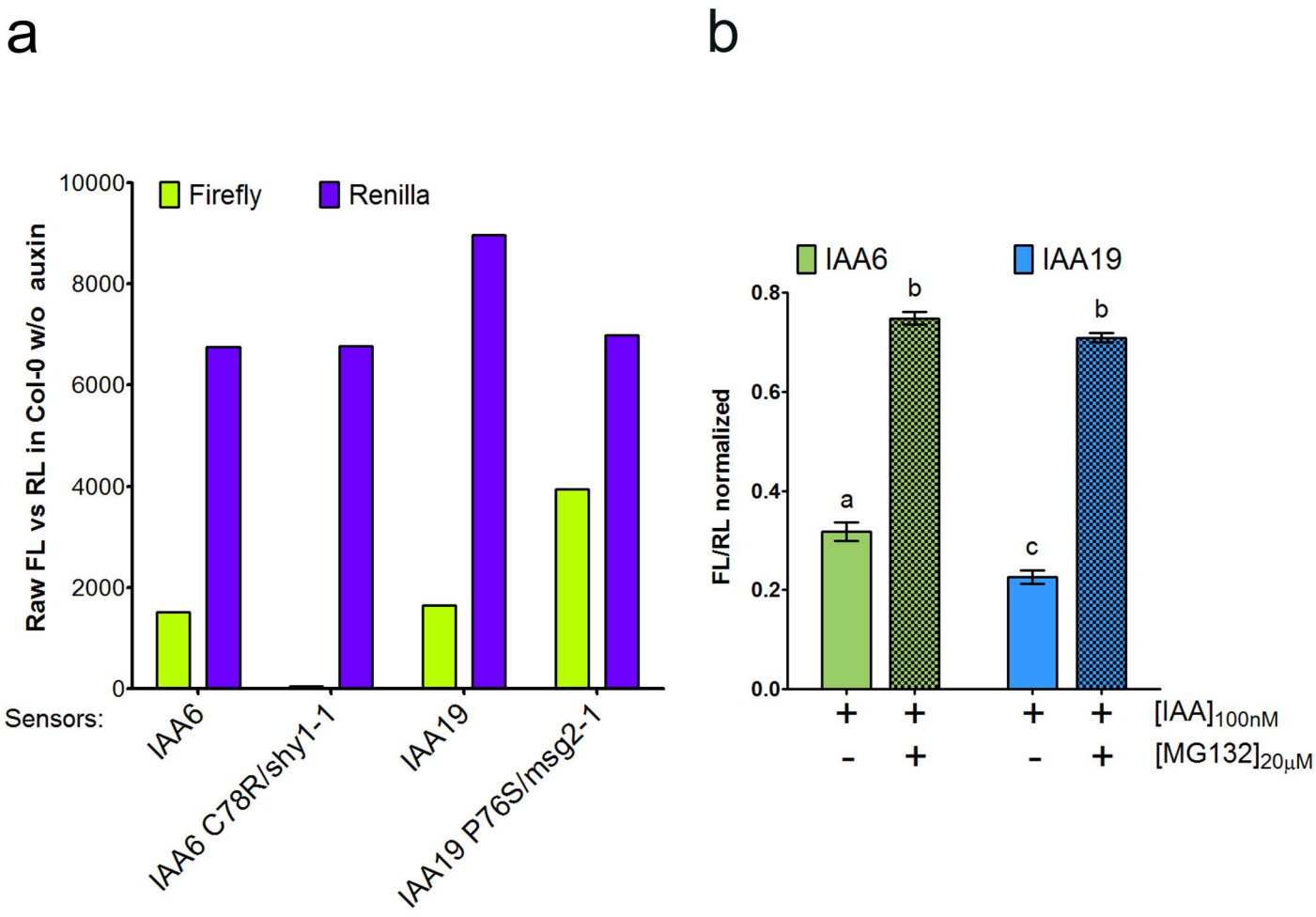

Supplementary Figure 16. (**a**) Raw values of Firefly luciferase (FL) -fused IAA6, IAA6$^{C78R/shy1-1}$, IAA19, IAA19$^{P76S/msg2-1}$ sensors and Renilla luciferase (RL) fluorescence of the normalization element in *Col-0* protoplasts without exogenous IAA treatment. While IAA6, IAA19, and IAA19$^{P76S/msg2-1}$ sensors are similarly expressed, IAA6$^{C78R/shy1-1}$ sensor is highly unstable and not suitable for ratiometric analyses. (**b**) Ratiometric analysis of IAA6 and IAA19 sensors in protoplasts of *Col-0 (WT)* plants are degraded in response to 100 nM IAA and stabilized upon combined treatment of IAA and 20 μM proteasome inhibitor MG132. Error bars, s.e.m. Different letters denote statistically significant differences as assessed by two-way ANOVA with $P<0.001$, $P>0.05$ (n.s.).

Supplementary Table 1. IAA6 ubiquitylated peptides identified in LC-MS analyses

IAA6 w/o Auxin

		Mascot			MaxQuant						
Sequence	# PSMs	Modifications	IonScore	Exp Value	Modifications	Score	PEP*	MH+ [Da]	Charge	m/z [Da]	RT	Exp
AGFMAKEGLALEITELR	6	K6(di-Gl)	78	3.14019E-07	K6(di-Gl)	101	1.53E-16	1963.0252	3	655.0132	67.64	1
AIGYVKVSMDGVPYMR	1	K6(di-Gl)	58	3.29577E-05	K6(di-Gl)	69	3.50E-07	1899.9508	3	633.9885	57.37	1
KAGFMAKEGLALEITELR	2	K7(di-Gl)	26	0.044766853	K7(di-Gl)	43	7.78E-05	2091.1251	4	523.5367	57.96	1
LGLPGDNYSEISVCGSSKK	4	C14(Carbamidomethyl); K19(di-Gl)	77	3.82786E-07	C14(Carbamidomethyl); K18(di-Gl)	71	2.88E-24	2125.0210	2	1063.0142	47.49	1
LGLPGDNYSEISVCGSSKKK	6	C14(Carbamidomethyl); K20(di-Gl)	37	0.003597134	C14(Carbamidomethyl); K18(di-Gl)	83	5.54E-27	2253.1139	3	751.7130	41.33	1
NNEEASKAIGYVK	3	K7(di-Gl)	92	1.31207E-08	K7(di-Gl)	102	4.29E-14	1536.7666	2	768.8856	30.79	1
AGFMAKEGLALEITELR	4	K6(di-Gl)	78	2.99886E-07	K6(di-Gl)	108	2.79E-18	1963.0272	3	655.0139	67.44	2
AIGYVKVSMDGVPYMR	1	K6(di-Gl)	46	0.00055457	K6(di-Gl)	50	0.00012455	1899.9364	3	633.9836	57.71	2
KAGFMAKEGLALEITELR	1	K7(di-Gl)	14	0.856952141	n.d.	n.d.	n.d.	2091.1228	4	523.5362	58.53	2
LGLPGDNYSEISVCGSSKK	4	C14(Carbamidomethyl); K19(di-Gl)	105	6.20807E-10	C14(Carbamidomethyl); K18(di-Gl)	104	5.47E-37	2125.0191	2	1063.0132	48.02	2
LGLPGDNYSEISVCGSSKK	2	C14(Carbamidomethyl); K18(LRGG)	19	0.279226459	n.d.	n.d.	n.d.	2394.2069	4	599.3072	43.57	2
LGLPGDNYSEISVCGSSKKK	3	C14(Carbamidomethyl); K18(di-Gl); K19(di-Gl)	21	0.155223177	C14(Carbamidomethyl); K18(di-Gl); K19(di-Gl)	43	7.86E-17	2367.1559	4	592.5444	41.21	2
LGLPGDNYSEISVCGSSKKK	6	C14(Carbamidomethyl); K18(di-Gl)	48	0.000305462	C14(Carbamidomethyl); K18(di-Gl)	83	7.86E-17	2253.1149	3	751.7099	41.27	2
NNEEASKAIGYVK	3	K7(di-Gl)	92	1.30004E-08	K7(di-Gl)	101	2.05E-13	1536.7624	2	768.8840	31.13	2
AGFMAKEGLALEITELR	4	K6(di-Gl)	72	1.34573E-06	K6(di-Gl)	63	5.08E-07	1963.0292	3	655.0146	68.24	3
AIGYVKVSMDGVPYMR	1	K6(di-Gl)	29	0.02582002	K6(di-Gl)	69	3.92E-07	1899.9406	3	633.9850	58.05	3
KAGFMAKEGLALEITELR	2	K7(di-Gl)	25	0.069655685	K7(di-Gl)	n.d.	n.d.	2091.1278	4	523.5374	58.55	3
LGLPGDNYSEISVCGSSKK	4	C14(Carbamidomethyl); K19(di-Gl)	83	9.54897E-08	C14(Carbamidomethyl); K18(di-Gl)	92	1.94E-16	2125.0210	3	709.0118	48.10	3
LGLPGDNYSEISVCGSSKK	2	C14(Carbamidomethyl); K18(LRGG)	38	0.003012705	C14(Carbamidomethyl); K18(LRGG)	62	1.94E-16	2394.2085	3	798.7410	43.84	3
LGLPGDNYSEISVCGSSKKK	6	C14(Carbamidomethyl); K18(di-Gl)	45	0.000642623	C14(Carbamidomethyl); K18(di-Gl)	65	5.26E-20	2253.1203	3	751.7128	41.66	3
LGLPGDNYSEISVCGSSKKK	2	C14(Carbamidomethyl); K18(di-Gl); K19(di-Gl)	16	0.519943997	C14(Carbamidomethyl); K18(di-Gl); K19(di-Gl)	42	5.26E-20	2367.1513	4	592.5433	41.57	3
NNEEASKAIGYVK	2	K7(di-Gl)	92	1.23867E-08	K7(di-Gl)	122	9.80E-13	1536.7674	2	768.8873	31.29	3

IAA6 with 4 µM IAA

		Mascot			MaxQuant						
Sequence	# PSMs	Modifications	IonScore	Exp Value	Modifications	Score	PEP*	MH+ [Da]	Charge	m/z [Da]	RT	Exp
AGFMAKEGLALEITELR	7	K6(di-Gl)	83	9.95306E-08	K6(di-Gl)	106	2.77E-16	1963.0272	3	655.0139	71.26	1
AIGYVKVSMDGVPYMR	1	K6(di-Gl)	62	1.2559E-05	K6(di-Gl)	77	5.87E-07	1899.9461	3	633.9869	57.51	1
KAGFMAKEGLALEITELR	2	K7(di-Gl)	30	0.019676895	n.d.	n.d.	n.d.	2091.1239	4	523.5364	57.94	1
KIDLGSSNSYINLVTVLENLFGCLGIGVAK	1	K1(di-Gl); C23(Carbamidomethyl)	37	0.004374784	n.d.	n.d.	n.d.	3308.7418	3	1103.5854	120.04	1
KNNEEASKAIGYVK	2	K8(di-Gl)	37	0.003908018	K8(di-Gl)	70	6.75E-06	1664.8572	3	555.6239	24.18	1
LGLPGDNYSEISVCGSSKK	6	C14(Carbamidomethyl); K19(di-Gl)	74	7.85157E-07	C14(Carbamidomethyl); K18(di-Gl)	84	9.73E-23	2125.0242	2	1063.0157	47.74	1
LGLPGDNYSEISVCGSSKKK	3	C14(Carbamidomethyl); K18(di-Gl); K19(di-Gl)	24	0.088299159	C14(Carbamidomethyl); K18(di-Gl); K19(di-Gl)	60	3.87E-25	2367.1574	4	592.5448	41.06	1
LGLPGDNYSEISVCGSSKKK	3	C14(Carbamidomethyl); K18(di-Gl)	38	0.003364779	C14(Carbamidomethyl); K18(di-Gl)	119	3.87E-25	2253.1144	4	564.0341	41.18	1
NNEEASKAIGYVK	4	K7(di-Gl)	81	1.62913E-07	K7(di-Gl)	93	1.15E-08	1536.7672	2	768.8866	30.86	1
AGFMAKEGLALEITELR	5	K6(di-Gl)	90	1.90527E-08	K6(di-Gl)	103	3.30E-45	1963.0240	2	982.0156	67.84	2
AIGYVKVSMDGVPYMR	1	K6(di-Gl)	45	0.000617955	K6(di-Gl)	80	3.15E-08	1899.9382	3	633.9843	58.23	2
KAGFMAKEGLALEITELR	4	K7(di-Gl)	85	6.0528E-08	K7(di-Gl)	84	7.35E-09	2091.1244	4	523.5366	58.60	2
KCEYIIIYEDKDR	1	K1(di-Gl); C2(Carbamidomethyl)	20	0.185761867	K1(di-Gl); C2(Carbamidomethyl)	47	7.72E-12	1858.8969	3	620.3038	38.53	2
LGLPGDNYSEISVCGSSKK	8	C14(Carbamidomethyl); K19(di-Gl)	85	6.71362E-08	C14(Carbamidomethyl); K19(di-Gl)	57	2.06E-10	2125.0218	2	1063.0145	48.14	2
LGLPGDNYSEISVCGSSKKK	11	C14(Carbamidomethyl); K19(di-Gl)	39	0.002517425	C14(Carbamidomethyl); K19(di-Gl)	95	6.45E-14	2253.1163	3	751.7095	41.23	2
LGLPGDNYSEISVCGSSKKK	3	C14(Carbamidomethyl); K18(LRGG)	22	0.13211635	C14(Carbamidomethyl); K18(LRGG); K19(di-Gl)	63	6.45E-14	2522.3004	5	505.2659	38.40	2
LGLPGDNYSEISVCGSSKKK	9	C14(Carbamidomethyl); K18(di-Gl); K20(di-Gl)	43	0.000924606	C14(Carbamidomethyl); K18(di-Gl); K19(di-Gl)	95	6.45E-14	2367.1516	3	789.7233	41.15	2
NNEEASKAIGYVK	3	K7(di-Gl)	92	1.36131E-08	K7(di-Gl)	141	5.06E-16	1536.7632	2	768.8849	31.41	2
AGFMAKEGLALEITELR	6	K6(di-Gl)	84	8.78935E-08	K6(di-Gl)	84	1.36E-11	1963.0259	3	655.0135	69.77	3
KAGFMAKEGLALEITELR	4	K7(di-Gl)	72	1.27338E-06	K7(di-Gl)	81	1.30E-09	2091.1288	3	697.7151	58.42	3
KNNEEASKAIGYVK	2	K8(di-Gl)	30	0.02055685	n.d.	n.d.	n.d.	1664.8606	3	555.6251	24.30	3
LGLPGDNYSEISVCGSSKK	6	C14(Carbamidomethyl); K18(di-Gl)	83	1.01148E-07	C14(Carbamidomethyl); K18(di-Gl)	88	2.89E-13	2125.0206	3	709.0117	47.75	3
LGLPGDNYSEISVCGSSKK	2	C14(Carbamidomethyl); K18(LRGG)	42	0.00130004	C14(Carbamidomethyl); K18(LRGG)	34	2.89E-13	2394.2085	3	798.7410	43.56	3
LGLPGDNYSEISVCGSSKKK	6	C14(Carbamidomethyl); K18(di-Gl)	42	0.001180203	C14(Carbamidomethyl); K18(di-Gl)	63	7.78E-10	2253.1177	3	751.7108	41.33	3
LGLPGDNYSEISVCGSSKKK	3	C14(Carbamidomethyl); K18(di-Gl); K19(di-Gl)	21	0.170591178	C14(Carbamidomethyl); K18(di-Gl); K19(di-Gl)	63	7.78E-10	2367.1601	4	592.5455	41.13	3
LGLPGDNYSEISVCGSSKKK	3	C14(Carbamidomethyl); K18(LRGG)	21	0.146877939	C14(Carbamidomethyl); K18(LRGG)	17	7.78E-10	2522.3024	5	505.2663	37.97	3
NNEEASKAIGYVK	1	K7(di-Gl)	72	1.29705E-06	K7(di-Gl)	142	3.71E-37	1536.7665	3	512.9270	31.29	3
NNEEASKAIGYVK	1	K7(LRGG)	16	0.509279938	K7(LRGG)	58	3.71E-37	1805.9509	4	452.2432	29.27	3

*PEP: Posterior error probability
n.d. : not detected

Supplementary Table 2. IAA19 ubiquitylated peptides identified in LC-MS analyses

IAA19 w/o Auxin

		Mascot			MaxQuant							
Sequence	# PSMs	Modifications	IonScore	Exp Value	Modifications	Score	PEP	MH+ [Da]	Charge	m/z [Da]	RT	Exp
AGFMEKEGLGLEITELR	1	M4(Oxidation); K6(di-Gl)	43	0.001016147	M4(Oxidation); K6(di-Gl)	56	1.40E-24	2023.0063	3	675.0070	59.26	1
AGFMEKEGLGLEITELR	1	K6(di-Gl)	53	9.93E-05	K6(di-Gl)	69	1.40E-24	2007.0161	3	669.6769	64.69	1
EASTTKVGLGYVK	1	K6(LRGG)	29	0.023656831	K6(LRGG)	20	0.00095458	1735.9674	4	434.7473	29.65	1
KAGFMEKEGLGLEITELR	2	K7(di-Gl)	51	0.000167478	n.d.	n.d.	n.d.	2135.1066	3	712.3737	55.77	1
KMDLGSSQGYDDLAFALDK	1	K1(LRGG)	66	5.31E-06	K1(LRGG)	81	1.75E-246	2457.2028	4	615.0562	57.59	1
KMDLGSSQGYDDLAFALDK	2	K1(di-Gl); M2(Oxidation)	74	8.09E-07	K1(di-Gl); M2(Oxidation)	67	1.75E-246	2204.0151	3	735.3432	58.72	1
KMDLGSSQGYDDLAFALDK	4	K1(di-Gl)	156	5.12E-15	K1(di-Gl)	190	1.75E-246	2188.0196	2	1094.5134	63.66	1
LGLPGRDVAEKMMK	1	K11(di-Gl)	16	0.558414348	K11(di-Gl)	50	2.86E-06	1658.8687	3	553.6278	43.92	1
VGLGYVKVSMDGVPYLR	1	K7(di-Gl)	64	8.63E-06	K7(di-Gl)	128	3.75E-31	1967.0354	3	656.3500	65.19	1
VNDSPAAKSQVVGWPPVCSYR	2	K8(di-Gl); C18(Carbamidomethyl)	60	1.87E-05	K8(di-Gl); C18(Carbamidomethyl)	75	1.64E-13	2431.1748	3	811.0631	51.52	1
AGFMEKEGLGLEITELR	1	M4(Oxidation); K6(di-Gl)	33	0.009659543	M4(Oxidation); K6(di-Gl)	29	9.57E-80	2023.0147	3	675.0098	59.56	2
AGFMEKEGLGLEITELR	2	K6(di-Gl)	53	9.79E-05	K6(di-Gl)	62	9.57E-80	2007.0192	3	669.6779	65.13	2
DVAEKMMK	4	K5(di-Gl); M7(Oxidation)	16	0.497687311	K5(di-Gl); M7(Oxidation)	79	6.03E-07	1081.5008	2	541.2540	16.86	2
DVAEKMMKK	2	K5(di-Gl); K8(di-Gl)	20	0.190966227	K5(di-Gl); K8(di-Gl)	52	0.00067398	1307.6402	2	654.3237	20.18	2
EASTTKVGLGYVK	2	K6(LRGG)	29	0.02666592	K6(LRGG)	40	4.98E-06	1735.9709	4	434.7476	29.79	2
EASTTKVGLGYVK	1	K6(di-Gl)	14	0.751547732	K6(di-Gl)	32	4.98E-06	1466.7848	3	489.5998	33.28	2
GIGVALKDGDNCEYVTIYEDK	1	K7(di-Gl); C12(Carbamidomethyl)	85	6.68E-08	K7(di-Gl); C12(Carbamidomethyl)	54	4.69E-40	2473.1561	3	825.0569	58.68	2
KAGFMEKEGLGLEITELR	2	K1(di-Gl); K7(di-Gl)	59	2.58E-05	K1(di-Gl); K7(di-Gl)	68	3.73E-44	2249.1555	3	750.3900	55.76	2
KMDLGSSQGYDDLAFALDK	1	K1(LRGG)	64	8.41E-06	K1(LRGG)	87	7.38E-113	2457.2072	4	615.0573	58.01	2
KMDLGSSQGYDDLAFALDK	3	K1(di-Gl); M2(Oxidation)	94	7.89E-09	K1(di-Gl); M2(Oxidation)	95	7.38E-113	2204.0151	3	735.3432	59.09	2
KMDLGSSQGYDDLAFALDK	4	K1(di-Gl)	134	8.43E-13	K1(di-Gl)	148	7.38E-113	2188.0218	2	1094.5145	64.18	2
LGLPGRDVAEKMMK	3	K11(di-Gl)	19	0.250009533	K11(di-Gl)	82	1.44E-10	1658.8703	4	415.4730	44.53	2
NSCKEASTTKVGLGYVK	1	C3(Carbamidomethyl); K4(di-Gl); K10(di-Gl)	72	1.16E-06	n.d.	n.d.	n.d.	2070.0320	3	690.6822	27.69	2
NSCKEASTTKVGLGYVK	2	C3(Carbamidomethyl); K10(di-Gl)	24	0.082216043	n.d.	n.d.	n.d.	1955.9884	4	489.7526	26.8	2
VGLGYVKVSMDGVPYLR	1	K7(LRGG)	16	0.463400575	n.d.	n.d.	n.d.	2236.2211	4	559.8107	59.82	2
VGLGYVKVSMDGVPYLR	1	K7(di-Gl)	57	3.97E-05	K7(di-Gl)	97	1.26E-18	1967.0398	3	656.3514	65.51	2
VNDSPAAKSQVVGWPPVCSYR	2	K8(LRGG); C18(Carbamidomethyl)	32	0.013550539	n.d.	n.d.	n.d.	2700.3656	4	675.8469	46.98	2
VNDSPAAKSQVVGWPPVCSYR	3	K8(di-Gl); C18(Carbamidomethyl)	60	1.95E-05	K8(di-Gl); C18(Carbamidomethyl)	82	1.65E-17	2431.1762	3	811.0636	51.56	2
AGFMEKEGLGLEITELR	2	K6(di-Gl)	102	1.15E-09	K6(di-Gl)	139	4.29E-175	2007.0162	2	1004.0117	65.28	3
EASTTKVGLGYVK	1	K6(di-Gl)	34	0.007942488	K6(di-Gl)	27	1.35E-09	1466.7843	3	489.5996	32.31	3
EASTTKVGLGYVK	1	K6(LRGG)	15	0.587430604	n.d.	n.d.	n.d.	1735.9710	4	434.7482	29.98	3
KMDLGSSQGYDDLAFALDK	2	K1(di-Gl)	136	4.99E-13	K1(di-Gl)	165	8.41E-97	2188.0228	2	1094.5150	64.22	3
KMDLGSSQGYDDLAFALDK	1	K1(LRGG)	47	0.000386328	K1(LRGG)	116	8.41E-97	2457.2079	4	615.0574	58.04	3
LGLPGRDVAEKMMK	1	K11(di-Gl)	16	0.534510903	K11(di-Gl)	80	3.17E-06	1658.8698	3	553.6281	44.54	3
NSCKEASTTKVGLGYVK	2	C3(Carbamidomethyl); K10(di-Gl)	29	0.022592098	n.d.	n.d.	n.d.	1955.9857	4	489.7519	26.69	3
VGLGYVKVSMDGVPYLR	1	K7(di-Gl)	45	0.000612289	K7(di-Gl)	74	6.70E-09	1967.0350	3	656.3499	65.59	3
VNDSPAAKSQVVGWPPVCSYR	2	K8(di-Gl); C18(Carbamidomethyl)	58	3.20E-05	K8(di-Gl); C18(Carbamidomethyl)	110	1.82E-22	2431.1788	3	811.0645	52.07	3

IAA19 with 4 µM IAA

		Mascot			MaxQuant							
Sequence	# PSMs	Modifications	IonScore	Exp Value	Modifications	Score	PEP	MH+ [Da]	Charge	m/z [Da]	RT	Exp
AGFMEKEGLGLEITELR	1	M4(Oxidation); K6(di-Gl)	73	1.10E-06	M4(Oxidation); K6(di-Gl)	58	1.13E-50	2023.0136	3	675.0094	58.99	1
AGFMEKEGLGLEITELR	2	K6(LRGG)	23	0.111932594	K6(LRGG)	36	1.13E-50	2276.2140	4	569.8090	58.88	1
AGFMEKEGLGLEITELR	3	K6(di-Gl)	84	7.55E-08	K6(di-Gl)	92	1.13E-50	2007.0154	2	1004.0114	64.48	1
DVAEKMMK	8	M6(Oxidation); K8(di-Gl)	22	0.115068531	n.d.	n.d.	n.d.	1081.4987	2	541.2537	17.58	1
EASTTKVGLGYVK	2	K6(LRGG)	26	0.053574308	K6(LRGG)	27	8.78E-07	1735.9676	4	434.7473	29.53	1
GIGVALKDGDNCEYVTIYEDK	3	K7(di-Gl); C12(Carbamidomethyl)	104	7.87E-10	K7(di-Gl); C12(Carbamidomethyl)	38	2.63E-41	2473.1471	3	825.0539	57.72	1
KAGFMEKEGLGLEITELR	4	K7(di-Gl)	65	6.44E-06	K7(di-Gl)	113	2.26E-40	2135.1125	4	534.5336	55.69	1
KAGFMEKEGLGLEITELR	2	K1(di-Gl); K7(di-Gl)	100	1.81E-09	K1(di-Gl); K7(di-Gl)	142	2.26E-40	2249.1522	3	750.3889	55.6	1
KMDLGSSQGYDDLAFALDK	1	K1(LRGG)	59	2.71E-05	K1(LRGG)	100	2.01E-194	2457.2045	4	615.0566	57.49	1
KMDLGSSQGYDDLAFALDK	6	K1(di-Gl); M2(Oxidation)	94	7.13E-09	K1(di-Gl); M2(Oxidation)	79	2.01E-194	2204.0136	3	735.3427	58.56	1
KMDLGSSQGYDDLAFALDK	5	K1(di-Gl)	156	5.03E-15	K1(di-Gl)	204	2.01E-194	2188.0203	2	1094.5138	63.62	1
NSCKEASTTKVGLGYVK	2	C3(Carbamidomethyl); K4(di-Gl); K10(di-Gl)	46	0.000493124	C3(Carbamidomethyl); K4(di-Gl); K10(di-Gl)	57	1.03E-06	2070.0229	3	690.6791	27.3	1
VGLGYVKVSMDGVPYLR	1	K7(di-Gl); M10(Oxidation)	26	0.053945667	K7(di-Gl); M10(Oxidation)	24	1.34E-39	1983.0351	3	661.6832	58.18	1

Supplementary Table 2 continued. IAA19 ubiquitylated peptides identified in LC-MS analyses

IAA19 with 4 µM IAA

		Mascot			MaxQuant							
Sequence	# PSMs	Modifications	IonScore	Exp Value	Modifications	Score	PEP	MH+ [Da]	Charge	m/z [Da]	RT	Exp
VGLGYVKVSMDGVPYLR	2	K7(di-Gl)	88	3.03E-08	K7(di-Gl)	142	1.34E-39	1967.0392	2	984.0233	64.91	1
VNDSPAAKSQVVGWPPVCSYR	5	K8(di-Gl); C18(Carbamidomethyl)	66	4.61E-06	K8(di-Gl); C18(Carbamidomethyl)	89	1.64E-17	2431.1762	3	811.0636	51.35	1
AGFMEKEGLGLEITELR	1	K6(di-Gl)	62	1.39E-05	K6(di-Gl)	114	2.15E-113	2007.0187	3	669.6777	65.17	2
EASTTKVGLGYVK	2	K6(di-Gl)	45	0.00058608	K6(di-Gl)	39	4.04E-07	1466.7840	3	489.5995	32.11	2
EASTTKVGLGYVK	2	K6(LRGG)	26	0.051045395	K6(LRGG)	26	4.04E-07	1735.9694	4	434.7478	29.75	2
GIGVALKDGDNCEYVTIYEDK	1	K7(di-Gl); C12(Carbamidomethyl)	62	1.27E-05	K7(di-Gl); C12(Carbamidomethyl)	37	3.63E-104	2473.1556	3	825.0567	58.26	2
KMDLGSSQGYDDLAFALDK	2	K1(di-Gl)	117	3.89E-11	K1(di-Gl)	194	2.38E-114	2188.0218	2	1094.5145	64.21	2
KMDLGSSQGYDDLAFALDK	2	K1(di-Gl); M2(Oxidation)	93	8.95E-09	K1(di-Gl); M2(Oxidation)	101	2.38E-114	2204.0167	3	735.3438	59.03	2
KMDLGSSQGYDDLAFALDK	2	K1(LRGG)	84	8.15E-08	K1(LRGG)	122	2.38E-114	2457.2045	3	819.7397	58.12	2
LGLPGRDVAEKMMK	2	K11(di-Gl)	13	0.988454239	K11(di-Gl)	52	0.00017596	1658.8719	2	829.9396	44.6	2
NSCKEASTTKVGLGYVK	5	C3(Carbamidomethyl); K10(di-Gl)	55	6.81E-05	C3(Carbamidomethyl); K10(di-Gl)	80	8.73E-10	1955.9851	4	489.7523	26.77	2
NSCKEASTTKVGLGYVK	1	C3(Carbamidomethyl); K4(di-Gl); K10(di-Gl)	14	0.79059956	C3(Carbamidomethyl); K4(di-Gl); K10(di-Gl)	26	8.73E-10	2070.0285	4	518.2626	27.89	2
VGLGYVKVSMDGVPYLR	1	K7(di-Gl)	60	2.00E-05	K7(di-Gl)	105	5.87E-17	1967.0425	3	656.3524	65.5	2
VNDSPAAKSQVVGWPPVCSYR	2	K8(di-Gl); C18(Carbamidomethyl)	60	1.91E-05	K8(di-Gl); C18(Carbamidomethyl)	120	8.62E-28	2431.1806	3	811.0651	51.98	2
VNDSPAAKSQVVGWPPVCSYR	1	K8(LRGG); C18(Carbamidomethyl)	15	0.608074188	K8(LRGG); C18(Carbamidomethyl)	18	8.62E-28	2700.3666	4	675.8471	46.77	2
AGFMEKEGLGLEITELR	1	K6(di-Gl)	60	1.79E-05	K6(di-Gl)	89	1.19E-96	2007.0157	3	669.6768	65.49	3
EASTTKVGLGYVK	1	K6(di-Gl)	58	3.31E-05	K6(di-Gl)	39	1.12E-05	1466.7834	3	489.5993	32.81	3
EASTTKVGLGYVK	2	K6(LRGG)	24	0.074637411	K6(LRGG)	28	3.94E-28	1735.9707	4	434.7481	30.39	3
GIGVALKDGDNCEYVTIYEDK	1	K7(di-Gl); C12(Carbamidomethyl)	65	7.08E-06	K7(di-Gl); C12(Carbamidomethyl)	48	1.48E-63	2473.1545	3	825.0563	58.65	3
KMDLGSSQGYDDLAFALDK	2	K1(di-Gl)	130	1.88E-12	K1(di-Gl)	191	5.11E-115	2188.0247	2	1094.5160	64.52	3
KMDLGSSQGYDDLAFALDK	1	K1(di-Gl); M2(Oxidation)	66	4.93E-06	K1(di-Gl); M2(Oxidation)	71	5.11E-115	2204.0083	3	735.3409	59.74	3
NSCKEASTTKVGLGYVK	4	C3(Carbamidomethyl); K10(di-Gl)	37	0.003980674	C3(Carbamidomethyl); K10(di-Gl)	45	0.00046473	1955.9811	3	652.6652	27.23	3
NSCKEASTTKVGLGYVK	1	C3(Carbamidomethyl); K4(di-Gl); K10(di-Gl)	36	0.004644688	C3(Carbamidomethyl); K4(di-Gl); K10(di-Gl)	31	0.00046473	2070.0324	3	690.6823	28.22	3
VGLGYVKVSMDGVPYLR	1	K7(di-Gl)	63	1.01E-05	K7(di-Gl)	93	1.22E-11	1967.0387	3	656.3511	65.95	3
VNDSPAAKSQVVGWPPVCSYR	3	K8(di-Gl); C18(Carbamidomethyl)	60	2.04E-05	K8(di-Gl); C18(Carbamidomethyl)	91	8.32E-15	2431.1812	3	811.0653	52.53	3

Supplementary Note 1

Population genetic and gene expression analyses

AtGenExpress[1] (http://jsp.weigelworld.org/AtGenExpress/resources/), and *Arabidopsis* eFP[2] (http://www.bar.utoronto.ca/) browsers were used to retrieve and compare *A. thaliana* expression profiles for *IAA6* and *IAA19* in different natural accessions[3], and developmental stages, as well as different tissues including: root cells types[4, 5], microgametogenesis[6], embryo development[7], flowers[3], xylem & cork[8], guard & mesophyll cells[9], stem epidermis[10], stigma & ovaries[11], pollen germination[12], shot apical[13], trichomes[14, 15].

References

1. Schmid, M. *et al.* A gene expression map of Arabidopsis thaliana development. *Nat Genet* **37**, 501-506 (2005).
2. Winter, D. *et al.* An "Electronic Fluorescent Pictograph" browser for exploring and analyzing large-scale biological data sets. *PLoS One* **2**, e718 (2007).
3. Lempe, J. *et al.* Diversity of flowering responses in wild Arabidopsis thaliana strains. *PLoS Genet* **1**, 109-118 (2005).
4. Birnbaum, K. *et al.* A gene expression map of the Arabidopsis root. *Science* **302**, 1956-1960 (2003).
5. Nawy, T. *et al.* Transcriptional profile of the Arabidopsis root quiescent center. *Plant Cell* **17**, 1908-1925 (2005).
6. Honys, D. & Twell, D. Transcriptome analysis of haploid male gametophyte development in Arabidopsis. *Genome Biol* **5**, R85 (2004).
7. Casson, S., Spencer, M., Walker, K. & Lindsey, K. Laser capture microdissection for the analysis of gene expression during embryogenesis of Arabidopsis. *Plant J* **42**, 111-123 (2005).
8. Zhao, C., Craig, J.C., Petzold, H.E., Dickerman, A.W. & Beers, E.P. The xylem and phloem transcriptomes from secondary tissues of the Arabidopsis root-hypocotyl. *Plant Physiol* **138**, 803-818 (2005).
9. Yang, Y., Costa, A., Leonhardt, N., Siegel, R.S. & Schroeder, J.I. Isolation of a strong Arabidopsis guard cell promoter and its potential as a research tool. *Plant Methods* **4**, 6 (2008).
10. Suh, M.C. *et al.* Cuticular lipid composition, surface structure, and gene expression in Arabidopsis stem epidermis. *Plant Physiol* **139**, 1649-1665 (2005).

11. Swanson, R., Clark, T. & Preuss, D. Expression profiling of Arabidopsis stigma tissue identifies stigma-specific genes. *Sexual Plant Reproduction* **18**, 163-171 (2005).
12. Qin, Y. *et al.* Penetration of the stigma and style elicits a novel transcriptome in pollen tubes, pointing to genes critical for growth in a pistil. *PLoS Genet* **5**, e1000621 (2009).
13. Yadav, R.K., Girke, T., Pasala, S., Xie, M. & Reddy, G.V. Gene expression map of the Arabidopsis shoot apical meristem stem cell niche. *Proc Natl Acad Sci U S A* **106**, 4941-4946 (2009).
14. Gilding, E.K. & Marks, M.D. Analysis of purified glabra3-shapeshifter trichomes reveals a role for NOECK in regulating early trichome morphogenic events. *Plant J* **64**, 304-317 (2010).
15. Marks, M.D., Wenger, J.P., Gilding, E., Jilk, R. & Dixon, R.A. Transcriptome analysis of Arabidopsis wild-type and gl3-sst sim trichomes identifies four additional genes required for trichome development. *Mol Plant* **2**, 803-822 (2009).

7.2 Supplementary Information for 2.2 Niemeyer M. *et al.* (2020)

Supplementary Information

Flexibility of intrinsically disordered degrons in AUX/IAA proteins reinforces auxin co-receptor assemblies

Niemeyer *et al.*

Supplementary Figures 1-15

Supplementary Tables 1-3

Supplementary Methods

Supp. Fig. 1

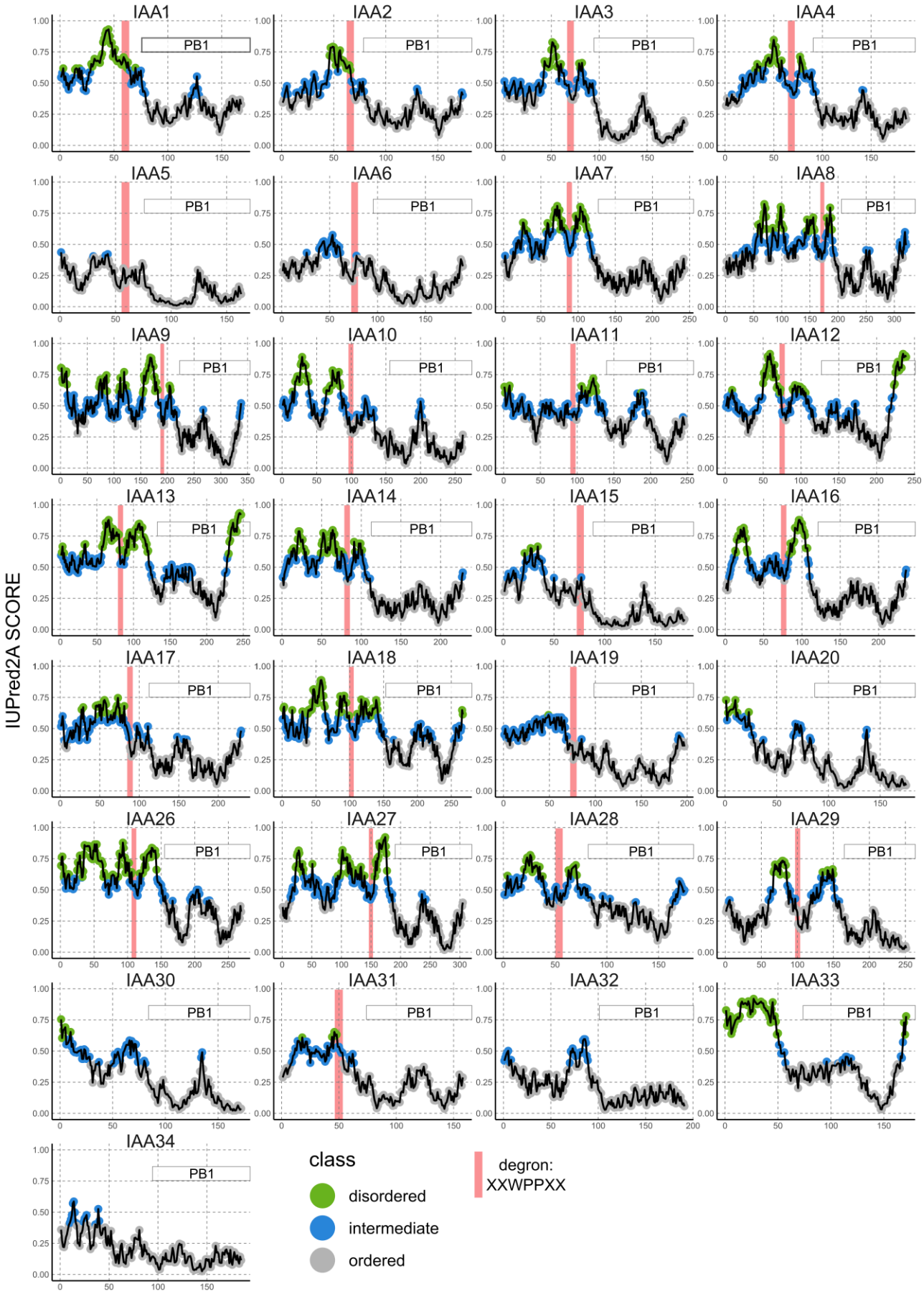

Supplementary Figure 1| IUPred2A disorder prediction along the sequence of *Arabidopsis thaliana* AUX/IAA proteins. The x-axis corresponds to the full length of each AUX/IAA protein sequence, and the y-axis shows the IUPred2A score for each amino acid (probability between 0-1). Amino acid residues are colored according to their disorder probability (disordered: ≥ 0.6, green; intermediate: 0.4-0.6, blue and ordered: ≤0.4, gray). The resolved, ordered PB1 domain is located along the sequence, as indicated, starting with the conserved VKV motif.

Supp. Fig. 2

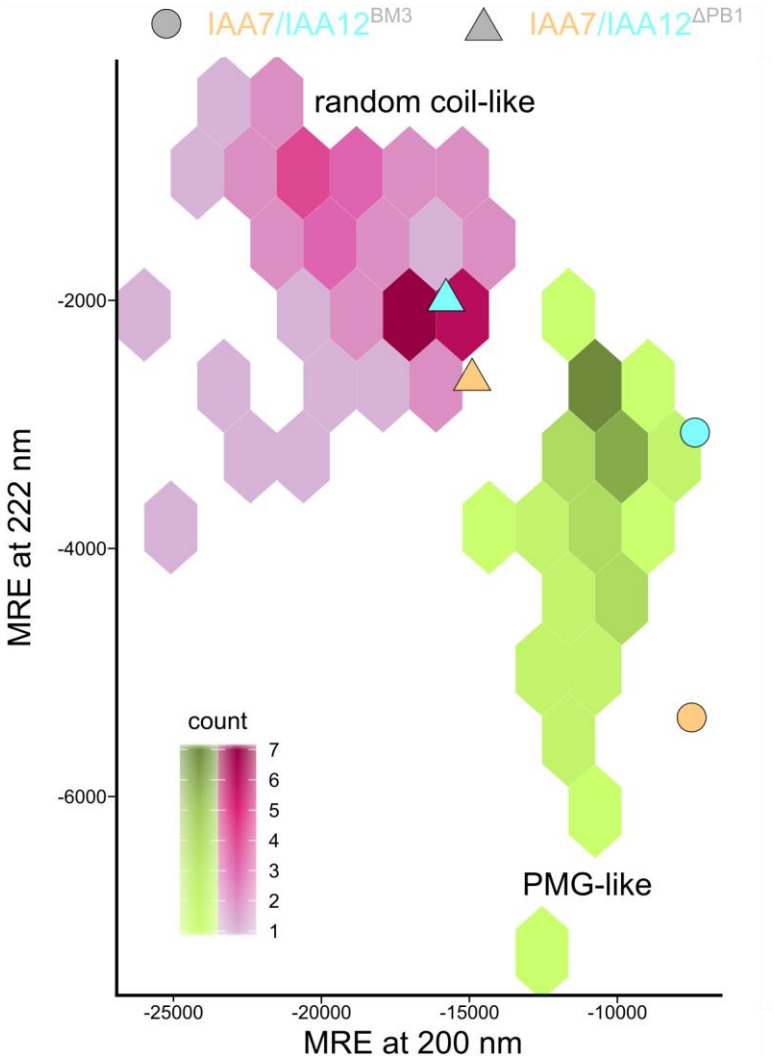

Supplementary Figure 2| Classification of IAA7 and IAA12 variants according to their CD spectra. CD spectral data classifies IAA7 (light orange) and IAA12 (aquamarine) as PMG-like proteins with random coil elements in their N-terminal half[1-3]. Molar residual ellipticity (MRE) at 200 nm and 222 nm is shown for the specified AUX/IAA protein variants on top of hexagonal binned reference proteins, with either unfolded, random coil-like proteins (purple) or premolten globule-like (PMG-like; green) proteins. Truncated versions (triangles, ΔPB1) lack the conserved folded PB1 domain. IAA7^{BM3} and IAA12 ^{BM3} variants (circles) carry 3 amino acid exchanges in their PB1 domain to render them oligomerization deficient.

Supp. Fig. 3

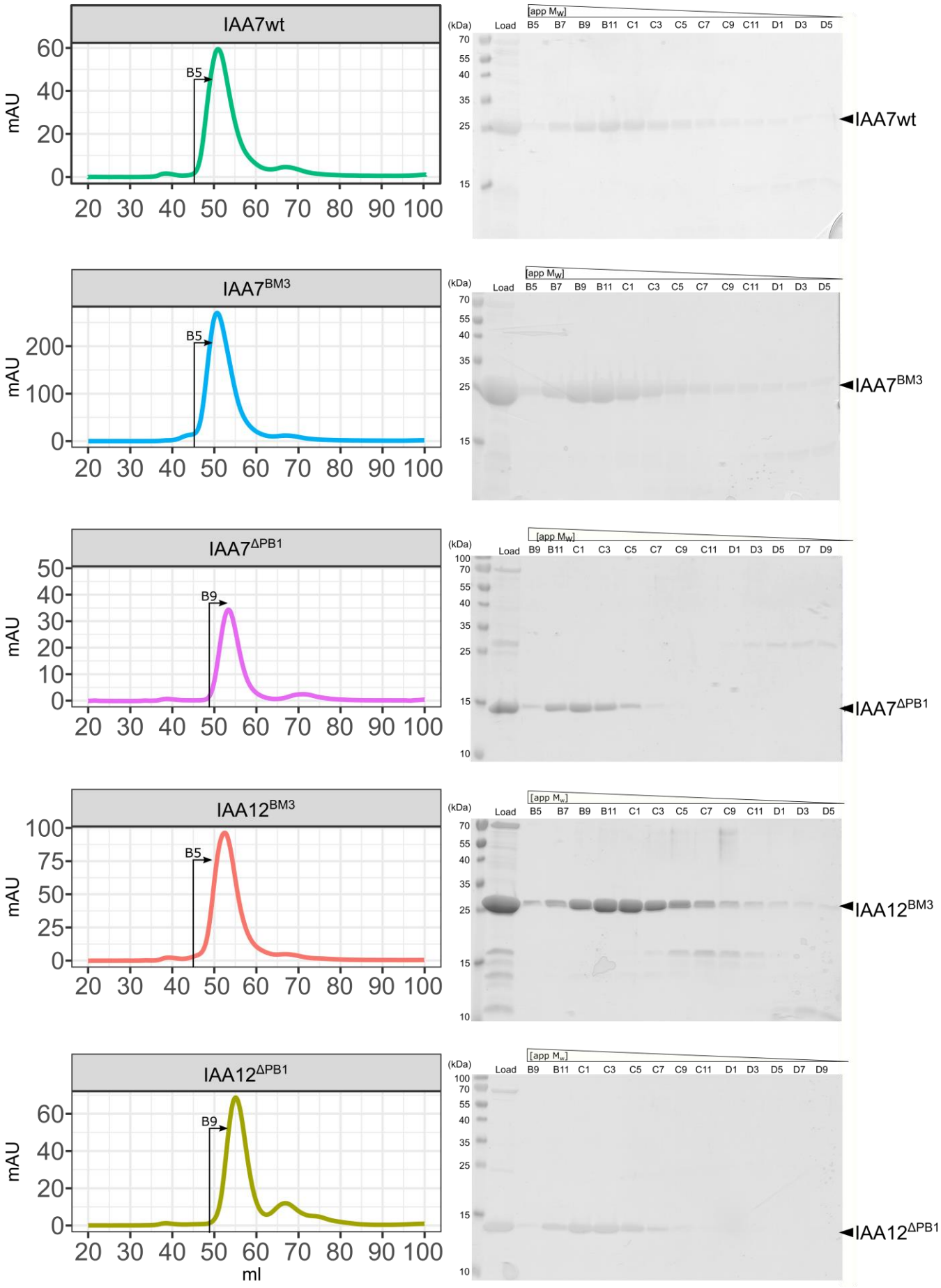

Supplementary Figure 3| Representative size exclusion chromatography runs for the untagged AUX/IAA protein variants. Elution profiles were obtained from semi-preparative size exclusion chromatography runs on a calibrated HiPrep 16/60 Sephacryl S100 High Resolution column (left panels). Indicated is the first fraction analyzed by SDS-PAGE shown in the right panels. Impurities could be separated from the protein of interest (indicated).

Supp. Fig. 4

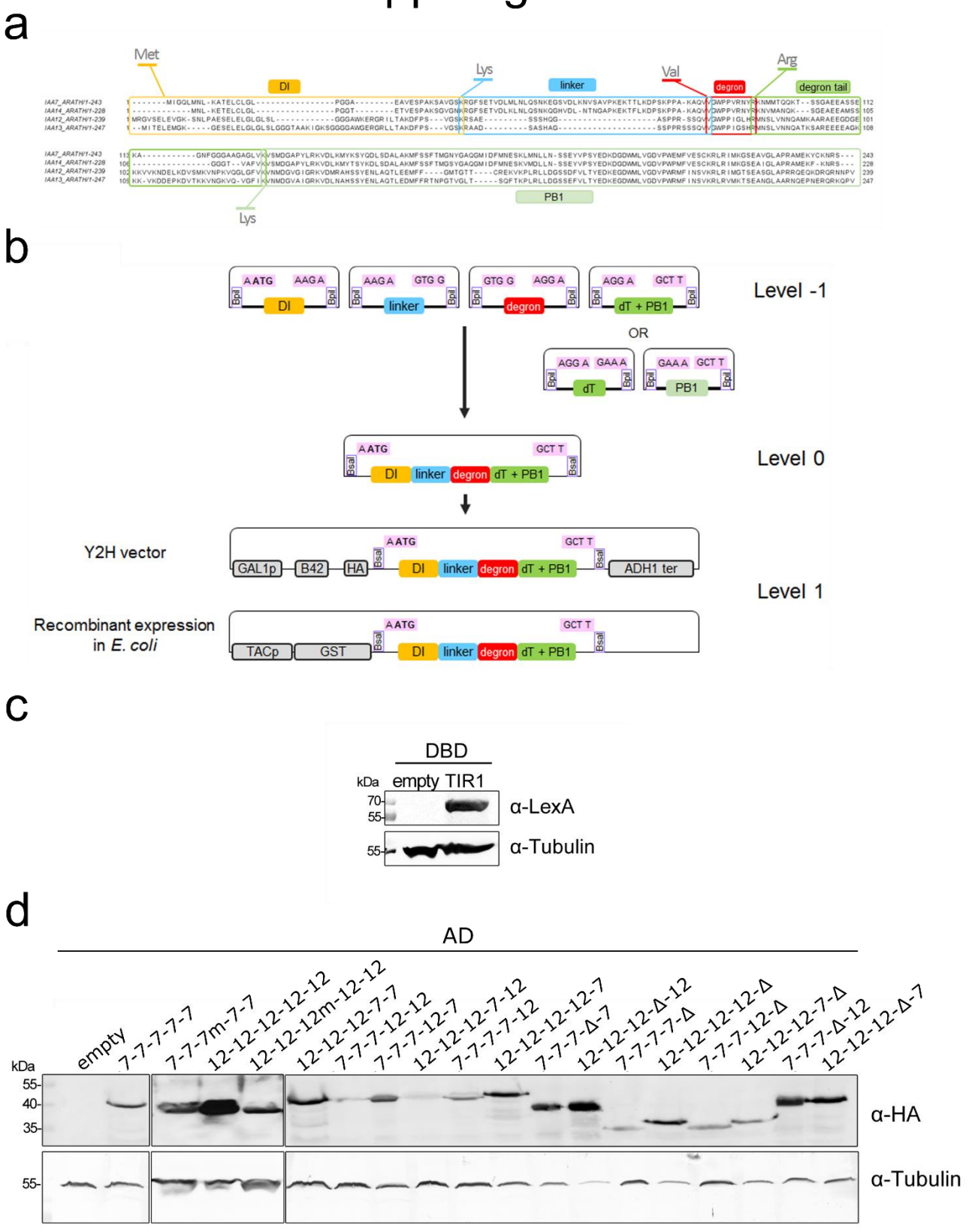

Supplementary Figure 4| Design principle for 4- and 5-module AUX/IAA chimeras. (**a**) Sequence alignment of IAA7, IAA14, IAA12, IAA13 from *Arabidopsis thaliana* showing conserved amino acid residues selected as start and end of each module: DI (orange), linker (blue), core degron (red), degron tail (dark green) and the PB1 domain (light green). Conserved amino acids used as Golden Gate assembly sites are highlighted. (**b**) Golden Gate cloning strategy to assemble level -1, 0, and 1 constructs for either yeast-two hybrid assays or recombinant *E.coli* expression as GST-fusion proteins using *Bpi*I and *Bsa*I restriction enzymes. (**c-d**) Immunoblots for LexA-DBD-tagged TIR1 (**c**) and HA-tagged AUX/IAA chimeras (**d**) from haploid yeast cells grown in Gal/Raff –Trp or Gal/Raff –Ura –His medium, respectively. 7m and 12m correspond to the gain-of-function mutations *axr2-1* and *bdl*, respectively. Detection was carried out using anti-LexA, anti-HA (F7), and anti-tubulin (loading control) antibodies.

Supp. Fig. 5

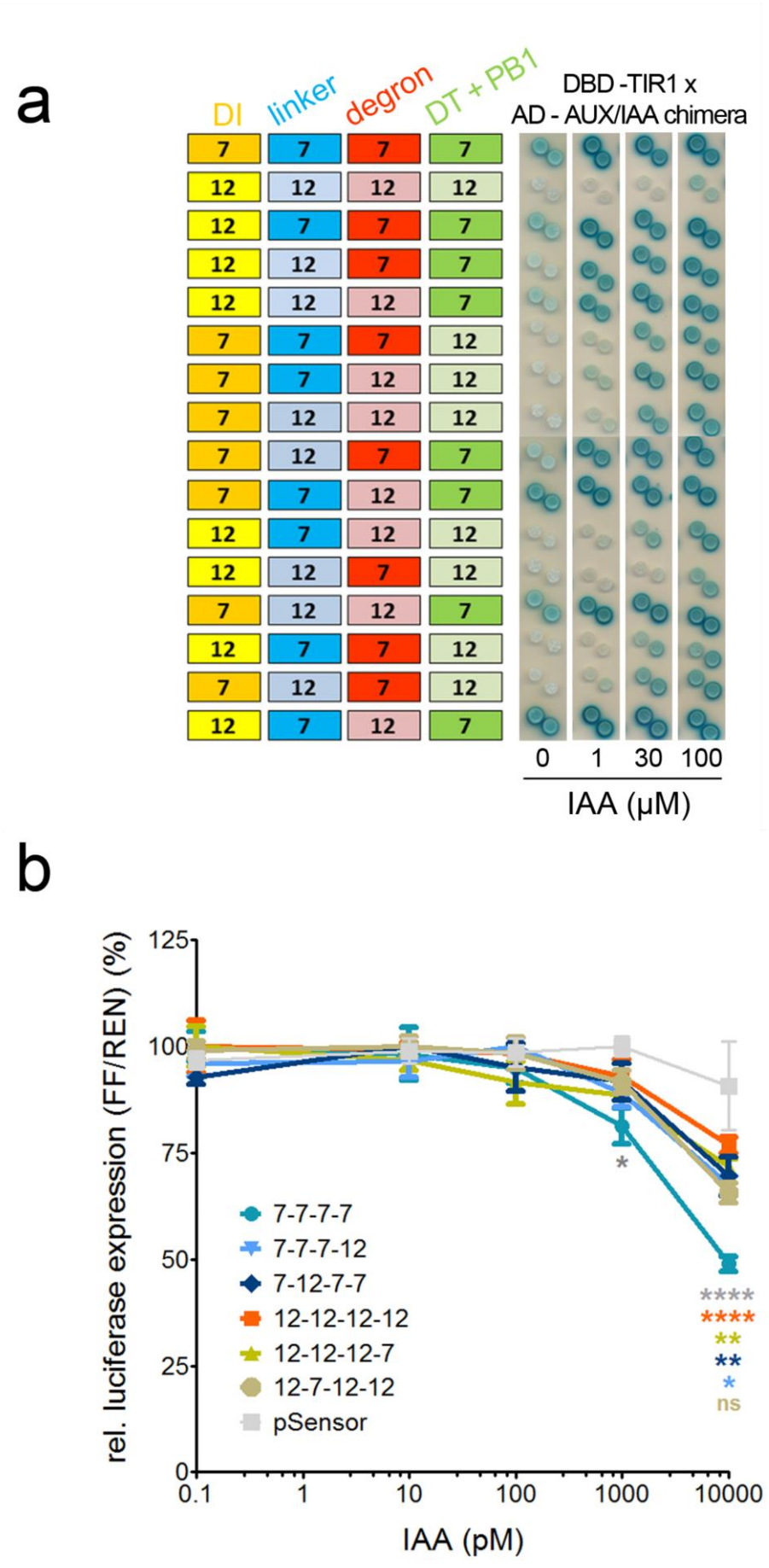

Supplementary Figure 5| Design of 4-module chimeras, where module 4 consists of the degron tail and the PB1 domain of IAA7 or IAA12 combined. (**a**) Yeast two hybrid assay shows auxin-dependent interaction of TIR1 and chimeric AUX/IAAs is strongly driven by the presence of the IAA7 degron tail, and the PB1 domain -containing module. (**b**) Ratiometric luminescent biosensor[4] to track degradation of 4-module AUX/IAA chimeric proteins in *Arabidopsis* protoplasts.

Supp. Fig. 6

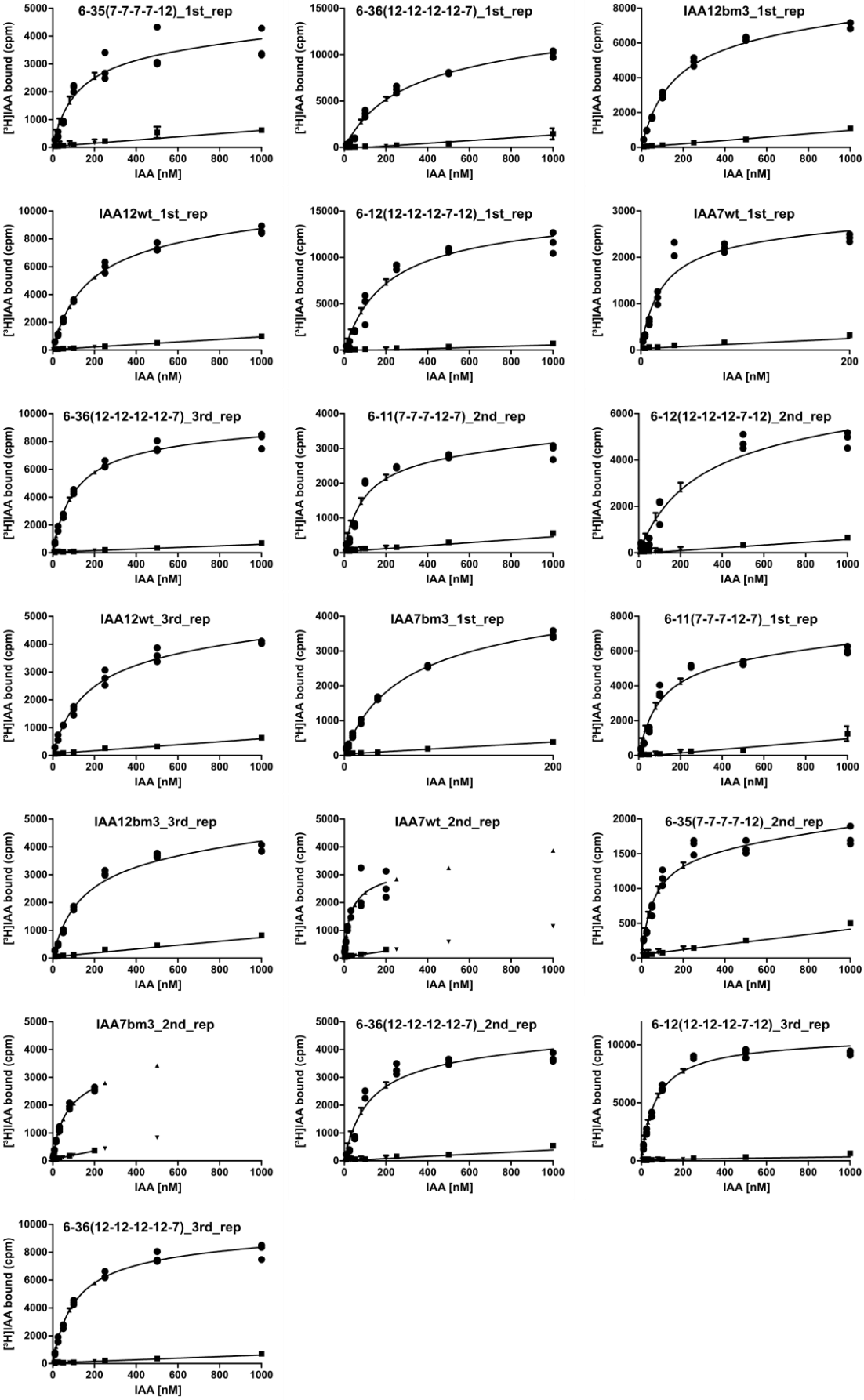

Supplementary Figure 6| Single non-normalized [³H]IAA radioligand binding curves. Single binding curves for each AUX/IAA variant and chimeric construct. Datapoints of each [³H]IAA concentration are shown as individual points for each technical replica (circles) together with non-specific binding in the presence of 2 mM cold IAA (squares).

Supp. Fig. 7

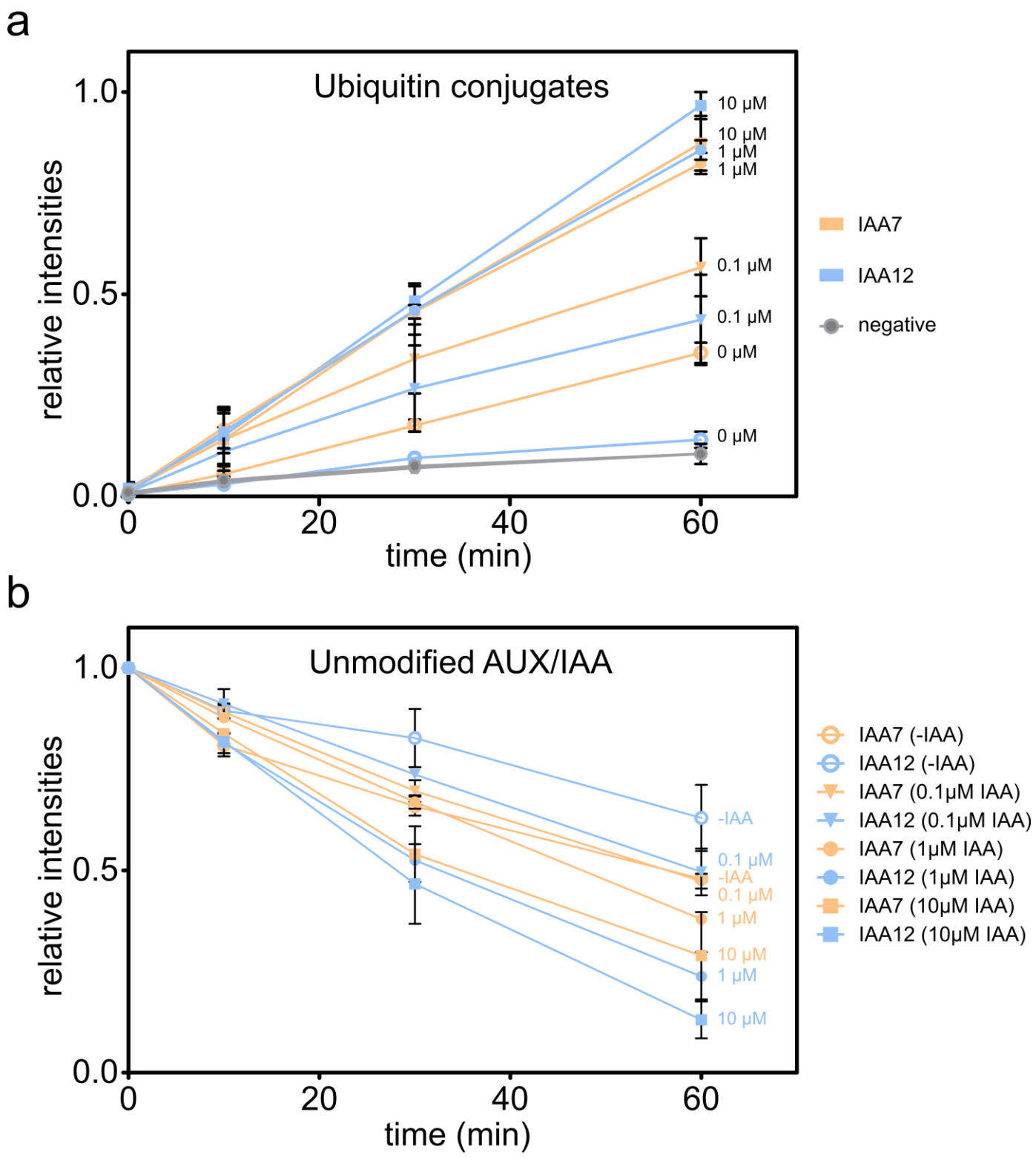

Supplementary Figure 7| Quantification of auxin- and time-dependent ubiquitylation of IAA7 and IAA12. (**a**) Increase in ubiquitin conjugates over time measured as the in-gel ubiquitin-fluorescein signal intensity above the ubiquitin-modified Cullin1 (asterisk, **Figure 3a).** Signal was normalized by the strongest signal (IAA12, 10 µM IAA). (**b**) Decrease of unmodified GST-AUX/IAA protein signal after immunoblotting detected by an Alexa Fluor Plus 647-coupled secondary antibody. Signals were normalized to the intensities at time point "0". Depicted are mean values from three independent experiments with standard deviation as error bars. Results for GST-IAA7 and GST-IAA12 are depicted in light orange and light blue, respectively.

Supp. Fig. 8

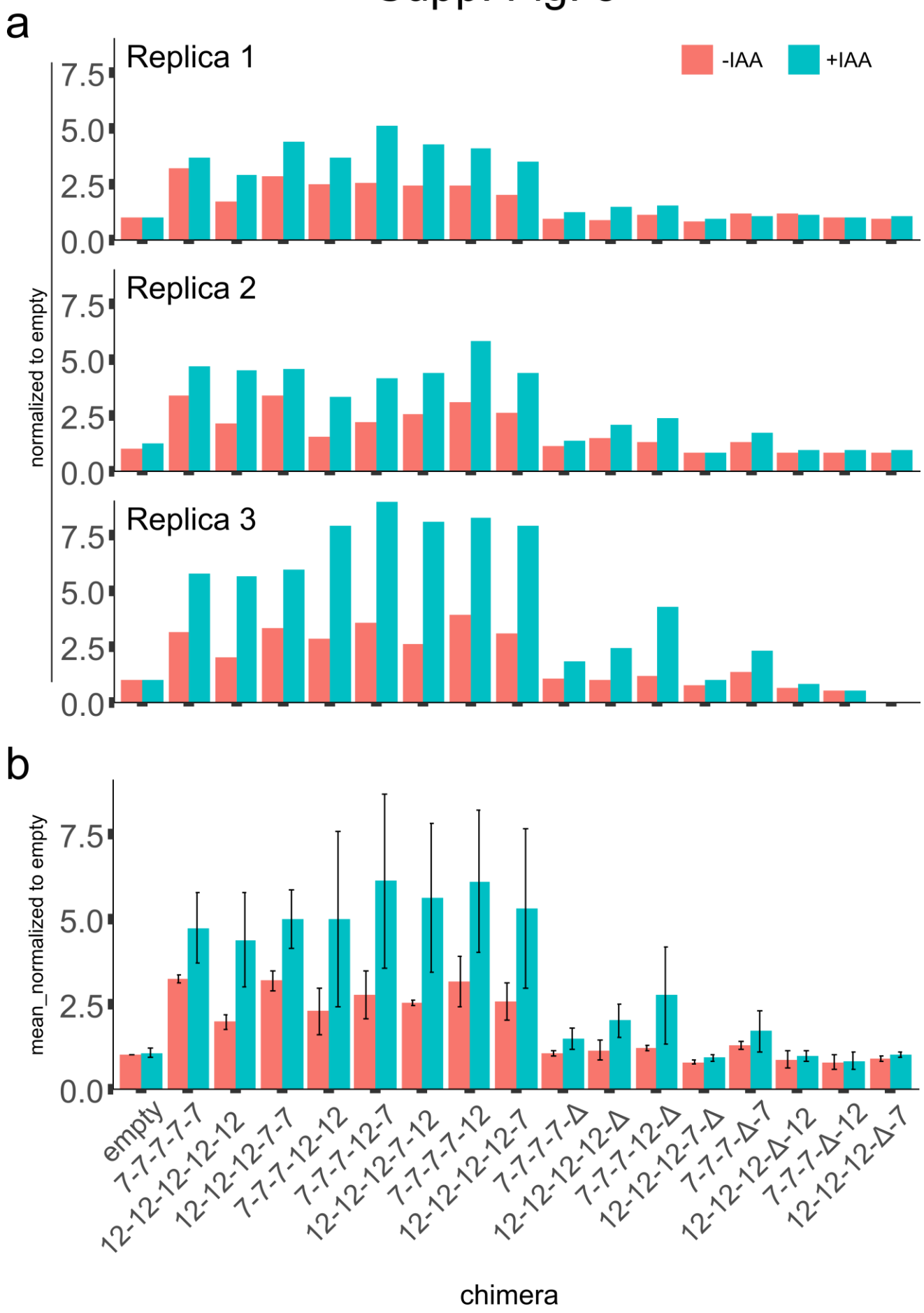

Supplementary Figure 8| Quantification of auxin-triggered chimera ubiquitylation. As in Supplementary Figure 7 ubiquitin conjugates on chimeric AUX/IAAs were measured via fluorescein signal intensities in the presence (teal) or absence (salmon) of auxin (IAA) after 1 h reaction time. (**a**) Raw signal intensities for each individual replica. (**b**) Auxin-triggered fold induction of chimera ubiquitylation as mean values with standard deviation using data from **a**. Chimeras consisting mainly of IAA7 or IAA12 modules are displayed.

Supp. Fig. 9

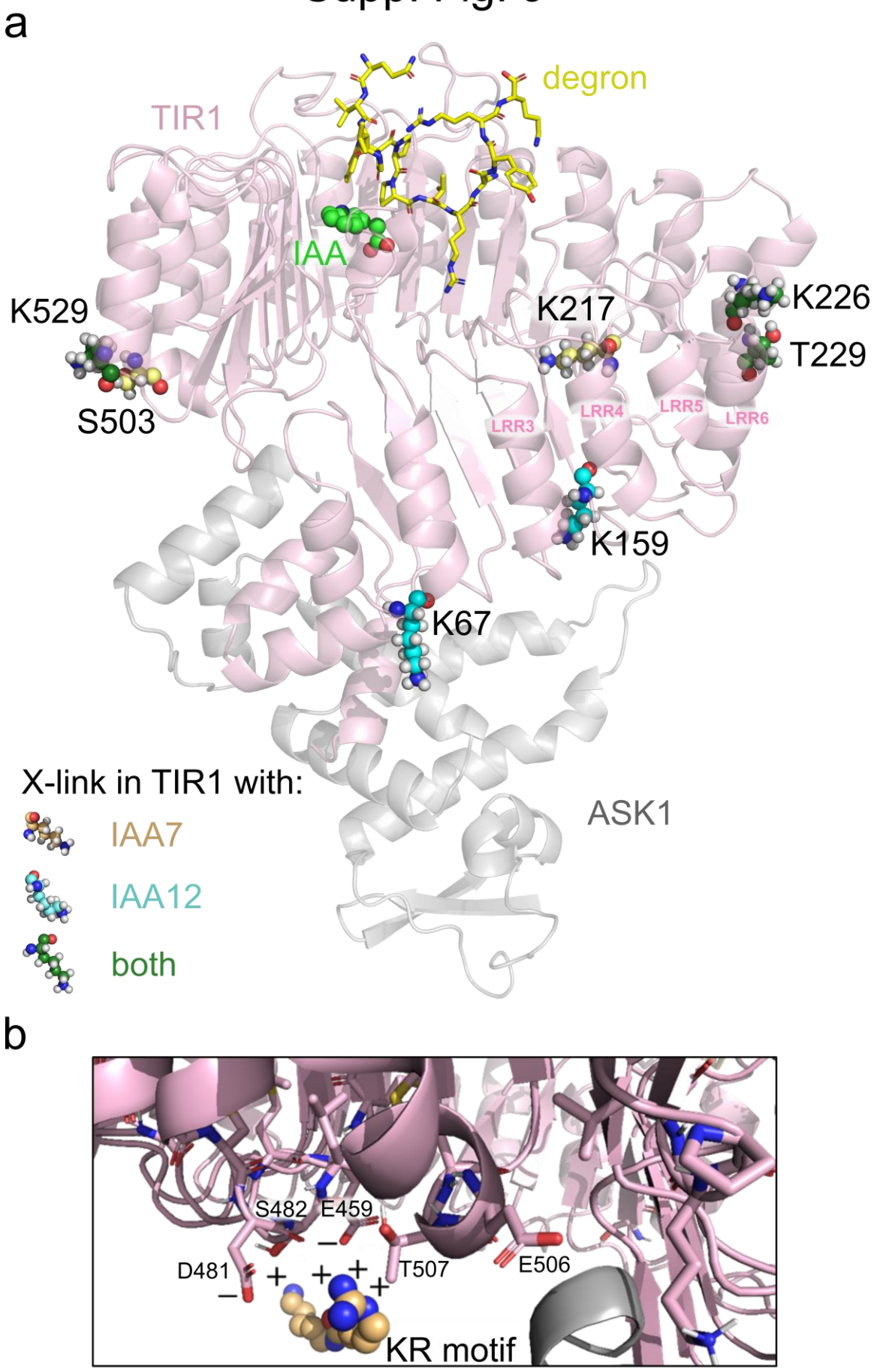

Supplementary Figure 9| Crosslinked residues in TIR1 either with IAA7, IAA12 or both. (**a**) Depicted is the crystal structure of ASK1·TIR1·auxin·IAA7 degron (2P1Q, gray, light pink) with highlighted residues found to be crosslinked with either IAA7 (light orange), IAA12 (aquamarine) or both (green) shown as spheres. Leucine-rich repeats carrying PB1 domain-interacting are labeled. (**b**) Patch enriched with negative charge potential, close to KR motif-cross-linked residues, acting as a plausible interaction site.

Supp. Fig. 10

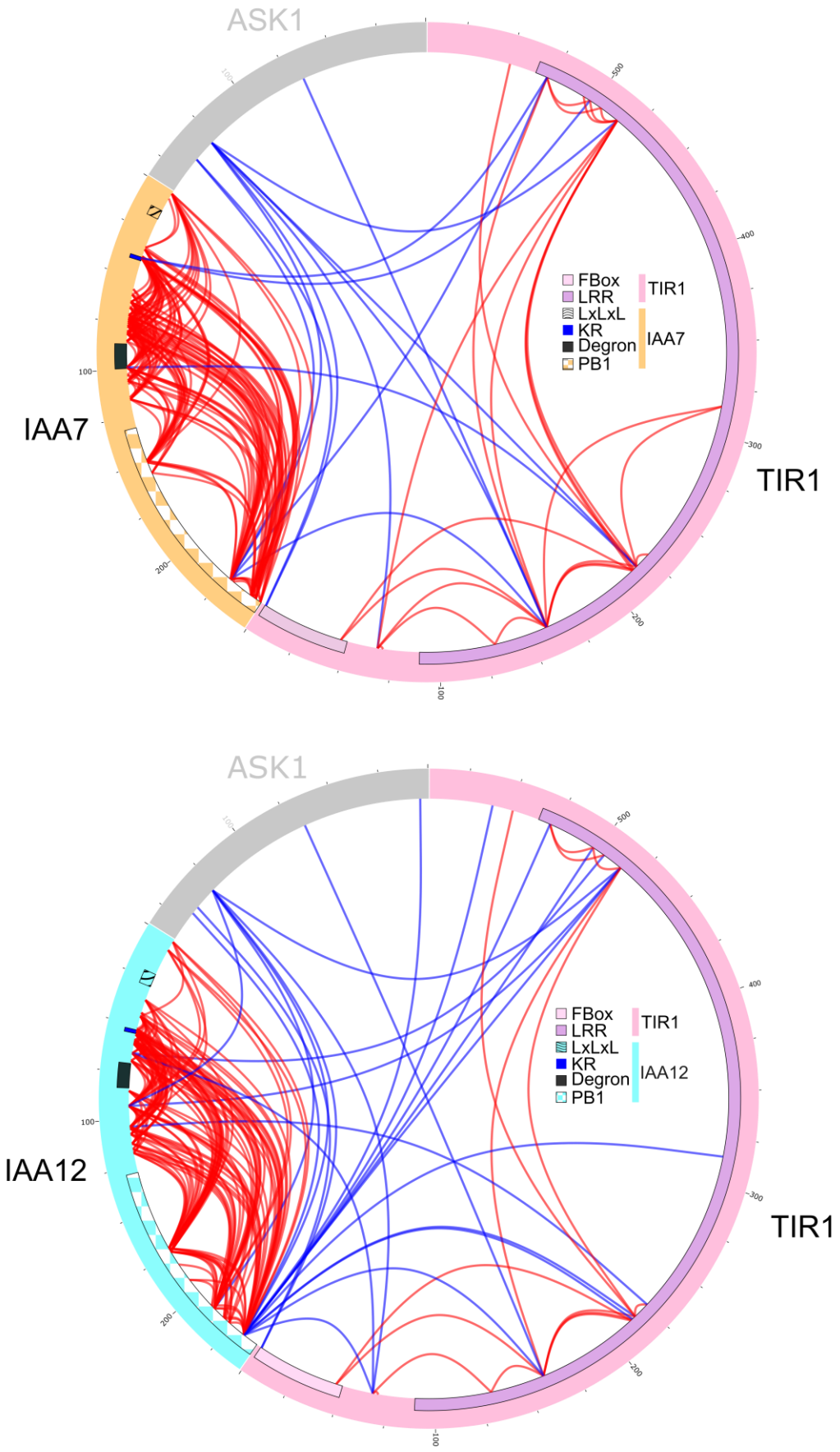

Supplementary Figure 10| Crosslinks identified in ASK1·TIR1 and AUX/IAAs in the absence of auxin. Displayed are all crosslinks within (intra-protein, red) or in between (inter-protein, blue) ASK1 (gray), TIR1 (light pink) and IAA7 (light orange) or IAA12 (aquamarine) as connecting lines along the circular depicted amino acid sequence. Lines correspond to all crosslinked peptides collected from multiple replica.

Supplementary Figure 11| Workflow for cross-linking-based docking using HADDOCK. Homology models from *At*IAA7^{PB1} and *At*IAA12^{PB1} domains were created using multi-template-based comparative modelling with MODELLER. Docking models using HADDOCK were generated by docking the PB1 homology models on the modified ASK1·TIR1·auxin·degron crystal structure (2P1Q) using as distant restraints the cross-linking information and the degron tail length. Potential conformational space was visualized via DisVis.

Supp. Fig. 12

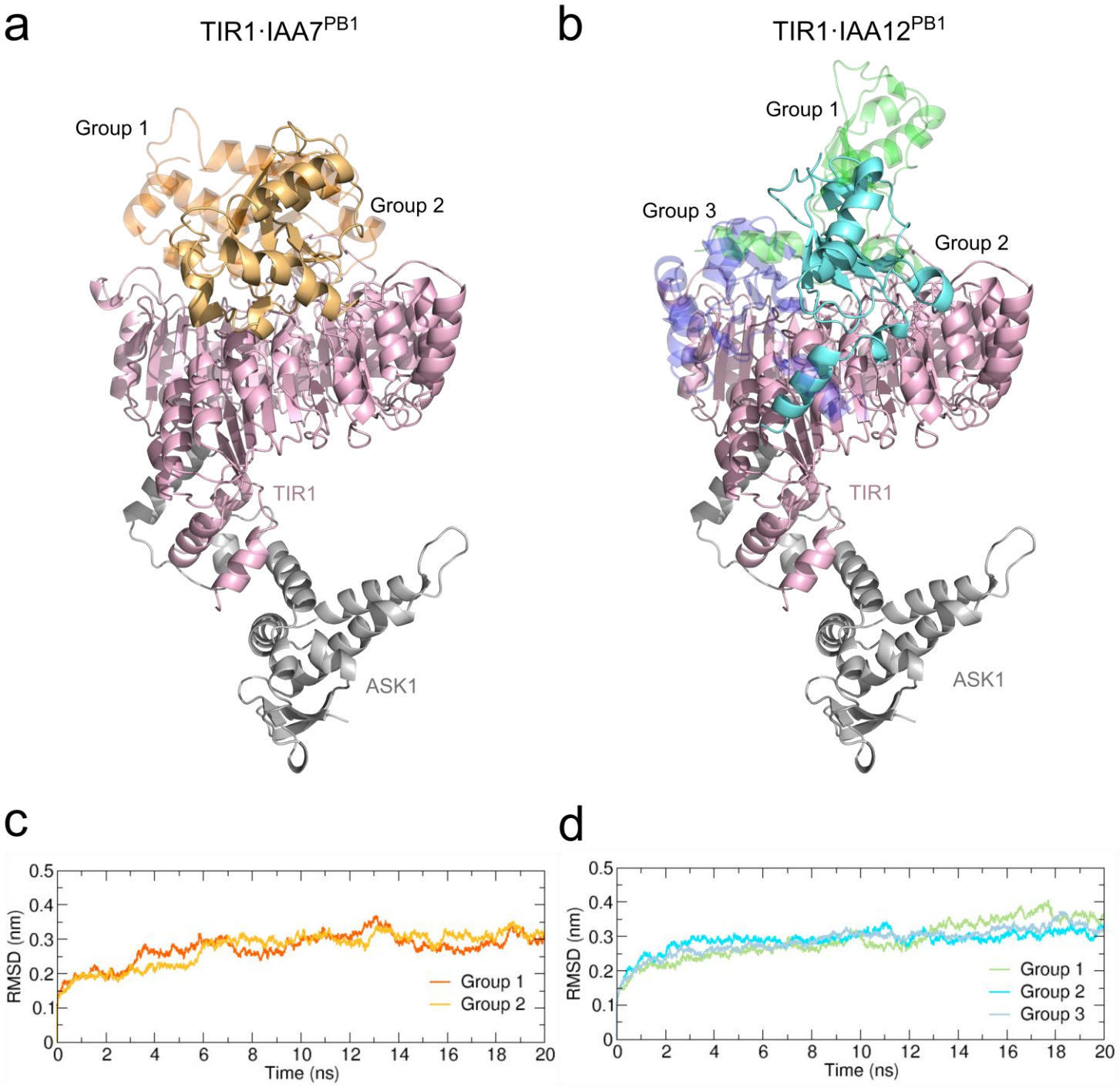

Supplementary Figure 12| HADDOCK docking using crosslinking data restrictions generated stable structural models of TIR1·AUX/IAA^{PB1} complexes. A representative structure for each group of TIR1·IAA7^{PB1} (**a**) (group 1: dark orange, group 2: light orange); and TIR1·IAA12^{PB1} (**b**) (group 1: green, group 2: aquamarine, group 3: dark blue) HADDOCK models are shown. Time evolution (ns) of RMSD values for the backbone atoms of (**c**) TIR1·IAA7^{PB1}and (**d**) TIR1·IAA12^{PB1}models, respect to their initial structure.

Supp. Fig.13

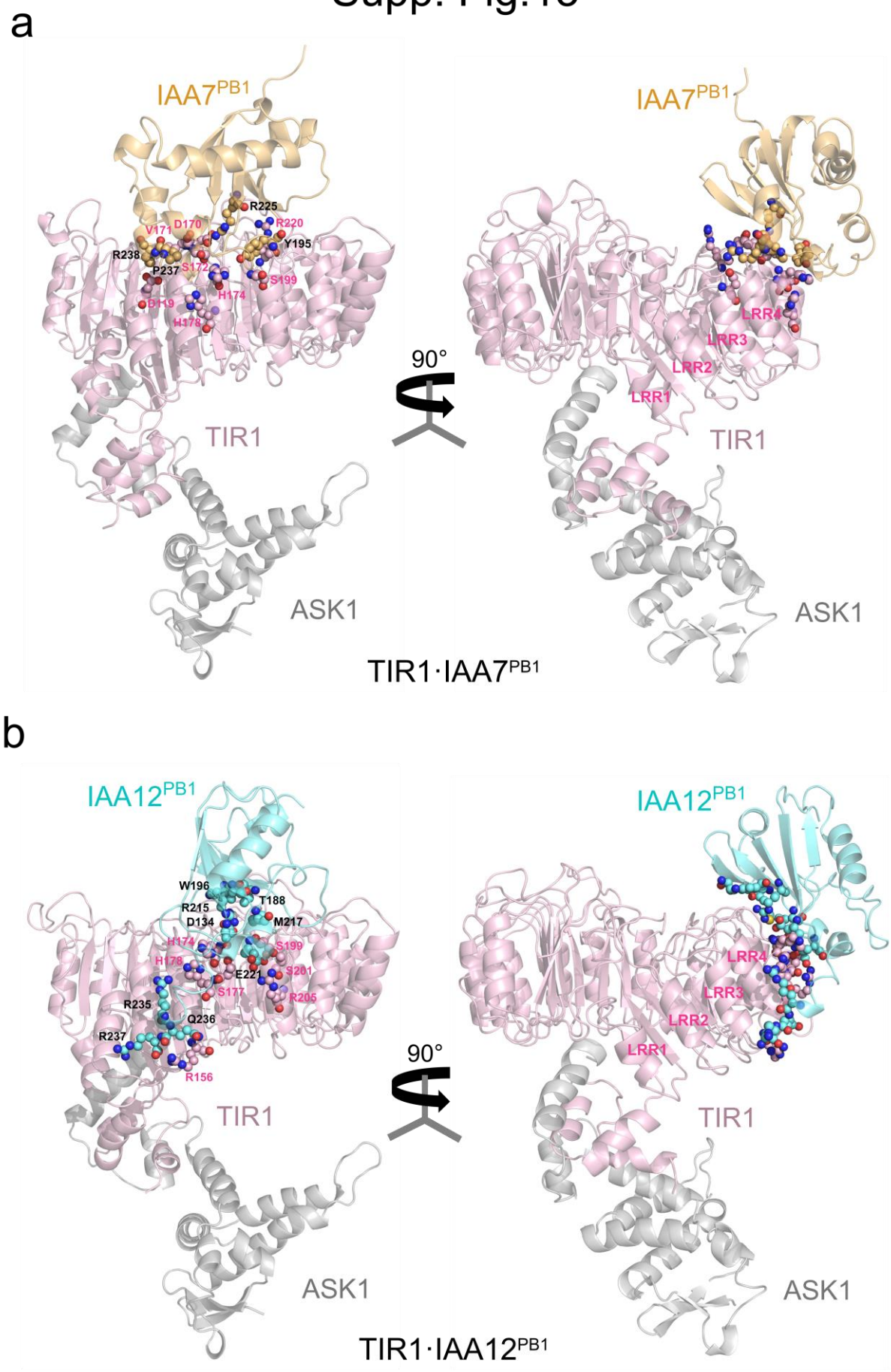

Supplementary Figure 13| Molecular dynamics (MD) simulations revealed the most energetically favorable model from HADDOCK-based docking. (**a-b**) PB1 domains from both IAA7 and IAA12 are positioned over TIR1, interacting with residues from leucine-rich-repeat 3 to 7 (LRR3-7). Energetically relevant residues (small spheres) from TIR1 (light pink), IAA7^{PB1} (light orange), and IAA12^{PB1} (aquamarine) domains for complex stabilization are located in the TIR1·AUX/IAA^{PB1} interface.

Supp. Fig. 14

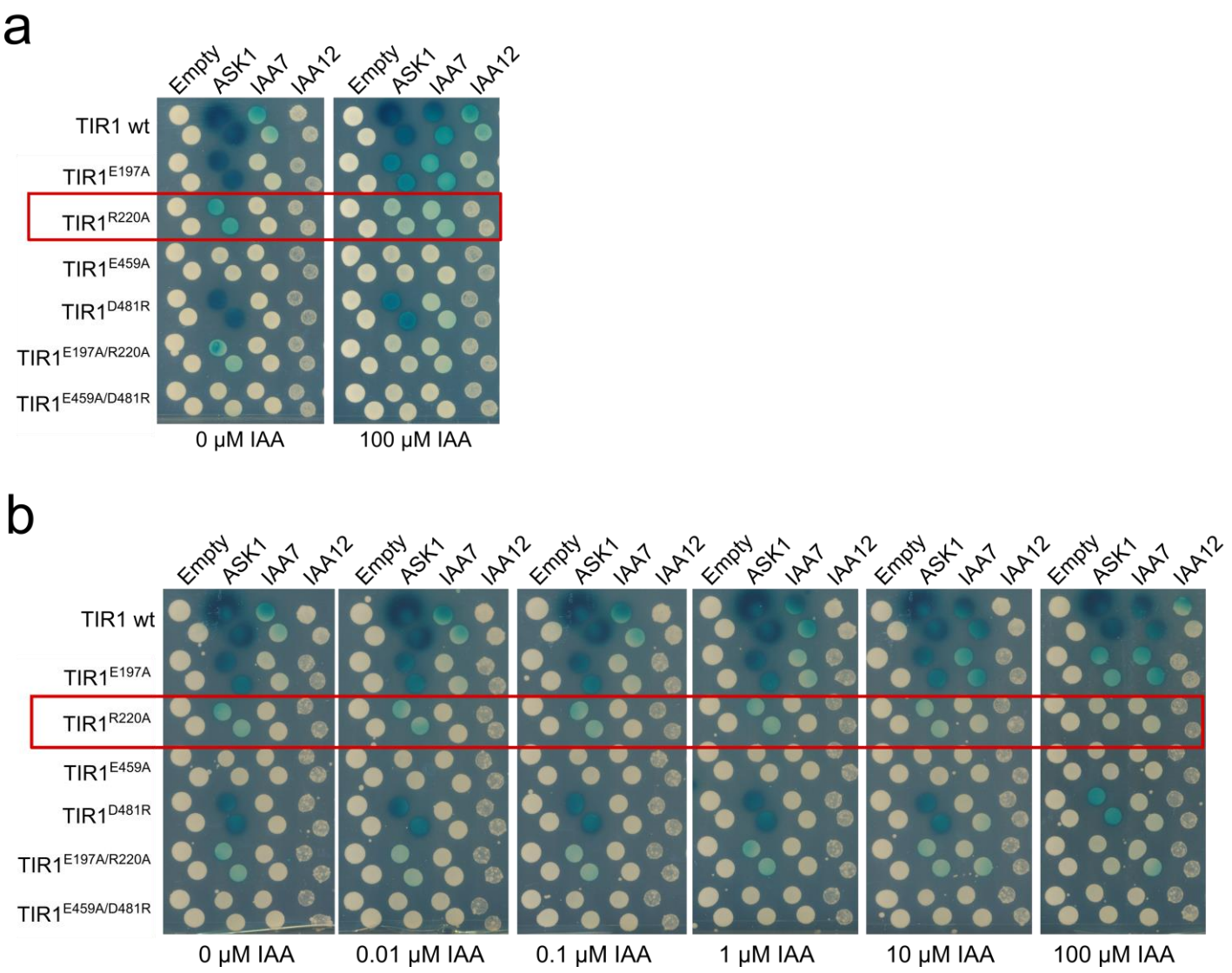

Supplementary Figure 14| Mutation R220A in TIR1 only partially affects TIR1·ASK1 interaction. Initial Y2H screen 1 and 2 (**a-b**, respectively) showing TIR1^{R220A} is only partially impaired in ASK1 recruitment.

Supp. Fig. 15

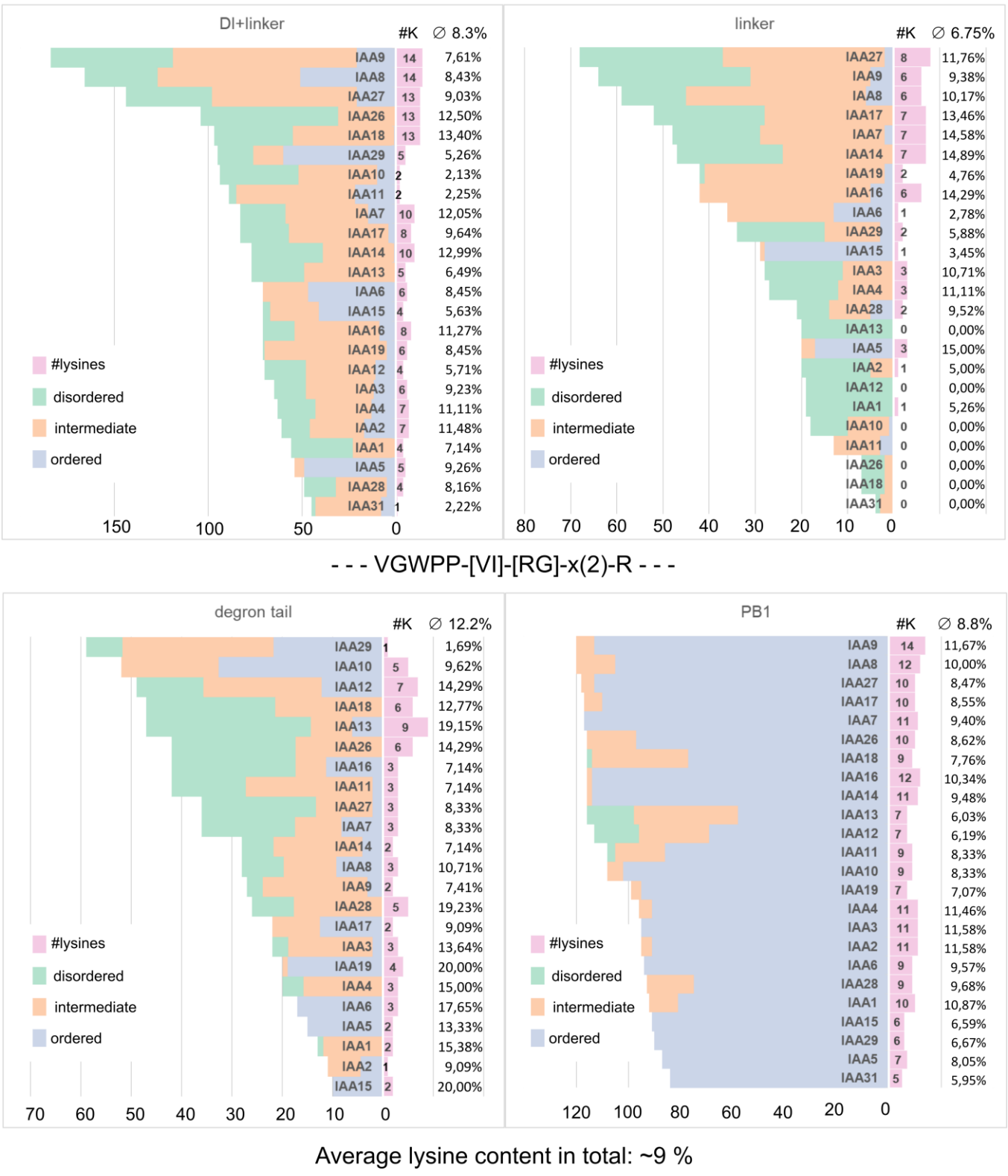

Supplementary Figure 15| Disorder probability and lysine content in different regions of the canonical *At*AUX/IAA proteins. IUPred2A-based prediction for disordered (green), intermediate (orange) and ordered (blue) amino acid residues is shown. Length in AUX/IAA IDRs partially correlate with lysine content and/or disorder. AUX/IAAs with less than 5 lysine residues (pink) in the degron tail show increased lysine content in the PB1 domain (≥10). AUX/IAA degron tails are enriched in ubiquitin acceptors sites (lysine residues, average 12.2% of total residues).

Suppl. Table 1. Restraints used in HADDOCK and DisVis.

Complex	Restraint#	Residue 1	Residue 2	Min. distance (Å)	Max. distance(Å)	Type of restraint
ASK1·TIR1·IAA7	1	TIR1, K226	IAA7, K223	8.0	34.0	Inter XL
	2	TIR1, S229	IAA7, K223	8.0	34.0	Inter XL
	3	IAA7, K94	IAA7, K237	8.0	34.0	Inter XL
	4	IAA7, K94	IAA7, G124	20.0	27.0	Degron tail restraint
ASK1·TIR1·IAA12	1	TIR1, K226	IAA12, K231	8.0	34.0	Inter XL
	2	TIR1, K67	IAA12, K231	8.0	34.0	Inter XL
	3	IAA12, M81	IAA12, P119	24.8	35.0	Degron tail restraint

Supplementary Table 1| Distance restraints used in HADDOCK-based docking and DisVis calculations. Restraints used for generating interaction surfaces with DisVis and/or molecular models with HADDOCK. Defined are the restraints used based on their type and origin.

Suppl. Table 2. Crosslinking-based docking by HADDOCK

Input	# grouped refined structures	group	# structures per group	HADDOCK scores	Buried surface	Van der Waals energy	Electrostatic energy	Restraint violation
ASK1·TIR1·IAA7 without degron tail restraint	175	1	124	-75.7 +/- 4.6	1390.6 +/- 29.4	-37.9 +/- 3.1	-279.1 +/- 15.2	2.5 +/- 0.72
		2	24	-63.8 +/- 10.8	1503.0 +/- 127.2	-47.9 +/- 8.8	-214.5 +/- 95.6	2.7 +/- 1.50
		6	5	-59.4 +/- 10.2	1627.6 +/- 95.8	-46.7 +/- 6.5	-210.5 +/- 15.6	2.3 +/- 1.02
		3	10	-53.6 +/- 9.1	1451.2 +/- 59.6	-32.4 +/- 6.2	-265.6 +/- 60.2	1.6 +/- 0.53
		5	6	-46.7 +/- 7.6	1019.5 +/- 31.2	-38.8 +/- 3.9	-127.3 +/- 32.5	2.5 +/- 0.56
		4	6	-34.2 +/- 7.4	1031.6 +/- 41.0	-22.7 +/- 2.5	-234.4 +/- 27.5	2.1 +/- 0.54
ASK1·TIR1·IAA7 with degron tail restraint	193	2	72	-89.1 +/- 2.5	1689.6 +/- 146.4	-43.5 +/- 3.0	-419.7 +/- 33.1	3.2 +/- 0.84
		1	121	-66.7 +/- 9.3	1395.2 +/- 162.7	-33.5 +/- 3.8	-272.7 +/- 39.0	1.6 +/- 0.36
ASK1·TIR1·IAA12 without degron tail restraint	132 in 13 groups	2	18	-76.3 +/- 10.0	1588.8 +/- 70.0	-38.1 +/- 4.8	-293.4 +/- 45.0	2.5 +/- 0.44
		1	47	-67.1 +/- 12.1	990.6 +/- 15.7	-30.3 +/- 1.6	-260.0 +/- 31.6	1.9 +/- 0.62
		4	9	-66.8 +/- 4.0	1548.8 +/- 140.0	-44.8 +/- 11.7	-257.4 +/- 46.3	2.6 +/- 0.39
		9	5	-66.5 +/- 10.6	1090.0 +/- 38.5	-23.9 +/- 1.4	-381.9 +/- 33.2	3.1 +/- 1.26
		8	5	-61.5 +/- 22.4	1218.9 +/- 164.4	-27.5 +/- 5.4	-404.8 +/- 62.1	2.5 +/- 0.69
		11	5	-51.9 +/- 4.1	1425.8 +/- 80.1	-29.5 +/- 2.0	-357.4 +/- 35.3	2.0 +/- 0.69
		10	5	-45.7 +/- 5.6	1434.8 +/- 70.1	-38.3 +/- 3.4	-230.4 +/- 29.4	1.9 +/- 0.33
		7	6	-41.5 +/- 3.5	1129.3 +/- 38.6	-27.1 +/- 2.5	-267.7 +/- 10.3	2.0 +/- 0.99
		3	10	-35.6 +/- 3.7	1193.6 +/- 31.5	-30.6 +/- 1.7	-89.6 +/- 21.8	2.9 +/- 0.74
		13	4	-33.1 +/- 8.6	1161.6 +/- 120.1	-24.3 +/- 4.5	-207.1 +/- 21.8	1.9 +/- 0.42
ASK1·TIR1·IAA12 with degron tail restraint	196	1	187	-94.2 +/- 9.9	1619.0 +/- 85.6	-35.4 +/- 2.4	-469.4 +/- 48.7	1.8 +/- 0.30
		3	4	-59.8 +/- 14.5	1541.9 +/- 116.0	-40.6 +/- 2.8	-252.6 +/- 58.2	2.8 +/- 0.44
		2	5	-53.9 +/- 10.2	1429.8 +/- 104.0	-38.0 +/- 4.5	-229.1 +/- 35.9	3.0 +/- 1.58

Supplementary Table 2| Resulting clusters from HADDOCK-based docking and their characteristics. Different relevant energetic values from ASK1·TIR1·IAA7 and ASK1·TIR1·IAA12 clusters either in presence or absence of the disorder (degron tail) restraint are shown together with the respective grouping. Results indicate a more defined and more reliable complex identification in the presence of the disorder restraint.

Supp. Table 3. Per-residue energy contributions to the formation of the TIR1·AUX/IAA^{PB1} complexes

Complexes	TIR1 Residues	Conservation within 21 TIR1/AFB-like proteins	prEFED protocol		CAS protocol	
			ΔG$_{sc}$ (kcal/mol) GB^{OBC1}	ΔG$_{sc}$ (kcal/mol) GB^{OBC2}	ΔΔG (kcal/mol) GB^{OBC1}	ΔΔG (kcal/mol) GB^{OBC2}
TIR1·IAA7^{PB1}	D170	5 (+8)	-3.746 +/- 1.11	-5.317 +/- 1.32	-13.678 +/- 2.06	-16.533 +/- 2.36
	R220	9 (+4)	-6.543 +/- 1.35	-6.975 +/- 1.46	-9.585 +/- 2.29	-10.623 +/- 2.54
	D119	19	-2.264 +/- 0.76	-3.364 +/- 0.98	-8.632 +/- 1.48	-10.414 +/- 1.86
	H174	2	-4.902 +/- 0.85	-5.418 +/- 0.97	-7.387 +/- 1.57	-8.255 +/- 1.78
	S172	5	-4.011 +/- 0.62	-4.241 +/- 0.65	-6.671 +/- 1.23	-7.447 +/- 1.28
	S199	2	-3.103 +/- 1.23	-3.375 +/- 1.30	-4.558 +/- 2.04	-5.032 +/- 2.18
	H178	1 (+3)	-2.841 +/- 0.59	-3.041 +/- 0.64	-2.899 +/- 0.95	-3.160 +/- 1.02
	V171	1	-2.536 +/- 0.49	-2.278 +/- 0.51	-2.483 +/- 0.90	-2.099 +/- 0.95
	E197	11 (+4)	2.437 +/- 1.07	2.331 +/- 1.22	-0.149 +/- 2.73	-0.807 +/- 3.14
	D146	8 (+2)	1.988 +/- 0.89	1.959 +/- 0.88	0.709 +/- 1.34	0.385 +/- 1.55
	K226	2	0.685 +/- 0.56	1.077 +/- 0.91	-	-
TIR1· IAA12^{PB1}	R205	6 (+2)	-7.99 +/- 0.90	-7.662 +/- 1.00	-15.253 +/- 1.84	-16.056 +/- 2.03
	R156	19 (+2)	-7.44 +/- 0.97	-7.555 +/- 1.05	-11.491 +/- 1.88	-12.437 +/- 1.99
	H174	2	-4.267 +/- 1.52	-5.195 +/- 1.98	-9.27 +/- 2.46	-10.690 +/- 2.89
	S201	2	-4.058 +/- 0.60	-4.508 +/- 0.64	-7.689 +/- 1.15	-8.963 +/- 1.23
	S199	2	-3.942 +/- 1.15	-4.439 +/- 1.18	-7.448 +/- 2.19	-8.731 +/- 2.36
	H178	1 (+3)	-1.706 +/- 0.93	-2.27 +/- 1.15	-4.349 +/- 1.78	-5.392 +/- 2.09
	S177	11 (+2)	-1.521 +/- 1.32	-1.738 +/- 1.40	-2.833 +/- 2.32	-3.307 +/- 2.54
	K130	2 (+1)	-1.041 +/- 1.27	-0.877 +/- 1.18	-1.745 +/- 2.72	-1.658 +/- 2.82
	S196	5 (+2)	-1.247 +/- 0.41	-1.281 +/- 0.47	-1.286 +/-0.66	-1.423 +/- 0.78
	V171	1	-1.784 +/- 0.38	-1.548 +/- 0.41	-0.767 +/- 0.87	-0.459 +/- 0.94
	A153	5	-1.259 +/- 0.24	-1.286 +/- 0.24	-	-
	D170	5 (+8)	0.459 +/- 0.16	0.059 +/- 0.23	-	-

Supplementary Table 3| Energy contribution of single amino acids to TIR1·AUX/IAA^{PB1} complex formation. Conservation of residues was checked in TIR1/AFB-like proteins in *Arabidopsis thaliana* (uniprot ID: Q570C0, Q9ZR12, Q9LW29, Q9LPW7, A0A178UVM5, A0A178UB83), *Selaginella moellendorffii* (uniprot ID: D8RF91, D8SDE6, D8SG63, D8R5Z3), *Physcomitrella patens* (uniprot ID: A9SYG2, A9TAY1, A9T980, A9SZ50, A9TE08, A9TP16), *Oryza sativa* (uniprot ID: Q0DKP3, Q7XVM8, Q2R3K5, Q8H7P5) and *Marchantia polymorpha* (uniprot ID: A0A2R6WBN4).

Supplementary Methods

Molecular dynamic simulations (MDS) of protein-protein complexes

One refined structure of each group, derived from the cross-link-based docking by HADDOCK incorporating the disorder restraint (2 groups for TIR1·IAA7^{PB1}; 3 groups for TIR1·IAA12^{PB1}), was used as starting structure for MD simulations. The 5 structures were prepared using structure preparation and protonate 3D (pH = 7.5) modules and subsequently minimized with AMBER10 force-field[5] in MOE 2019.0101 (Chemical Computing Group Inc., Montreal, Quebec, Canada).

Molecular dynamic simulations were performed with the GROMACS software package (version 4.6.5)[6]. The parameters corresponding to the proteins were generated with AMBER99SB-ILDN force-field[7] and TIP3P explicit solvation model[8]. Electro-neutrality was guaranteed by adding Na^+ and Cl^- ions into the unit cells at an appropriate ratio to reach a final NaCl concentration of 0.2 mol/L. The protocol employed here to perform MD simulations involves prior energy minimization (EM) and position-restrained equilibration, as outlined by Lindahl [9] for lysozyme in water. The systems were subjected to 50 000 steps of steepest descents minimization with a step size of 0.01 nm[10]. The maximum tolerance was set to 1 000 kJ*mol^{-1}*nm^{-1} and cutoff radii of 1.2 nm were established for the calculation of both van der Waals and short-range electrostatic interactions. The particle mesh Ewald algorithm was used to handle long-range electrostatic interactions[11,12]. The Verlet cutoff-scheme was used, as well as the potential modifier potential-shift-Verlet for both Coulomb and van der Waals interactions. Bond lengths were left unconstrained during EM. Next, the solvent was equilibrated around the system for 50 ps using position restraint dynamics, with force constant of 1,000 kJ*mol^{-1}*nm^{-2} to all the heavy atoms of the proteins. Cutoff radii of 1.2 nm were established for the calculation of van der Waals and electrostatic

interactions. Again, the Verlet cutoff-scheme was used, as well as the potential modifier potential-shift-Verlet for both Coulomb and van der Waals interactions. Newton's equation of motion was solved using the leap-frog integrator[13], with a time step of Δt = 2 fs for a total time of 50 ps (25,000 integration steps). The system was simulated at constant temperature and pressure of 310 K and 1 atm, respectively. In order to accomplish this, we used the Berendsen algorithm[14] for the pressure and Velocity rescaling[15] for the temperature, with time constant (τ) of 3 ps and 0.1 ps, respectively[10]. Bond lengths were constrained by the Linear Constraints Solver algorithm[16]. Random initial velocities were assigned to each atom prior to the MD simulations, obeying the Maxwell-Boltzmann distribution from 50 K to 310 K.[10]

Once the system was equilibrated, we proceeded to the productive dynamic simulation without position restraint[17] for 20 ns. The system simulation was carried out at T = 310 K and p = 1 atm. The Parrinello-Rahman coupling algorithm[18,19] was used to keep pressure constant with a time constant (τ) of 1 ps.[10] The temperature, non-bonded interaction and time step were controlled or set up similarly as in the equilibration run. The snapshots of all runs were saved each 10 ps. Root Mean Square Deviation (RMSD) values for the backbone atoms of TIR1·IAA7^{PB1} and TIR1·IAA12^{PB1} compared to its initial structure, were calculated during the entire simulation using the *g_rms* program (GROMACS v4.6.5)[6].

Effective binding free energy calculations using MM-GBSA

The effective binding free energy (ΔG_{eff}) of the protein-protein complexes formation was calculated using MMPBSA.py from Amber18 package employing the MM-GBSA method[20]. We followed the single trajectory approach, in which the trajectories for the free proteins were extracted from that of the protein-protein complexes. GB^{OBC1} and GB^{OBC2} implicit solvation models were employed[20]. The ΔG_{eff} values were obtained

every 10 ps from the productive MD simulation (20 000 ps). We calculated the cumulative mean (also referred to as accumulated mean) for each of the 2 000 ΔG_{eff} values. We computed the accumulated mean for each position by summing over all previous values and dividing by their number.

Energetically-relevant residues (hot-spots) at the interfaces of TIR1·AUX/IAA PB1 complexes were predicted by using the per-residue effective free energy decomposition (prEFED) protocol implemented in MMPBSA.py[20]. Hot-spot residues were defined as those with a side-chain energy contribution (ΔG_{sc}) of ≤ -1.0 kcal/mol. We used Computational Alanine Scanning (CAS)[20] to further assess per-residue free energy contributions. Alanine single-point mutations were generated on previously identified hot-spots from the prEFED protocol. Both prEFED and CAS protocols were performed from the last 10 ns of the MD simulation.

Supplementary References

1 Uversky, V. N. Natively unfolded proteins: a point where biology waits for physics. *Protein Sci* **11**, 739-756, doi:10.1110/ps.4210102 (2002).

2 Hamdi, K. *et al.* Structural disorder and induced folding within two cereal, ABA stress and ripening (ASR) proteins. *Sci Rep* **7**, 15544, doi:10.1038/s41598-017-15299-4 (2017).

3 Uversky, V. N. What does it mean to be natively unfolded? *Eur J Biochem* **269**, 2-12, doi:10.1046/j.0014-2956.2001.02649.x (2002).

4 Wend, S. *et al.* A quantitative ratiometric sensor for time-resolved analysis of auxin dynamics. *Sci Rep* **3**, 2052, doi:10.1038/srep02052 (2013).

5 AMBER10 (University of California, San Francisco, 2008).

6 Pronk, S. *et al.* GROMACS 4.5: a high-throughput and highly parallel open source molecular simulation toolkit. *Bioinformatics* **29**, 845-854, doi:10.1093/bioinformatics/btt055 (2013).

7 Hornak, V. *et al.* Comparison of multiple Amber force fields and development of improved protein backbone parameters. *Proteins* **65**, 712-725, doi:10.1002/prot.21123 (2006).

8 Jorgensen, W. L., Chandrasekhar, J., Madura, J. D., Impey, R. W. & Klein, M. L. Comparison of Simple Potential Functions for Simulating Liquid Water. *J Chem Phys* **79**, 926-935, doi:Doi 10.1063/1.445869 (1983).

9 Lindahl, E. Molecular dynamics simulations. *Methods Mol Biol* **1215**, 3-26, doi:10.1007/978-1-4939-1465-4_1 (2015).

10 Páll, S., Abraham, M. J., Kutzner, C., Hess, B. & Lindahl, E. in *Solving Software Challenges for Exascale* Vol. 8759 (eds S Markidis & E Laure) 3-27 (2015).

11 Darden, T., York, D. & Pedersen, L. Particle Mesh Ewald: An W log(N) Method for Ewald Sums in Large Systems. *J. Chem. Phys.* **98**, 10089-10093 (1993).

12 Essmann, U. *et al.* A Smooth Particle Mesh Ewald Method. *J. Chem. Phys.* **103**, 8577-8592 (1995).

13 Verlet, L. Computer "Experiments" on Classical Fluids. I. Thermodynamical Properties of Lennard-Jones Molecules. *Phys. Rev.* **159**, 98-103 (1967).

14 Berendsen, H. J. C., Postma, J. P. M., DiNola, A. & Haak, J. R. Molecular Dynamics with Coupling to an External Bath. . *J. Chem. Phys.* **81** (1984).

15 Bussi, G., Donadio, D. & Parrinello, M. Canonical sampling through velocity rescaling. *J. Chem. Phys.* **126** (2007).

16 Hess, B. & et al. A linear constraint solver for molecular simulations. *J. Comput. Chem.* **18**, 1463–1472 (1997).

17 Schneider, T. & Stoll, E. Molecular-Dynamics study of a 3-dimensional one-component model for distortive phase-transitions. *Phys. Rev. B* **17**, 1302-1322 (1978).

18 Parrinello, M. & Rahman, A. Polymorphic Transitions in Single Crystals: A New Molecular Dynamics Method. *J. Appl. Phys.* **52**, 7182-7190 (1981).

19 Nosé, S. & Klein, M. L. Constant pressure molecular dynamics for molecular systems. *Mol. Phys.* **50**, 1055-1076 (1983).

20 AMBER 2018 (University of California, San Francisco, 2018).

7.3 Supplementary Information for 2.3 Bagchi R. *et al.* (2018)

Supporting Information

The Arabidopsis ALF4 protein is a regulator of SCF E3 ligases

Bagchi *et al.*

Supplementary Figures 1-15

Supplementary Tables 1-3

Supplementary Methods

Expanded View Figures

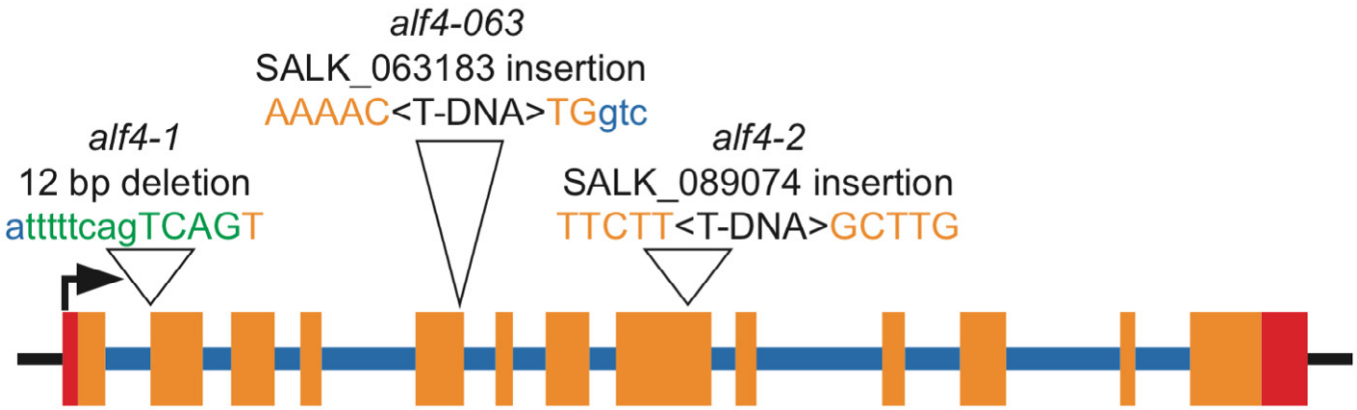

Figure EV1. Genomic locations of the *Arabidopsis* ALF4 mutations.

A schematic of the *ALF4* genomic region showing the *alf4-1* deletion (green letters) and the *alf4-2* and *alf4-063* SALK T-DNA insertions. UTRs are red, exons orange with uppercase letters, introns blue with lowercase letters. T-DNA insertion information based on sequencing from the left border.

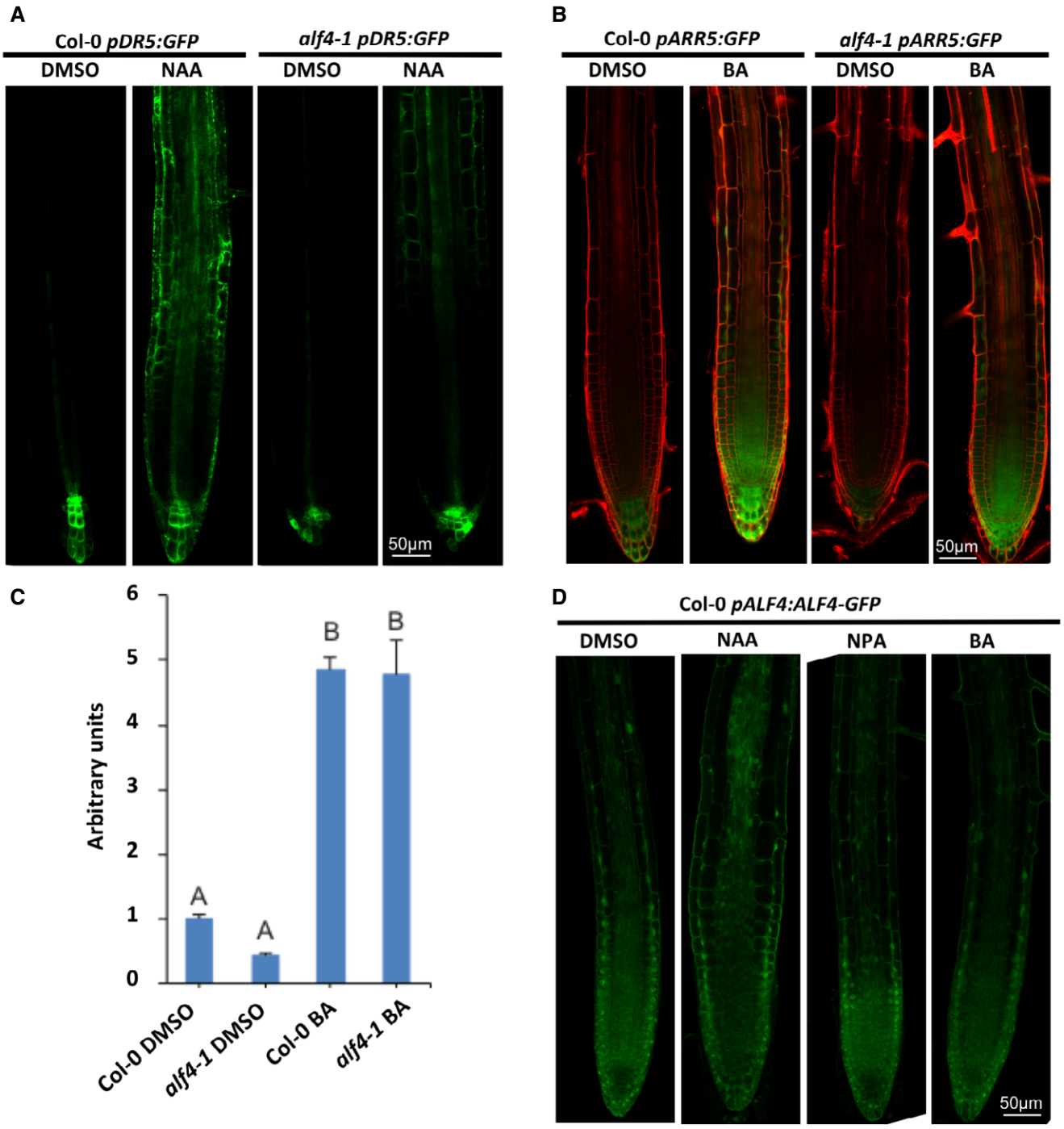

Figure EV2. ALF4 does not affect cytokinin response and is not substantially affected by auxin or cytokinin treatments.

A Expression of the auxin-responsive marker, *pDR5:GFP* (green signal), imaged in the presence or absence of synthetic auxin NAA for 24 h. These images are the same as those presented in Fig 1G, but without the red channel.

B Expression of the cytokinin responsive marker *pARR5:GFP* in Col-0 and *alf4-1* roots in the presence or absence of synthetic cytokinin (BA) for 24 h. Roots are counterstained with propidium iodide (red signal).

C BA treatment caused a strong ARR5 response in both wild-type plants and *alf4-1* plants, whereas DMSO did not (mean ± SE, n = 5–10 root tips/treatment, ANOVA with Tukey's *post hoc* test, $P < 0.01$).

D Levels of *pALF4:ALF4-GFP* in root tips were not substantially affected by treatment with NAA, BA, or the auxin transport inhibitor NPA compared to DMSO controls. Increases in root vascular signal upon NAA treatment coincided with lateral root induction.

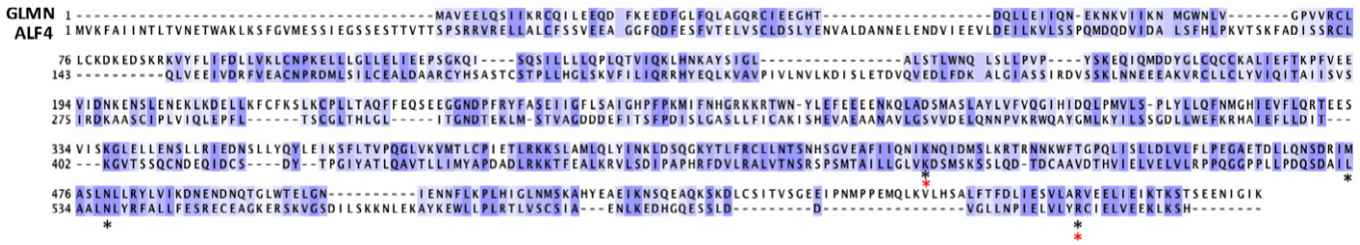

Figure EV3. Alignment of the ALF4 and human GLMN sequence.

Shading indicates conserved amino acids. Residues shown to be important for interaction between GLMN and RBX1 are indicated with black asterisks. ALF4 residues mutated to generate ALF4^{A484} and ALF4^{A614} are indicated with red asterisks.

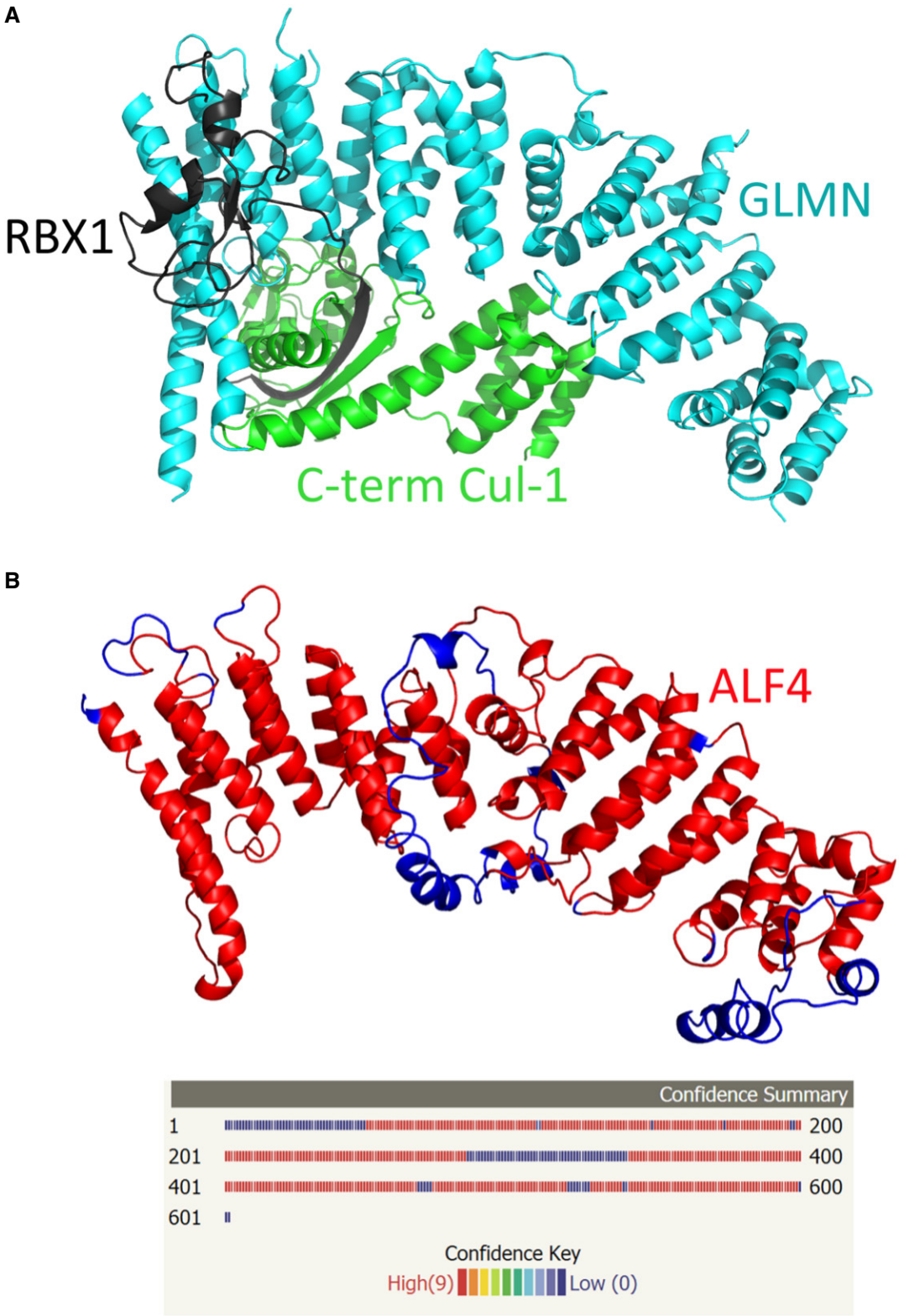

Figure EV4. Structure of GLMN and ALF4.

A X-ray structure of the Glomulin–RBX1–CUL1 complex. Adapted from PDB:4F52 originally published in Duda *et al* (2012).

B ALF4 schematic of the homology model generated with Phyre2 (webportal for protein modeling, prediction, and analysis; Kelley *et al*, 2015). 79% of ALF4 residues were modeled with > 90% confidence (red, see confidence key). 129 residues were modeled *ab initio* (blue).

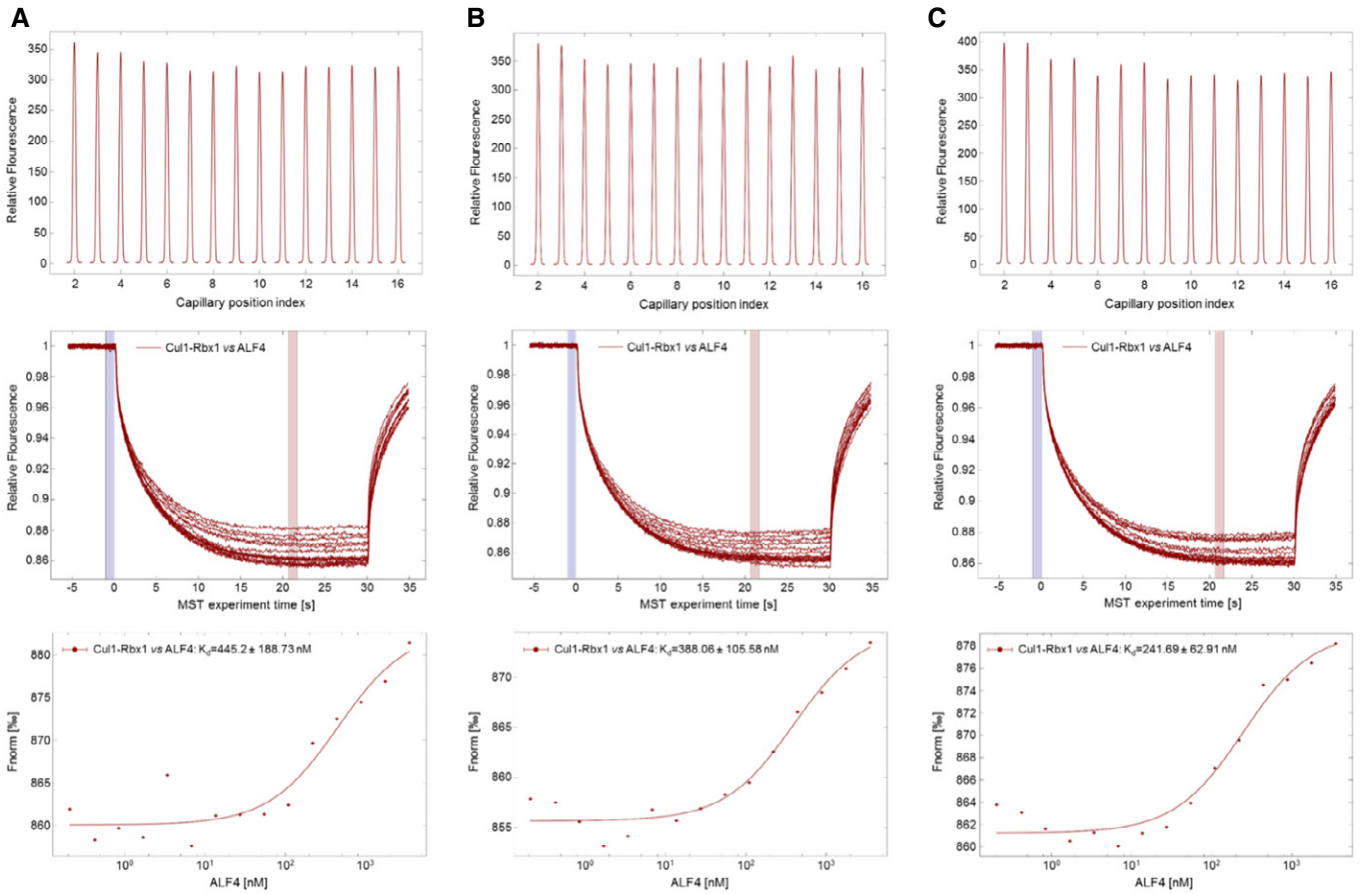

Figure EV5. Raw data of MST measurements for the interaction between labeled HsCul1–MmRBX1 vs. *At*ALF4 isoform F4JWD6.

A–C Three independent biological replicates of MST measurements depict ALF4 (red) binding to Cul1–RBX1. These measurements were combined for calculation of the dissociation constant (see Fig 3C). For each replicate, the capillary scan (up), MST traces (middle), and binding curves (low) are shown.

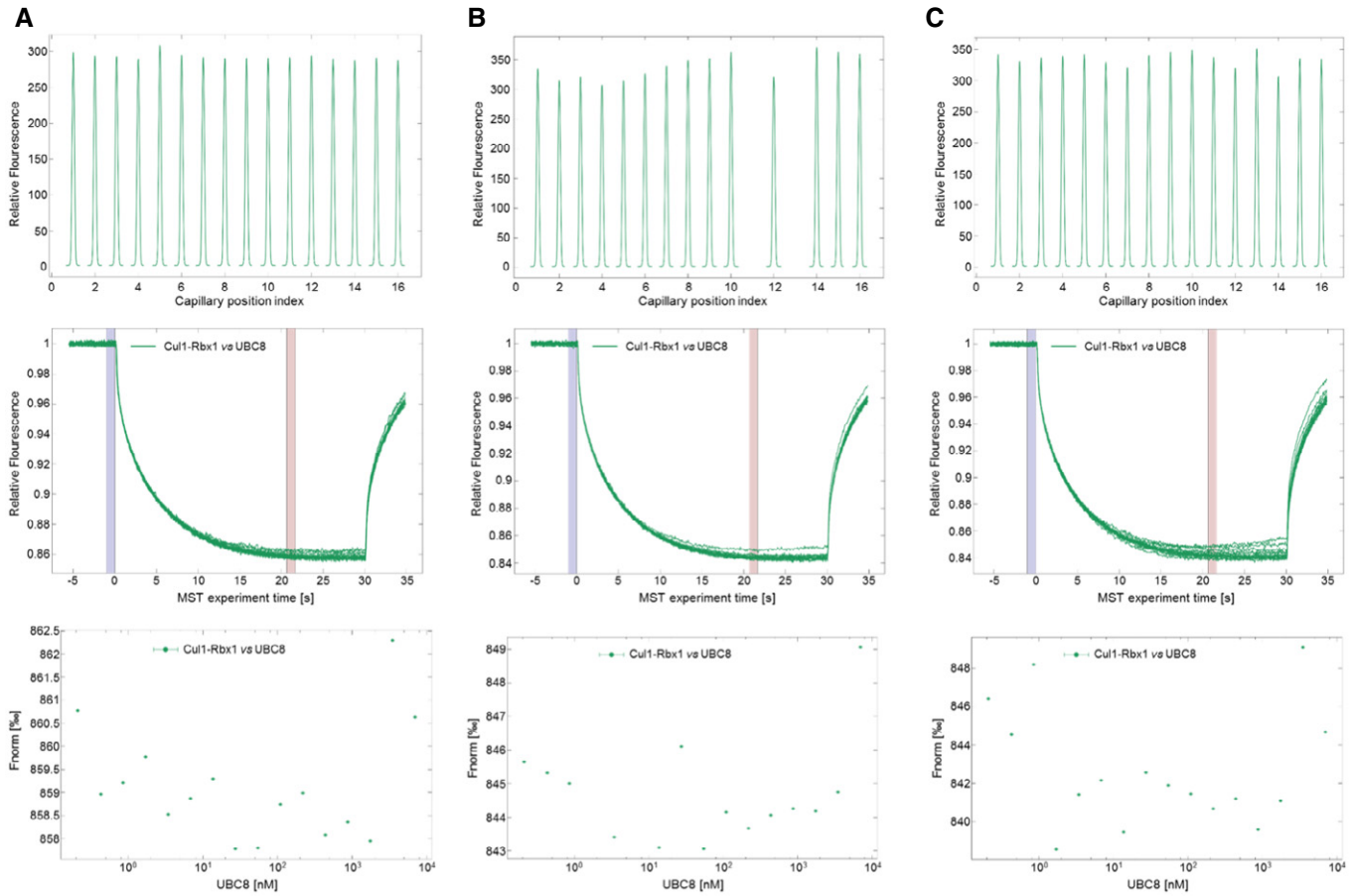

Figure EV6. Raw data of MST measurements for the interaction between labeled *Hs*Cul1–*Mm*RBX1 vs. *At*UBC8.

A–C Three independent biological replicates of MST measurements depict uncharged UBC8 (without ubiquitin) (green) does not bind to Cul1–RBX1. These measurements were used as a control for ALF4–Cul1–RBX1 interaction in Fig 3C. For each replicate, the capillary scan (up), MST traces (middle), and binding curves (low) are shown.

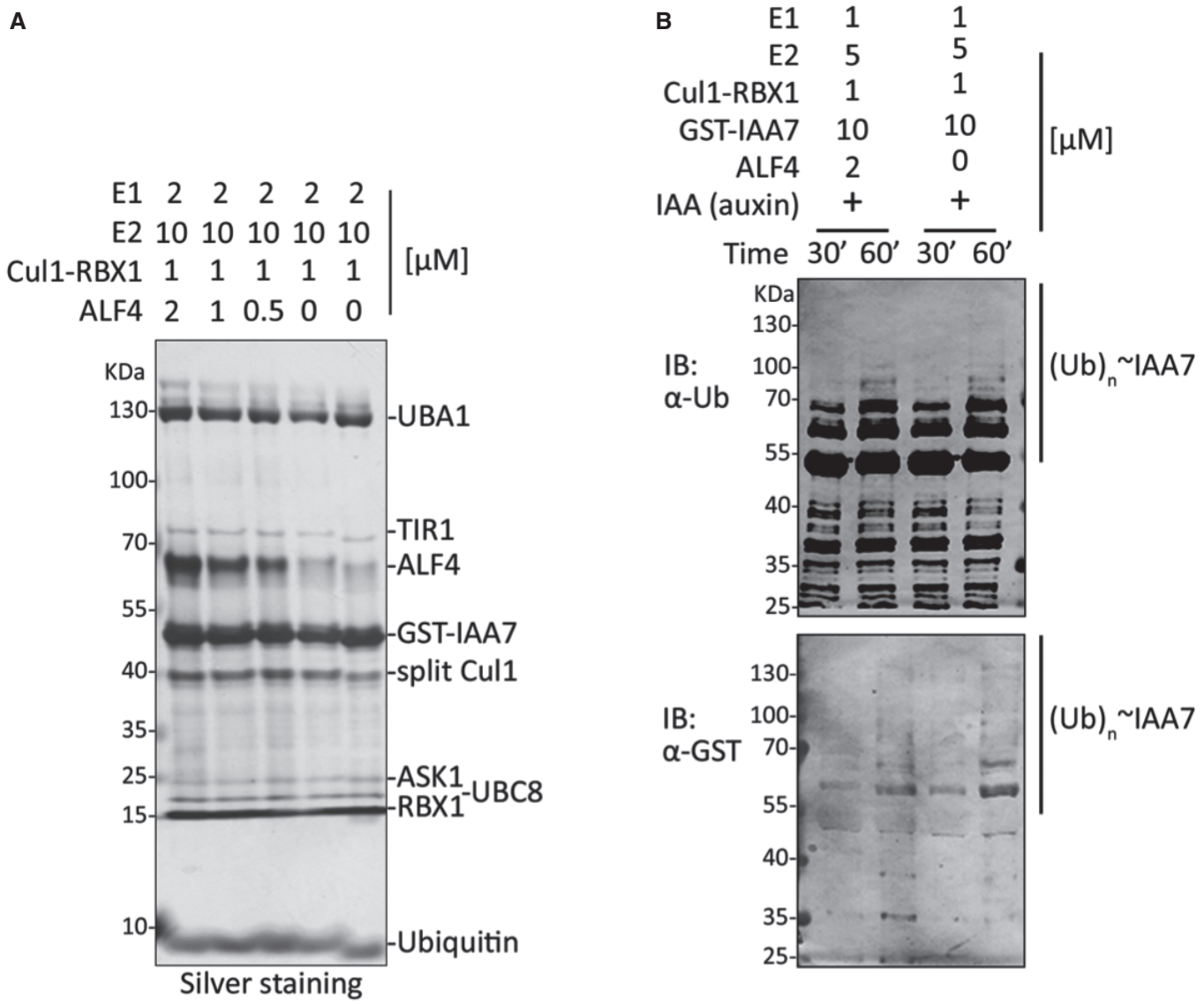

Figure EV7. Quality control of IVU components and IVU replicate using isoform F4JWD6.

A Silver staining of a gradient gel for quality control of proteins involved in the IVU reaction of GST-IAA7.

B Polyubiquitination of GST-IAA7 is also compromised by the presence of ALF4 isoform F4JWD6. IVU reactions after 30 and 60 min depict SCF^{TIR1}- and auxin-dependent transfer of ubiquitin to GST-IAA7. Each reaction consists of a mixture of 1 μM UBA1 (E1), 5 μM UBC8 (E2), 100 μM ubiquitin, and 1 μM Cul1–RBX1, 1 μM TIR1-ASK1, and 10 μM GST-IAA7 (mixture B) without or with 2 μM ALF4. Immunoblots show ubiquitinated conjugates on IAA7 using anti-GST (rabbit) or anti-ubiquitin (P4D1) (mouse) antibodies. For details, see Materials and Methods.

Source data are available online for this figure.

7.4 List of publications

- **Niemeyer M**, Moreno Castillo E, Ihling CH, Iacobucci C, Wilde V, Hellmuth A, Hoehenwarter W, Samodelov SL, Zurbriggen MD, Kastritis PL, Sinz A, Calderón Villalobos LIA. (**2020**) Flexibility of intrinsically disordered degrons in AUX/IAA proteins reinforces auxin co-receptor assemblies. ***Nat Commun*** May 8;11(1):2277. doi: 10.1038/s41467-020-16147-2.

- Bagchi R, Melnyk CW, Christ G, Winkler M, Kirchsteiner K, Salehin M, Mergner J, **Niemeyer M**, Schwechheimer C, Calderón Villalobos LIA, Estelle M (**2018**) The Arabidopsis ALF4 protein is a negative regulator of SCF E3 ligases. **EMBO J.** Jan 17;37(2):255-268. doi: 10.15252/embj.201797159. Epub 2017 Dec 12.

- Winkler M, **Niemeyer M**, Hellmuth A, Janitza P, Christ G, Samodelov S, Wilde V, Majovsky P, Trujillo M, Zurbriggen M, Hoehenwarter W, Quint M, Calderón Villalobos LIA (**2017**). Variation in auxin sensing guides AUX/IAA transcriptional repressor ubiquitylation and destruction ***Nat Commun*** Jun 7;8:15706;
  doi: 10.1038/ncomms15706.

7.5 List of figures

Acknowledgements

This work would have never been possible without the help of many lovely human beings, and here I want to thank them for their support, help and contributions.

First, I want to thank Luz Irina for her guidance through my doctoral work and an excellent supervision. Besides the extensive helpful scientific discussions we had, I especially want to thank her for the continuous dedication to improve my scientific and non-scientific skills. Under your supervision I tremendously evolve as not only a scientist, presenter and writer, but also as a person.

Further, I want to thank Steffen, who hosted me as a doctorate and always supported me and showed interest in my project. The supportive discussions, especially during the final phase of my thesis work, helped me a lot and I am grateful for the time you spend. Thank you for reviewing my thesis.

Speaking of thesis reviewing, I also want to thank Prof. Andrea Sinz for her input, especially regarding XL-MS and the straightforward offer to review my thesis. Additionally, I am glad that Prof. Dolf Weijers accepted to review my thesis and complete this great committee. The scientific input I gained from your publications and the personal communication was very insightful.

Many thanks also to Prof. Elmar Wahle, who was my mentor during this time and earlier, and always lend me an open ear. Same is true for Jun.-Prof. Panagiotis Kastritis. Thank you a lot Panos for the input and nice discussion during our collaboration and the additional fun time we spent together. I am looking forward to our next collaborative project.

Ein ganz großes Dankeschön auch an Verona unsere Laborfee! Ohne dich wäre dieses Labor einfach nicht funktionsfähig und ohne deine Hilfe meine Arbeit so niemals möglich gewesen. Auf zwei weitere großartige Jahre mit dir!
Außerdem möchte ich den Menschen danken, die die Basis für dieses Projekt gelegt haben, Antje, Martin und Gideon. Es war mir eine Freude mit euch zu arbeiten auch wenn es nur kurz war und eure vorherigen Arbeiten haben mir den Start sehr erleichtert! Ich denke, dass ich eure Arbeit angemessen fortgeführt habe.

I also want to thank my new lab companions, Elena and Tobi, for the fun we have working together. My new colleague, Jhonny, who is continuing my project, I not only want to thank him, but especially want to wish him all the best with the further development of the project!

Additionally, I want acknowledge the other people directly involved in my project, Claudio Iacobucci, Christian Ihling and Michael Götze for assistance with XL-MS, and Wolfgang Höhenwarter regarding MS-based Ub site identification. I also want to thank the Mark Estelle lab for the collaboration on the ALF4 project.

Danke auch an all die helfenden Hände am IPB, die eine großartige Arbeitsumgebung ermöglichen!

Insbesondere möchte ich meiner Familie und meinen Freunden für ihre Unterstützung während der jetzt doch vielen Jahre danken. Vielen vielen Dank! Ich bin sehr dankbar euch alle zu haben und das gilt nochmal besonders für meine Mutter und meinen Vater. Ich kann mir keine bessere Unterstützung in all den Jahren vorstellen.
Auch meinen Freunden in und außerhalb von Halle möchte ich danken für die offenen Ohren, wenn ich mal wieder von der Arbeit genervt und für die vielen Stunden des Zusammenseins und Feierns. Besondere Dank an Christian, Kaiser, Malte und Sarah für die Jahre des gemeinsamen Studiums und die Zeit danach. Außerdem erwähnt werden muss Willi, mein allerliebster Boulderkumpane. Schön, dass du wieder in Halle bist. Ebenso wichtig sind meine Freunde am IPB selbst für die vielen gemeinsamen Stunden insbesondere im Kaffeeschuppen und auf zahlreichen IPB-Feiern! Greetings to KMG crew, too!

Zu guter Letzt:
Christine, ich bin unendlich froh dich in meinem Leben zu haben. Deine Unterstützung während dieser Zeit und mein Dank dafür sind nicht in Worte zu fassen. Die gemeinsamen Stunden mit dir sind wunderbar und helfen mir auch durch die schwerste Zeit. Ich liebe dich!

DANKESCHÖN!

Curriculum vitae

Name: Michael Niemeyer

Nationality: German

Day of birth: 03.09.1990

Place of birth: Goslar, Germany

Education and research experience

11/2015 – present	Doctorate Faculty of Natural Science – Biological Sciences Martin-Luther Universität of Halle-Wittenberg Dissertation thesis "Dynamics of auxin sensing by an SCF-E3 type ubiquitin ligase and its degradation targets" Supervisor: Dr. Luz Irina A. Calderón Villalobos Leibniz Institute of Plant Biochemistry, Halle (Saale)
10/2015 – 10/2015	Student assistant / research assistant AG Signalintegration Supervisor: Dr. Luz Irina A. Calderón Villalobos Leibniz Institute of Plant Biochemistry, Halle (Saale)
10/2013 – 09/2015	**Master student**, Martin-Luther Universität of Halle-Wittenberg Graduation: Master of Science, final grade 1.2
11/2014 – 03/2015	**Internship**, Fraunhofer Institute for Cell Therapy and Immunology IZI, Department of Drug Design and Target Validation Supervisor: Dr. Holger Cynis
06/2014 – 07/2014	**Internship**, Alfred Wegener Institute Helmholtz Center for Polar and Marine Research Division Supervisor: Dr. Uwe John
01/2013 – 04/2013	**Internship**, Institute for Biochemistry, MLU Halle-Wittenberg, Group Allgemeine Biochemie Supervisor: Prof. Elmar Wahle / Michael Götze
10/2010 – 09/2013	**Bachelor student**, Martin-Luther Universität of Halle-Wittenberg Graduation: Master of Science, final grade 2.3
08/2003 – 07/2010	**High-School education** at Ratsgymnasium Goslar Graduation: Abitur, final grade 2.2

Conference attendances

- *"Practical course on ubiquitin and ubiquitin-like proteins"*, Frankfurt, GER, 05.09. - 09.10.2015
- *"Plant Science student conference 2016"*, Halle (Saale), GER, 17. - 24.09.2016
- *EMBO training course: "New approaches to study Ub and UbL modifications"*, Alghero, ITA, 17. - 24.09.2016
- *"Proteasome Hub 2018", München, GER, 12. - 14.02.2018*
- *"PROTEOSTASIS Final Meeting and 5th MC Meeting"*, Athen, GRC, 22. - 24.02.2018
- *"Plant Science Student Conference", Halle (Saale), GER, 18. - 21.06.2019*
- *"Plant Proteostasis", Freiburg, GER, 1. - 13.09.2019*

Halle (Saale), July 2020

Michael Niemeyer

Eidesstattliche Erklärung (Statutory declaration)

Hiermit erkläre ich an Eides statt, dass ich mich mit der vorliegenden wissenschaftlichen Arbeit erstmals um die Erlangung des Doktorgrades bewerbe, die Arbeit selbstständig und ohne fremde Hilfe verfasst, nur die angegebenen Quellen und Hilfsmittel genutzt und die den benutzten werken wörtlich oder inhaltlich entnommenen Stelle als solche kenntlich gemacht habe.

Halle (Saale), den _____ _____

Michael Niemeyer